8-9-2014

SYNTHESIS AND CHARACTERIZATION OF POLYMER NANOMATERIALS USING CONTROLLED RADICAL POLYMERIZATION

Lei Wang
University of South Carolina - Columbia

SYNTHESIS AND CHARACTERIZATION OF POLYMER NANOMATERIALS USING CONTROLLED RADICAL POLYMERIZATION

by

Lei Wang

Bachelor of Science
Wuhan Polytechnic University, 2009

Submitted in Partial Fulfillment of the Requirements

For the Degree of Doctor of Philosophy in

Chemistry

College of Arts and Sciences

University of South Carolina

2014

Accepted by:

Brian C. Benicewicz, Major Professor

John J. Lavigne, Committee Member

Thomas Vogt, Committee Member

Alan W. Decho, Committee Member

Lacy Ford, Vice Provost and Dean of Graduate Studies

ACKNOWLEDGEMENTS

I would like to express my sincere and deepest gratitude to my Ph.D. advisor Prof. Brian Benicewicz for his patient guidance, incredible encouragement and support, and inspirational advice on my Ph.D. research. His insight and wisdom have inspired me most in my graduate school life. I really enjoyed the conversations with him about the research, work and life. And I am very proud of being a member of the Benicewicz group.

I would like to acknowledge Dr. Alan W. Decho, Dr. Yung Pin Chen and Kristen Miller for their contributions and advices on this work. I also would like to thank Prof. Linda Schadler and Ying Li at Rensselaer Polytechnic Institute, Prof. Chuanbing Tang, Dr. Yali Qiao for their support and suggestions on the cooperation projects.

I also would like to thank my committee Prof. John J. Lavigne and Prof. Thomas Vogt for their suggestions and help in my Ph.D. research.

I would like to thank present and past Benicewicz group members for their assistances and discussions in my graduate study. I learned a lot from the group and really enjoyed working with the excellent team.

Finally, I would like to express my gratitude to my parents and my brother. Their faith and love give me the strength I need to proceed. Without their support and encouragement, I would never have finished this work.

ABSTRACT

This research focuses on creating and investigating polymer/organic bound interfaces on nanoparticles with advanced architectures to tailor the properties of polymer nanocomposites for various applications. Reversible addition-fragmentation chain transfer (RAFT) polymerization and a toolbox of surface functionalization from the simple to the advanced were developed to prepare the polymer nanomaterials.

In the first part (Chapter 2), a variety of RAFT agents (xanthate, dithiocarbamate and trithiocarbonate) were used to mediate the polymerizations of several classes of free radical polymerizable monomers. These monomers consist of styrene, methyl acrylate, methyl methacrylate, vinyl acetate and isoprene, which have different activities and require different classes of RAFT agents to control the polymerizations. RAFT agents containing the tertiary and α-EWG R groups demonstrated excellent control over the molecular weights with little effect on the PDIs. MADIX agents and trithiocarbonate RAFT agents containing the similar R groups generated polystyrene with a high PDI (~ 2.0) and a low PDI (~ 1.1) respectively with control over the polymer molecular weights. These differences can result in either sharp or fuzzy interfaces on nanoparticles with similar chain lengths and chain densities. A dithiocarbamate RAFT agent exhibited excellent control over the polymerization of vinyl acetate. In addition, trithiocarbonates were used as thermally stable RAFT agents that could mediate the polymerization of isoprene with predictable molecular weights. Polyisoprene grafted silica particles are

expected to improve the dispersion of particles in rubber matrices, which is critical for mechanical reinforcement.

In the second part, two classes of water soluble polymers were grafted on nanoparticles via surface-initiated RAFT polymerizations. A new RAFT agent, 4-cyanopentanoic acid N-pyrroledithiocarboxylate (CPDC) was invented for mediating the polymerization of N-vinylpyrrolidone. The synthesis of poly(vinylpyrrolidone) (PVP) grafted nanoparticles was confirmed by FTIR, TGA, ^{1}H NMR and TEM. The synthesis of dye-labeled poly(methacrylic acid) (PMAA) grafted silica nanoparticles was studied with two methods. In the first method, "one-pot" click reactions between azide attached silica nanoparticles and alkyne functionalized molecules (alkyne based dye and 4-pentynoic acid) were used. In the second method, surface-initiated RAFT polymerization of *tert*-butylmethacrylate (*t*BuMA) was conducted on dye-labeled CPDB coated silica nanoparticles followed by sequential removal of the thiocarbonylthio end groups and the *tert*-butyl moieties. Additionally, as a more straightforward strategy, direct polymerization of methacrylic acid on silica nanoparticles with a diameter size as small as 15 nm was conducted via the RAFT polymerization technique. A variety of PMAA brushes with different lengths and densities were prepared on nanoparticle surfaces with excellent control.

In the third part (Chapter 5), a direct-coprecipitation of iron salts strategy was used to generate superparamagnetic nanoparticles with a saturation magnetization of 59.5 emu/g. A silica coating was applied and used to stabilize the magnetic nanoparticles and create a convenient platform for further functionalization. PMAA brushes were prepared on the magnetic nanoparticles with an average diameter size as small as 10 nm via

surface-initiated RAFT polymerization of methacrylic acid while maintaining good dispersibility in solutions. The synthesis was confirmed by FTIR, TGA, VSM, TEM and AFM. The polymer grafted magnetic nanoparticles were removed from water solutions after antimicrobial testing using a magnet, thereby avoiding nano-based pollution of the environment.

In the last part (Chapter 6), the surface of silica nanoparticles was modified with a variety of functionalities, from the simple to the advanced. A series of luminescent particles with different sizes were prepared. Dye-labeled monolayer carboxylic acid coated silica nanoparticles with a range of graft densities were synthesized and the particles have strong fluorescence. It was shown that when the commonly-used antibiotics, such as penicillin-G, were linked to carboxylic acid grafted silica nanoparticles, their bacteriocidal efficiencies were increased significantly, even to antibiotic-resistant MRSA. We hypothesize that the increased antimicrobial activity is ascribed to locally high concentrations of antibiotics bound to nanoparticles, which overwhelms the resistance of bacterial strains. β-Cyclodextrin grafted nanoparticles were prepared to capture acyl-homoserine lactone molecules in the bacterial quorum sensing (QS) process. Advanced bimodal PEG and PMAA grafted nanoparticles, and poly(MAA-*b*-NIPAM) grafted particles were designed and prepared via the “grafting to” and “grafting from” techniques. A new strategy of aqueous-based surface functionalization of particles with water soluble polymers was developed.

TABLE OF CONTENTS

ACKNOWLEDGEMENTS iii

ABSTRACT iv

LIST OF TABLES x

LIST OF FIGURES xi

LIST OF SCHEMES xviii

CHAPTER 1: INTRODUCTION 1

1.1 REVERSIBLE ADDITION-FRAGMENTATION CHAIN TRANSFER POLYMERIZATION 2

1.2 SURFACE FUNCTIONALIZATION OF NANOPARTICLES 4

1.3 POLYMER CHEMISTRY ON VARIOUS SUBSTRATES 15

1.4 WATER SOLUBLE POLYMERS 19

1.5 RESEARCH OUTLINE 22

1.6 REFERENCE 24

CHAPTER 2: DESIGN AND SYNTHESIS OF RAFT AGENTS FOR MEDIATING POLYMERIZATION OF VARIOUS MONOMERS 31

2.1 INTRODUCTION 31

2.2 EXPERIMENTAL 35

2.3 RESULTS AND DISCUSSION 42

2.4 SUMMARY 66

2.5 REFERENCE 66

CHAPTER 3: SYNTHESIS AND CHARACTERIZATION OF POLY(VINYLPYRROLIDONE) GRAFTED NANOPARTICLES VIA RAFT POLYMERIZATION 68

3.1 INTRODUCTION 68

3.2 EXPERIMENTAL 70

3.3 RESULTS AND DISCUSSION 74

3.4 SUMMARY 83

3.5 REFERENCE 83

CHAPTER 4: SYNTHESIS AND CHARACTERIZATION OF DYE-LABELED POLY(METHACRYLIC ACID) GRAFTED NANOPARTICLES 85

4.1 INTRODUCTION 86

4.2 EXPERIMENTAL 89

4.3 RESULTS AND DISCUSSION 93

4.4 SUMMARY 112

4.5 REFERENCE 113

CHAPTER 5: PREPARATION AND CHARACTERIZATION OF RECYCLABLE MAGNETIC NANOPARTICLES WITH SURFACE-GRAFTED POLY(METHACRYLIC ACID) VIA RAFT POLYMERIZATION 115

5.1 INTRODUCTION 115

5.2 EXPERIMENTAL 118

5.3 RESULTS AND DISCUSSION 123

5.4 SUMMARY 136

5.5 REFERENCE 137

CHAPTER 6: SURFACE FUNCTIONALIZATION OF NANOPARTICLES: FROM THE SIMPLE TO THE ADVANCED 139

6.1 INTRODUCTION 140

6.2 EXPERIMENTAL 143

6.3 Results and Discussion 149
6.4 Summary 176
6.5 Reference 177
Chapter 7: Conclusions and Future Work 180
Appendix A: Permission to Reprint 186

LIST OF TABLES

Table 4.1 Surface-initiated RAFT polymerization of AHMA on silica nanoparticles in THF 95

Table 5.1 The Microemulsion Method for Preparation of Fe_3O_4/SiO_2 Magnetic Nanoparticles 123

Table 6.1 Europium (III)-doped silica nanoparticles size distribution 151

Table 6.2 Dye-labeled monolayer carboxylic acid coated nanoparticles 155

Table 6.3 RAFT Polymerization of NIPAM.....175

LIST OF FIGURES

Figure 1.1 Surface functionalization of nanoparticles: from the simple to the complex...11

Figure 1.2 The structures of several categories of water soluble polymers.....20

Figure 2.1 Process of radical addition to thiocarbonylthio chain transfer agents (CTA) and fragmentation 31

Figure 2.2 The structure of O-ethyl S-prop-2-yn-1-yl carbonodithioate (**1**), 6-azidohexyl 2-((ethoxycarbonothioyl)thio)-2-methylpropanoate (**2**), S-(2-cyanopropan-2-yl) O-ethyl carbonodithioate (**3**) and S-(cyano(phenyl)methyl) O-ethyl carbonodithioate (**4**).....42

Figure 2.3 ^{1}H NMR spectra of O-ethyl S-prop-2-yn-1-yl carbonodithioate.....43

Figure 2.4 ^{13}C NMR spectra of O-ethyl S-prop-2-yn-1-yl carbonodithioate.....44

Figure 2.5 ^{1}H NMR spectra of 6-azidohexyl 2-bromo-2-methylpropanoate.....45

Figure 2.6 ^{1}H NMR spectra of 6-azidohexyl 2-((ethoxycarbonothioyl)thio)-2-methylpropanoate.....46

Figure 2.7 ^{1}H NMR spectra of S-(2-cyanopropan-2-yl) O-ethyl carbonodithioate.....47

Figure 2.8 The structure of (4-cyano-4-diethyldithiocarbamyl) pentanoic acid (CDPA) .48

Figure 2.9 ^{1}H NMR spectra of CDPA (E.A.: Ethyl Acetate) 49

Figure 2.10 UV-vis standard absorption curve of CDSS at 299 nm.....51

Figure 2.11 (a) Kinetic plots and (b) dependence of the GPC molecular weight (filled triangles), theoretical molecular weight (solid line) and polydispersity (filled squares) on the conversion for the MADIX polymerization of styrene ([Styrene]:[CTA]:[AIBN] = 300:1:0.1) at 70 ^{o}C mediated by O-ethyl S-prop-2-yn-1-yl carbonodithioate (**1**) 52

Figure 2.12 (a) Kinetic plots and (b) dependence of the GPC molecular weight (filled triangles), theoretical molecular weight (solid line) and polydispersity (filled squares) on the conversion for the MADIX polymerization of methyl acrylate in THF (monomer concentration: 5.14 mol/L) at 70 ^{o}C mediated by O-ethyl S-prop-2-yn-1-yl carbonodithioate (**1**).....54

Figure 2.13 (a) Kinetic plots and (b) dependence of the GPC molecular weight (filled triangles), theoretical molecular weight (solid line) and polydispersity (filled circles) on the conversion for the MADIX polymerization of vinyl acetate ([Monomer]:[CTA]:[AIBN] = 300:1:0.1) at 70 ^{o}C mediated by O-ethyl S-prop-2-yn-1-yl carbonodithioate (**1**) 56

Figure 2.14 (a) Kinetic plots and (b) dependence of the GPC molecular weight (filled squares), theoretical molecular weight (solid line) and polydispersity (unfilled circles) on the conversion for the MADIX polymerization of styrene ([Monomer]:[CTA]:[AIBN] = 300:1:0.1) at 70 ^{o}C mediated by 6-azidohexyl 2-((ethoxycarbonothioyl)thio)-2-methylpropanoate (**2**) 57

Figure 2.15 (a) Kinetic plots and (b) dependence of the GPC molecular weight (filled squares), theoretical molecular weight (solid line) and polydispersity (unfilled circles) on the conversion for the MADIX polymerization of methyl acrylate in THF (monomer concentration: 4.40 mol/L) at 70 ^{o}C mediated by 6-azidohexyl 2-((ethoxycarbonothioyl)thio)-2-methylpropanoate (**2**) 59

Figure 2.16 (a) Kinetic plots and (b) dependence of the GPC molecular weight (filled squares), theoretical molecular weight (solid line) and polydispersity (unfilled circles) on the conversion for the MADIX polymerization of styrene ([Monomer]:[CTA]:[AIBN] = 300:1:0.1) at 80 ^{o}C mediated by S-(2-cyanopropan-2-yl) O-ethyl carbonodithioate (**3**) ... 61

Figure 2.17 (a) Kinetic plots and (b) dependence of the GPC molecular weight (filled squares), theoretical molecular weight (solid line) and polydispersity (unfilled circles) on the conversion for the RAFT polymerization of styrene ([Monomer]:[CTA]:[AIBN] = 500:1:0.1) at 70 ^{o}C mediated by 4-cyano-4-(dodecylsulfanylthiocarbonyl)sulfanylpentanoic acid 62

Figure 3.1 The structure of 4-Cyanopentanoic acid N-pyrroledithiocarboxylate (CPDC) 75

Figure 3.2 ^{1}H NMR spectra of the intermediate 1H-pyrrole-1-carbothioic dithioperoxyanhydride 75

Figure 3.3 ^{1}H NMR spectra of CPDC 76

Figure 3.4 UV-vis spectra of CPDC 76

Figure 3.5 Mass spectrum of CPDC 77

Figure 3.6 IR spectra of CPDC 77

Figure 3.7 (a) Kinetic study and (b) GPC molecular weight (inverted triangle), theoretical molecular weight (solid line) and polydispersity (unfilled circles) for the CPDC mediated RAFT polymerization of styrene in THF ([Styrene]:[CPDC]:[AIBN] = 475:1:0.1) at 75 ^{o}C 79

Figure 3.8 UV-vis standard absorption curve of CPDC in THF.....81

Figure 3.9 IR spectra of PVP grafted silica nanoparticles.....82

Figure 3.10 TGA of (a) CPDC; (b) CPDC coated nanoparticles; and (c) PVP grafted nanoparticles.....82

Figure 3.11 TEM image of PVP grafted nanoparticles. Inset: Photograph of PVP grafted nanoparticles in DMSO.....83

Figure 4.1 IR spectra of PAHMA grafted nanoparticles (a) before and (b) after "click" reaction.....86

Figure 4.2 Photograph of column purification of polyacid grafted nanoparticles after "click" reaction.....96

Figure 4.3 UV-vis standard absorption curve of NBD-COOH.....98

Figure 4.4 TGA of dye-labeled poly(*t*BuMA) grafted silica nanoparticle.....99

Figure 4.5 UV-vis absorption of (a) dye-labeled CPDB coated silica nanoparticle; (b) dye-labeled CPDB removed silica nanoparticle.....100

Figure 4.6 The structures of amino coumarin and the fluorescein derivative.....101

Figure 4.7 (a) Kinetic plots and (b) dependence of the GPC molecular weight (filled squares), theoretical molecular weight (solid line) and polydispersity (unfilled circles) on the conversion for the surface-initiated RAFT polymerization of *tert*-butylmethacrylate ([*t*BuMA]:[CPDB]:[AIBN] = 1000:1:0.1) at 60 ^{o}C.....102

Figure 4.8 IR spectra of SiO_2-g-poly(*t*BuMA) (a) after and (b) before TMSBr treatment.....103

Figure 4.9 ^{1}H NMR spectra of PMAA grafted silica nanoparticles.....104

Figure 4.10 TGA in nitrogen: (a) poly(*tert*-butyl methacrylate), Mn=7000 g/mol; (b) poly(*tert*-butyl methacrylate) grafted silica nanoparticles without RAFT group chain end capped); (c) PMAA grafted silica nanoparticles.....104

Figure 4.11 TEM image of poly(methacrylic acid) grafted silica nanoparticles.....105

Figure 4.12 ^{1}H NMR spectra of PMAA grafted silica nanoparticles at different time in the kinetic study (for calculation of the conversion at certain time in the polymerization). (A): t=0 h; (B): t=1.58 h; (C): t=4.05 h; (D): t= 6 h; (E): t= 8.7 h; (F): t=10.82 h.....107

Figure 4.13 IR spectra of PMAA grafted silica nanoparticle before and after methylation

by trimethylsilyldiazomethane.....107

Figure 4.14 ^{1}H NMR of PMAA grafted silica nanoparticle before and after methylation by trimethylsilyldiazomethane.....108

Figure 4.15 TGA of dye-labeled PMAA grafted silica nanoparticle.....108

Figure 4.16 Photograph of dye-labeled PMAA grafted silica nanoparticles in DMSO ..109

Figure 4.17 Photograph of dye-labeled PMAA grafted silica nanoparticles in water 109

Figure 4.18 TEM of dye-labeled PMAA grafted silica nanoparticles. Size bar = 300 nm 109

Figure 4.19 (a) Kinetic plot and (b) dependence of the GPC molecular weight (inverted triangle), theoretical molecular weight (solid line) and polydispersity (unfilled circles) on the conversion for the surface-initiated RAFT polymerization of methacrylic acid ([MAA]:[CPDB]:[AIBN] = 1000:1:0.1).....111

Figure 5.1 Photograph of Fe_3O_4/SiO_2 magnetic nanoparticles prepared via the microemulsion method.....125

Figure 5.2 TEM of Fe_3O_4/SiO_2 nanoparticles prepared by microemulsion method with the standard recipe (Group A in Table 5.1) 125

Figure 5.3 Photograph of Fe_3O_4/SiO_2 nanoparticles prepared via microemulsion method: a)10X TEOS of the standard recipe; b) 5X TEOS of the standard recipe; c) Standard Recipe; d) 2X iron of the standard recipe 126

Figure 5.4 TEM of Fe_3O_4/SiO_2 nanoparticles prepared by the recipe with 2X water (Group E in Table 5.1) 126

Figure 5.5 XRD of Fe_3O_4/SiO_2 magnetic nanoparticles 128

Figure 5.6 IR of Fe_3O_4/SiO_2 and Fe_3O_4 magnetic nanoparticles.....128

Figure 5.7 General procedure of fabrication of Fe_3O_4/SiO_2 magnetic nanoparticles 129

Figure 5.8 VSM of superparamagnetic Fe_3O_4 nanoparticles (59.5 emu/g) and Fe_3O_4/SiO_2 nanoparticles (29.1 emu/g).....129

Figure 5.9 TGA of Fe_3O_4, Fe_3O_4/SiO_2, and PMAA grafted Fe_3O_4/SiO_2 magnetic nanoparticles 129

Figure 5.10 TEM of Fe_3O_4/SiO_2 nanoparticles.....130

Figure 5.11 CPDB coated Fe_3O_4/SiO_2 nanoparticles.....131

Figure 5.12 IR spectra of PMAA grafted Fe_3O_4/SiO_2 magnetic nanoparticles before and after methylation.....132

Figure 5.13 PMAA grafted SiO_2/Fe_3O_4 nanoparticles in DMF: (A) Normal state; (B) After magnetic separation; (C) Sonication Recovery and 14 days later.....133

Figure 5.14 TEM of PMAA grafted magnetic nanoparticles 133

Figure 5.15 AFM of PMAA grafted Fe_3O_4/SiO_2 magnetic nanoparticles. Size bar = 200 nm.....133

Figure 5.16 Inhibition activities of free-PenG (light blue), and PenG complexed to carboxylated polymers on magnetic nanoparticles (navy) as tested by bacterial culture solution with *E. coli*.....135

Figure 6.1 TEM image of silica nanoparticles prepared by Stober method with different sizes (a) 20 nm; (b) 90-100 nm.....149

Figure 6.2 Photoluminescence spectrum of Eu (III)-doped silica nanoparticles. Using the excitation wavelength of 365 nm, the maximum emission was 538 nm 150

Figure 6.3 Confocal scanning laser micrographs showing time-resolved fluorescence of Eu (III)-doped silica nanoparticles: (A) 25-30 nm size; (B) 95-100 nm size. Note: the sizes of light spots are larger than the actual particle size due to inherent resolution limitations of light microscopy and partial agglomeration of particles prepared on glass slides 151

Figure 6.4 Transmission electron microscopy (TEM) micrographs of Eu (III)-doped silica nanoparticles with a variety of ligands: (1) Tris(2,2,6,6-tetramethyl-3,5-heptanedionato) Europium (Eu : Si = 0.33 mol%), 25-30 nm; (2) Europium chloride hexahydrate (Eu : Si = 0.68 mol%), 40-50 nm; (3) Europium chloride hexahydrate (Eu : Si = 1.34 mol%),150-170 nm; (4) Europium acetate hydrate (Eu : Si = 0.5 mol%), 95-100 nm.....152

Figure 6.5 Eu (III)-doped silica nanoparticles with a variety of ligands: (1) Tris(2,2,6,6-tetramethyl-3,5-heptanedionato) Europium (Eu : Si = 0.33 mol%), 25-30 nm; (2) Europium chloride hexahydrate (Eu : Si = 0.68 mol%), 40-50 nm; (3) Europium acetate hydrate (Eu : Si = 0.5 mol%), 95-100 nm; (4) Europium chloride hexahydrate (Eu : Si = 1.34 mol%), 150-170 nm 152

Figure 6.6 (a), (b), (c): TEM micrographs of Ru(II)-doped silica nanoparticles, 40-50 nm; (d): photograph of ruthenium(II) doped silica nanoparticles.....153

Figure 6.7 UV-vis standard absorption curve of NBD-COOH at 326 nm.....155

Figure 6.8 Photograph of dye-labeled carboxylic acid coated nanoparticles in ethanol after several washes 156

Figure 6.9 TEM and AFM image of polymer grafted sNPs: (a) poly(tert-butyl methacrylate) grafted sNPs with RAFT group chain end capped; (b) poly(tert-butyl methacrylate) grafted sNPs without RAFT group chain end capping; (c) poly(methacrylic acid) grafted sNPs. Scale bar for all the TEM images: 200 nm. (d) AFM image of poly(methacrylic acid) grafted sNPs.....157

Figure 6.10 Results of disk-diffusion assays using (A) S. typhimurium and (B) E. coli. Disks 1, 2, and 3 represent 2.5, 5.0, and 7.5 µg of PenG added in soluble form, respectively. Disks 1', 2', and 3' have 2.5, 5.0, and 7.5 µg of PenG complexed to 'monomeric' surface-carboxylated silica nanoparticles (sNPs), respectively. 159

Figure 6.11 Inhibition activity of free-PenG (white), PenG-complexed to the surface monolayer on sNPs (black), and PenG-complexed to carboxylated polymers on sNPs (hatched), as tested by disk-diffusion assays using B. cereus (A), P. aeruginosa (B), K. pneumoniae (C), P. vulgaris (D), E. aerogenes (E), S. typhimurium (F), CA-MRSA (G), HA-MRSA (H), E. coli (I), and S. aureus (J) 161

Figure 6.12 ^{1}H NMR spectra of the as-synthesized β-CD coated silica nanoparticles. a) before dialysis; b) after dialysis 165

Figure 6.13 TGA of (a) dye-labeled monolayer carboxylic acid coated silica nanoparticles (graft density: 0.24 groups/nm^2); (b) dye-labeled monolayer β-CD silica coated nanoparticles.....165

Figure 6.14 TGA of (a) dye-labeled poly(methacrylic acid) grafted silica nanoparticles (graft density: 0.3 groups/nm^2); (b) dye-labeled poly(β-CD) grafted silica nanoparticles 166

Figure 6.15 Photograph of dye-labeled poly(β-CD) grafted silica nanoparticles in DMSO 166

Figure 6.16 IR spectra of the click reaction progress between alkyne-oligoglutamate and PAHMA grafted silica nanoparticles 168

Figure 6.17 TGA of glutamate attached nanoparticles 169

Figure 6.18 ^{1}H NMR of 1-(2-thioxothiazolidin-3-yl)pent-4-yn-1-one 171

Figure 6.19 Photograph of nanoparticles in water (a) SiO_2; (b) PEG (Mn=550 g/mol) functionalized SiO_2; (c) PEG (Mn=5000 g/mol) functionalized SiO_2.....172

Figure 6.20 TGA of (a) SiO_2-COOH; (b) PEG (Mn=550 g/mol) functionalized SiO_2; (c) PEG (Mn=5000 g/mol) functionalized SiO_2 172

Figure 6.21 TGA of (a) PEG (Mn=5000 g/mol) grafted SiO_2 Nanoparticles; (b) Bimodal PEG and PMAA grafted SiO_2 Nanoparticles 173

Figure 6.22 ^{1}H NMR of (a) PMAA grafted silica nanoparticles; (b) poly(MAA-*b*-NIPAM) grafted nanoparticles.....176

Figure 6.23 ^{1}H NMR of (a) PMAA grafted silica nanoparticles; (b) poly(MAA-*b*-NIPAM) grafted nanoparticles.....176

Figure A.1 Permission to reprint for Chapter 1. 186

Figure A.2 Permission to reprint for Chapter 4. 187

Figure A.3 Permission to reprint for Chapter 6. 188

Figure A.4 Permission to reprint for Chapter 4 and Chapter 6.. 189

LIST OF SCHEMES

Scheme 1.1 Mechanism of RAFT polymerization 3

Scheme 2.1 Two methods of immobilization of RAFT agents containing alkyne or azide moieties on silica nanoparticles via the click reaction and subsequent surface-initiated polymerizations.....34

Scheme 2.2 The synthetic strategy of xanthate O-ethyl S-prop-2-yn-1-yl carbonodithioate.....43

Scheme 2.3 The synthetic strategy of 6-azidohexyl 2-((ethoxycarbonothioyl)thio)-2-methylpropanoate.....45

Scheme 2.4 The synthesis of (a) intermediate O,O-diethyl bisxanthate; (b) S-(2-cyanopropan-2-yl) O-ethyl carbonodithioate **(E)** 47

Scheme 2.5 The synthesis of S-(cyano(phenyl)methyl) O-ethyl carbonodithioate (**4**) 48

Scheme 2.6 Synthesis of RAFT agent CDPA.....49

Scheme 2.7 Synthesis of CDSS anchored silica nanoparticles.....50

Scheme 2.8 Synthesis of CDPA anchored silica nanoparticles 51

Scheme 3.1 Synthesis of RAFT agent CPDC.....75

Scheme 3.2 Scheme for synthesis of PVP grafted silica nanoparticles 80

Scheme 4.1 Synthesis of dye-labeled poly(carboxylic acid) grafted silica nanoparticles .94

Scheme 4.2 “Deprotection” strategy for preparation of dye-labeled PMAA grafted silica nanoparticles 97

Scheme 4.3 Synthetic scheme for preparation of dye-labeled PMAA grafted silica nanoparticles via direct polymerization of MAA 106

Scheme 5.1 Synthetic scheme for preparation of PMAA grafted Fe_3O_4/SiO_2 nanoparticles via direct polymerization of MAA.....130

Scheme 5.2 Scheme of recycling magnetic nanoparticles to deliver antibiotics for killing bacteria 134

Scheme 6.1 Synthesis of dye and carboxylic acid functionalized nanoparticles 154

Scheme 6.2 Synthesis of Penicillin G covalently attached nanoparticles 158

Scheme 6.3 Synthetic method for preparation of glutamate attached nanoparticles 168

Scheme 6.4 Synthetic method for bimodal PMAA and PEG grafted silica nanoparticles via RAFT polymerization in water 170

Scheme 6.5 Synthetic method for poly(MAA-*b*-NIPAM) grafted silica nanoparticles ..174

CHAPTER 1

INTRODUCTION[1]

[1] Li, Y.; Krentz, T. M.; Wang, L.; Benicewicz, B. C.; Schadler, L. S. Ligand Engineering of Polymer Nanocomposites: From the Simple to the Complex. *ACS Appl. Mater. Interfaces* **2014**, *6*, 6005−6021. Reprinted here with permission of publisher

1.1 Reversible Addition-Fragmentation Chain Transfer Polymerization

Free radical polymerization has been widely used for industry applications due to its advantages, such as being adaptable to various monomers and less strict polymerization conditions.[1] In addition, very high molecular weights of certain polymers can be easily achieved. However, free radical polymerization is usually accompanied with irreversible termination resulting in a large amount of dead chains formed during the polymerization. It also can not be used to build more complicated molecular architectures, such as block copolymers and star-shape polymers. Thus, controlled radical polymerization (CRP) was developed to prepare polymers with controllable molecular weights, polydispersity and sophisticated architectures.[2]

Reversible addition-fragmentation chain transfer (RAFT) polymerization has been recognized as an important reversible addition radical polymerization (RDRP) technique to prepare polymers with controllable molecular weights and low polydispersities since its invention by Moad and co-workers in 1998.[3] RAFT polymerization has many advantages, such as being adaptable to almost all free radical polymerizable monomers, without participation of inorganic catalysts and mild operational conditions. Also in 1998, macromolecular design by interchange of xanthates (MADIX)[4,5] was reported by Rhodia Chimie in France. MADIX and RAFT techniques operate on identical mechanisms, and the only difference lies on the choice of Z substituent of the chain-transfer agent (CTA) structure. RAFT terminology indicates structures of Z-C(=S)-S-R generally, while MADIX was named for xanthates only with Z = OZ'.

Being different from nitroxide-mediated polymerization (NMP)[6] and atom-transfer radical polymerization (ATRP),[7] the RAFT/MADIX technique uses a degenerative chain

transfer method to control polymerization, rather than employing a persistent radical in the system.[8] One of unique features of the RAFT/MADIX technique is its applicability to functional monomers, such as vinyl acetate and N-vinyl pyrrolidone. It has been successfully applied in mediating polymerizations of a variety of monomers under mild conditions with controllable molecular weights, narrow polydispersity and sophisticated architectures.

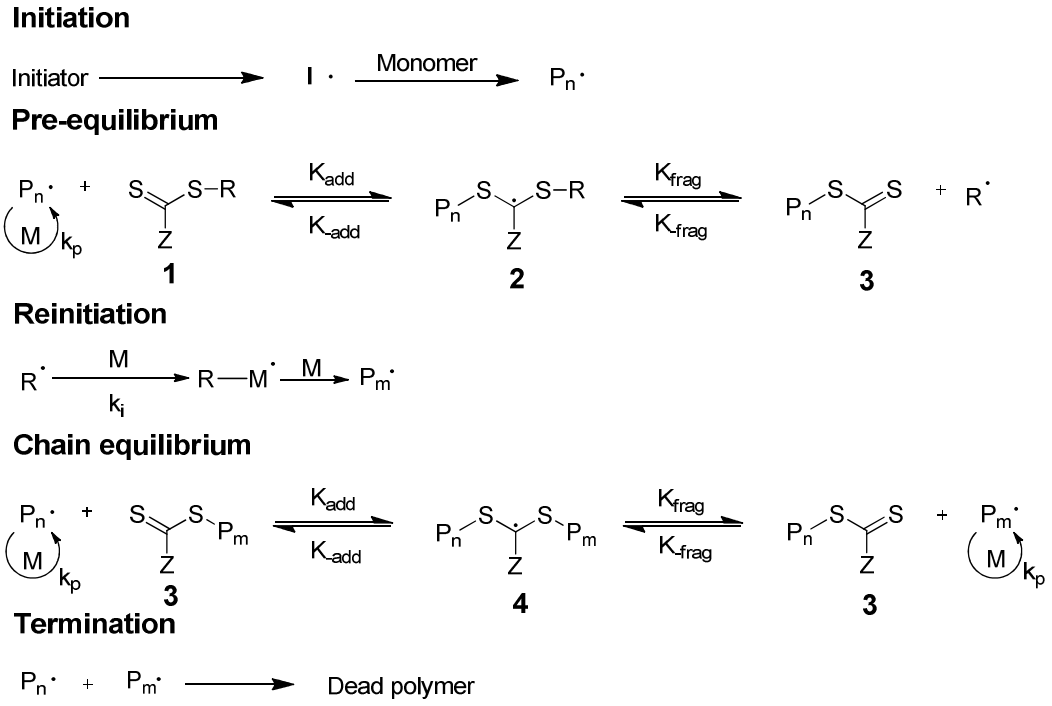

Scheme 1.1 Mechanism of RAFT polymerization.[3]

The mechanism for a RAFT polymerization is shown in Scheme 1.1.[3] In the initiation stage, the initiators decompose into free radicals, which add to monomers and grow into oligomeric propagating radicals $P_n\cdot$. A variety of initiation methods have been conducted for a RAFT polymerization, such as the thermal initiation,[9] photochemical stimulation by ultraviolet light,[10] γ radiation,[11] and pulsed laser irradiation.[12] However, the most widely utilized method is the thermal decomposition of radical initiators. Then, the addition of

$P_n^{\cdot}$ to the chain transfer agent (**1**) generates adduct intermediate radicals (**2**), which can transfer back to the original state (**1**) or form a macro RAFT agent (**3**) by fragmentation. Hence, the R ideally should be a good leaving and reinitiating group. After initiation, polymer chains grow by monomer addition, and they rapidly exchange between dormant adduct transient radicals (**4**) and the macro RAFT agent (**3**). The rapid exchange guarantees that the growing radicals are at lower concentrations than the stabilized intermediate radicals (**4**), thus minimizing termination.

In chain polymerization, chain transfer constant (C_{tr}) represents the ratio of the rate constant of transfer (k_{tr}) to that of propagation (k_p), $C_{tr} = k_{tr}/k_p$. As the transfer process for CTA is associated with the both addition and fragmentation process, the C_{tr}(**X**) is expressed as Equation (1). [13]

$$C_{tr}(\mathbf{X}) = (k_a/k_p)[k_\beta/(k_{-a}+k_\beta)] \qquad (\mathbf{1})$$

where k_a, k_β and k_{-a} are the rate constant for addition, fragmentation, and reverse addition steps respectively. From the equation, it was known that C_{tr}(**X**) is associated with the rate constant of addition (k_a), and the probability ($k_\beta/(k_{-a}+k_\beta)$) of fragmentation.[13] The higher the transfer constant, the faster for chain transfer in equilibrium, then the closer the experimental molecular weight is to the theoretical molecular weight.

1.2 Surface Functionalization of Nanoparticles

Surface functionalization of nanoparticles is very appealing due to their applications in coatings, biomedical engineering, organic light-emitting devices (OLEDs) and chemosensors.[14] Surface functionalization plays a critical role in tailoring the properties of nanoparticles for applications, such as enhanced particle dispersion in polymer

matrices and the resulting optoelectronic properties,[15] mechanical properties,[16] improved cellular internalization,[17] enhanced binding ability for therapeutic delivery,[17] and selective recognition to bio-systems.[18]

1.2.1 Surface Functionalization with Small Molecule Ligands (SMLs)

Small molecules represent a significant class of materials which have been widely used to modify surfaces and have many advantages, such as low molecular weights, easy coordination onto nanoparticles, and easy processing conditions.[19-21] Compared to macromolecules, the small size of these molecules makes surface functionalizations with multiple ligands much easier. In this section, only non-charged SMLs for surface modification will be reviewed and discussed.

A wide range of small molecule ligands (SMLs) have been coated onto nanoparticles for applications in biosensing and drug delivery.[22,23] These ligands can alter the nanoparticle's stability, hydrophobic/hydrophilic properties, zeta potential, cytotoxicity, and the interactions with cells.[24-26]

Small molecules provide a repulsive layer on particle surfaces which can enhance the stability of nanoparticles in suspension and minimize nanoparticle aggregations. Two factors should be considered while choosing SMLs for stabilization of nanoparticles, one is the substrate particles, and the other one is the dispersion solvent. Rotello and co-workers have summarized the surface functionalization of a variety of nanoparticles with corresponding SMLs.[27] Generally, silane SMLs are used to modify SiO_2 nanoparticles, thio SMLs are suitable to coat Au nanoparticles and phosphate based SMLs can be employed to functionalize iron oxide and TiO_2 nanoparticles. In the nanoparticle surface

functionalizations, SMLs are bound to surfaces via chemical absorption or physical absorption (hydrophobic/hydrophilic interactions). The dispersion solvents consists of organic solvents and water. Choosing appropriate solvents with close polarity to the dispersion particles is quite necessary to store the particles.

1.2.2 Surface Functionalization with Charge Moieties

Surface modification on nanoparticles with charged moieties was reported to load and release drugs,[28] and affects the interaction between nanoparticles and cell membrane structures, which further alters the cell uptake.[29] Positive charge, negative charge and zwitterionic moieties have been functionalized on nanoparticle surfaces.[30]

Cationic compounds have been applied on substrates as important candidates of antimicrobial agents in the past few decades. Quaternary ammonium (QA)[31] is the most important and commonly used cationic material to kill bacteria. Matyjaszewski and coworkers[32] modified magnetic nanoparticles with poly(quaternary ammonium) (PQA) to kill *E. coli* with a retained 100% biocidal efficiency during eight-cycles usage of the nanoparticles. Klibanov and coworkers[33] functionalized glass slides with poly(4-vinyl-N-alkylpyridinium bromide) to kill airborne bacteria on contact. The antimicrobial properties of QA compounds are probably ascribed to the interaction with bacterial cell membranes and further results in the disruption of the membranes.[34-36] Carmona-Ribeiro reviewed the specific functions of cationic materials when interacting with bacterial cell membranes and summarized the general steps for disruption of cell membranes.[37]

QA compounds can also be used as drug delivery vehicles to load and release antibiotics. Lee *et al.* have demonstrated that mesoporous silica nanoparticles (MSN) can

be functionalized with surface positive charges to deliver an anionic anti-inflammatory drug, sulfasalazine, with controllable loading and release by changing the pH value.[28] The positively charged surface was synthesized by a condensation reaction between trimethylammonium (TA)-silane and tetraethoxysilane (TEOS) of MSN. Sulfasalazine was loaded into the nanoparticle and stayed in the framework of MSN under acidic conditions, and was sustainly released by electrostatic repulsion from the gradually formed negative charge surface under neutral conditions.

Surface functionalization with negatively charged compounds has also been widely investigated for antimicrobial or other biomedical applications. It was reported that positively charged nanoparticles demonstrated higher internalization while negatively charged nanoparticles showed cell uptake by direct diffusion.[38,39] Surface attached anionic compounds can be employed as drug delivery vehicles to kill bacteria. Riffle and coworkers[40] modified Fe_3O_4 nanoparticles with block copolymers PEO-*b*-PAA. The unattached segments of PAA provide thousands of anionic carboxylates which were used to conjugate with cationic aminoglycoside antibiotics via ionic complexation for therapeutic applications. The delivery vehicles can also be used to deliver moieties ranging from antibiotics to metal ions. Anionic poly(3-sulfopropylmethacrylate) brushes were prepared on a Si/SiO_2 surface and employed to coordinate silver ions inside the brushes.[41] The surface attached silver-coordinated brushes inhibited the growth of both gram negative and gram positive bacteria.

Zwitterionic materials (also called inner salts) with one pair or multiple pairs of positive and negative charges in the structures have been anchored on a variety of surfaces. Surface attached zwitterionic materials were shown to be resistant to bacterial

adhesion and biofilm formation.[42] However, most of the applications of these surface attached zwitterionic moieties are still in the antifouling field. These anchored zwitterionic materials were found to be highly resistant to protein adsorption. The two main zwitterionic materials are based on sulfobetaine (SB) and carboxybetaine (CB). Thus, SB based sulfobetaine methacrylate and CB based carboxybetaine methacrylate materials have been widely investigated as antifouling materials.[42,43]

Surface functionalization with different charge moieties can be characterized by zeta potential tests.[44] It reveals the surface electrical potential which can be used to analyze the stability in solutions. Generally, nanoparticles have demonstrated stable dispersions in solution when the zeta potential is above ±30 mV. It is well known that the surface charge can inhibit aggregation of nanoparticles, thus surface modification to introduce appropriate amounts of charges is an effective method to store nanoparticle suspensions.

1.2.3 Surface Grafting Chemistry

Generally, surface functionalization of nanoparticles includes two strategies, namely "grafting from" and "grafting to". In the "grafting to" method, free molecules/polymers, containing functional groups react with nanofiller surface functional groups to create a covalent linkage. Due to steric hindrance, the graft density depends on the molecular weight and flexibility of the molecules.

Silane coupling, phosphate coupling, and "click chemistry" can all be used for "grafting to" a variety of nanoparticles, such as TiO_2,[45] ITO,[19] and SiO_2.[46-50] Silane coupling has been widely reviewed.[50,51] More phosphate functional groups have been used to attach molecules to the surface of titania[45,52] and barium titanate.[53] In addition, the

use of copper-catalyzed azide-alkyne cycloaddition ("click chemistry") has become a common tool for grafting to and can be used on polymers synthesized using a variety of methods[19,45-49] due to the easy preparation of clickable blocks (alkyne and azido end-capped moieties), high efficiency and specificity of the reaction. It does, however, leave a copper catalyst in the mixture.

One technique that can be used to tailor the brushes before attachment is RAFT polymerization which is adaptable to almost all radical polymerizable monomers. For example, it can be used to prepare alkyne and azido end-capped polymers for "click" reaction or through the use of a trimethoxysilane containing RAFT agent[50] to create a polymer that can couple to the hydroxyl groups common on metal oxide nanoparticles. ATRP[51] was also used to graft previously prepared triblock copolymers to silicon wafers.

In the "grafting from" method, polymerization is initiated on the nanofiller surface and the polymer grows *in-situ*. This technique can generate a relatively high graft density due to the absence of steric hindrance. A variety of controlled radical polymerizations (CRP), such as ATRP, nitroxide-mediated polymerization (NMP) and RAFT, have been employed to graft a wide range of polymers from surfaces over a broad range of graft densities with controllable chain lengths, polydispersity and morphology.[54-56] These surface-attached polymers have well-defined and advanced structures, such as block copolymers, branch copolymers, and star-shape polymers. The first work of surface functionalization using ATRP was reported by Wirth and co-workers in 1997.[57] Acrylamide was polymerized via ATRP on benzyl chloride attached silica surfaces. Then, Matyjaszewski and co-workers[58-60] significantly expanded grafting polymers from surfaces via ATRP. The first report of surface functionalization using NMP was in 1999

by Hawker and Russell on silicon wafers.[61] Since the invention of RAFT in 1998, it was firstly reported to modify surfaces by Tsuji *et al.* in 2001.[62] They prepared the RAFT agent *in-situ* by conversion of a surface-supported ATRP initiator followed by surface initiated RAFT polymerization of styrene. Brittain and co-workers[63] employed azoundecylchlorosilane as the anchored initiator to initiate RAFT polymerization on silica particles. Brittain *et al.*[64] also employed the "click" reaction to anchor RAFT agents on silica particles to mediate the polymerization of styrene and methyl methacrylate. Benicewicz *et al.*[65,66] employed a RAFT agent 4-cyanopentanoic acid dithiobenzoate (CPDB) to prepare a wide range of polymers from silica nanoparticle surfaces with a variety of graft densities of 0.01 - 0.68 chains/nm^2. Thus, CRP methods are tremendously important techniques for the "grafting from" method to prepare polymer grafted nanoparticles.[54-56]

Usually, NMP requires high reaction temperatures and ATRP generates residual copper or other metals after polymerization which is extremely difficult to be completely removed. Thus, both NMP and ATRP have not been widely applied on nanoparticle surfaces for biomedical applications. RAFT, generally employing mild reaction conditions without residual metal issues after polymerization, is adaptable to a variety of functional monomers.[9] Due to the advantages of the RAFT technique, it has been widely applied for the surface functionalization of nanoparticles to conjugate lactose[67] and peptides,[68] to deliver therapeutic agents[69] and siRNA.[70]

Both "grafting to" and "grafting from" have been demonstrated as effective methods to graft monomodal polymer brushes on surfaces. These methods have been reviewed by Benicewicz,[71] Brittain,[72] Matyjaszewski,[73,74] and Perrier.[75] In addition, these two

strategies can work cooperatively to functionalize nanoparticles with ligands from the simple to the complex for various applications, as shown in Figure 1.1.[15]

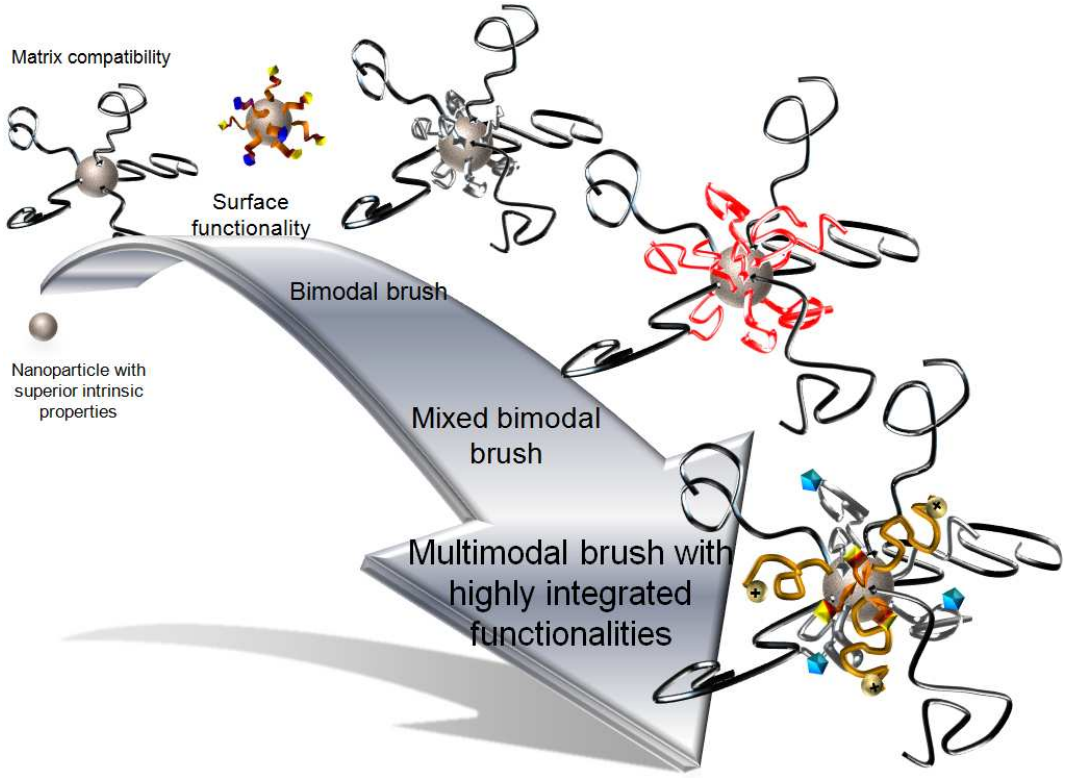

Figure 1.1 Surface functionalization of nanoparticles: from the simple to the complex.[15]

Recently, nanofillers with bimodal polymer brushes have been developed to decrease the entropic interfacial tension between the grafted and the matrix polymer brushes, and suppress dewetting in polymer matrices.[52] There are only a few reports on the preparation of bimodal brush grafted surfaces. Minko *et al.*[76] grafted two incompatible polymer brushes, carboxyl-terminated polystyrene and poly(2-vinylpyridine), to silicon wafer consecutively via a "grafting to" technique. Zhao and He[77] reported using a surface anchored "Y" shaped initiator to consecutively conduct ATRP and NMP for grafting poly(acrylic acid) and polystyrene mixed bimodal brushes on silicon wafer. Benicewicz *et al.*[78] firstly reported preparing bimodal polymer brushes on small size SiO_2

nanoparticles (diameter: 15 nm), which is significant for polymer nanocomposites because bimodal brushes had previously only been grafted on silicon wafer or 150 nm SiO_2 particles. Two rounds of surface-initiated RAFT polymerizations were used to graft the bimodal polymer brushes. The original SiO_2 nanoparticles were reacted with 3-aminopropyldimethylethoxysilane to form amino functionalized SiO_2 nanoparticles followed by the reaction with mercaptothiazoline-activated RAFT agent (CPDB) to obtain RAFT agent coated nanoparticles. After the first surface-initiated RAFT polymerization, the terminal dithiobenzoate moiety was removed by treating with excess amount of AIBN. The exact surface chemistry was repeated one more time to obtain a second population of polymer brushes. This synthesis strategy can be widely employed to prepare bimodal homopolymer brushes and mixed brushes on surfaces including PS/PMMA, PS/PS, PMMA/PMMA (1^{st} population/2^{nd} population of polymers).

For some nanofillers, such as TiO_2, ITO, and CdSe quantum dots (QDs), ligand exchange is an important strategy to prepare polymer brushes that are firmly attached to the nanoparticles. In this process, weakly bound molecules are replaced by molecules that can strongly bond to enhance the interactions between surface attached polymers and substrates. Oleic acid has been used as an important and common ligand in the synthesis of many metal oxide nanoparticles. It is quite helpful to stabilize the nanoparticles and improve the dispersity in some organic solvents. However, oleic acid is a weak binder and is usually replaced with a silane agent[79] and phosphonic acid/phosphate[80-83] moiety to obtain stronger binding. Schadler *et al.* reported using a phosphate-azide ligand to replace oleic acid on TiO_2[80] and ITO[82] surfaces, followed by further functionalization via "click chemistry" on the new ligand. They also directly used phosphate-terminated PDMS to

replace oleic acid on TiO_2[84] and QD[81] surfaces. Long chain and short chain phosphate-terminated PDMS chains were attached on QDs sequentially to form bimodal PDMS-brush-grafted QDs which demonstrated an excellent dispersion in the high molecular weight silicone matrix.

Generally, oleic acid or oleylamine are added to stabilize magnetic iron oxide nanoparticles in the preparation process. However, it limits the surface functionalization of particles and reduces the dispersion of the particles in hydrophilic media. Thus, ligand exchange is quite necessary for further applications of magnetic iron oxide nanoparticles. Bronstein and co-workers[79] used N-(6-aminohexyl)-aminopropyltrimethoxysilane to replace oleic acid on iron oxide nanoparticles to stabilize the particles. Binder and co-workers[85] employed 1,2-diols bearing ω-azido or ω -bromo ligands to replace octylamine or oleic acid on γ-Fe_2O_3 nanoparticles followed by post-functionalization of the new ligand to obtain fluorescent properties. Sun and coworkers[86] replaced oleylamine via ligand exchange to convert the nanoparticles from hydrophobic to hydrophilic for stable dispersion in an aqueous environment. Hatton *et al.*[87] replaced oleic acid with various hydroxyl group containing ligands followed by post-functionalization for surface-initiated ATRP polymerizations.

Ligand exchange is also an important tool for surface modification of nanocrystals. Murray and co-workers[88] used nitrosonium tetrafluoroborate to replace oleic acid or oleylamine on nanocrystals to stabilize the nanocrystals in various hydrophilic solvents and made the ligand exchange reversible. Talapin *et al.*[89,90] used metal chalcogenide complexes to exchange ligands on nanocrystals resulting in a hydrophilic property.

1.2.4 Characterization of Surface Functionalization

The characterization of ligand functionalized nanoparticles is a critical component of research on surface functionalities with monomodal, bimodal, mixed bimodal and multi-modal distributions. There are several factors that need to be well characterized in surface ligand engineering. The first one is graft density. A variety of small molecule ligand functionalized nanoparticles have been analyzed using their unique UV-vis and/or IR absorptions.[56,91] The amount of small molecules bound to the surface can be measured quantitatively based on the comparison between the absorbance of ligand functionalized particles and a standard UV-vis absorption curve plotted from known concentration of free ligands. The graft density of polymer grafted nanoparticles can be determined by TGA when the polymer brushes have a narrow length distribution. The second factor is grafting distributions. The polymer length distribution can be easily characterized by GPC analysis of cleaved polymer chains. However, the characterization of spatial distribution of the brushes on particle surfaces is not easy. Recently, significant progress has been achieved in characterization of spatially symmetric and asymmetric distributions of surface functionalities.[92-94] TEM so far is the main technique to qualitatively characterize the asymmetric distribution of surface functionalities.[95,96] The third factor is the morphology of surface grafted brushes. The specific morphology of the brushes is affected by the interactions between the brush and the dispersion solvent or polymer matrix. The dimensions of the brush have been characterized by dynamic light scattering accompanied with theory and simulations.[97-104] In benign solvents, the dimensions of the nanoparticle-attached spherical brushes are in agreement with the dimensions of free chains in the same solvents.[105] In polymer matrices, small-angle neutron scattering

(SANS) accompanied with selective labeling demonstrated that there is a significant reduction of the brush dimensions in the polymer matrix compared to normal organic solvents.[106] Kumar *et al.*[16] recently specifically discussed the characterization of nanoparticle-attached brush structures in organic solvents and polymer matrices. In addition, the characterization involved in surface ligand engineering of polymer nanocomposites has been reviewed by Kumar,[16] Koo,[107] Mittal,[108] and Hussain.[109]

1.3 Polymer Chemistry on Various Substrates

A wide variety of substrates have been modified to graft polymer chains by "grafting to" or "grafting from" techniques. The functional groups on substrates can be initiator; chain transfer agents (CTA) that allow surface-initiated (SI)-ATRP, Si-NMP and Si-RAFT; or other groups required to couple with free polymer chain end groups. This section will discuss the different surface chemistries among silica, metal oxides, gold, carbon and polymer nanomaterials.

Silica Surfaces

Silica substrates, such as silica nanoparticles, silica gel, glass and quartz have been extensively used to graft polymer brushes. A general strategy to functionalize the silica substrates is using organosilanes to incorporate functional groups on nanoparticles including amino, carboxylic acid, and bromo groups. The further post-functionalization can introduce initiator or CTA groups to mediate surface-initiated controlled radical polymerization. In this method, a condensation reaction between silanol groups (Si-OH) on silica surfaces and alkoxysilane or halogensilane molecules occurs resulting in the formation of a Si-O-Si bond.[9,56,110-112] A series of mono- and tri-functional silanes have

been widely employed, such as -$SiMe_2Cl$, -SIM_2OEt, -$Si(OMe)_3$ and -$Si(OEt)_3$. Trifunctional organosilanes have been reported to polymerize with unreacted functional silane moieties in water, which is not good to form a monolayer of surface functionalized groups.[113] As a different approach, silane-containing initiators or CTAs were employed to directly modify silica surfaces. Benicewicz *et al* developed a silane-containing RAFT agent by a multistep synthesis to react with silanol groups on the surface of silica nanoparticles.[110]

Silica nanoparticles have been applied in the delivery of enzymes, antibiotics and DNA.[114] The biocompatibility makes silica nanoparticles as ideal carriers for bio-applications associated with the human body. As an important class of silica materials, mesoporous silicas have attracted huge interests since its first synthesis by Mobil Corporation researchers in 1992.[115] Mesoporous silicas have been applied in the fields of catalysis and biomedical devices because of their unique properties, pore morphologies and easy surface functionalization.[116,117] In the last few years, mesoporous silica nanoparticles (MSN) particles have been used in the delivery of bio-molecules, especially drug molecules.[118]

Metal Oxide Surfaces

Metal oxide nanoparticles provide unique properties of local heating and magnetic properties. The surface functionalization of these nanoparticles varies depending on the nature of the substrates. The most widely used metal oxide nanoparticles for grafting polymers are iron oxide, titanium and aluminum surfaces.

Alumina substrates have been functionalized with organosilanes to form Al-O-Si bonds via a condensation reaction between Al-OH moieties and organosilane agents. The post functionalization can introduce an ATRP initiator by coupling with 2-bromo-2-methylpropionyl bromide for surface-initiated ATRP polymerization.[119] Iron oxide nanoparticles (Fe_3O_4 and Fe_2O_3) contain various surface groups depending on the synthetic recipes. Oleic acid containing iron oxide nanoparticles can be functionalized by ATRP initiators via a ligand-exchange process resulting in a surface-initiated ATRP platform.[120,121] Carboxylic acids and phosphonic acids were used to bind Fe_3O_4 nanoparticles inspiring the development of a series of initiators or CTAs containing these acids for surface binding followed by Si-CRP.[122-127] TiO_2 substrates have been modified by organosilanes to form Ti-O-Si bonds on the surfaces or coordinated by acid derivatives.[122] Similarly, initiators containing organosilane were used to functionalize TiO_2 surfaces followed by SI-ATRP. An acid containing RAFT agent has been used to coordinate the surface of TiO_2 nanoparticles for Si-RAFT with three indentified approaches, namely monodentate, bridging or chelating bidentate between carboxylic acid moieties and the Ti atom.[122] A series of other metal oxide nanoparticles have been functionalized employing similar strategies as the above three substrates.[128,129]

Gold Surfaces

The general strategy to functionalize gold nanoparticles is forming an Au-S bond on the surface. The first strategy is preparing gold nanoparticles *in-situ* under the stabilization of polymers containing thio end groups. Lowe and coworkers[130] reduced several RAFT end group containing polymers and a gold precursor complex simultaneously in water resulting in a variety of polymer stabilized gold nanoparticles.

The second strategy is preparing initiator or RAFT agent coated gold nanoparticles followed by Si-CRP. Fukuda *et al.* reduced $HAuCl_4 \cdot 4H_2O$ and ATRP initiator containing a disulfide bond simultaneously to prepare ATRP initiator functionalized gold nanoparticles followed by SI-ATRP.[131] Dithioesters or trithiocarbonates has been reported to directly attach on gold substrates.[132] This straightforward strategy provides a simple tool to prepare polymer grafted gold nanoparticles by Si-RAFT technique.

Carbon Surfaces

Generally, there is no functional group on carbon nanotubes or nanoparticles. Thus, the modification of the carbon nanomaterials needs an oxidative activation with HNO_3 or H_2SO_4 to introduce carboxylic acid moieties on the surfaces. The further conversion of carboxylic acid with initiator containing groups via an esterification reaction resulted in ATRP initiator modified carbon nanotubes[133] or nanoparticles.[134]

Polymer Surfaces

The surface functionalization of polymer nanomaterials varies depending on the nature of the substrates. Generally, there are two categories of the substrate polymer surfaces, namely functional group containing and inert polymer nanomaterials. The strategy to modify functional group containing polymer substrates is either converting these groups with initiators/RAFT agents followed by Si-CRP or coupling with other free functional group containing polymers. Cellulose with hydroxyl groups were coupled with ATRP initiators by condensation reactions.[135] Halogen and epoxide containing polymer substrates were treated with sodium N,N-diethyldithiocarbamate and carboxylic acid

containing ATRP initiators respectively to incorporate initiators and/or RAFT agents on surfaces.[136]

The inert polymer substrates need to be pretreated to incorporate functional groups on the surface followed by the above-mentioned strategies or directly used as a platform for growing polymers employing irradiation or plasma procedures. The pretreatment method varies depending on the inert polymer substrates. For example, polypropylene, poly(tetrafluoroethylene) (PTFE), and rubbers were subjected to ozone treatment,[137] hydrogen plasma/ozone,[138] and $NaOH/KMnO_4$[139] respectively. The newly generated -OH groups on the polymer substrates can be postfunctionalized with initiators or RAFT agents followed by SI-CRP. An alternative strategy to grow polymers on inert polymer substrates employs irradiation or plasma techniques. UV, γ-radiation and plasma have been employed to generate radicals on poly(vinylidene fluoride), polyethylene and PTFE surfaces followed by Si-RAFT or Si-ATRP to grow polymers.[140-142]

1.4 Water Soluble Polymers

Water soluble polymers have been applied in membrane transport,[143] coatings[144] and biomedical areas.[145] These polymers offer water solubility to nanoparticles when they are grafted on nanoparticles, which is very appealing for industrial applications. In this section, the main categories of water soluble polymers (Figure 1.2) will be discussed.

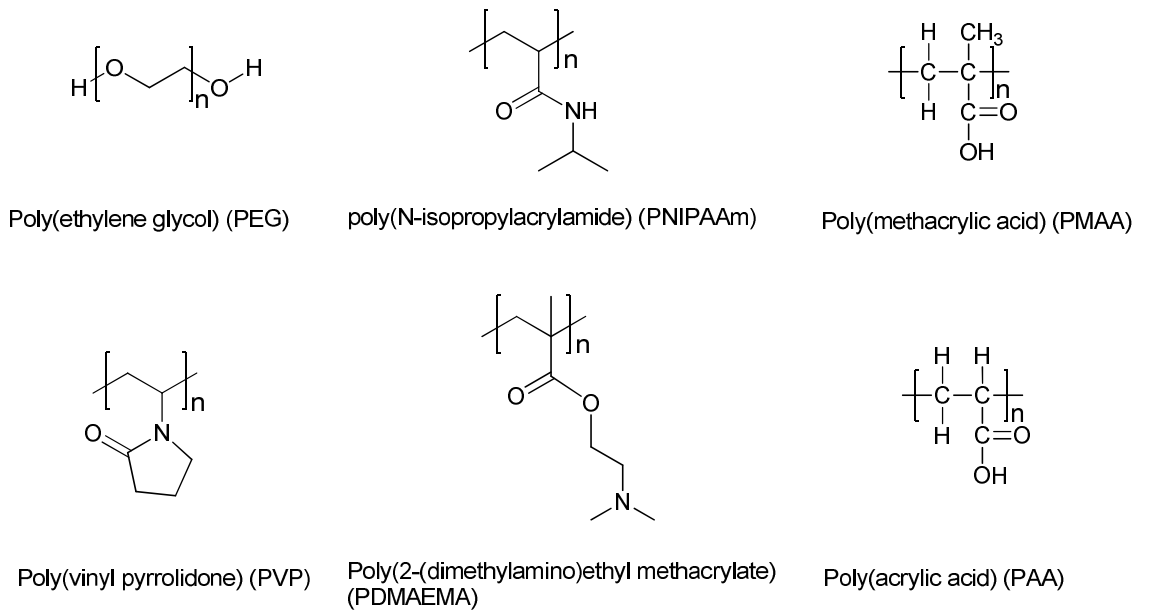

Figure 1.2 The structures of several categories of water soluble polymers.

Poly(ethylene glycol) (PEG), a hydrophilic polymer generally used to enhance the water solubility of materials, is a significant polymer material that has been used in bioapplications due to its unique properties, including exceptional biocompatibility and non-toxicity.[146] Surface coating with PEG prevents protein absorption and minimizes cell attachment as antifouling materials.[146,147] The surface anchored PEGs have also been reported to prevent protein absorption, enhance circulation time, improve tumor targeting, and increase stabilization in salt solutions.[148-150]

pH responsive water soluble polymers usually contain ionizable groups in the structures. They can protonate and deprotonate under different pH conditions. Generally, there are two classes of pH responsive water soluble polymers, namely polyacids and polybases. The representatives of polyacids are poly(acrylic acid) (PAA) and poly(methacrylic acid) (PMAA). Both of them contain multiple carboxylic acids which can be used to chemically or physically bind small molecules, thus they have been coated

on nanoparticles to kill bacteria as antibiotic delivery materials.[40,151] The representative polybase is PDMAEMA. It has also been applied in biomedical devices.[152-154]

The representative temperature-responsive water soluble polymer is poly(N-isopropylacrylamide) (PNIPAAm), which alters its conformation under different temperature conditions. When the temperature is higher than the lower critical solution temperature (LCST), the PNIPAM transits from a swollen hydrated phase to a shrunken dehydrated phase.[155,156] PNIPAAm has a LCST around 32 °C in water, which is suitable for applications of drug delivery[157,158] and bio-separations.[159,160] PDMAEMA is another important temperature-responsive water soluble polymer with a LCST around 45 °C in water at pH 8.5.[161,162] The LCST varies at different pH values.

Poly(vinyl pyrrolidone) (PVP), a very important water soluble polymer, has been applied in the biomedical area and cosmetic industry due to its nontoxic and nonionic characteristics, and its biocompatibility.[163] It is particularly attractive in the drug delivery field for its abilities to conjugate active biomolecules and prolong the circulation lifetime of antibiotics in blood.[163] Although PVP has been synthesized via free radical polymerization of N-vinylpyrrolidone (NVP),[164] the preparation of PVP with great control on polymer chain length and architecture is desirable and extremely important for biomedical applications. NMP, ATRP and organocobalt-mediated radical polymerization (OMRP)[165] have demonstrated no effect or very little effect after careful design and operation, on the mediated polymerization of NVP in a controlled manner. The reason is the special polar lactam structure in the monomer, which interacts with the catalysts and further interrupts them in these polymerization systems.

1.5 Research Outline

The goal of this research was to functionalize nanoparticles with new surface chemistries to obtain desired properties for various applications. The beauty of polymer grafted nanoparticles is that the properties of the composites can be tailored by choosing different substrate nanoparticles and polymer shells. Thus, surface functionalization is critical to prepare the composite materials and also will affect the dispersion of nanoparticles in small molecule or polymer matrices which would further influence the properties. This research would be helpful to understand the structure-property relationship of polymer grafted nanoparticles.

The first part of this work (Chapter 2) is design and synthesis of RAFT agents to mediate the polymerizations of main classes of free radical polymerizable monomers, such as styrene, methyl acrylate, methyl methacrylate, vinyl acetate and isoprene in solutions and on nanoparticles. There is no universal RAFT to control the polymerization of all monomers. Thus, a variety of RAFT agents, such as xanthate, dithiocarbamate and trithiocarbonate were employed for monomers with different activities. The effects of different R groups were investigated and it was found that tertiary and α-EWG R groups were effective for controlling molecular weight. Some RAFT agents were able to control the molecular weight but with high PDI (*e.g.* PDI = ~2.0), which was helpful to design polymer grafted nanoparticles with broad PDI to improve the dispersion of these nanoparticles in polymer matrices by overcoming the loss of interface entropy. New polymer chemistries were also developed for controlling the polymerizations of vinyl acetate and isoprene. Polyisoprene grafted silica particles are expected to improve the dispersion of particles in rubber matrices, which is critical for mechanical reinforcement.

The second part of this work (Chapter 3 and 4) is grafting water soluble polymers on nanoparticles. In Chapter 3, a new RAFT agent was developed to control the polymerization of N-vinylpyrrolidone on silica nanoparticles, which has not been previously reported in the literature. The as-synthesized poly(vinyl pyrrolidone) grafted nanoparticles may have many applications in the antimicrobial area. In Chapter 4, dye-labeled and poly(methacrylic acid) grafted nanoparticles were prepared via two new classes of chemistries. The direct RAFT polymerization of methacrylic acid on small size nanoparticles provides a new window to prepare pH responsive nanocomposites.

The third part of this work (Chapter 5) is synthesis of poly(methacrylic acid) grafted superparamagnetic nanoparticles. An effective method was used to prepare Fe_3O_4/SiO_2 superparamagnetic nanoparticles with sizes as low as 10 nm and a high saturation magnetization using very mild synthetic conditions. The direct surface-initiated RAFT polymerization of MAA was conducted on very small size Fe_3O_4/SiO_2 magnetic nanoparticles while maintaining good dispersibility in solutions. The as-synthesized magnetic nanoparticles can be used as a recyclable platform in the biomedical area thus avoiding nano-based pollution of the environment.

The last part of this research (Chapter 6) is surface functionalization of silica nanoparticles with a strategy of “from the simple to the advanced”. A variety of functionalities were precisely built on nanoparticles and the resulting tailored architectures exhibited different properties. The simple surface functionalization consists of coating small molecules, such as fluorescent dyes and carboxylic acids onto particles while the advanced surface modification consists of block copolymers and bimodal

polymers with tailored graft densities. In addition, a new strategy of surface functionalization of particles with polymers in water was developed.

1.6 Reference

1. Huh, D. S.; K., M. S.; Choe, S. J. *Bull. Korean Chem. Soc.* **2001**, *22*, 769-771.
2. Braunecker, W. A.; Matyjaszewski, K. *Prog. Polym. Sci.* **2007**, *32*, 93-146.
3. Chiefari, J.; Chong, Y. K.; Ercole, F.; Krstina, J.; Jeffery, J.; Le, T. P. T.; Mayadunne, R. T. A.; Meijs, G. F.; Moad, C. L.; Moad, G.; Rizzardo, E.; Thang, S. H. *Macromolecules*. **1998**, *31*, 5559-5562.
4. Charmot, D.; Corpart, P.; Adam, H.; Zard, S.; Biadatti, T.; Bouhadir, G. *Macromol. Symp.* **2000**, *150*, 23-32.
5. Charmot, D.; Corpart, P.; Michelet, D.; Zard, S.; Biadatti, T. In *Chem Abstr* 1999; Vol. 130, p 82018.
6. Hawker, C. J.; Bosman, A. W.; Harth, E. *Chem. Rev.* **2001**, *101*, 3661-3688.
7. Matyjaszewski, K.; Xia, J. *Chem. Rev.* **2001**, *101*, 2921-2990.
8. Barner-Kowollik, C. In *Handbook of RAFT Polymerization*; Barner-Kowollik, C., Ed.; Wiley-VCH: Weinheim: Germany, **2008**, p 1-4.
9. Li, C.; Han, J.; Ryu, C. Y.; Benicewicz, B. C. *Macromolecules*. **2006**, *39*, 3175-3183.
10. Lu, L.; Yang, N.; Cai, Y. *Chem. Commun.* **2005**, 5287-5288.
11. Millard, P.-E.; Barner, L.; Stenzel, M. H.; Davis, T. P.; Barner-Kowollik, C.; Müller, A. H. *Macromol. Rapid Commun.* **2006**, *27*, 821-828.
12. Buback, M.; Junkers, T.; Vana, P. *Macromol. Rapid Commun.* **2005**, *26*, 796-802.
13. Destarac, M.; Brochon, C.; Catala, J. M.; Wilczewska, A.; Zard, S. Z. *Macromol. Chem. Phys.* **2002**, *203*, 2281-2289.
14. Zou, H.; Wu, S.; Shen, J. *Chem. Rev*. **2008**, *108*, 3893-3957.
15. Li, Y.; Krentz, T. M.; Wang, L.; Benicewicz, B. C.; Schadler, L. S. *ACS Appl. Mater. Interfaces*. **2014**, *6*, 6005-6021.
16. Kumar, S. K.; Jouault, N.; Benicewicz, B.; Neely, T. *Macromolecules*. **2013**, *46*, 3199-3214.
17. Saha, K.; Bajaj, A.; Duncan, B.; Rotello, V. M. *Small*. **2011**, *7*, 1903-1918.
18. Elghanian, R.; Storhoff, J. J.; Mucic, R. C.; Letsinger, R. L.; Mirkin, C. A. *Science*. **1997**, *277*, 1078-1081.
19. Tomovska, R.; Daniloska, V.; Asua, J. M. *Appl. Surf. Sci.* **2013**, *264*, 670-673.
20. Zhao, J.; Milanova, M.; Warmoeskerken, M. M. C. G.; Dutschk, V. *Colloid Surface A*, **2012**, *413*, 273-279.
21. Goodwin, J. W.; Harbron, R. S.; Reynolds, P. A. *Colloid Polym Sci* **1990**, *268*, 766-777.
22. Bajaj, A.; Miranda, O. R.; Kim, I.-B.; Phillips, R. L.; Jerry, D. J.; Bunz, U. H.; Rotello, V. M. *Proc. Natl. Acad. Sci.* **2009**, *106*, 10912-10916.
23. Dreaden, E. C.; Mackey, M. A.; Huang, X.; Kang, B.; El-Sayed, M. A. *Chem. Soc. Rev.* **2011**, *40*, 3391-3404.
24. Mout, R.; Moyano, D. F.; Rana, S.; Rotello, V. M. *Chem. Soc. Rev.* **2012**, *41*, 2539-2544.

25. Tam, Y. Y.; Chen, S.; Zaifman, J.; Tam, Y. K.; Lin, P. J.; Ansell, S.; Roberge, M.; Ciufolini, M. A.; Cullis, P. R. *Nanomedicine : nanotechnology, biology, and medicine*. **2013**, *9*, 665-674.
26. Yeh, Y. C.; Saha, K.; Yan, B.; Miranda, O. R.; Yu, X.; Rotello, V. M. *Nanoscale* **2013**, *5*, 12140-12143.
27. De, M.; Ghosh, P. S.; Rotello, V. M. *Adv. Mater.* **2008**, *20*, 4225-4241.
28. Lee, C. H.; Lo, L. W.; Mou, C. Y.; Yang, C. S. *Adv. Funct. Mater.* **2008**, *18*, 3283-3292.
29. Nel, A. E.; Mädler, L.; Velegol, D.; Xia, T.; Hoek, E. M.; Somasundaran, P.; Klaessig, F.; Castranova, V.; Thompson, M. *Nat. Mater.* **2009**, *8*, 543-557.
30. Mout, R.; Moyano, D. F.; Rana, S.; Rotello, V. M. *Chem. Soc. Rev.* **2012**, *41*, 2539-2544.
31. Wang, J.; Chen, Y. P.; Yao, K.; Wilbon, P. A.; Zhang, W.; Ren, L.; Zhou, J.; Nagarkatti, M.; Wang, C.; Chu, F.; He, X.; Decho, A. W.; Tang, C. *Chem. Commun.* **2012**, *48*, 916-918.
32. Dong, H.; Huang, J.; Koepsel, R. R.; Ye, P.; Russell, A. J.; Matyjaszewski, K. *Biomacromolecules* **2011**, *12*, 1305-1311.
33. Tiller, J. C.; Liao, C. J.; Lewis, K.; Klibanov, A. M. *Proc. Natl. Acad. Sci.* **2001**, *98*, 5981-5985.
34. Ikeda, T.; Yamaguchi, H.; Tazuke, S. *Antimicrob. Agents Chemother.* **1984**, *26*, 139-144.
35. Imazato, S.; Russell, R.; McCabe, J. *J Dent* **1995**, *23*, 177-181.
36. Marchisio, M.; Bianciardi, P.; Longo, T.; Ferruti, P.; Ranucci, E.; Neri, M. *J. Biomater. Sci., Polym. Ed.* **1995**, *6*, 533-539.
37. Carmona-Ribeiro, A. M.; de Melo Carrasco, L. D. *Int. J. Mol. Sci.* **2013**, *14*, 9906-9946.
38. Cho, E. C.; Xie, J.; Wurm, P. A.; Xia, Y. *Nano Lett.* **2009**, *9*, 1080-1084.
39. Shi, X.; Thomas, T. P.; Myc, L. A.; Kotlyar, A.; Baker Jr, J. R. *Phys. Chem. Chem. Phys.* **2007**, *9*, 5712-5720.
40. Pothayee, N.; Pothayee, N.; Jain, N.; Hu, N.; Balasubramaniam, S.; Johnson, L. M.; Davis, R. M.; Sriranganathan, N.; Riffle, J. S. *Chem. Mater.* **2012**, *24*, 2056-2063.
41. Ramstedt, M.; Cheng, N.; Azzaroni, O.; Mossialos, D.; Mathieu, H. J.; Huck, W. T. *Langmuir* **2007**, *23*, 3314-3321.
42. Cheng, G.; Zhang, Z.; Chen, S.; Bryers, J. D.; Jiang, S. *Biomaterials* **2007**, *28*, 4192-4199.
43. Zhang, Z.; Chen, S.; Jiang, S. *Biomacromolecules* **2006**, *7*, 3311-3315.
44. Singh, R.; Lillard, J. W., Jr. *Exp. Mol. Pathol.* **2009**, *86*, 215-223.
45. García-González, C. A.; Fraile, J.; López-Periago, A.; Domingo, C. *J. Colloid Interface Sci.* **2009**, *338*, 491-499.
46. Li, J.; Wang, L.; Benicewicz, B. C. *Langmuir* **2013**, *29*, 11547-11553.
47. Ranjan, R.; Brittain, W. J. *Macromolecules* **2007**, *40*, 6217-6223.
48. Ranjan, R.; Brittain, W. J. *Macromol. Rapid Commun.* **2008**, *29*, 1104-1110.
49. Ranjan, R.; Brittain, W. J. *Macromol. Rapid Commun.* **2007**, *28*, 2084-2089.
50. Huang, Y.; Liu, Q.; Zhou, X.; Perrier, S. b.; Zhao, Y. *Macromolecules* **2009**, *42*, 5509-5517.

51. Pyun, J.; Jia, S.; Kowalewski, T.; Matyjaszewski, K. *Macromol. Chem. Phys.* **2004**, *205*, 411-417.
52. Natarajan, B.; Neely, T.; Rungta, A.; Benicewicz, B. C.; Schadler, L. S. *Macromolecules* **2013**, *46*, 4909-4918.
53. Hsiue, G. H.; Chu, L. W.; Lin, I. *Colloids Surf., A.* **2007**, *294*, 212-220.
54. Husseman, M.; Malmström, E. E.; McNamara, M.; Mate, M.; Mecerreyes, D.; Benoit, D. G.; Hedrick, J. L.; Mansky, P.; Huang, E.; Russell, T. P.; Hawker, C. J. *Macromolecules* **1999**, *32*, 1424-1431.
55. Gao, J.; Li, J.; Benicewicz, B. C.; Hillborg, H.; Schadler, L. S. *Polymers* **2012**, *4*, 187-210.
56. Gao, J.; Li, J.; Zhao, S.; Benicewicz, B. C.; Hillborg, H.; Schadler, L. S. *Polymer* **2013**, *54*, 3961-3973.
57. Huang, X.; W., M. J. *Anal. Chem.* **1997**, *69*, 4577-4580.
58. Matyjaszewski, K.; Miller., P. J.; Shukla, N.; Immaraporn, B.; Gelman, A.; Luokala., B. B.; Siclovan, T. M.; Kickelbick, G.; Vallant, T.; Hoffmann, H.; Pakula, T. *Macromolecules* **1999**, *32*, 8716-8724.
59. Pyun, J.; Jia, S.; Kowalewski, T.; Patterson, G. D.; Matyjaszewski, K. *Macromolecules* **2003**, *36*, 5094-5104.
60. Pyun, J.; Matyjaszewski, K.; Kowalewski, T.; Savin, D.; Patterson, G.; Kickelbick, G.; Huesing, N. *J. Am. Chem. Soc.* **2001**, *123*, 9445-9446.
61. Husseman, M.; Malmström; E. E.; McNamara, M.; Mate, M.; Mecerreyes, D.; Benoit, D. G.; Hedrick, J. L.; Mansky, P.; Huang, E.; Russell, T. P.; Hawker, C. J. *Macromolecules* **1999**, *32*, 1424-1431.
62. Tsujii, Y.; Ejaz., M.; Sato, K.; Goto, A.; Fukuda, T. *Macromolecules*. **2001**, *34*, 8872-8878.
63. Baum, M.; Brittain, W. *Macromolecules* **2002**, *35*, 610-615.
64. Ranjan, R.; Brittain, W. *Macromol. Rapid Commun.* **2008**, *29*, 1104-1110.
65. Wang, L.; Benicewicz., B. *ACS Macro Lett.* **2013**, *2*, 173-176.
66. Douglas, D.; Li, Y.; Lewis, S.; Benicewicz, B.; Schadler, L.; Kumar S. K. *Macromolecules* **2010**, *43*, 1564-1570.
67. Guo, T.-Y.; Liu, P.; Zhu, J.-W.; Song, M.-D.; Zhang, B.-H. *Biomacromolecules* **2006**, *7*, 1196-1202.
68. Boyer, C.; Bulmus, V.; Priyanto, P.; Teoh, W. Y.; Amal, R.; Davis, T. P. *J. Mater. Chem.* **2009**, *19*, 111-123.
69. Rowe, M. D.; Thamm, D. H.; Kraft, S. L.; Boyes, S. G. *Biomacromolecules* **2009**, *10*, 983-993.
70. Boyer, C.; Priyanto, P.; Davis, T. P.; Pissuwan, D.; Bulmus, V.; Kavallaris, M.; Teoh, W. Y.; Amal, R.; Carroll, M.; Woodward, R. *J. Mater. Chem.* **2010**, *20*, 255-265.
71. Li, Y.; Schadler, L. S.; Benicewicz, B. C. *Handbook of RAFT Polymerization*.; Barner-Kowollik, C., Ed.; Wiley-VCH: Weinham, Germany 2008; p 423-453.
72. Radhakrishnan, B.; Ranjan, R.; Brittain, W. J. *Soft Matter*. **2006**, *2*, 386-396.
73. Pyun, J.; Matyjaszewski, K. *Chem. Mater.* **2001**, *13*, 3436-3448.
74. Pyun, J.; Kowalewski, T.; Matyjaszewski, K. *Macromol. Rapid Commun.* **2003**, *24*, 1043-1059.

75. Moraes, J.; Ohno, K.; Maschmeyer, T.; Perrier, S. *Chem. Commun.* **2013**, *49*, 9077-9088.
76. Minko, S.; Patil, S.; Datsyuk, V.; Simon, F.; Eichhorn, K.-J.; Motornov, M.; Usov, D.; Tokarev, I.; Stamm, M. *Langmuir* **2002**, *18*, 289-296.
77. Zhao, B.; He, T. *Macromolecules* **2003**, *36*, 8599-8602.
78. Rungta, A.; Natarajan, B.; Neely, T.; Dukes, D.; Schadler, L. S.; Benicewicz, B. C. *Macromolecules* **2012**, *45*, 9303-9311.
79. Huang, X.; Schmucker, A.; Dyke, J.; Hall, S.; Retrum, J.; Stein, B.; Remmes, N.; Baxter, D.; Dragnea, B.; Bronstein, L.M. *J. Mater. Chem.* **2009**, *19*, 4231-4239.
80. Tao, P. Li, Y.; Rungta, A.; Viswanath, A.; Gao, J.; Benicewicz, B.; Siegel, R.; Schadler, L. *J. Mater. Chem.* **2011**, *21*, 18623-18629.
81. Tao, P. L., Y.; Siegel, R. W.; Schadler, L. S. *J. Mater. Chem. C*. **2013**, *1*, 86-94.
82. Tao, P. Viswanath, A.; Schadler, L.; Benicewicz, B.; Siegel, R. *ACS Appl. Mater. Interfaces*. **2011**, *3*, 3638-3645.
83. White, M. A.; Johnson, J. A.; Koberstein, J. T.; Turro, N. J. *J. Am. Chem. Soc.* **2006**, *128*, 11356-11357.
84. Li, Y. Tao, P.; Viswanath, A.; Benicewicz, B. C.; Schadler, L. S. *Langmuir*. **2013**, *29*, 1211-1220.
85. Binder, W. W. H. *Monatshefte für Chemie*. **2007**, *138*, 315-320.
86. Peng, S.; Wang, C.; Xie, J.; Sun, S. *J. Am. Chem. Soc.* **2006**, *128*, 10676-10677.
87. Lattuada, M.; Hatton, T. A. *Langmuir* **2007**, *23*, 2158-2168.
88. Dong, A.; Ye, X.; Chen, J.; Kang, Y.; Gordon, T.; Kikkawa, J. M.; Murray, C. B. *J. Am. Chem. Soc.* **2011**, *133*, 998-1006.
89. Kovalenko, M. V.; Scheele, M.; Talapin, D. V. *Science* **2009**, *324*, 1417-1420.
90. Kovalenko, M. V.; Spokoyny, B.; Lee, J.-S.; Scheele, M.; Weber, A.; Perera, S.; Landry, D.; Talapin, D. V. *J. Am. Chem. Soc.* **2010**, *132*, 6686-6695.
91. Wu, N.; Fu, L.; Su, M.; Aslam, M.; Wong, K. C.; Dravid, V. P. *Nano Lett.* **2004**, *4*, 383-386.
92. Lattuada, M.; Hatton, T. A. *Nano Today* **2011**, *6*, 286-308.
93. Walther, A.; Muller, A. H. *Chem. Rev.* **2013**, *113*, 5194-5261.
94. Hu, J.; Zhou, S.; Sun, Y.; Fang, X.; Wu, L. *Chem. Soc. Rev.* **2012**, *41*, 4356-4378.
95. Hu, S.-H.; Gao, X. *J. Am. Chem. Soc.* **2010**, *132*, 7234-7237.
96. Wu, L. Y.; Ross, B. M.; Hong, S.; Lee, L. P. *Small*. **2010**, *6*, 503-507.
97. Verso, F. L.; Yelash, L.; Egorov, S. A.; Binder, K. *Soft Matter* **2012**, *8*, 4185-4196.
98. Reith, D.; Milchev, A.; Virnau, P.; Binder, K. *Macromolecules* **2012**, *45*, 4381-4393.
99. Ndoro, T. V. M.; Voyiatzis, E.; Ghanbari, A.; Theodorou, D. N.; Bo□hm, M. C.; Mu□ller-Plathe, F. *Macromolecules* **2011**, *44*, 2316-2327.
100. Ghanbari, A.; Ndoro, T. V. M.; Leroy, F.; Rahimi, M.; Bohm, M. C.; Mu□ller-Plathe, F. *Macromolecules* **2011**, *45*, 572-584.
101. LoVerso, F.; Egorov, S. A.; Binder, K. *Macromolecules* **2012**, *45*, 8892-8902.
102. Ndoro, T. V. M.; Böhm, M. C.; Müller-Plathe, F. *Macromolecules*. **2011**, *45*, 171-179.
103. Milchev, A.; Binder, K. *J Chem Phys* **2012**, *136*, 1-8.
104. Egorov, S. A.; Binder, K. *J Chem Phys* **2012**, *137*, 1-8.

105. Vlassopoulos, D. *J. Polym. Sci., Part B: Polym. Phys.* **2004**, *42*, 2931-2941.
106. Chevigny, C.; Jestin, J.; Gigmes, D.; Schweins, R.; Di-Cola, E.; Dalmas, F.; Bertin, D.; Boué, F. *Macromolecules* **2010**, *43*, 4833-4837.
107. Koo, J. H. *Polymer nanocomposites: processing, characterization, and applications*; McGraw-Hill, New York, 2006.
108. Mittal, V. *Characterization techniques for polymer nanocomposites*; Mittal, V., Ed.; Wiley-VCH: Weinheim, Germany, 2012; Chapter 1, pp 1 − 12.
109. Hussain, F.; Hojjati, M.; Okamoto, M.; Gorga, R. E. *J Compos Mater* **2006**, *40*, 1511-1575.
110. Li, C.; Benicewicz, B. C. *Macromolecules* **2005**, *38*, 5929-5936.
111. Akcora, P.; Liu, H.; Kumar, S. K.; Moll, J.; Li, Y.; Benicewicz, B. C.; Schadler, L. S.; Acehan, D.; Panagiotopoulos, A. Z.; Pryamitsyn, V.; Ganesan, V.; Ilavsky, J.; Thiyagarajan, P.; Colby, R. H.; Douglas, J. F. *Nat. Mater.* **2009**, *8*, 354-359.
112. Akcora, P.; Kumar, S.; Sakai, V. G.; Li, Y.; Benicewicz, B. C.; Schadler, L. S. *Macromolecules* **2010**, *43*, 8275-8281.
113. Fadeev, A. Y.; McCarthy, T. J. *Langmuir* **2000**, *16*, 7268-7274.
114. Sekhon, B. S.; Kamboj, S. R. *Nanomedicine*. **2010**, *6*, 612-618.
115. Kresge, C.; Leonowicz, M.; Roth, W.; Vartuli, J.; Beck, J. *Nature* **1992**, *359*, 710-712.
116. Van Der Voort, P.; Baltes, M.; Vansant, E. *J. Phys. Chem. B* **1999**, *103*, 10102-10108.
117. Shi, J.-l.; Zhang, L.-X. *J. Mater. Chem.* **2004**, *14*, 795-806.
118. Chen, Y.; Chen, H.; Guo, L.; He, Q.; Chen, F.; Zhou, J.; Feng, J.; Shi, J. *ACS Nano* **2009**, *4*, 529-539.
119. Cui, Y.; Tao, C.; Tian, Y.; He, Q.; Li, J. *Langmuir* **2006**, *22*, 8205-8208.
120. An, L.; Li, Z.; Wang, Z.; Zhang, J.; Yang, B. *Chem. Lett.* **2005**, *34*, 652-653.
121. Parvin, S.; Sato, E.; Matsui, J.; Miyashita, T. *Polym. J.* **2006**, *38*, 1283-1287.
122. Kobayashi, M.; Matsuno, R.; Otsuka, H.; Takahara, A. *Sci Tech Adv Mater* **2006**, *7*, 617-628.
123. Lattuada, M.; Hatton, T. A. *Langmuir* **2006**, *23*, 2158-2168.
124. Maliakal, A.; Katz, H.; Cotts, P. M.; Subramoney, S.; Mirau, P. *J. Am. Chem. Soc.* **2005**, *127*, 14655-14662.
125. Matsuno, R.; Otsuka, H.; Takahara, A. *Soft Matter* **2006**, *2*, 415-421.
126. Matsuno, R.; Yamamoto, K.; Otsuka, H.; Takahara, A. *Chem. Mater.* **2003**, *15*, 3-5.
127. Matsuno, R.; Yamamoto, K.; Otsuka, H.; Takahara, A. *Macromolecules* **2004**, *37*, 2203-2209.
128. Liu, P.; Wang, T. *Polym. Eng. Sci.* **2007**, *47*, 1296-1301.
129. Liu, P.; Wang, T. *Curr. Appl. Phys.* **2008**, *8*, 66-70.
130. Lowe, A. B.; Sumerlin, B. S.; Donovan, M. S.; McCormick, C. L. *J. Am. Chem. Soc.* **2002**, *124*, 11562-11563.

131. Ohno, K.; Koh, K.-M.; Tsujii, Y.; Fukuda, T. *Macromolecules* **2002**, *35*, 8989-8993.
132. Duwez, A.-S.; Guillet, P.; Colard, C.; Gohy, J.-F.; Fustin, C.-A. *Macromolecules* **2006**, *39*, 2729-2731.
133. Qin, S.; Qin, D.; Ford, W. T.; Resasco, D. E.; Herrera, J. E. *J. Am. Chem. Soc.* **2003**, *126*, 170-176.
134. Yang, Q.; Wang, L.; Xiang, W.; Zhou, J.; Tan, Q. *J. Polym. Sci., Part A: Polym. Chem*. **2007**, *45*, 3451-3459.
135. Carlmark, A.; Malmström, E. *J. Am. Chem. Soc.* **2002**, *124*, 900-901.
136. Liu, Y.; Klep, V.; Zdyrko, B.; Luzinov, I. *Langmuir* **2005**, *21*, 11806-11813.
137. Yao, F.; Fu, G.-D.; Zhao, J.; Kang, E.-T.; Neoh, K. G. *J. Membr. Sci.* **2008**, *319*, 149-157.
138. Liu, Y.-L.; Luo, M.-T.; Lai, J.-Y. *Macromol. Rapid Commun.* **2007**, *28*, 329-333.
139. Coiai, S.; Passaglia, E.; Ciardelli, F. *Macromol. Chem. Phys.* **2006**, *207*, 2289-2298.
140. Barner, L.; Zwaneveld, N.; Perera, S.; Pham, Y.; Davis, T. P. *J. Polym. Sci., Part A: Polym. Chem*. **2002**, *40*, 4180-4192.
141. Chen, Y.; Deng, Q.; Xiao, J.; Nie, H.; Wu, L.; Zhou, W.; Huang, B. *Polymer*. **2007**, *48*, 7604-7613.
142. Yu, W. H.; Kang, E. T.; Neoh, K. G. *Langmuir* **2004**, *21*, 450-456.
143. Hollman, A. M.; Scherrer, N. T.; Cammers-Goodwin, A.; Bhattacharyya, D. *J. Membr. Sci.* **2004**, *239*, 65-79.
144. Moya, S.; Azzaroni, O.; Farhan, T.; Osborne, V. L.; Huck, W. T. *Angew. Chem. Int. Ed.* **2005**, *44*, 4578-4581.
145. Chen, H.; Hsieh, Y. L. *Biotechnol. Bioeng.* **2005**, *90*, 405-413.
146. Lan, S.; Veiseh, M.; Zhang, M. *Biosens. Bioelectron.* **2005**, *20*, 1697-1708.
147. Chen, H.; Brook, M. A.; Sheardown, H. *Biomaterials* **2004**, *25*, 2273-2282.
148. Choi, C. H. J.; Alabi, C. A.; Webster, P.; Davis, M. E. *Proc. Natl. Acad. Sci.* **2010**, *107*, 1235-1240.
149. Niidome, T.; Yamagata, M.; Okamoto, Y.; Akiyama, Y.; Takahashi, H.; Kawano, T.; Katayama, Y.; Niidome, Y. *J Control Release* **2006**, *114*, 343-347.
150. Peer, D.; Karp, J. M.; Hong, S.; Farokhzad, O. C.; Margalit, R.; Langer, R. *Nat. Nanotechnol.* **2007**, *2*, 751-760.
151. Cash, B. M.; Wang, L.; Benicewicz, B. C. *J. Polym. Sci., Part A: Polym. Chem*. **2012**, *50*, 2533-2540.
152. Zhang, M.; Liu, L.; Zhao, H.; Yang, Y.; Fu, G.; He, B. *J. Colloid Interface Sci.* **2006**, *301*, 85-91.
153. Singh, N.; Wang, J.; Ulbricht, M.; Wickramasinghe, S. R.; Husson, S. M. *J. Membr. Sci.* **2008**, *309*, 64-72.
154. Zhang, X.-Z.; Yang, Y.-Y.; Chung, T.-S.; Ma, K.-X. *Langmuir* **2001**, *17*, 6094-6099.
155. Purushotham, S.; Chang, P.; Rumpel, H.; Kee, I.; Ng, R.; Chow, P.; Tan, C.; Ramanujan, R. *Nanotechnology* **2009**, *20*, 305101.
156. Yavuz, M. S.; Cheng, Y.; Chen, J.; Cobley, C. M.; Zhang, Q.; Rycenga, M.; Xie, J.; Kim, C.; Song, K. H.; Schwartz, A. G. *Nat. Mater.* **2009**, *8*, 935-939.

157. Zhou, Z.; Zhu, S.; Zhang, D. *J. Mater. Chem.* **2007**, *17*, 2428-2433.
158. Jayaraman, A.; Schweizer, K. S. *J. Chem. Phys.* **2008**, *128*, 164904.
159. Nagase, K.; Kobayashi, J.; Kikuchi, A.; Akiyama, Y.; Kanazawa, H.; Okano, T. *Biomacromolecules* **2008**, *9*, 1340-1347.
160. Nagase, K.; Kobayashi, J.; Kikuchi, A.; Akiyama, Y.; Kanazawa, H.; Okano, T. *Langmuir* **2007**, *23*, 9409-9415.
161. Yuk, S. H.; Cho, S. H.; Lee, S. H. *Macromolecules* **1997**, *30*, 6856-6859.
162. Cho, S. H.; Jhon, M. S.; Yuk, S. H.; Lee, H. B. *J. Polym. Sci., Part B: Polym. Phys.* **1997**, *35*, 595-598.
163. Devasia, R.; Bindu, R. L.; Borsali, R.; Mougin, N.; Gnanou, Y. *Macromol. Symp.* **2005**, *229*, 8-17.
164. Luo, L.; Ranger, M.; Lessard, D. G.; Le Garrec, D.; Gori, S.; Leroux, J.-C.; Rimmer, S.; Smith, D. *Macromolecules* **2004**, *37*, 4008-4013.
165. Debuigne, A.; Willet, N.; Jérôme, R.; Detrembleur, C. *Macromolecules* **2007**, *40*, 7111-7118.

CHAPTER 2

DESIGN AND SYNTHESIS OF RAFT AGENTS FOR MEDIATING POLYMERIZATION OF VARIOUS MONOMERS

2.1 Introduction

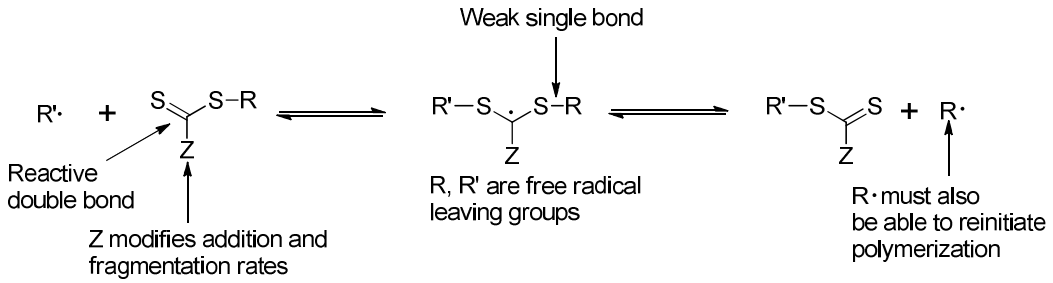

Figure 2.1 Process of radical addition to thiocarbonylthio chain transfer agents (CTA) and fragmentation.[1]

RAFT agents play an extremely significant role in RAFT polymerizations. As shown in Figure 2.1, it contains R and Z groups in the structure.[1] For an effective RAFT agent, R should be a good leaving group to facilitate the rapid fragmentation and must be effective in reinitiating polymerization to guarantee effective chain transfer. The Z group activates the thiocarbonyl bond to radical addition and provides the stability for the adduct radical (Figure 2.1).

The R group of RAFT agents can greatly affect the control of molecular weight while the Z group can influence the PDI of polymers.[2,3] Generally, increasing the substitution and stability of the R leaving group increases the chain transfer constant.[2] This explains

why tertiary R groups usually facilitate control over the polymerization of a variety of monomers. All of these modifications and effects can be understood in terms of the radical stability of the radical leaving group. The Z group affects the polydispersity of polymers by changing the electron density of the thiocarbonyl in the CTA.[3] Usually, conjugation is a effective method to greatly affect the electron density of C=S bond. Z groups possessing lone-pair donors such as OR, NR_2 and SR increase the stability of the CTA, reduce the addition rate constant of radical to the thiocarbonyl, and further enhance the PDI via the conjugation effect between the lone-pair electrons on oxygen, nitrogen or sulfur atom and the thiocarbonyl. PDIs of polymers, such as polystyrene and poly(methyl methacrylate), mediated by MADIX agents, are usually higher, varying from 1.5 to 2.4, compared to those mediated by dithiobenzoate based RAFT agents.[1,2] It was observed that the PDI for polystyryl chains is around 2 by calculation from the formula (**1**):[3,4]

$$PDI = 1+1/C_{tr}(P_nX) \qquad (\mathbf{1})$$

As introduced above, the proper design of the R and Z substituents as well as choice of monomer determine the control of molecular weight and PDIs. Other items, such as temperature, solvent, feed ratio between species should also be considered when designing and operating RAFT polymerization. Moad *et al.* reviewed the appropriate selection of various Z and R groups to different monomers.[1]

In early results of nanocomposite systems using polymer grafted nanoparticles, the dispersion of the particles in polymer matrices was usually poor.[5] This behavior can be controlled by understanding the effects of surface grafted brush molecular weight, matrix molecular weight, and the chain density on the surface of the nanoparticles on

interactions between particles and matrix. An important reason underlying the polymer grafted nanoparticle phase separation from matrices is the loss of entropy associated with the interface. Broadening the brush/matrix interface is a potential method to overcome the loss of interface entropy, which can be implemented by using widely distributed polymer chains on the nanoparticle surface.

It is known that under the same conditions, particularly with commonly used monomers, such as styrene and methyl acrylate, the PDIs of these polymer chains mediated by xanthates or dithiocarbamates are larger than that mediated by dithiobenzoate based RAFT agents.[1,2] In general, the former is 1.5-2.4, while the later is around 1.2 or even smaller. Hence, we are motivated to develop xanthates and dithiocarbamates to mediate the RAFT polymerization from nanoparticle surfaces to form relatively high polydisperse polymer chains. It is anticipated that these surface-attached brushes with high PDI will significantly alter the interactions with polymer matrices resulting in better dispersion of the polymer grafted nanoparticles.

The click reaction (azide-alkyne Huisgen cycloaddition) has been widely used as an efficient method to connect different molecules or blocks.[6] Our initial design targeted RAFT/MADIX agents containing alkyne or azide moieties, which can be easily anchored on the corresponding azide or alkyne functionalized nanoparticles via the click reaction, as shown in Scheme 2.1. There are two methods of attaching a RAFT agent on the surface of nanoparticles via click chemistry. The first one is using a RAFT agent containing azide moiety, which then was reacted with alkyne functionalized silica nanoparticles using the click reaction (Scheme 2.1, a). The second method is employing a

RAFT agent containing alkyne moiety, which then was reacted with azide functionalized silica nanoparticles (Scheme 2.1, b).

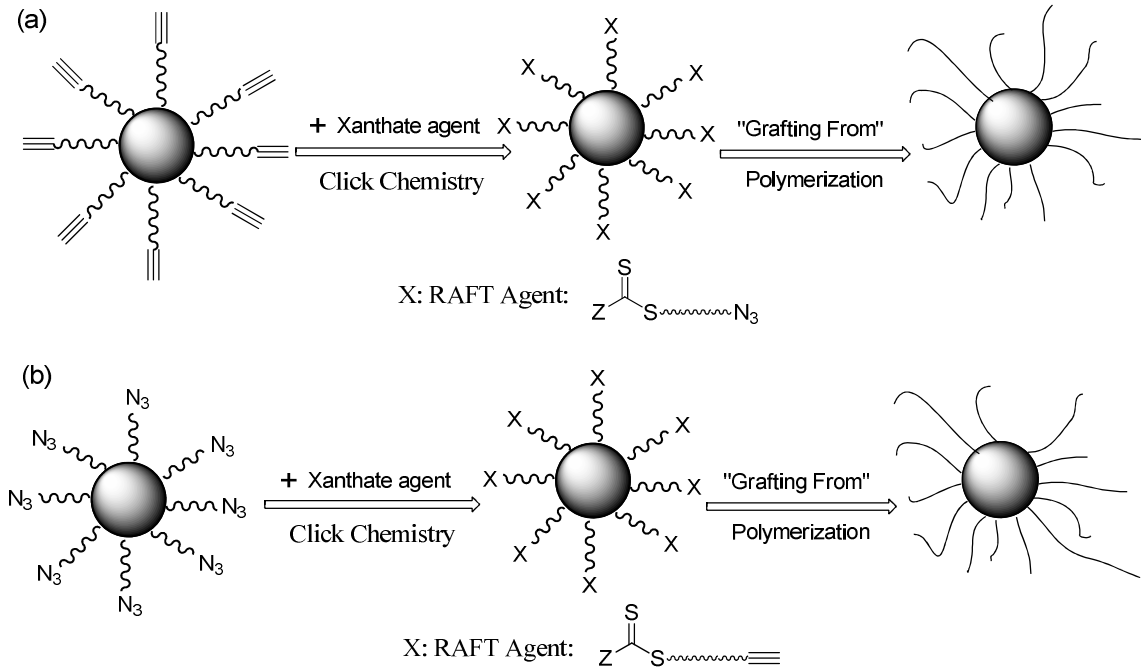

Scheme 2.1. Two methods of immobilization of RAFT agents containing alkyne or azide moieties on silica nanoparticles via the click reaction and subsequent surface-initiated polymerizations.

Polyisoprene has been recognized as an important class of rubber materials for the automotive industry since its first application in 1917.[7] Polyisoprene has been prepared by anionic, cationic, and radical polymerizations.[8-10] However, few people have reported the RAFT polymerization of isoprene in a controlled manner.[11,12] Silica particles have been used to improve the mechanical properties of rubber materials, such as polyisoprene.[13] However, bare silica particles are usually agglomerated in polymer rubber matrices due to the incompatibility. Even though particle surface functionalization, such as silane chemistry modification, has been conducted to improve the dispersion of particles, the effects were still limited. In this work, we report the surface-initiated RAFT polymerization of isoprene on silica nanoparticles to obtain polyisoprene grafted silica

nanoparticles with controllable polymer chain lengths. These polyisoprene grafted particles are expected to disperse well in polymer matrices even at high particle loading, which could find applications in the rubber industry.

2.2 Experimental

2.2.1 Materials

All chemicals were obtained from Fisher or Acros and used as-received unless otherwise specified. 4-Cyano-4-(dodecylsulfanylthiocarbonyl)sulfanylpentanoic acid was obtained from Strem Chemical Inc. Aminopropyldimethylethoxysilane was obtained from Gelest and used as-received. Styrene, methyl methacrylate and methyl acrylate were purified by passing through an activated neutral alumina column. AIBN was recrystallized from methanol before use.

2.2.2 Instrumentation

^{1}H NMR (Varian Mercury spectrometer 300/400) was conducted using $CDCl_3$ or CD_3OD as the solvent. Molecular weights and PDI were determined using a gel permeation chromatography (GPC) equipped with a 515 HPLC pump, a 2410 refractive index detector, and three Styragel columns. The columns consisted of HR1, HR3 and HR4 in the effective molecular weight ranges of 100-5000, 500-30000, and 5000-500000, respectively. The GPC used THF as eluent at 30 °C and a flow rate of 1.0 mL/min and was calibrated with poly(methyl methacrylate) or polystyrene standards obtained from Polymer Laboratories. Samples were filtered through microfilters with a pore size of 0.2 μm before injection. Infrared spectra were recorded with a PerkinElmer Spectrum 100 spectrometer. UV-vis spectra were measured with a Perkin-Elmer Lambda 4C UV-vis

spectrophotometer. TEM images were examined using a Hitachi 8000 transmission electron microscope with an operating voltage of 200 kV. Carbon-coated copper grids were used to prepare samples by dropping sample solutions on the grids followed by drying in a fume hood before use. TGA measurement was conducted using a TA Instruments Q5000 with a heating rate of 10°C/min form 25°C to 1000°C under nitrogen flow. Differential scanning calorimetry (DSC) measurement was conducted using a TA Instruments Q2000 under nitrogen flow.

2.2.3 Synthesis of O-ethyl S-prop-2-yn-1-yl carbonodithioate

Phosphorus tribromide (14.16g, 0.052 mol) was added dropwise to propargyl alcohol (8.04 g, 0.143 mol) cooled in an ice bath. The reaction solution was then stirred at 0 ˚C for 2 hours and at room temperature for 1 hour. The mixture was diluted with 100 ml of water and then went through extraction with pentane (3×50 mL), drying with anhydrous magnesium sulfate, filtration and followed by comcentration. The crude compound was purified via silica gel column chromatography using pentane as an eluent. After removal of the solvent, the colorless oil product was obtained. A THF suspention (10 mL) of Potassium ethyl xanthogenate (1.00g, 6.00×10^{-3} mol) and propargyl bromide (1.02g, 7.00×10^{-3} mol) was stirred at rt overnight under dark environment. After filtration of the formed precipitate, the resulting solution was added to 100 mL water. The solution went through extraction with diethyl ether (3×30 mL), drying with anhydrous magnesium sulfate and followed by filtration. The compound was purified via silica gel column chromatography using pentane as an eluent. After removal of the solvent, a pale-yellow oil was obtained and dried under vacuum to constant weight (0.81g, 81% yield). ^{1}H NMR (300 MHz, $CDCl_3$): δ (ppm) 1.40 (t, 3H, CH_3), 2.20 (t, 1H, CH), 3.86 (d, 2H, CH_2S), 4.64

(q, 2H, CH_2O). ^{13}C NMR (400 MHz, $CDCl_3$): δ (ppm) 13.67 (CH_3), 24.25 (CH_2S), 70.2 (CH_2O), 71.57 (CH), 77.65 (C), 211.92 (C=S).

2.2.4 Synthesis of 1-azido-6-hydroxyhexane

1-Chlorohexanol (6.83g, 0.05 mol) and sodium azide (6.50g, 0.10 mol) were dissolved in 50 ml water. The resulting solution was stirred at 80 °C for 12 h. The cooled solution went through extraction with diethyl ether (3×50 mL), drying with anhydrous sodium sulfate and followed by filtration. After removal of the solvent, a colorless liquid was obtained and dried under vacuum to constant weight (yield, 7.04g, 98.4%). ^1H NMR (400 MHz, $CDCl_3$): δ (ppm) 1.40 (m, 4H, CH_2), 1.51-1.62 (m, 4H, CH_2), 3.27 (t, 2H, CH_2-N_3), 3.63 (t, 2H, CH_2O).

2.2.5 Synthesis of 6-azidohexyl 2-((ethoxycarbonothioyl)thio)-2-methylpropanoate

A THF solution (25 mL) of α-bromoisobutyryl bromide (16.69g, 72.63mmol) was added dropwise to a solution of 6-azido-1-hexanol (7.054g, 49.26mmol) and triethylamine (7.35g, 72.63mmol) in THF (45mL) and cooled in ice bath. The resulting solution was then transfered to room temperature and stirred for 1 hr. Then, 10 mL methanol was added and the formed triethylammonium bromide salt was filtered off. After removal of the solvent, the product was dissolved in methylene chloride followed by washing with a saturated ammonium chloride solution (two times) and DI water (two times). After drying with anhydrous sodium sulfate, filtration, and removal of the solvent, the crude yellow oil was purified via silica column chromatography (hexane/ethyl acetate, 20/1). A colorless oil was obtained and dried under vacuum to constant weight (yield: 11.351g, 78.9%). ^1H NMR (400 MHz, $CDCl_3$): δ (ppm) 1.41 (m, 4H, CH_2), 1.52-

1.82 (m, 4H, CH_2), 1.94 (s, 6H, $C(CH_3)_2$), 3.27 (t, 2H, CH_2-N_3), 4.17 (t, 2H, CH_2-O-C(=O)).

A DMSO solution (45 mL) of 6-azidohexyl 2-bromo-2-methylpropanoate (9.525g, 32.60mmol) and 3-fold excess of potassium ethyl xanthate (15. 68g, 97.82 mmol) was stirred at rt overnight. The resulting solution was added to 100 mL water. After filtration of the generated white precipitate, the solution was extracted with diethyl ether (3×50 mL), drying with anhydrous sodium sulfate and followed by filtration. After removal of the solvent, the product was purified via silica column chromatography (hexane/ethyl acetate, 20/1). A yellow oil was obtained and dried under vacuum to constant weight (9.18g, yield 84.5%). ^{1}H NMR (400 MHz, $CDCl_3$): δ (ppm) 1.40 (m, 4H, CH_2), 1.48 (t, 3H, CH_3), 1.51-1.82 (m, 4H, CH_2), 1.67 (s, 6H, $C(CH_3)_2$), 3.26 (t, 2H, CH_2-N_3), 4.11 (t, 2H, CH_2-O-C(=O)), 4.62 (q, 2H, CH_2O). ^{13}C NMR (400 MHz, $CDCl_3$): δ (ppm) 14.1, 25.4, 25.6, 26.5, 28.7, 30.3, 50.1, 50.3, 65.6, 70.1, 172.4, 215.5.

2.2.6 Synthesis of *O,O*-diethyl bisxanthate

3.17 g iodine was added slowly into a water solution (10 mL) of potassium *O*-ethyl xanthate (4.01 g, 0.025 mol). After stirring for 4 hrs, the product went through extraction with hexane (3 × 20 mL) and washing with 5% sodium thiosulfate solution (2 × 10 mL). The hexane layer was dried with anhydrous sodium sulfate and followed by filtration. After removal of the solvent, the product was purified via silica column chromatography (100% hexane). A yellow solid was obtained and dried under vacuum to constant weight (2.87g, yield=94.5%). ^{1}H NMR (400 MHz, $CDCl_3$): δ (ppm) 1.42 (t, 6H, CH_3), 4.66 (q, 4H, CH_2).

2.2.7 Synthesis of S-(2-cyanopropan-2-yl) O-ethyl carbonodithioate

A toluene solution (40 mL) of *O*,*O*-diethyl bisxanthate (1.43 g, 5.9×10^{-3} mol) and AIBN (1.21 g, 7.35×10^{-3} mol) was purged with N_2 for 30 min then stirred at 80 ºC. After 2 h an additional amount of AIBN (0.8 g, 4.87×10^{-3} mol) was added. The reaction was stopped after 7.5 h. After removal of solvent, the product was purified via silica column chromatography (hexane/ethyl acetate: 95/5) (1.83g, 65.4 % yield). ^{1}H NMR (400 MHz, $CDCl_3$): δ (ppm) 1.55 (t, 3H, CH_3), 1.76 (s, 6H, $C(CH_3)_2$), 4.74 (q, 2H, CH_2O).

2.2.8 Synthesis of (4-cyano-4-diethyldithiocarbamyl) Pentanoic Acid (CDPA)

Tetraethylthiuram disulfide (7.62g, 25.7 mmol) and 4,4'-azobis(4-cyanopentanoic acid) (10.0 g, 35.7 mmol) were dissolved in 100 mL ethyl acetate. The reaction solution was heated at 75 °C for 18 h. Then solvent was removed and the crude product was purified via silica gel column chromatography (hexane : ethyl acetate = 3:2). The product was obtained as a yellow liquid (yield: 11.0 g, 78%). ^{1}H NMR (300 MHz, CD_3OD): δ (ppm) 1.26 (t, 6H, $\mathbf{CH_3}CH_2$), 1.89 (s, 3H, $\mathbf{CH_3}C(CN)$), 2.42 (t, 2H, $\mathbf{CH_2}C(CN)$), 2.61(t, 2H, $\mathbf{CH_2}$-C(=O)-O), 3.76-4.00 (m, 4H, $\mathbf{CH_2}N$).

2.2.9 Activation of CDPA

CDPA (4.14 g, 15.1 mmol) and 2-mercaptothiazoline (1.80 g, 15.1 mmol), and dicyclohexylcarbodiimide (DCC) (3.74 g, 18.1 mmol) were dissolved in 40 mL dry mixture of dichloromethane and THF (dichloromethane : THF = 1 : 1), followed by the addition of dimethylaminopyridine (DMAP) (183.4 mg, 1.50 mmol). The resulting solution was stirred at rt for 6 h. After removal of the solvent, the crude product was purified via silica gel column chromatography (hexane : ethyl acetate = 4:1). ^{1}H NMR

(300 MHz, $CDCl_3$): δ (ppm) 1.28 (t, 6H, **CH_3**CH_2), 1.95 (s, 3H, **CH_3**C(CN)), 2.63 (t, 2H, **CH_2**C(CN)), 2.75 (t, 2H, **CH_2**-C(=O)-O), 3.32 (t, 2H, **CH_2**SC(=S)), 3.60-4.06 (m, 4H, **CH_2**N), 4.59 (t, 2H, C(=O)N**CH_2**).

2.2.10 Activation of 4-Cyano-4-(dodecylsulfanylthiocarbonyl)sulfanylpentanoic acid (CDSS)

CDSS (0.81 g, 2 mmol) and 2-mercaptothiazoline (0.24 g, 2 mmol), and dicyclohexylcarbodiimide (DCC) (0.52 g, 2.5 mmol) were dissolved in 20 mL dichloromethane followed by the addition of 4-dimethylaminopyridine (DMAP) (24.4 mg, 0.2 mmol). The resulting solution was stirred at rt for 6 h. After removal of the solvent, the crude product was purified via silica gel column chromatography (hexane : ethyl acetate = 4:1). The yellow product was dried overnight under vacuum (yield: 0.72g, 71.3%).

2.2.11 Synthesis of CDPA Functionalized SiO_2 Nanoparticles

A THF stock solution (2.8 mL) of activated CDPA (63.97 g/L) was diluted in ~20 mL dry THF. A THF solution of amino-functionalized silica nanoparticles (approx. 1.5 g) was added slowly to the above activated CDPA solution and the resulting mixture was stirred at rt overnight. After the reaction, the solution was precipitated into cyclohexane and ethyl ether mixture. (200 mL, cyclohexane : ethyl ether = 4 : 1), centrifuged at 3000 rpm for 5 minutes, and redispersed in dry THF. This procedure was repeated several times until the supernatant solution was colorless after centrifugation. The final nanoparticles were dried under vacuum at rt for further usage.

2.2.12 Synthesis of CDSS Functionalized SiO_2 Nanoparticles

A THF stock solution (2.6 mL) of activated CDSS (17.72 g/L) was diluted in 25 mL dry THF. A THF solution (15 mL) of amino-functionalized silica nanoparticles (approx. 1.5 g) was added slowly to the above activated CDSS solution and the resulting mixture was stirred at rt for 6h. After the reaction, the solution was precipitated into cyclohexane and ethyl ether mixture. (300 mL, cyclohexane : ethyl ether = 4 : 1), centrifuged at 3000 rpm for 5 minutes, and redispersed in dry THF. This procedure was repeated several times until the supernatant solution was colorless after centrifugation. The yellow nanoparticles were dried under vacuum at rt for further usage.

2.2.13 Polymerization of Styrene Mediated by RAFT/MADIX Agent

Styrene (3.47 mL, 30.33 mmol), O-ethyl S-prop-2-yn-1-yl carbonodithioate (16.2 mg, 0.1013 mmol) and dry THF (4 mL) were added to a 25 mL Schlenk flask. AIBN (1.011 mL, 10mM in THF) was added and the solution was degassed by four freeze-pump-thaw cycles, filled with nitrogen, and then placed in an oil bath of 70 °C for various intervals. The polymerization was stopped by quenching the Schlenk flask in ice water.

2.2.14 Polymerization of Vinyl Acetate Mediated by Dithiocarbamate RAFT Agent

Vinyl acetate (776.5 µL, 8.425 mmol), CDPA (4.625 mg, 1.685×10^{-5} mol) and anisole (0.594 mL) were added to a Schlenk tube. AIBN (0.337 mL, 5 mM in anisole) was added and the solution was degassed by three freeze-pump-thaw cycles, filled with nitrogen, and then placed in an oil bath of 80 °C for various intervals. The polymerization was stopped by quenching the Schlenk tube in ice water.

2.2.15 Bulk RAFT Polymerization of Isoprene

Isoprene (0.5 mL, 5.0 mmol), CDSS (4.04 mg, 10.0 µmol) and dicumyl peroxide initiator (0.54 mg, 2.0 µmol) were added to a 15 mL Schlenk tube. The mixture was degassed by three freeze-pump-thaw cycles, filled with nitrogen, and then placed in an oil bath of 115 °C. The polymerization was stopped by quenching the Schlenk tube in ice water.

2.3 Results and Discussion

2.3.1 Synthesis of RAFT/MADIX Agents

Four O-ethyl (Z group) based MADIX agents were synthesized, as shown in Figure 2.2. The classic method to synthesize ethoxyl based MADIX agents is employing the coupling reaction between ethyl xanthogenate salt (potassium or sodium) and halogen based R group.

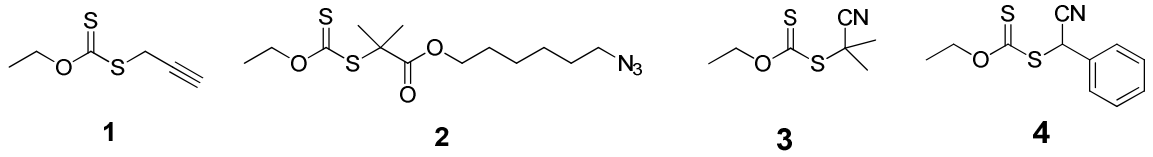

Figure 2.2 The structure of O-ethyl S-prop-2-yn-1-yl carbonodithioate (**1**), 6-azidohexyl 2-((ethoxycarbonothioyl)thio)-2-methylpropanoate (**2**), S-(2-cyanopropan-2-yl) O-ethyl carbonodithioate (**3**) and S-(cyano(phenyl)methyl) O-ethyl carbonodithioate (**4**).

The synthesis of alkyne-based MADIX agent O-ethyl S-prop-2-yn-1-yl carbonodithioate was conducted according to Scheme 2.2. Propargyl alcohol was reacted with phosphorus tribromide to generate propargyl bromide, which then was reacted with a xanthogenate to form the yellow O-ethyl S-prop-2-yn-1-yl carbonodithioate (**1**). The synthetic strategy has a high efficiency with a yield (last step) of 81%. The ^{1}H NMR

(Figure 2.3) and ^{13}C NMR (Figure 2.4) spectra reveal the successful formation of O-ethyl S-prop-2-yn-1-yl carbonodithioate. The alkyne-based O-ethyl S-prop-2-yn-1-yl carbonodithioate can be easily anchored on azide functionalized nanoparticles via "click" chemistry, which allows for further surface-initiated RAFT polymerization.

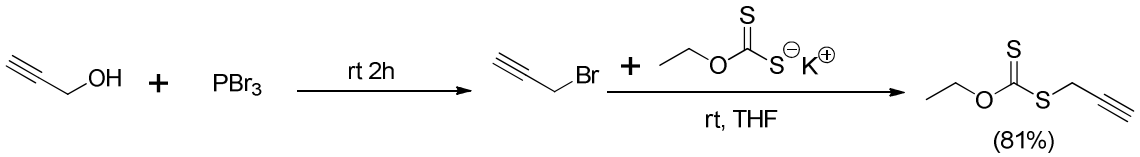

Scheme 2.2 The synthetic strategy of xanthate O-ethyl S-prop-2-yn-1-yl carbonodithioate.

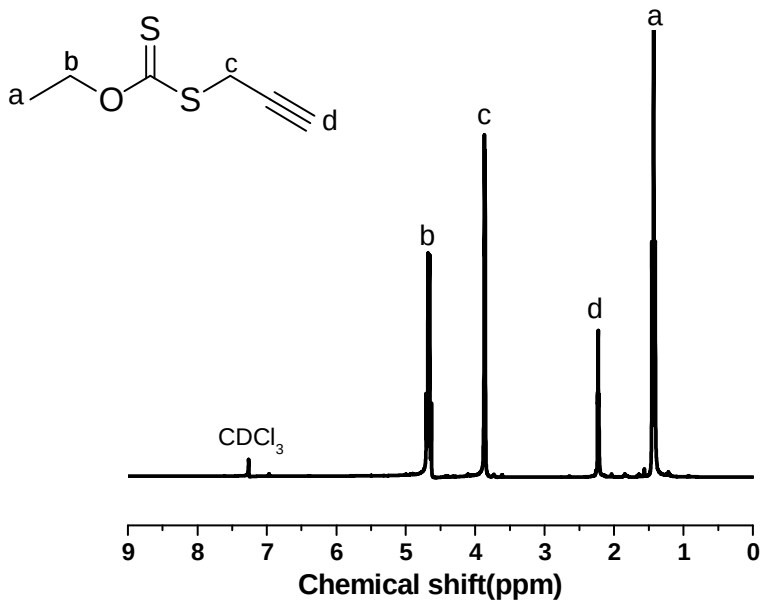

Figure 2.3 ^{1}H NMR spectra of O-ethyl S-prop-2-yn-1-yl carbonodithioate.

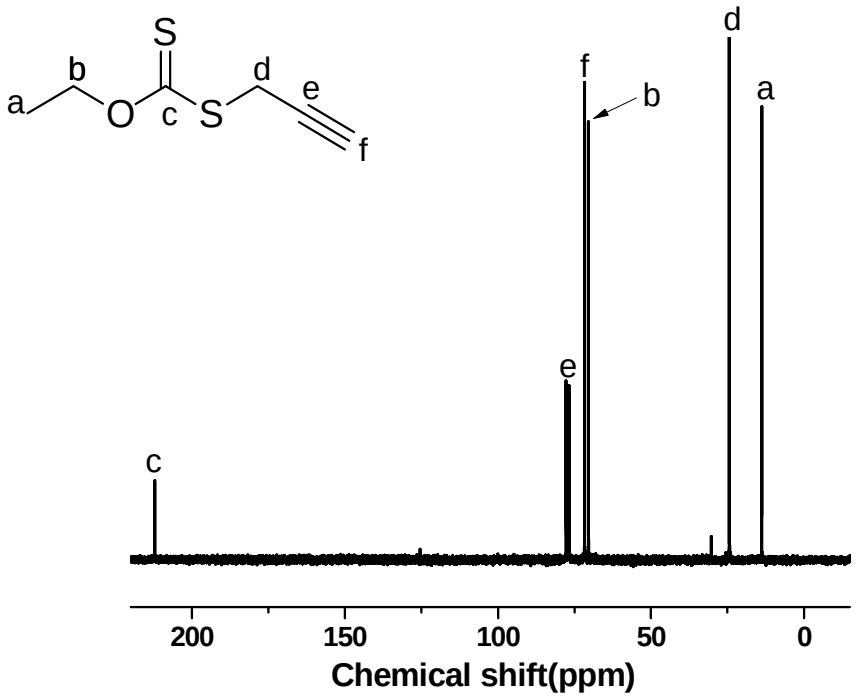

Figure 2.4 ^{13}C NMR spectra of O-ethyl S-prop-2-yn-1-yl carbonodithioate.

The preparation of azide-based MADIX agent (**2)** 6-azidohexyl 2-((ethoxycarbonothioyl)thio)-2-methylpropanoate (AECM) was conducted according to Scheme 2.3. 1-Azido-6-hydroxyhexane was first prepared by reacting 1-chloro-6-hydroxyhexane with sodium azide. This aqueous based reaction has a high yield of 98.4%. The subsequent esterification of α-bromoisobutyryl bromide with 1-azido-6-hydroxyhexane gave the oil 6-azidohexyl 2-bromo-2-methylpropanoate in good yield (78.8%) under mild reaction conditions, which was confirmed by the ^{1}H NMR spectra (Figure 2.5). It was then reacted with potassium ethyl xanthogenate to generate the MADIX agent **2** AECM (yield: 84.5%). The ^{1}H NMR (Figure 2.6) spectra reveals the successful formation of AECM. The azide-based MADIX agent **2** AECM can be easily attached on alkyne functionalized nanoparticles via “click” chemistry. This strategy can

be employed to graft polymer brushes on nanoparticles via both “grafting from” and “grafting to” techniques.

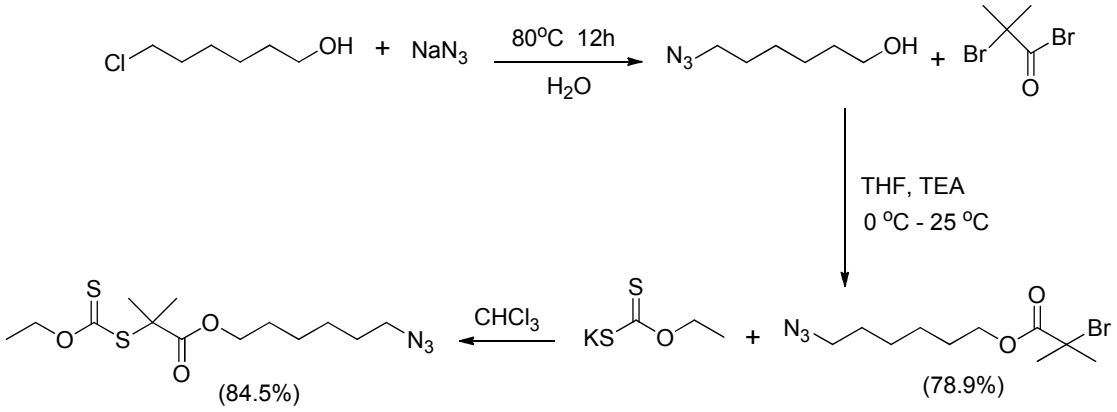

Scheme 2.3 The synthetic strategy of 6-azidohexyl 2-((ethoxycarbonothioyl)thio)-2-methylpropanoate.

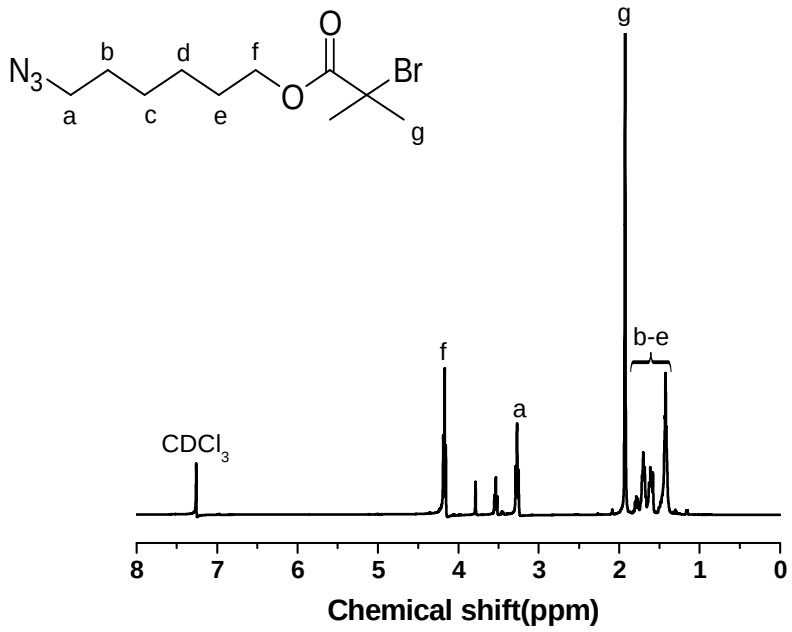

Figure 2.5 ^{1}H NMR spectra of 6-azidohexyl 2-bromo-2-methylpropanoate.

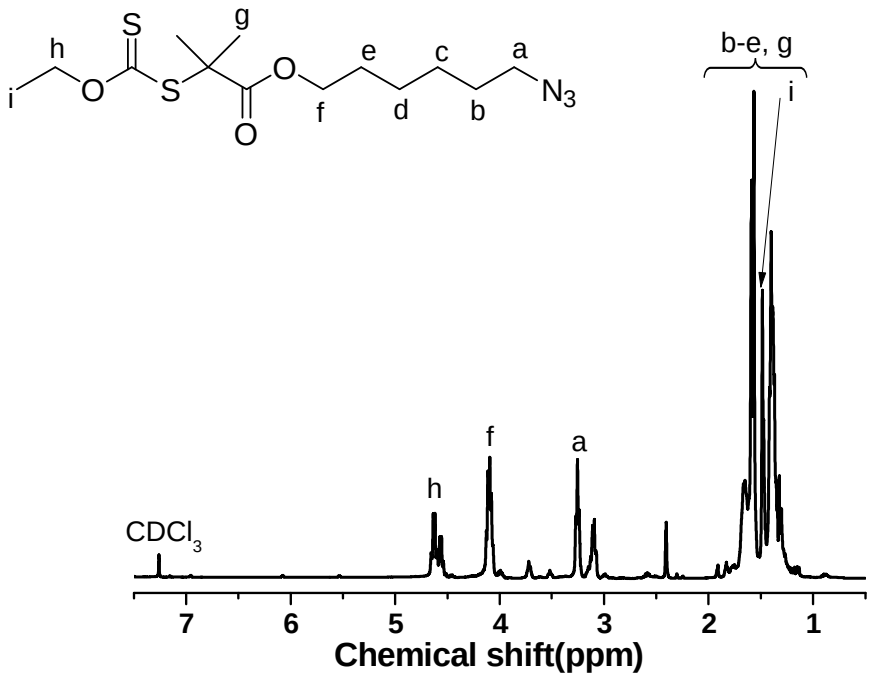

Figure 2.6 ^{1}H NMR spectra of 6-azidohexyl 2-((ethoxycarbonothioyl)thio)-2-methylpropanoate.

The MADIX agent S-(2-cyanopropan-2-yl) O-ethyl carbonodithioate (**3)** was synthesized by a two-step reaction.[14,15] O,O-diethyl bisxanthate was first prepared by reacting potassium ethyl xanthogenate with iodine. The subsequent radical reaction between O,O-diethyl bisxanthate and 2,2'-Azobisisobutyronitrile (AIBN) gave the yellow oil S-(2-cyanopropan-2-yl) O-ethyl carbonodithioate with a yield of 65.4% (Scheme 2.4). The ^{1}H NMR (Figure 2.7) spectra reveals the successful formation of S-(2-cyanopropan-2-yl) O-ethyl carbonodithioate.

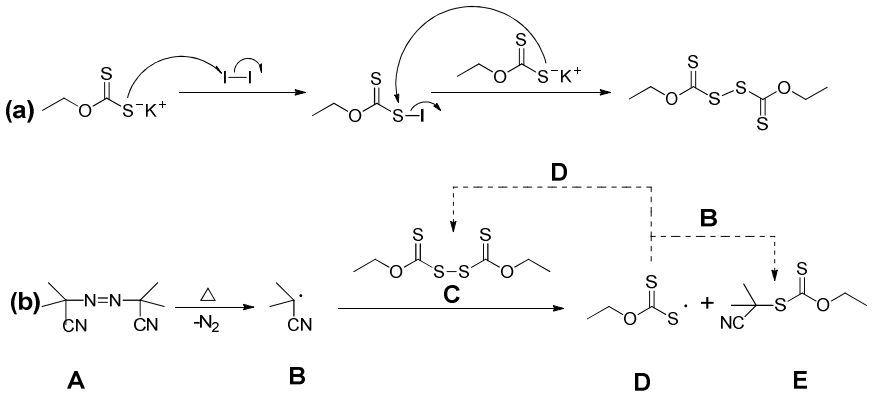

Scheme 2.4 The synthesis of (a) intermediate O,O-diethyl bisxanthate; (b) S-(2-cyanopropan-2-yl) O-ethyl carbonodithioate **(E).**[14,15]

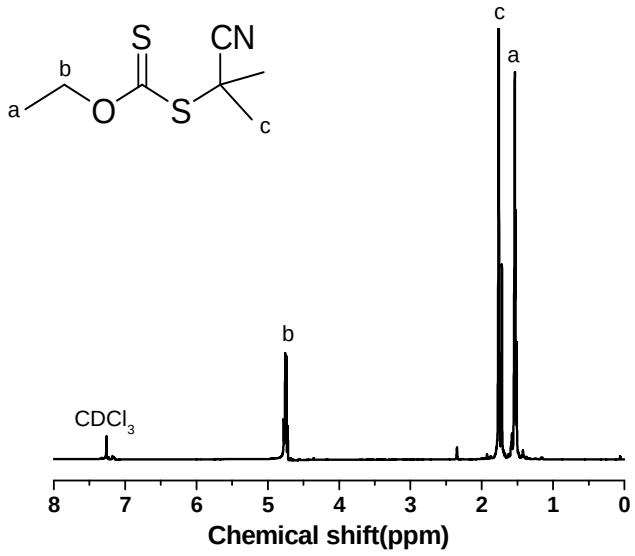

Figure 2.7 ^{1}H NMR spectra of S-(2-cyanopropan-2-yl) O-ethyl carbonodithioate.

The MADIX agent **4** was synthesized by the reaction between 2-bromo-2-phenylacetonitrile and potassium ethyl xanthogenate (Scheme 2.5). This synthesis is straightforward and the S-(cyano(phenyl)methyl) O-ethyl carbonodithioate was successfully prepared.

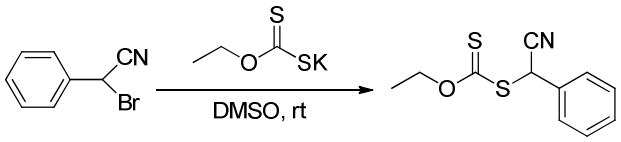

Scheme 2.5 The synthesis of S-(cyano(phenyl)methyl) O-ethyl carbonodithioate (**4**).

Another RAFT agent with the tertiary cyanopentanoic R group was synthesized for mediating the polymerization of vinyl acetate, as shown in Figure 2.8. It contains a diethylamino based Z group. The method for synthesis of RAFT agent (4-cyano-4-diethyldithiocarbamyl) pentanoic acid (CDPA) is shown in Scheme 2.6. Tetraethylthiuram disulfide was allowed to react with 4,4'-azobis(4-cyanopentanoic acid) to form the yellow liquid CDPA. ^{1}H NMR spectra (Figure 2.9) showed peaks at 1.26 ppm, 1.89 ppm, 2.42 ppm, 2.61 ppm, 3.76-4.00 ppm ascribed to the protons in CDPA. Activated CDPA was prepared by the coupling reaction between CDPA and 2-mercaptothiazoline for further use.

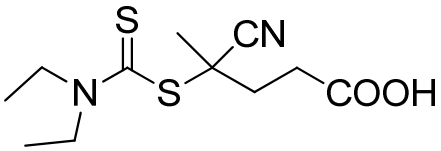

Figure 2.8 The structure of (4-cyano-4-diethyldithiocarbamyl) pentanoic acid (CDPA).

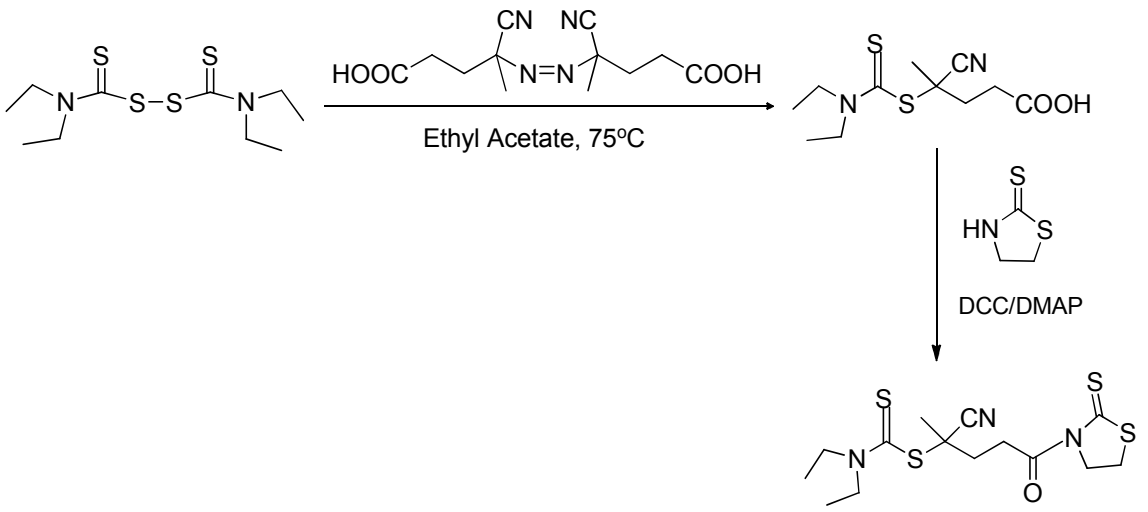

Scheme 2.6 Synthesis of RAFT agent CDPA.

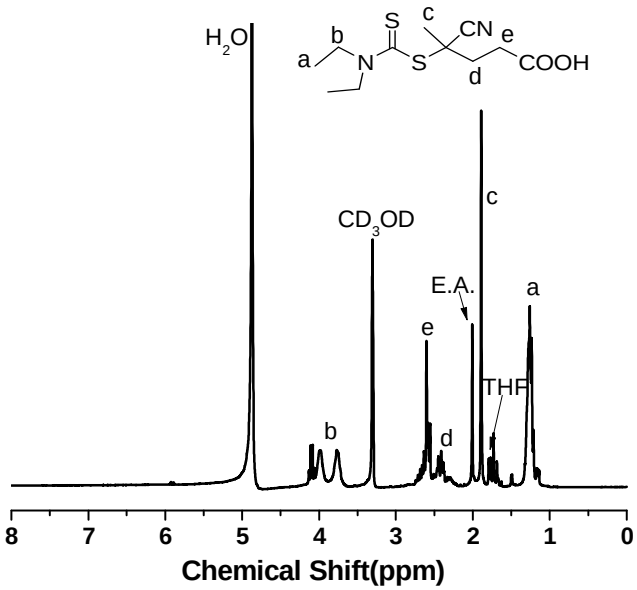

Figure 2.9 ^{1}H NMR spectra of CDPA (E.A.: Ethyl Acetate).

2.3.2 Synthesis of RAFT/MADIX Agents Grafted Nanoparticles

The strategy for synthesis of trithiocarbonate RAFT agent 4-cyano-4-(dodecylsulfanylthiocarbonyl)sulfanylpentanoic acid (CDSS) coated nanoparticles is shown in Scheme 2.7. Initially CDSS was activated by 2-mercaptothiazoline to form

activated CDSS with a yield of 71.3%. Then CDSS anchored silica nanoparticles were prepared by the reaction between amino immobilized nanoparticles with accurately measured densities and activated CDSS. The amount of CDSS coated on nanoparticles can be controlled by changing the feed ratio between amino coated particles and CDSS. The amount of CDSS covalently bound to the nanoparticle surface was determined quantitatively by comparing the absorbance for the CDSS modified particles to a standard UV-vis absorption curve prepared from known amounts of free CDSS at 299 nm (Figure 2.10). The as-synthesized CPSS modified silica nanoparticles used here possessed a graft density of 0.35 chains/nm^2.

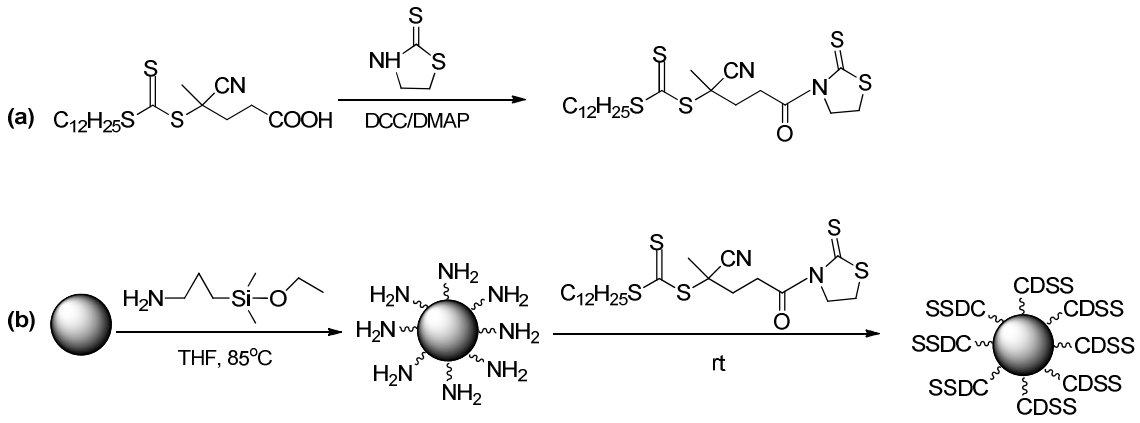

Scheme 2.7 Synthesis of CDSS anchored silica nanoparticles.

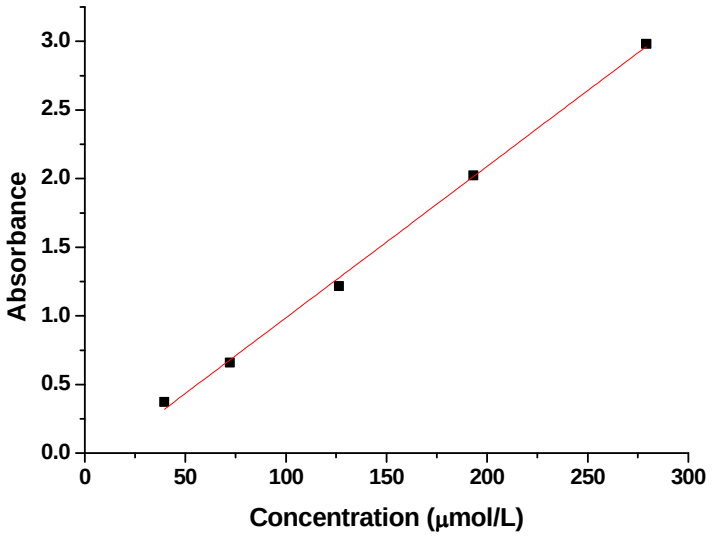

Figure 2.10 UV-vis standard absorption curve of CDSS at 299 nm.

The method for synthesis of CDPA coated nanoparticles is shown in Scheme 2.8. The CDPA anchored silica nanoparticles were prepared by the reaction between amino immobilized nanoparticles with accurately measured densities and activated CDPA. The amount of CDPA coated on nanoparticles can be controlled by changing the feed ratio between amino coated particles and CDPA. The as-synthesized CDPA modified particles possessed a graft density of 0.12 groups/nm^2.

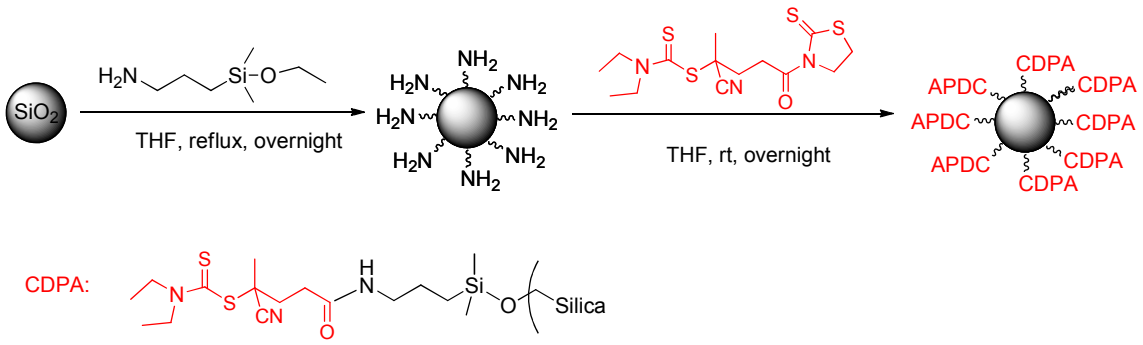

Scheme 2.8 Synthesis of CDPA anchored silica nanoparticles.

2.3.3 Polymerizations Mediated by O-ethyl Based MADIX Agents

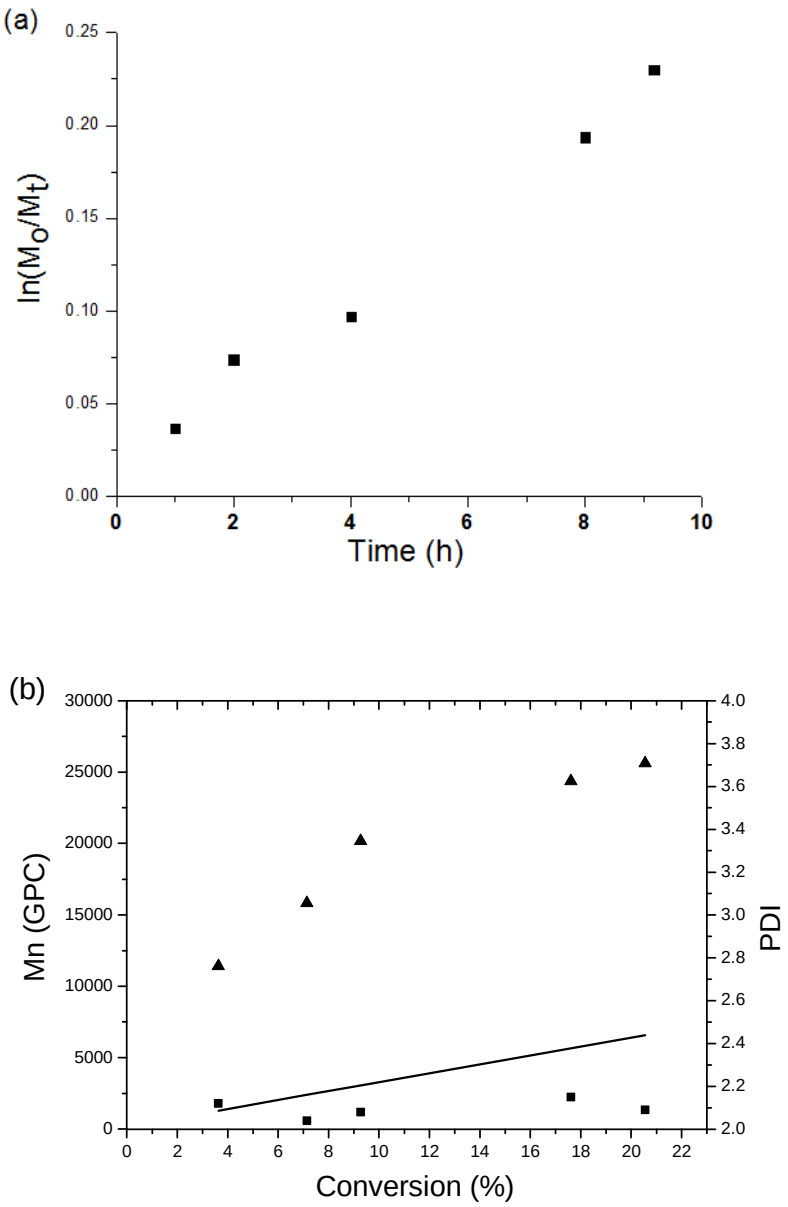

Figure 2.11 (a) Kinetic plots and (b) dependence of the GPC molecular weight (filled triangles), theoretical molecular weight (solid line) and polydispersity (filled squares) on the conversion for the MADIX polymerization of styrene ([Styrene]:[CTA]:[AIBN] = 300:1:0.1) at 70 ^{o}C mediated by O-ethyl S-prop-2-yn-1-yl carbonodithioate (**1**).

The results of the kinetic study of MADIX polymerization of styrene mediated by MADIX agent O-ethyl S-prop-2-yn-1-yl carbonodithioate (**1**) at 70 °C in THF with a

monomer concentration of 3.36 mol/L is shown in Figure 2.10. A linear relationship between $\ln(M_0/M_t)$ (where M_0 is the initial monomer concentration and M_t is the monomer concentration at time *t*) and polymerization time was observed, which implies a constant radical concentration. However, the Mn determined by GPC of the polymer chains was higher than theoretical molecular weight and the PDIs were around 2.1 during the polymerization. The reason for the molecular weight deviations may be that propargyl group with α-primary carbon is not a good leaving group, which leads to a low transfer constant of the O-ethyl S-prop-2-yn-1-yl carbonodithioate (**1**) over styryl monomer. As discussed previously, polystyryl is a less reactive propagating radical, which therefore requires a MADIX agent with increased C=S double bond reactivity to achieve controlled polymerizations. The C=S double bond reactivity of the MADIX agent (**1**) may be not high enough to control the propagating styryl radicals. To test whether O-ethyl S-prop-2-yn-1-yl carbonodithioate (**1**) is a good controlling agent to a more reactive radical monomer, such as methyl acrylate, the polymerization kinetic study was investigated.

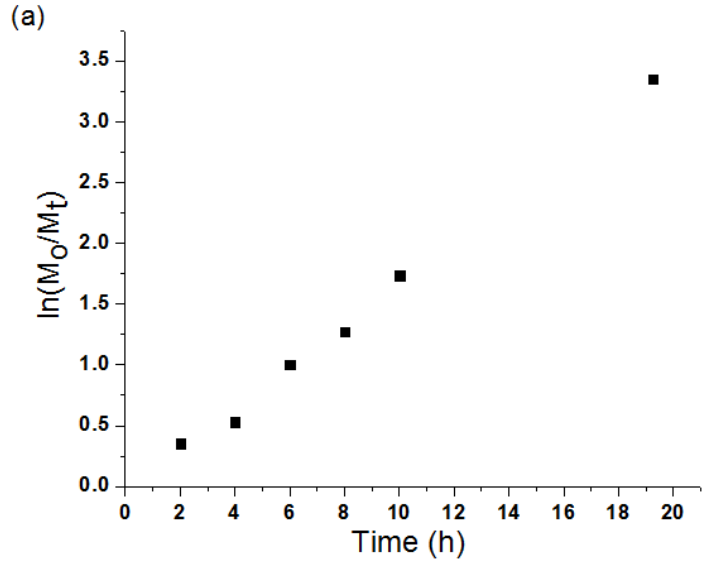

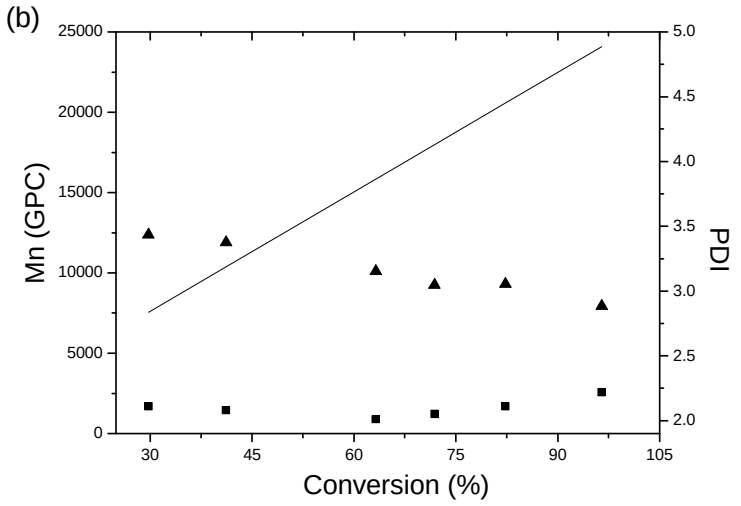

Figure 2.12 (a) Kinetic plots and (b) dependence of the GPC molecular weight (filled triangles), theoretical molecular weight (solid line) and polydispersity (filled squares) on the conversion for the MADIX polymerization of methyl acrylate in THF (monomer concentration: 5.14 mol/L) at 70 ^{o}C mediated by O-ethyl S-prop-2-yn-1-yl carbonodithioate (**1**).

The results of the kinetic study of MADIX polymerization of methyl acrylate mediated by MADIX agent O-ethyl S-prop-2-yn-1-yl carbonodithioate (**1**) with a ratio between species of [Monomer]:[CTA] = 288:1 at 70 °C in THF is shown in Figure 2.12. A linear relationship between $\ln(M_0/M_t)$ and polymerization time was observed, which implies a constant radical concentration. However, the Mn determined by GPC of the polymer chains decreased linearly with monomer conversion while the PDI slowly increased. The reason for the gradually decrease of molecular weights may be that some low Mn polymer chains were generated at high conversion, which results from chain transfer to monomer. This can be further rationalized by the slowly increased PDI. Compared to styryl radical, acrylyl radical is more reactive, which means the propagation for acrylyl radical is faster. This agrees with the observation that high molecular weights were achieved within 2h. Even though O-ethyl S-prop-2-yn-1-yl carbonodithioate (**1**) was

not able to control the polymerization of styrene and methyl acrylate, further polymerization tests were conducted with the highly reactive vinyl acetate.

The results of the kinetic study of the MADIX polymerization of vinyl acetate mediated by MADIX agent O-ethyl S-prop-2-yn-1-yl carbonodithioate (**1**) at 70 °C in THF with a monomer concentration of 5.19 mol/L is shown in Figure 2.13. A non-linear relationship between $\ln(M_0/M_t)$ and polymerization time was observed, which implies non-constant radical concentrations during the polymerization. In addition, the Mn determined by GPC of the polymer chains ($Mn,_{GPC}$) was higher than the theoretical Mn at low conversion, while theoretical Mn was higher than the $Mn,_{GPC}$ at high conversion. The PDIs varied from 1.15 to 1.83 during the polymerization. These results indicated that O-ethyl S-prop-2-yn-1-yl carbonodithioate (**1**) exhibited hybrid behavior between conventional and living free radical polymerization, which is a sudden increase of molecular weight at the beginning of the reaction, followed by a slight increase of molecular weight with conversion. Such behavior has been extensively described for the case of cumylphenyldithioacetate mediated methyl methacrylate polymerization[22]. However, O-ethyl S-prop-2-yn-1-yl carbonodithioate (**1**) is still more effective than some RAFT agents for controlling the polymerization of vinyl acetate.[9]

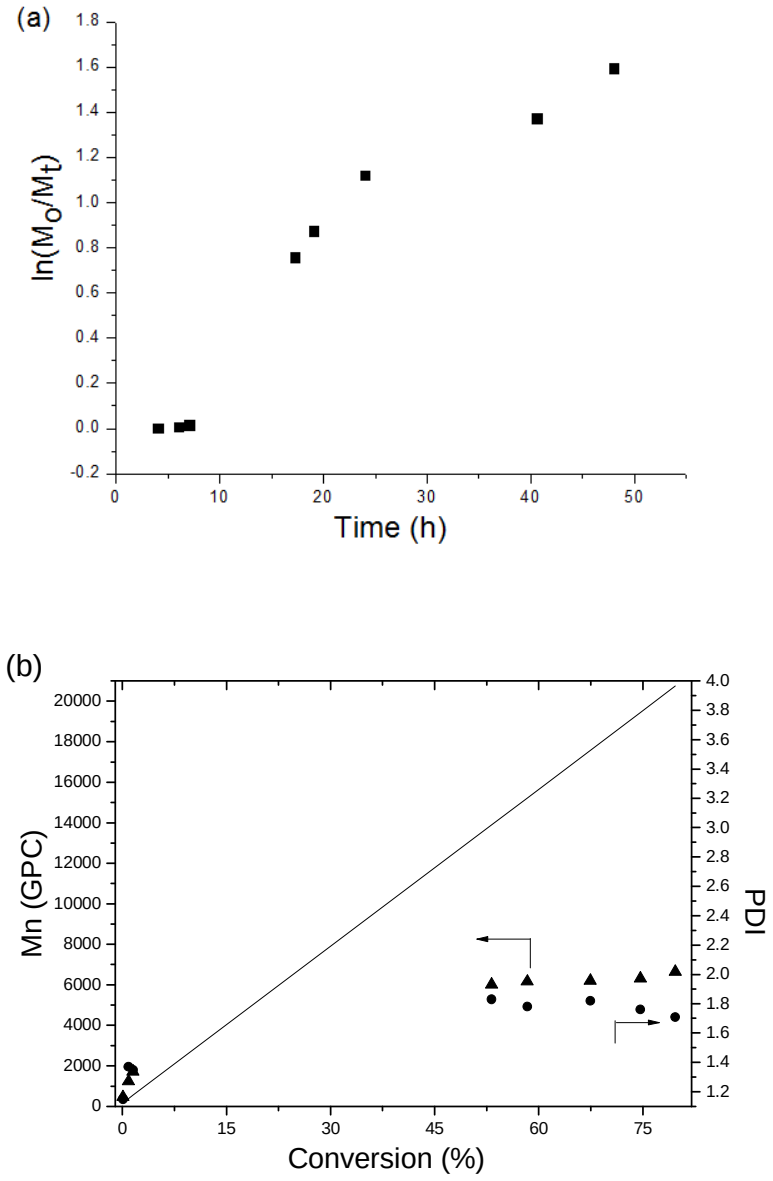

Figure 2.13 (a) Kinetic plots and (b) dependence of the GPC molecular weight (filled triangles), theoretical molecular weight (solid line) and polydispersity (filled circles) on the conversion for the MADIX polymerization of vinyl acetate ([Monomer]:[CTA]:[AIBN] = 300:1:0.1) at 70 ^{o}C mediated by O-ethyl S-prop-2-yn-1-yl carbonodithioate (**1**).

MADIX agent **1** was also used to mediate the polymerization of methyl methacrylate (MMA) in THF with a monomer concentration of 3.88 mol/L. It was conducted at 60 °C for 10 h, and the experimental Mn was 183,774 g/mol while the theoretical Mn was 4,622 g/mol, with a PDI of 2.48. Thus, it was not able to control the polymerization of MMA.

MADIX agent **1** did not control the polymerization of styrene, methyl acrylate, and vinyl acetate very well because of its low transfer constant. As introduced above, the more substituted and stabilized the R leaving group, the higher the transfer constant. Thus, a new MADIX agent bearing a tertiary R group, 6-azidohexyl 2-((ethoxycarbonothioyl)thio)-2-methylpropanoate **(2)** was designed and synthesized, as shown in Figure 2.1.

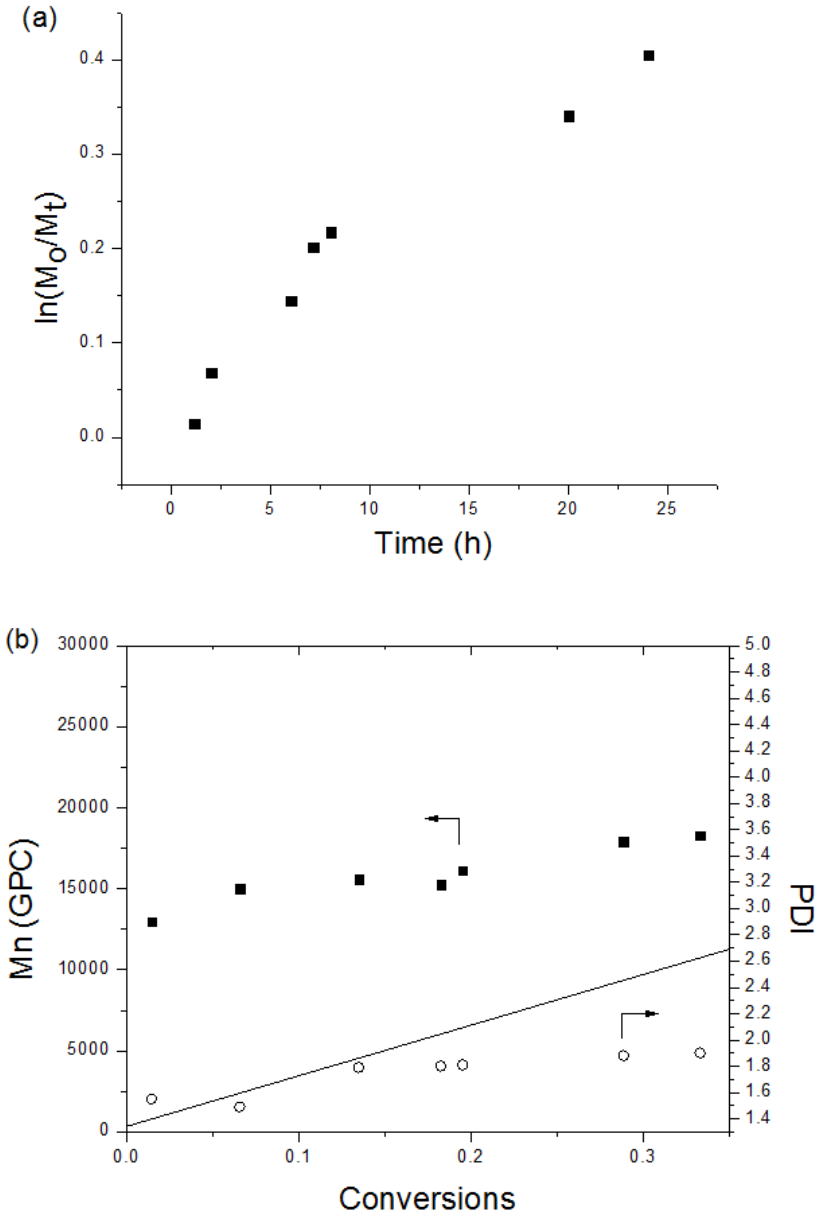

Figure 2.14 (a) Kinetic plots and (b) dependence of the GPC molecular weight (filled squares), theoretical molecular weight (solid line) and polydispersity (unfilled circles) on the conversion for the MADIX polymerization of styrene ([Monomer]:[CTA]:[AIBN] = 300:1:0.1) at 70 ^{o}C mediated by 6-azidohexyl 2-((ethoxycarbonothioyl)thio)-2-methylpropanoate (**2**).

The results of the kinetic study of MADIX polymerization of *styrene* mediated by 6-azidohexyl 2-((ethoxycarbonothioyl)thio)-2-methylpropanoate (**2**) at 70 °C in THF with a monomer concentration of 2.91 mol/L is shown in Figure 2.14. A linear relationship (generally linear) between $\ln(M_0/M_t)$ and polymerization time was observed, which implies a roughly constant radical concentration. However, the $Mn,_{GPC}$ of the polymer chains was higher than theoretical molecular weight and the PDIs varied from 1.49 to 1.90 during the polymerization. Even though the $Mn,_{GPC}$ is not very close to the theoretical Mn, the effect of MADIX agent **2** is much better than the MADIX agent **1** due to the closer agreement between the $Mn,_{GPC}$ and the theoretical Mn, which demonstrates the effect of the tertiary R group in the increasing transfer constant and further controlling the molecular weight during polymerization. Although it demonstrated some improvement compared to the MADIX agent **1**, the transfer constant of this MADIX agent **2** is still not high enough to control the polymerization of styrene well. For the same consideration as discussed in testing MADIX agent **1**, methyl acrylate was chosen to further investigate the nature of MADIX agent **2** for controlling the polymerization of a more reactive monomer.

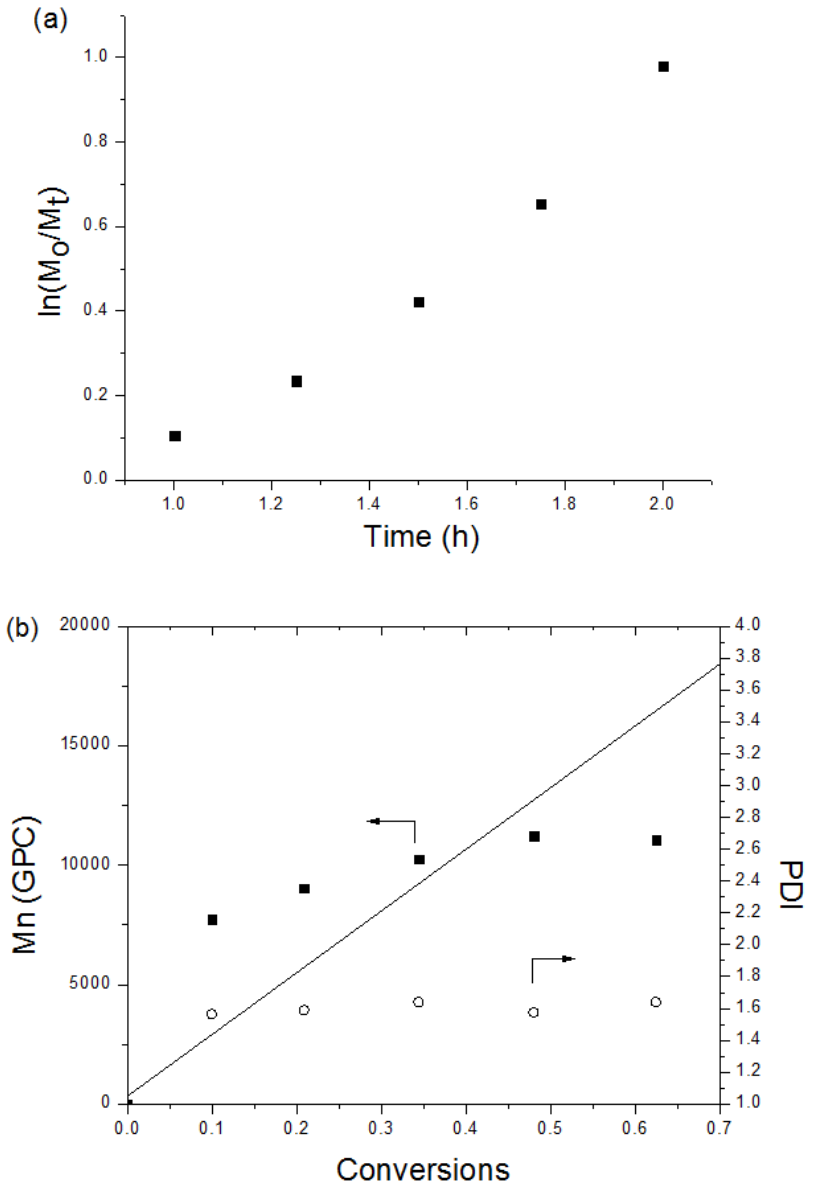

Figure 2.15 (a) Kinetic plots and (b) dependence of the GPC molecular weight (filled squares), theoretical molecular weight (solid line) and polydispersity (unfilled circles) on the conversion for the MADIX polymerization of methyl acrylate in THF (monomer concentration: 4.40 mol/L) at 70 ^{o}C mediated by 6-azidohexyl 2-((ethoxycarbonothioyl)thio)-2-methylpropanoate (**2**).

The results of the kinetic study of MADIX polymerization of methyl acrylate mediated by MADIX agent 6-azidohexyl 2-((ethoxycarbonothioyl)thio)-2-methylpropanoate (**2**) with a ratio between species of [Monomer]:[CTA] = 300:1 at 70 °C in THF is shown in Figure 2.15. A linear relationship between $\ln(M_0/M_t)$ (where M_0 is

the initial monomer concentration and M_t is the monomer concentration at time *t*) and polymerization time was observed, which implies a constant radical concentration. The Mn determined by GPC of the polymer chains gradually increased with monomer conversion, but did not correlate with the theoretical Mn. The possible reason is still the transfer constant. Even though the MADIX agent has tertiary R leaving group, the transfer constant is still not high enough to control the polymerization of methyl acrylate and the hybrid behavior described earlier is observed for this polymerization.

According to the literature[2], introducing electron withdrawing groups (EWG) on R can greatly increase the transfer constant of MADIX agent. Thus, the cyano-based MADIX agents **3** and **4** were targeted for further investigation (Figure 2.2).

The results of the kinetic study of MADIX polymerization of styrene mediated by S-(2-cyanopropan-2-yl) O-ethyl carbonodithioate **(3)** at 80 °C in THF with a monomer concentration of 3.12 mol/L is shown in Figure 2.16. A linear relationship between $\ln(M_0/M_t)$ and polymerization time was observed, which implies a constant radical concentration. Additionally, the Mn determined by GPC of the polymer chains increased linearly with monomer conversion and agreed closely with the theoretical molecular weight, especially at high conversions. The PDIs were approximately ~ 2.0 during the polymerization, which is consistent with the calculation from formula **1** for polystyryl chains. These features demonstrated the living/controlled nature of the MADIX polymerization of styrene mediated by S-(2-cyanopropan-2-yl) O-ethyl carbonodithioate. These also showed that the cyanoisopropyl group is a good leaving and reinitiating group for mediating the polymerization of styrene. Thus this MADIX agent has great potential to mediate the polymerization of styrene on nanoparticle surfaces with controllable

molecular weight but with high PDI, which may be able to overcome the loss of interface entropy and enhance the dispersion of polystyrene grafted nanoparticles in polystyrene matrices.

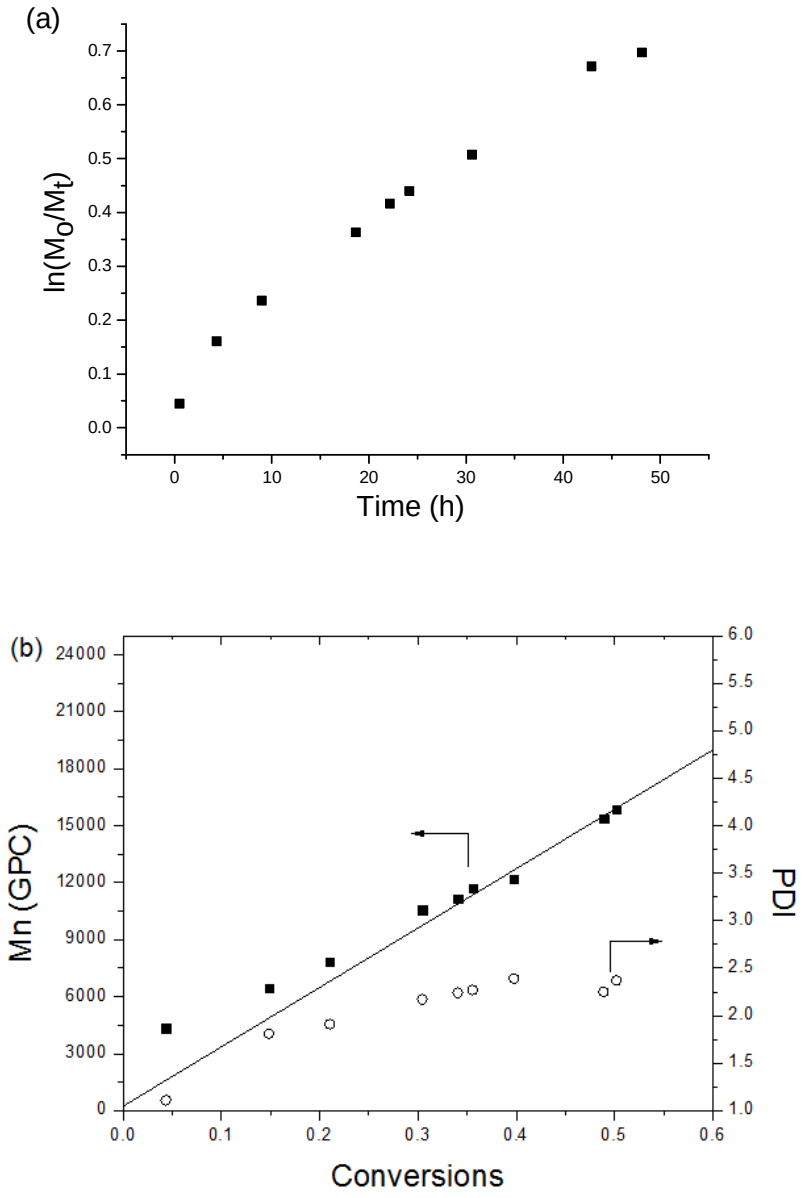

Figure 2.16 (a) Kinetic plots and (b) dependence of the GPC molecular weight (filled squares), theoretical molecular weight (solid line) and polydispersity (unfilled circles) on the conversion for the MADIX polymerization of styrene ([Monomer]:[CTA]:[AIBN] = 300:1:0.1) at 80 ^{o}C mediated by S-(2-cyanopropan-2-yl) O-ethyl carbonodithioate (**3**).

2.3.4 Polymerizations Mediated by Trithiocarbonate and Dithiocarbamate RAFT Agents

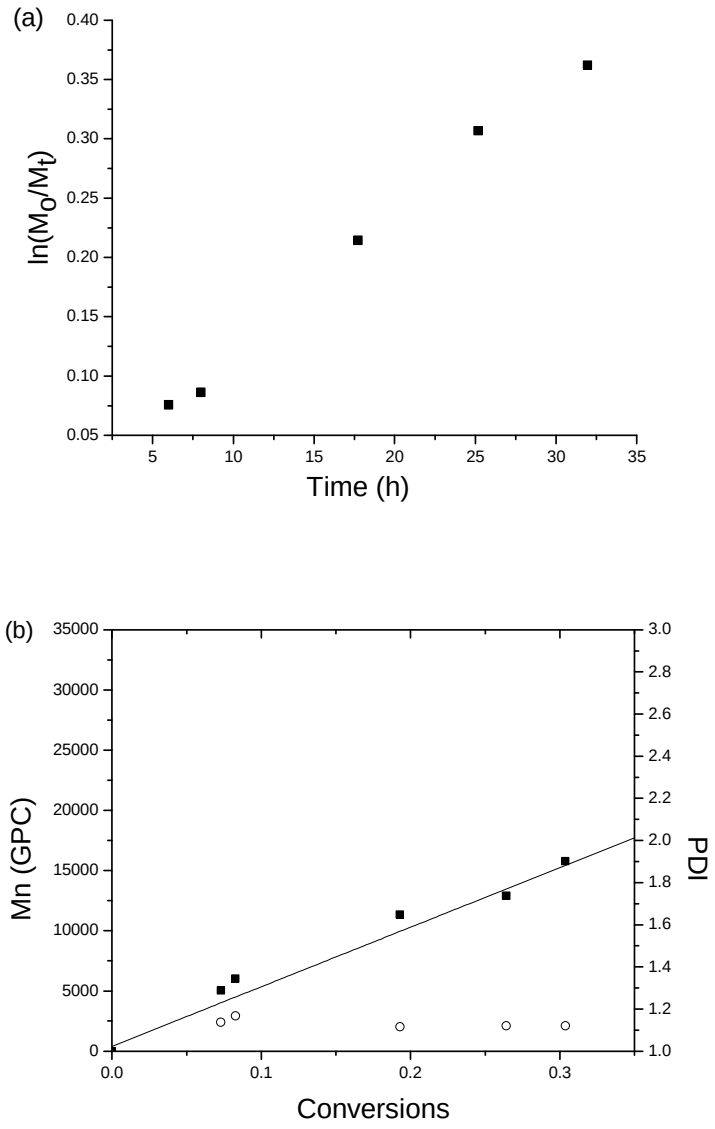

Figure 2.17 (a) Kinetic plots and (b) dependence of the GPC molecular weight (filled squares), theoretical molecular weight (solid line) and polydispersity (unfilled circles) on the conversion for the RAFT polymerization of styrene ([Monomer]:[CTA]:[AIBN] = 500:1:0.1) at 70 ^{o}C mediated by 4-cyano-4-(dodecylsulfanylthiocarbonyl)sulfanylpentanoic acid.

The results of the kinetic study of RAFT polymerization of *styrene* mediated by 4-cyano-4-(dodecylsulfanylthiocarbonyl)sulfanylpentanoic acid (CDSS) at 70 °C in THF

with a monomer concentration of 5.16 mol/L is shown in Figure 2.17. A linear relationship between $\ln(M_0/M_t)$ and polymerization time was observed, which implies a constant radical concentration. Additionally, the Mn determined by GPC of the polymer chains increased linearly with monomer conversion and agreed closely with the theoretical molecular weight. The PDIs were approximately 1.1 during the polymerization. These features demonstrated the living/controlled nature of the RAFT polymerization of styrene mediated by CDSS.

CDSS coated silica nanoparticles were also used to mediate the polymerization of styrene in DMF. After 24h, the conversion of the polymerization was 23%. The experimental Mn was 19,416 g/mol and the theoretical Mn was 17,055 g/mol, with a PDI of 1.2. The experimental Mn has a close agreement with the theoretical Mn. The RAFT polymerization of methyl acrylate was also conducted on CDSS coated nanoparticles at 60 °C. After 9.5 h, the conversion of the polymerization was 55.9%. The experimental Mn was 10,113 g/mol while the theoretical Mn was 33,858 g/mol, with a PDI of 1.18. In addition, the polymerization of MMA on CDSS coated nanoparticles was investigated. After 9h, the conversion was 34.1 %. The Mn obtained from GPC was 37800 g/mol and the theoretical Mn was 34,564 g/mol, with a PDI of 1.12. The experimental Mn agrees well with the theoretical Mn. Thus, CDSS was also demonstrated good control over the polymerization of styrene and MMA on nanoparticles.

All the O-ethyl, trithiocarbonate and dithiocarbonate based RAFT agents with similar tertiary R groups containing one cyano and two alkyl moieties are able to mediate the polymerization of styrene with controllable molecular weight. However, O-ethyl based RAFT/MADIX agent controlled polystyrene with a much higher PDI (~ 2.0) compared to

that of trithiocarbonate and dithiocarbonate controlled polystyrene (PDI = ~1.1). This difference can be used to design polymer grafted nanoparticles with broad polymer chain distribution (i.e., "fuzzy" interface) to improve the dispersion of these nanoparticles by overcoming the loss of interface entropy.

The dithiocarbamate RAFT agent CDPA was used to mediate the polymerization of vinyl acetate with a ratio between species of [Monomer]:[CDPA]:[AIBN] = 500:1:0.1 in anisole with a monomer concentration of 4.57 mol/L at 80 °C. After 17.5h, the experimental Mn was 9,857 g/mol and the theoretical Mn was 9,401 g/mol, with a PDI of 1.37. The experimental Mn has a close agreement with the theoretical Mn. In another experiment, after 24h, the experimental Mn was 24,120 g/mol and the PDI was 1.49. Thus, CDPA is a potential good RAFT agent to mediate the polymerization of vinyl acetate with controllable polymer chain length.

2.3.5 RAFT Polymerization of Isoprene

Many RAFT agents are not able to mediate the polymerization of isoprene which is usually ascribed to the high reaction temperature (above 100 ^{o}C). Most RAFT agents are not stable at this temperature, such as dithiobenzoates.[12] On the other hand, trithiocarbonates have demonstrated some advantages on mediating the polymerization of isoprene. Thus, 4-cyano-4-(dodecylsulfanylthiocarbonyl)sulfanylpentanoic acid (CDSS) was used to mediate the polymerization of isoprene in our work.

The bulk RAFT polymerization of isoprene was conducted in a sealed tube at 115 °C with a ratio between species of [isoprene]:[CDSS]:[Initiator] = 1082:1:0.2. The experimental Mn of the polyisoprene chains after 39 hr was 18,168 g/mol and the PDI

was 1.35. The conversion was 35.4% and the theoretical molecular weight was 26,814 g/mol. The experimental Mn was lower than theoretical Mn, which was also observed by Perrier *et al.*[12] They used another trithiocarbonate RAFT agent with similar reaction conditions in their work, and explained that the molecular weight difference was due to the GPC calibration standard. This also could be the reason for the difference between experimental and theoretical Mn in our work. Both Wooley[11] and Perrier[12] reported that the PDI of the synthesized polymers was around 1.30, which is similar to the current work. Thus, CDSS is an effective RAFT agent to mediate the polymerization of isoprene with predictable molecular weight.

The surface-initiated RAFT polymerization of isoprene was conducted in DMF at 115 ˚C with a ratio between species of [isoprene]:[CDSS]:[Initiator] = 348:1:0.14 and a monomer concentration of 1.07 mol/L. The generated polyisoprene grafted nanoparticles that produced an optically transparent solution indicate excellent dispersion. The experimental Mn of the anchored polyisoprene chains was 35,907 g/mol and the PDI was 1.21. Thus, CDSS is a thermally stable RAFT agent capable of mediating the RAFT polymerization of isoprene on nanoparticles. The polyisoprene grafted nanoparticles have a great potential to improve the dispersion of particles in rubber matrices, which is critical for mechanical reinforcement.

2.4 Summary

In conclusion, a series of new RAFT/MADIX agents were designed and synthesized to mediate the polymerization of styrene, MA, MMA, VAc and isoprene. The polymerizations of styrene, methyl acrylate, vinyl acetate mediated by O-ethyl S-prop-2-yn-1-yl carbonodithioate (**1**) and/or 6-azidohexyl 2-((ethoxycarbonothioyl)thio)-2-

methylpropanoate (**2**) were not well-controlled which probably was due to the low transfer constants of these MADIX agents. Both the RAFT agents containing the tertiary and α-EWG R groups of S-(2-cyanopropan-2-yl) O-ethyl carbonodithioate **(3)** and trithiocarbonate CDSS demonstrated excellent control over the polymerization of styrene. The former generated polystyrene has a high PDI (~ 2.0) while the later generated polymer has a low PDI (~ 1.1). These differences can result in either sharp or fuzzy interfaces on nanoparticles with similar chain lengths and chain densities. The fuzzy interface would be helpful to improve the dispersion of these nanoparticles in polymer matrices by overcoming the loss of interface entropy. CDSS anchored RAFT agent also demonstrated good control over the polymerization of styrene and MMA on nanoparticles. CDPA exhibited great control over the polymerization of vinyl acetate. In addition, CDSS is a thermally stable RAFT agent that could mediate the polymerization of isoprene with predictable molecular weights. Polyisoprene grafted silica particles are expected to improve the dispersion of particles in rubber matrices, which is critical for mechanical reinforcement.

2.5 Reference

1. Moad, G.; Rizzardo, E.; Thang, S. H. *Aust. J. Chem.* **2005,** *58*, 379-410.
2. Destarac, M.; Brochon, C.; Catala, J-M.; Wilczewska, A.; Zard, S. Z. *Macromol. Chem. Phys.* **2002**, *203*, 2281-2289.
3. Destarac, M.; Bzducha, W.; Taton, D.; Gauthier-Gillaizeau, I.; Zard, S. Z. *Macromol. Rapid Commun.* **2002**, *23*, 1049-1054
4. Muller, A. H. E.; Zhuang, R.; Yan, D.; Litvinenko, G. *Macromolecules* **1995**, *28*, 4326-4333.
5. Edgecombe, S. R.; Gardiner, J. M.; Matsen, M. W. *Macromolecules* **2002**, *35*, 6475-6477.
6. Demko, Z. P.; Sharpless, K. B. *Angew. Chem. Int. Ed.*, **2002**, *41*, 2110-2113.
7. Schoenberg, E.; Marsh, H. A.; Walters, S. J.; Saltman, W. M. *Rubber Chem. Technol.* **1979**, *52*, 526.
8. Hou, S.; Chan, W. K. *Macromolecules* **2002**, *35*, 850-856.
9. Peng, Y.; Wang, J.; Liu, J.; Dai, H.; Cun, L. *Polym. Int.* **1996**, *39*, 63-68.

10. Wootthikanokkhan, J.; Tongrubbai, B. *J. Appl. Polym. Sci.* **2003**, *88*, 921-927.
11. Germack, D. S.; Wooley, K. L. *J. Polym. Sci. Part A: Polym. Chem.* **2007**, *45*, 4100-4108.
12. Jitchum, V.; Perrier, S. *Macromolecules* **2007**, *40*, 1408-1412.
13. Nakamura, Y.; Honda, H.; Harada, A.; Fujii, S.; Nagata, K. *J. Appl. Polym. Sci.* **2009**, *113*, 1507-1514.
14. Bouhadir, G.; Legrand, N.; Quiclet-Sire, B.; Zard, S. Z. *Tetrahedron Lett.* **1999**, *40*, 277-280.
15. Jamir, L.; Yella, R.; Patel, B. K. *J. Sulfur Chem.* **2009**, *30*, 128-134.

CHAPTER 3

SYNTHESIS AND CHARACTERIZATION OF POLY(VINYLPYRROLIDONE) GRAFTED NANOPARTICLES VIA RAFT POLYMERIZATION

3.1 Introduction

As a significant water soluble polymer, poly(vinyl pyrrolidone) (PVP) has been applied in a variety of industries.[1,2] Free radical polymerization has been employed to prepare PVP, however the polymer molecular weight and architecture were not controllable.[3] Compared to other controlled radical polymerizations,[4-6] reversible addition-fragmentation chain transfer/macromolecular design by interchange of xanthates (RAFT/MADIX)[7,8] polymerization has been widely used to synthesize polymers in a controlled manner (both molecular weight and polydispersity) since it does not require the use of inorganic catalysts and is adaptable to a extremely wide range of functional monomers. So far, *O*-ethyl xanthate based RAFT/MADIX agents have been used in mediating the NVP polymerization.[9-12] However, it was reported that the terminal *O*-ethyl xanthate on PVP chains is unstable and decomposed in the polymerization.[13] In addition, the terminal *O*-ethyl xanthate on PVP chains was hydrolyzed to form a hydroxyl end group after 16 h in a 40 ^{o}C aqueous environment.[14] Thus, more thermally and chemically stable RAFT/MADIX agents are desirable for mediating the polymerization of NVP. Dithiocarbamates have been used as a thermally stable agent in RAFT polymerization. So

far, only a few groups have reported using dithiocarbamates to mediate the polymerization of NVP.[1,15] However, these dithiocarbamate RAFT agents contained either bulky Z groups or alkyne based primary R groups, which are not good living groups and interfere with the polymerization due to the alkyne moiety.[15] Therefore, we are motivated to design new dithiocarbamate RAFT agents to mediate the polymerization of NVP.

Polymer grafted nanoparticles are very appealing composite materials with broad applications in coatings, biomedical devices and chemosensors.[16,17] In addition, the properties of the composites can be tailored by choosing different substrate nanoparticles and polymer shells. The graft density and chain lengths of the surface attached polymers are able to greatly affect the dispersion and the final properties of the nanoparticles.

Few groups have reported placing PVP on nanoparticles.[18-21] In these reported PVP covered particles, PVP chains were physically absorbed on the particles surfaces or grafted on surfaces without control (by free radical polymerizations). Thus, we were motivated to graft PVP on particle surfaces in a controlled manner for advanced applications. This is the first report of mediating the polymerization of NVP on nanoparticles in a controlled manner via surface-initiated RAFT polymerization.

The growing phenomenon of bacterial resistance to antibiotics results in high morbidity and mortality, which is an exceptionally urgent healthcare problem.[22] A wide range of antibiotics, such as penicillin, have become ineffective or have limited effectiveness against bacteria since their first usages decades ago. MRSA (methicillin-resistant *Staphylococcus aureus*), is a well-known bacteria exhibiting resistance to antibiotics with beta lactam structures, such as penicillin. The resistance makes MRSA

caused infections much more difficult to overcome and thus results in an extremely dangerous infection. Nanoparticles with a series of advantages, such as high surface to volume ratio and unique nano-size effects, have been employed as drug delivery vehicles.[23] They have been widely used to carry and release active biomolecules to eukaryote cells, however few groups have applied it to target bacteria, especially MRSA. Thus, we were motivated to prepare PVP grafted nanoparticles with controllable chain length and graft densities for overcoming MRSA infections by conjugation to bacterial resistant penicillin.

3.2 Experimental

3.2.1 Materials

All chemicals were obtained from Fisher or Acros and used as-received unless otherwise specified. 3-Aminopropyldimethylethoxysilane was obtained from Gelest and used as-received. The amino-functionalized silica nanoparticles were prepared according to the literature.[24] N-vinylpyrrolidone was purified by distillation under reduced pressure before use. AIBN was recrystallized from methanol before use.

3.2.2 Instrumentation

^{1}H NMR (Varian Mercury spectrometer 300/400) was conducted using $CDCl_3$ or CD_3OD as the solvent. Molecular weights and PDI were determined using a gel permeation chromatography (GPC) equipped with a 515 HPLC pump, a 2410 refractive index detector, and three Styragel columns. The columns consisted of HR1, HR3 and HR4 in the effective molecular weight ranges of 100-5000, 500-30000, and 5000-500000, respectively. The GPC used THF as eluent at 30 °C and a flow rate of 1.0 mL/min and

was calibrated with poly(methyl methacrylate) or polystyrene standards obtained from Polymer Laboratories. The polymer grafted nanoparticles were cleaved by HF before GPC analysis. Samples were filtered through microfilters with a pore size of 0.2 μm before injection. Infrared spectra were recorded with a PerkinElmer Spectrum 100 spectrometer. UV-vis spectra were measured with a Perkin-Elmer Lambda 4C UV-vis spectrophotometer. TEM images were examined using a Hitachi 8000 transmission electron microscope with an operating voltage of 200 kV. Carbon-coated copper grids were used to prepare samples by dropping sample solutions on the grids followed by drying in a fume hood before use. TGA measurement was conducted using a TA Instruments Q5000 with a heating rate of 10°C/min form 25°C to 950°C under nitrogen flow. Differential scanning calorimetry (DSC) measurement was conducted using a TA Instruments Q2000 under nitrogen flow.

3.2.3 Synthesis of 4-Cyanopentanoic acid N-pyrroledithiocarboxylate (CPDC)

Pyrrole (2.68g, 0.04 mol) was added dropwise to a DMSO solution (30 mL) of sodium hydroxide (0.96 g, 0.04 mol) at rt. The resulting brown solution then was stirred at rt for 30 min. After that, carbon disulfide (3.04 g, 0.04 mol) was added to the solution followed by another 30 min stirring. Excess amount of aqueous solution of potassium ferricyanide (14.48 g) was added dropwise to the solution and the resulting mixture was stirred for 30 min. The product was formed and further washed by DI water until the washings were colorless. The product was dried overnight under vacuum and obtained as a coffee color solid (yield: 61%, 3.46 g). ^{1}H NMR (300 MHz, $CDCl_3$): δ (ppm) 6.45 (m, 4H, =CHN), 7.77 (m, 4H, =CH).

1H-pyrrole-1-carbothioic dithioperoxyanhydride (1.10g, 3.87 mmol) and 4,4'-azobis(4-cyanopentanoic acid) (1.69 g, 6.029 mmol) were dissolved in 70 mL ethyl acetate. The reaction solution was heated at 75 °C for 18 h. Then solvent was removed and the crude product was passed through silica gel column chromatography (hexane : ethyl acetate = 3:2). The product was obtained as a pale yellow solid (yield: 2.08 g, 88.3%). ^{1}H NMR (300 MHz, $CDCl_3$): δ (ppm) 1.90 (s, 3H, $C(CH_3)CN$), 2.39-2.61 (m, 2H, $C(CN)CH_2$), 2.64 (t, 2H, CH_2-C(=O)-O), 6.30 (m, 2H, =CHN), 7.54 (m, 2H, =CH). Melting point: 114 °C. Mass spectroscopy: m/z: 268 (theoretical m/z: 268).

3.2.4 Activation of CPDC

4-Cyanopentanoic acid N-pyrroledithiocarboxylate (0.285 g, 1.064 mmol) and 2-mercaptothiazoline (0.127 g, 1.064 mmol), and dicyclohexylcarbodiimide (DCC) (0.264 g, 1.277 mmol) were dissolved in 20 mL of dichloromethane. (Dimethylamino)pyridine (DMAP) (13.0 mg, 0.11 mmol) was subsequently added. The resulting solution was stirred at rt for 6 h. After removal of the solvent, the crude product was passed through silica gel column chromatography (hexane : ethyl acetate = 5:4). The product was obtained with a dark yellow color (yield: 0.246 g, 62.5 %). ^{1}H NMR (300 MHz, $CDCl_3$): δ (ppm) 1.91 (s, 3H, $C(CH_3)CN$), 2.60 (m, 2H, $C(CN)CH_2$), 3.26 (t, 2H, $-CH_2SC(=S)$), 3.66 (t, 2H, $-CH_2C(=O)N$), 4.52 (t, 2H, $-C(=O)NCH_2$), 6.30 (m, 2H, =CHN), 7.54 (m, 2H, =CH).

3.2.5 Synthesis of CPDC Functionalized SiO_2 Nanoparticles

A THF stock solution (4.10 mL) of activated CPDC (0.05 mol/L) was diluted in 20 mL dry THF. A THF solution of amino-functionalized silica nanoparticles (approx. 3g)

was added slowly to the above activated CPDC solution and the resulting mixture was stirred at rt for 6h. After the reaction, the solution was precipitated into cyclohexane and ethyl ether mixture. (300 mL, cyclohexane : ethyl ether = 4 : 1), centrifuged at 3000 rpm for 5 minutes, and redispersed in dry THF. This procedure was repeated several times until the supernatant solution was colorless after centrifugation. The light yellow CPDC anchored nanoparticles were dried under vacuum at rt.

3.2.6 Surface-Initiated RAFT Polymerization of NVP from CPDC Anchored SiO_2 Nanoparticles

NVP (0.44 mL, 4.114×10^{-3} mol), CPDC coated SiO_2 nanoparticles (50.26 mg), dry dioxane (1.5 mL) and anisole (1.5 mL) were added to a 20 mL Schlenk tube. After sonication for 1 min, AIBN (51 µL, 10 mM in dioxane) was added. The solution was degassed by four freeze-pump-thaw cycles, filled with nitrogen, and then placed in an oil bath at 80 °C for various intervals. The polymerization was stopped by quenching in ice water.

3.2.7 Cleavage of Grafted PVP from Silica Nanoparticles

Generally, 20- 50 mg of PVP grafted silica nanoparticles were dissolved in DMF (2 mL) in a plastic bottle. HF (1.0 mL, 49% in aq) was added, and the resulting solution was stirred at rt overnight. The solution was poured into a PTFE Petri dish and left in a fume hood overnight to remove the volatiles. The cleaved PVP was dissolved in DMF, and then characterized by GPC.

3.3 Results and Discussion

3.3.1 Synthesis and Characterization of RAFT Agent

The structure of the new RAFT agent is shown in Figure 3.1. It contains a pyrrole based Z group and a tertiary cyanopentanoic acid R group, which has been reported as a good leaving group.[20] The strategy for the synthesis of RAFT agent CPDC is shown in Scheme 3.1. Pyrrole was allowed to react with sodium hydroxide in DMSO, followed by addition of carbon disulfide to generate sodium N-pyrroledithiocarboxylate. An excess of potassium ferricyanide was added to oxidize sodium N-pyrroledithiocarboxylate resulting in 1H-pyrrole-1-carbothioic dithioperoxyanhydride, which was further allowed to react with 4,4'-azobis(4-cyanopentanoic acid) to form CPDC. ^{1}H NMR spectrum (Figure 3.2) confirmed the peaks at 6.4 ppm and 7.8 ppm assigned to the protons in the pyrrole rings of the intermediate 1H-pyrrole-1-carbothioic dithioperoxyanhydride. The ^{1}H NMR spectrum (Figure 3.3) showed peaks at 1.9 ppm, 2.4 ppm, 2.6 ppm, 6.4 ppm and 7.8 ppm ascribed to the protons in CPDC. The CPDC has a color of pale yellow with UV-vis strong absorption peaks at 308 nm and 288 nm (Figure 3.4). Mass spectrum (Figure 3.5) confirmed the molecular weight of CPDC of 268 g/mol. The IR spectra (Figure 3.6) demonstrated the presence of the peaks at ~1700 cm^{-1}ascribed to the carbonyl moiety in -COOH, the broad peak at 3400 ~ 2400 cm^{-1} due to the hydroxyl moiety in –COOH, and a range of strong absorption peaks at 1500 ~ 600 cm^{-1} assigned to the pyrrole moiety. Activated CPDC was prepared by the coupling reaction between CPDC and 2-mercaptothiazoline for further use.

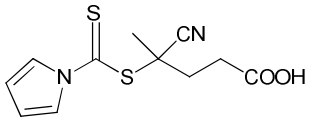

4-Cyanopentanoic acid N-pyrroledithiocarboxylate (CPDC)

Figure 3.1 The structure of 4-Cyanopentanoic acid N-pyrroledithiocarboxylate (CPDC).

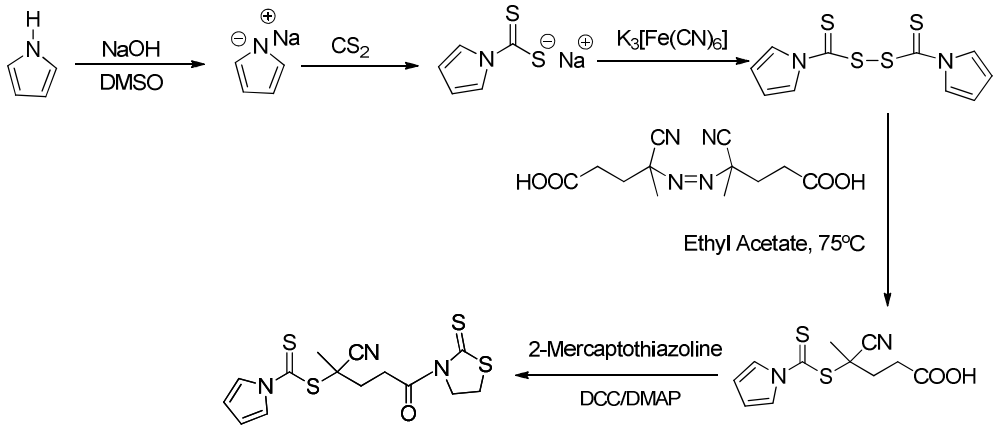

Scheme 3.1 Synthesis of RAFT agent CPDC.

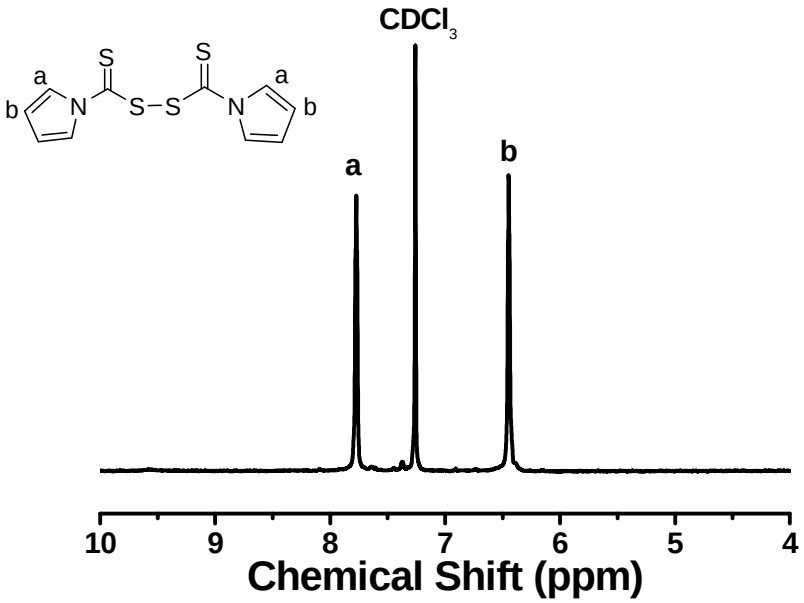

Figure 3.2.[1]H NMR spectra of the intermediate 1H-pyrrole-1-carbothioic dithioperoxyanhydride.

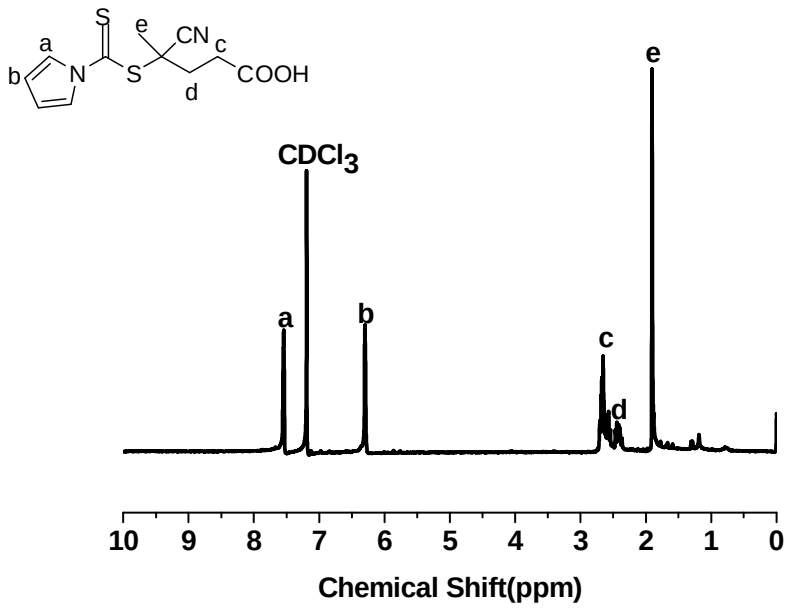

Figure 3.3 ^{1}H NMR spectra of CPDC.

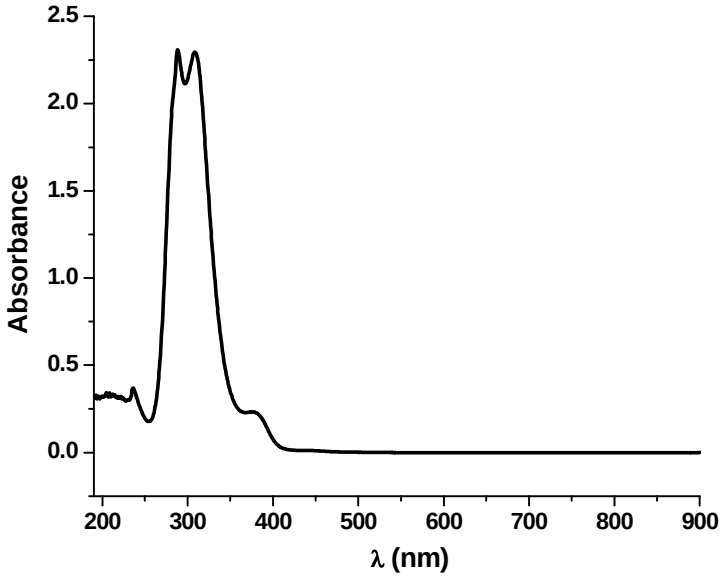

Figure 3.4 UV-vis spectra of CPDC.

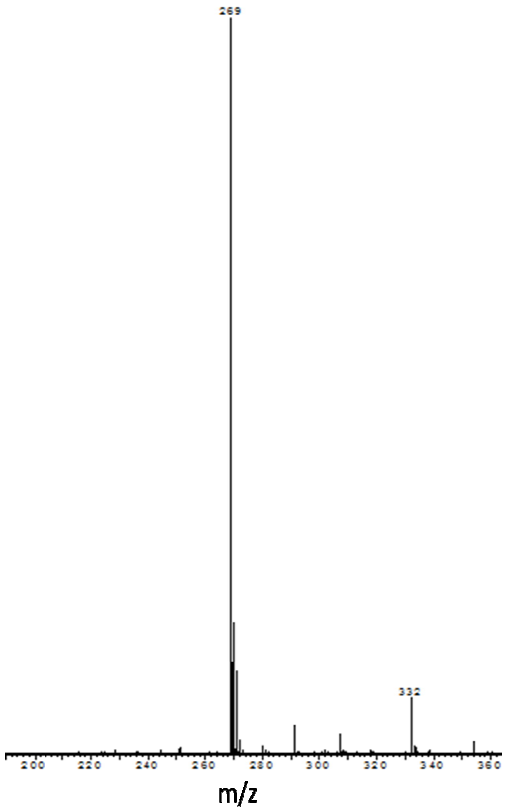

Figure 3.5 Mass spectrum of CPDC.

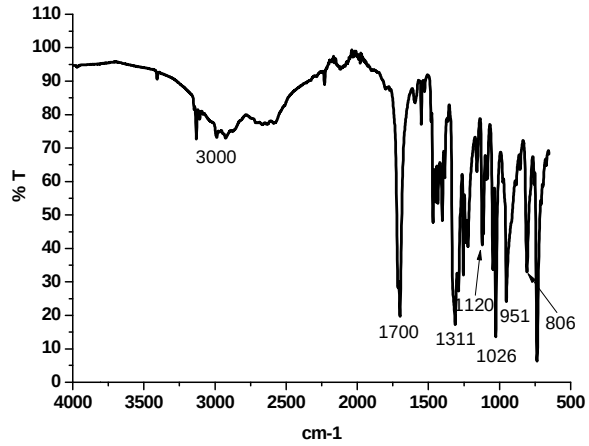

Figure 3.6. IR spectra of CPDC.

3.3.2 RAFT Polymerization of CPDC

The results of the kinetic study of RAFT polymerization of styrene mediated by CPDC in THF is shown in Figure 3.7. There was a linear relationship between $\ln(M_0/M_t)$ (where M_0 indicates the initial monomer concentration and M_t indicates the monomer concentration at time *t*) and polymerization time *t*, which means a constant radical concentration during the polymerization. In addition, the Mn measured by GPC of the polystyrene (PS) chains increased linearly with monomer conversion and matched well with the theoretical molecular weight. All of these confirmed the living/controlled nature of the RAFT polymerization of styrene mediated by CPDC. Compared to a traditional well-controlled RAFT polymerization with a narrow PDI (usually less than 1.2), the PDIs were slightly higher and around 1.3-1.5 during the polymerization. Nonetheless, a range of PS chains with controllable molecular weights can be prepared using the CPDC mediated RAFT polymerization.

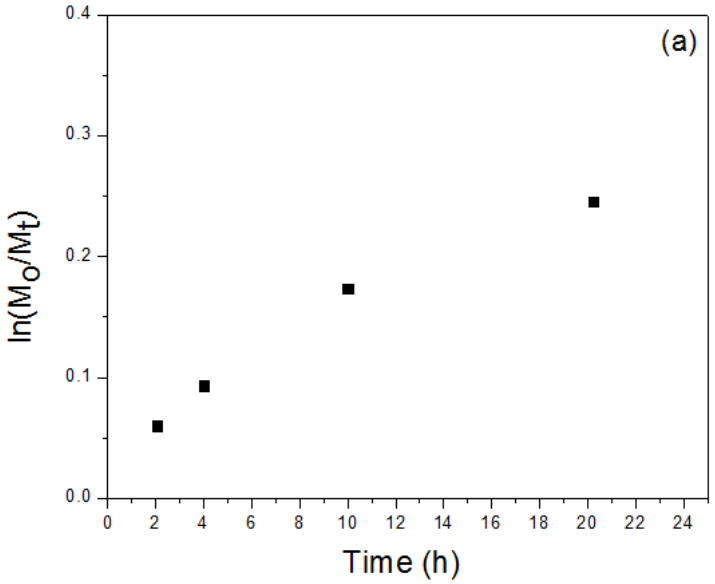

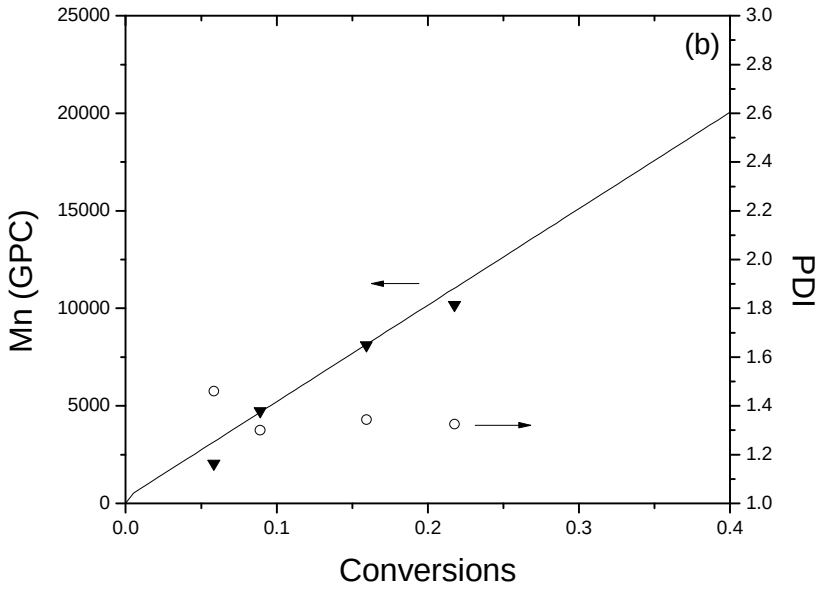

Figure 3.7 (a) Kinetic study and (b) GPC molecular weight (inverted triangle), theoretical molecular weight (solid line) and polydispersity (unfilled circles) for the CPDC mediated RAFT polymerization of styrene in THF ([Styrene]:[CPDC]:[AIBN] = 475:1:0.1) at 75 ^{o}C.

As a specially designed RAFT agent, CPDC was used to mediate the RAFT polymerization of NVP. The polymerization of NVP was conducted at 80 ^{o}C employing a ratio between species of [NVP]:[CPDC]:[AIBN] = 497:1:0.125 at 80 ^{o}C in 0.934 mL dioxane. After 24.5 h, the polymerization reached a conversion of 27 %. The molecular weight (Mn) of the PVP chains obtained from ^{1}H NMR was 11,320 g/mol and the theoretical Mn was 15100 g/mol. As a comparison, trithiocarbonate RAFT agent 4-cyano-4-(dodecylsulfanylthiocarbonyl)sulfanylpentanoic acid (CDSS) was used to mediate the polymerization of NVP under similar conditions. After 24.5 h, the polymerization resulted in a gel which was not worked up.

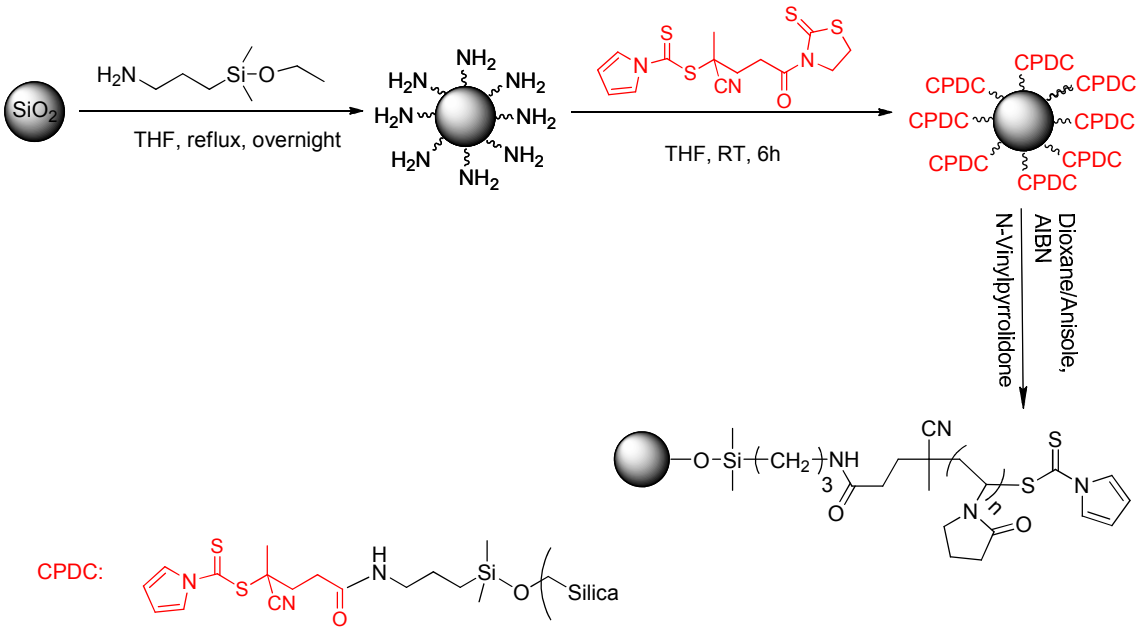

Scheme 3.2 Scheme for synthesis of PVP grafted silica nanoparticles.

The method for the synthesis of PVP grafted nanoparticles is shown in Scheme 3.2. The CPDC anchored silica nanoparticles were prepared by the reaction between amino immobilized nanoparticles with accurately measured densities and activated CPDC. The amount of CPDC coated on nanoparticles can be controlled by changing the feed ratio between amino coated particles and CPDC. A UV-*vis* absorption standard curve (absorbance VS concentration) of CPDC was made to precisely measure the graft density of CPDC on nanoparticles (Figure 3.8).

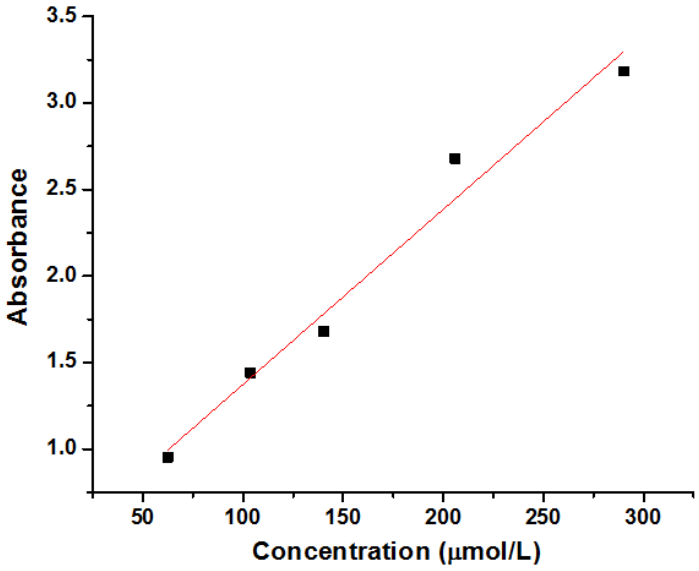

Figure 3.8 UV-vis standard absorption curve of CPDC in THF.

The surface-initiated RAFT polymerization of N-Vinylpyrrolidone was conducted using a recipe of [NVP]:[CPDC]:[AIBN] = 1438:1:0.18 at 80 ^{o}C in a mixed solvent of dioxane and anisole (dioxane/anisole = 1/1) with a monomer concentration of 1.18 mol/L. The ^{1}H NMR spectra exhibited the proton peaks at 1.3-1.8 ppm and 3.5-4.0 ppm ascribed to the attached polymer backbone. The IR spectra of the PVP grafted nanoparticles (Figure 3.9) showed the appearance of the absorption peaks at ~ 2955 cm^{-1}, 1655 cm^{-1}, 1423 cm^{-1}, 1287 cm^{-1}, 1065 cm^{-1}due to the methyl group, amide in lactam, -CH_2- in lactam, C-N in lactam, and SiO_2 moieties, respectively. The molecular weight (M_n) of the surface anchored PVP chains was 56900 g/mol and the PDI was 1.65. The thermogravimetric analysis (TGA) confirmed that the anchored PVP chains accounted for 48 % by weight (Figure 3.10, b). The PVP grafted silica nanoparticle solution was transparent in dimethylsulfoxide (DMSO) (Inset, Figure 3.11).The TEM image (Figure

3.11) shows the PVP grafted silica nanoparticles were dispersed and demonstrates that the size of the nanoparticles was around 20-30 nm (diameter)

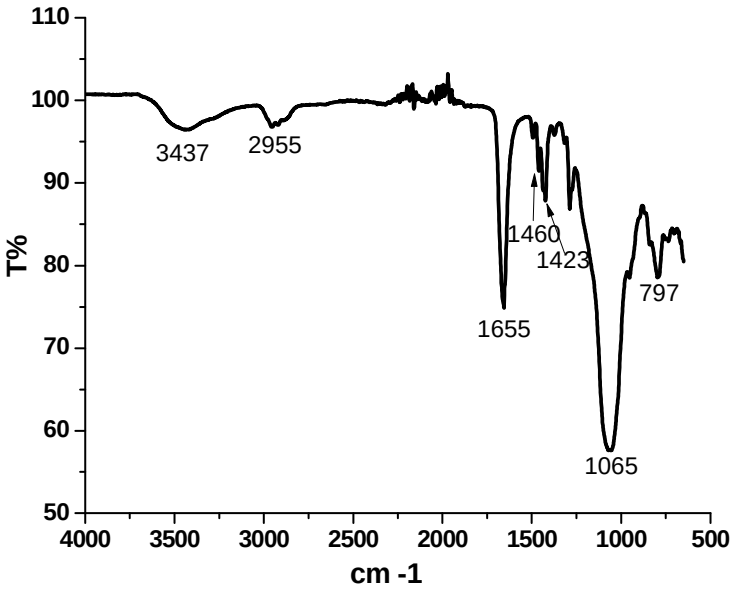

Figure 3.9 IR spectra of PVP grafted silica nanoparticles.

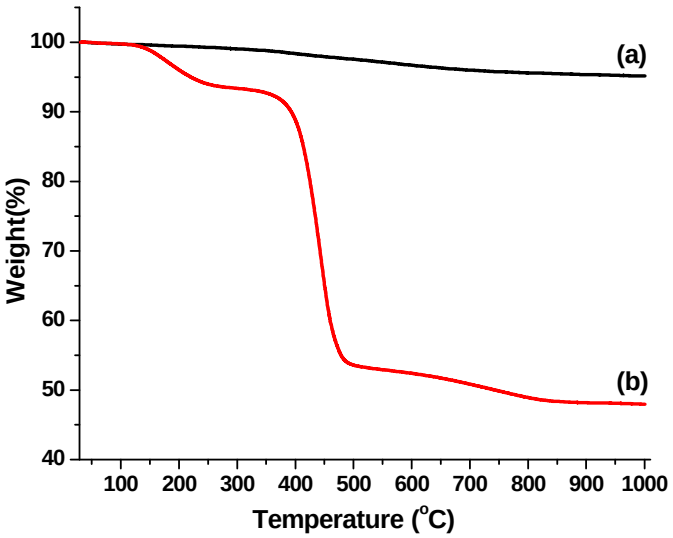

Figure 3.10 TGA of (a) CPDC coated nanoparticles; and (b) PVP grafted nanoparticles.

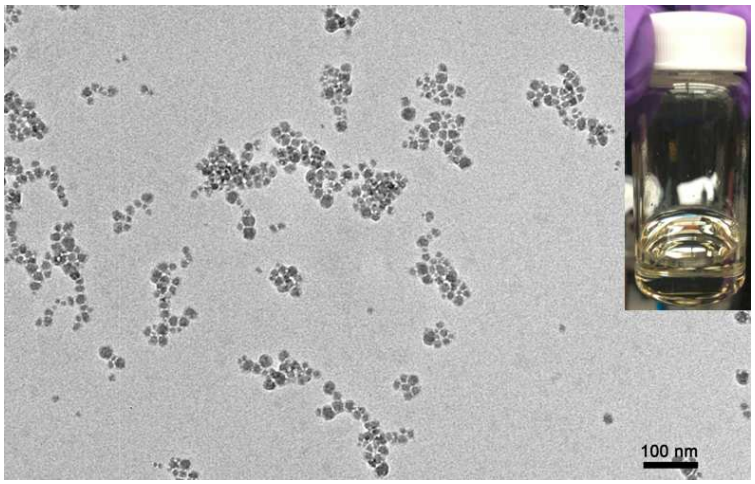

Figure 3.11 TEM image of PVP grafted nanoparticles. Inset: Photograph of PVP grafted nanoparticles in DMSO.

3.4 Summary

In conclusion, we designed and synthesized a new dithiocarbamate based RAFT agent CPDC for mediating RAFT polymerization of NVP. CPDC can also mediate the polymerization of styrene and methyl acrylate in a controlled manner. CPDC was coated on silica nanoparticles via surface silane coupling chemistry. The surface-initiated RAFT polymerization of NVP was conducted on 15 nm (diameter) silica nanoparticles resulting in well-dispersed particles. The synthesis of PVP grafted silica nanoparticles was confirmed by FTIR, TGA, ^{1}H NMR analysis and TEM. PVP grafted silica nanoparticles appear to be a new vehicle to efficiently restore antibiotic activity.

3.5 Reference

1. Devasia, R.; Bindu, R. L.; Borsali, R.; Mougin, N.; Gnanou, Y. *Macromol. Symp.* **2005**, *229*, 8-17.
2. Kaneda, Y.; Tsutsumi, Y.; Yoshioka, Y.; Kamada, H.; Yamamoto, Y.; Kodaira, H.; Tsunoda, S.; Okamoto, T.; Mukai, Y.; Shibata, H.; Nakagawa, S.; Mayumi, T. *Biomaterials* **2004**, *25*, 3259-3266.
3. Luo, L.; Ranger, M.; Lessard, D. G.; Le Garrec, D.; Gori, S.; Leroux, J. C.; Rimmer, S.; Smith, D. *Macromolecules* **2004**, *37*, 4008-4013.

4. Bilalis, P.; Zorba, G.; Pitsikalis, M.; Hadjichristidis, N. *J. Polym. Sci., Part A: Polym. Chem.* **2006**, *44*, 5719-5728.
5. Lu, X.; Gong, S.; Meng, L.; Li, C.; Yang, S.; Zhang, L. *Polymer*, **2007**, *48*, 2835-2842.
6. Debuigne, A.; Willet, N.; Jerome, R.; Detrembleur, C. *Macromolecules* **2007**, *40*, 7111-7118.
7. Chiefari, J.; Chong, Y. K.; Ercole, F.; Krstina, J.; Jeffery, J.; Le, T. P. T.; Mayadunne, R. T. A.; Meijs, G. F.; Moad, C. L.; Moad, G.; Rizzardo, E.; Thang, S. H. *Macromolecules* **1998**, *31*, 5559-5562.
8. Charmot, D.; Corpart, P.; Adam, H.; Zard, S. Z.; Biadatti, T.; Bouhadir, G. *Macromol. Symp.* **2000**, *150*, 23-32.
9. Wan, D.; Satoh, K.; Kamigaito, M.; Okamoto, Y. *Macromolecules* **2005**, *38*, 10397-10405.
10. Postma, A.; Davis, T. P.; Li, G.; Moad, G.; O'Shea, M. *Macromolecules* **2006**, *39*, 5307-5318.
11. Destarac, M.; Brochon, C.; Catala, J.-M.; Wilczewska, A.; Zard, S. Z. *Macromol. Chem. Phys.* **2002**, *203*, 2281-2289.
12. Adamy, M.; Van Herk, A. M.; Destarac, M.; Monteiro, M. J. *Macromolecules* **2003**, *36*, 2293-2301.
13. Pound, G.; Eksteen, Z.; Pfukwa, R.; McKenzie, J. M.; Lange, R. F. M.; Klumperman, B. *J. Polym. Sci., Part A: Polym. Chem.* **2008**, *46*, 6575-6593.
14. Pound, G.; McKenzie, J. M.; Lange, R. F. M.; Klumperman, B. *Chem. Commun.* **2008**, *44*, 3193-3195.
15. Mishra, V.; Kumar, R. *J. Appl. Polym. Sci.* **2012**, *124*, 4475-4485.
16. Zou, H.; Wu, S.; Shen, J. *Chem. Rev.* 2008, 108, 3893-3957.
17. Cash, B.; Wang, L.; Benicewicz, B. *J. Polym. Sci., Part A: Polym. Chem.* **2012**, *50*, 2533-2540.
18. Zelikin, A. N.; Such, G. K.; Postma, A.; Caruso, F. *Biomacromolecules* **2007**, *8*, 2950-2953.
19. Mosaiab, T.; Jeong, C. J.; Shin, G. J.; Choi, K. H.; Lee, S. K.; Lee, I.; In, I.; Park, S. Y. *Mater. Sci. Eng.: C* **2013**, *33*, 3786–3794.
20. Arsalani, N.;Fattahi, H.; Nazarpoor, M. *eXPRESS Polymer Letters* **2010**, *4*, 329–338.
21. Lakhwani, S.; Rahaman, M. N. *J. Mater. Sci.* **1999**, *34*, 3909-3912.
22. Evans, H. L.; Lefrak, S. N.; Lyman, J.; Smith, R. L.; Chong, T. W.; McElearney, S. T.; Schumlan, A. R.; Hughes, M. G.; Raymond, D. P.; Pruett, T. L.; Sawyer, R. G. *Crit. Care Med.* **2007**, *35*, 89-95.
23. Mahapatra, I.; Clark, J.; Dobson, P. J.; Owenc, R.; Lead, J. R. *Environ. Sci.: Processes & Impacts.* **2013**, *15*, 123-144.
24. Li, C.; Han, J.; Ryu, C. Y.; Benicewicz, B. C. *Macromolecules* **2006**, *39*, 3175-3183.

CHAPTER 4

SYNTHESIS AND CHARACTERIZATION OF DYE-LABELED POLY(METHACRYLIC ACID) GRAFTED NANOPARTICLES[2,3]

[2] Wang, L.; Benicewicz, B. Synthesis and Characterization of Dye-Labeled Poly(methacrylic acid) Grafted Silica Nanoparticles. *ACS Macro Lett.* **2013**, *2*, 173-176.
[3] Cash, B.; Wang, L.; Benicewicz, B. The Preparation and Characterization of Carboxylic Acid-Coated Silica Nanoparticles. *J. Polym. Sci. Part A: Polym. Chem.* **2012**, *50*, 2533-2540.

4.1 Introduction

Polymer grafted nanoparticles are of great interest because of their applications in chemosensors, coatings and organic light-emitting devices (OLEDs).[2] The RAFT polymerization technique has emerged as a powerful tool to modify nanoparticle surfaces with functional polymers containing predetermined molecular weights due to the straightforward attachment chemistry and controllable surface graft density.

Poly(methacrylic acid) (PMAA) and other polymers made from acid containing monomers represent an important class of stimuli-responsive polymers and have been widely used in membrane transport,[1] biomedical applications,[2] coatings,[3] and sensors.[4] There are few reports about the synthesis of PMAA or other multi acid containing polymers on nanoparticle surfaces. For example, Brittain *et al.*[5] synthesized poly(*tert*-butylacrylate) brushes on silica surface by atom transfer radical polymerization (ATRP), followed by pyrolysis at 200 ^{o}C resulting in PAA grafted silica substrates. Genzer *et al.*[6] prepared poly(*tert*-butylacrylate) grafted silicon wafer by ATRP, followed by acid hydrolysis of the polymer to form the immobilized PAA chains. Zhao *et al.*[7] sequentially prepared poly(*tert*-butylacrylate) brushes by ATRP and polystyrene brushes by nitroxide-mediated radical polymerization (NMRP) on the surface of silica nanoparticles. Subsequent deprotection of the *tert*-butyl moieties with trimethylsilane iodide (TMSI) led to environmentally-responsive nanoparticle materials. To avoid the toxicity issue of residual copper from ATRP catalysts in bioapplications, Benicewicz *et al.*[8] prepared PMAA grafted silica nanoparticles by surface-initiated RAFT polymerization of *tert*-butyl methacrylate, followed by deprotection of the *tert*-butyl groups by TMSI.

Very few groups have conducted direct surface-initiated RAFT polymerization of methacrylic acid or other acid containing monomers on nanoparticle surfaces. One particular challenge is maintaining good dispersibility of the polymer grafted nanoparticles using small size substrate nanoparticles. Generally, smaller size nanoparticles agglomerate more readily than larger particles. Thus, the size and nature of the substrate nanoparticles are important issues affecting the final dispersibility of polymer grafted nanoparticles. Charpentier *et al.*[9] used a RAFT agent with a carboxylic acid group to modify TiO_2 nanoparticles and conducted the surface-initiated polymerization of acrylic acid. Yusa *et al.*[10] synthesized poly(6-(acrylamide)hexanoic acid chains on 11 µm (diameter) size silica particles. The polymer grafted particles flocculated at low pH's (pH=3) and dispersed in water at high pH's (pH=10). However, the large (11 µm diameter) particles are much easier to disperse in solution. In this work, we report the direct polymerization of MAA on small diameter silica nanoparticles (as small as 15nm) in a controlled manner via surface-initiated RAFT polymerization which was compared to another procedure for attaching PMAA chains to nanoparticles. Cleavage of the methylated chains from the nanoparticle surface enabled accurate measurement of the molecular weights via organic phase GPC, and a precise determination of the polymerization kinetics.

In the microbiology field, resistant microbial infections, especially the bacterial biofilm infections, have increased greatly in the past decades.[11] Biofilm infections are capable of protecting bacterial cells by blocking free antibiotics outside of the "barrier" and coordinating their metabolic activity by quorum sensing, which allows the bacterial cells to operate, communicate, and function as a group rather than individual cells. To our

knowledge, antibiotics bound to nanoparticles have not been extensively used to combat biofilm infections. Our preliminary research has demonstrated that nanoparticle conjugated antibiotics with non-specifical binding via carboxyl groups are more bioactive against bacteria than free antibiotics in solution. In addition, carboxylic acid coated nanoparticles penetrated biofilms to a distance of approimately 50 μm within 24 h. Thus, modifying a nanoparticle with a controllable amount of carboxylic acids may be useful against biofilm related infections.

Fluorescent nanoparticles have been applied in bioimaging and nanomedicine fields.[12,13] Silica nanoparticles possess a series of properties, such as biocompatibility, controllable particle size, easy fabrication and powerful surface functionalization chemistry toolbox.[14] Fluorescent silica nanoparticles provide universal imaging probes with other functionalities by powerful surface multi-functionalization with a variety of biomolecules and polymers.[15,16] Aditionally, labeling the nanoparticle surface with fluorescent dyes is helpful in monitoring the presence and movement of particles in biological cells or other systems. Nanoparticles with anchored polymer chains containing carboxylic acid moieties have been reported to be useful for fighting bacterial infections and as drug delivery vehicles in the biomedical field.[8, 17] Based on the great potential bioapplications, we were motivated to prepare dye-labeled PMAA grafted silica nanoparticles as a powerful platform for such applications.

4.2 Experimental

4.2.1 Materials

All chemicals were obtained from Fisher or Acros and used as received unless otherwise specified. Colloid silica nanopartilces in methyl ethyl ketone was obtained from Nissan Chemical. Trimethylsilyldiazomethane (2.0 M in hexanes) was purchased from TCI. 4-Cyanopentanoic acid dithiobenzoate (CPDB) was obtained from Strem Chemical Inc. 2,2'-Azobis(4-methoxy-2,4-dimethyl valeronitrile) (V-70) was obtained from Wako and used as received. CPDB immobilized silica nanoparticles were synthesized according to the literature.[18] 3-Aminopropyldimethylethoxysilane was obtained from Gelest and used as received. *Tert*-butylmethacrylate (99%, Acros) and methacrylic acid (99.5%, Acros) were purified by passing through an activated neutral alumina column. AIBN was recrystallized from methanol before use.

4.2.2 Instrumentation

^{1}H NMR (Varian Mercury spectrometer 300/400) was conducted using $CDCl_3$ or CD_3OD as the solvent. Molecular weights and PDI were determined using a gel permeation chromatography (GPC) equipped with a 515 HPLC pump, a 2410 refractive index detector, and three Styragel columns. The columns consisted of HR1, HR3 and HR4 in the effective molecular weight ranges of 100-5000, 500-30000, and 5000-500000, respectively. The GPC used THF as eluent at 30 °C and a flow rate of 1.0 mL/min and was calibrated with poly(methyl methacrylate) standards obtained from Polymer Laboratories. The PMAA grafted nanoparticles were methylated by trimethylsilyldiazomethane[19] and then cleaved by HF before GPC analysis. Samples were

filtered through microfilters with a pore size of 0.2 μm before injection. Infrared spectra were recorded with a PerkinElmer Spectrum 100 spectrometer. UV-vis spectra were measured with a Perkin-Elmer Lambda 4C UV-vis spectrophotometer. TEM images were examined using a Hitachi 8000 transmission electron microscope with an operating voltage of 200 kV. Carbon-coated copper grids were used to prepare samples by dropping sample solutions on the grids followed by drying in a fume hood before use. Thermogravimetric analysis (TGA) was conducted using a TA Instruments Q5000 with a temperature ramping from 25 °C to 1000 °C at a rate of 10 °C/min under nitrogen.

4.2.3 Synthesis of 1-Azido-6-hydroxyhexane

1-Chlorohexanol (6.83g, 0.05 mol) and sodium azide (6.50g, 0.10 mol) were dissolved in 50 ml water. The resulting solution was stirred at 80 °C for 12 h. The cooled solution went through extraction with diethyl ether (3×50 mL), drying with anhydrous sodium sulfate and followed by filtration. After removal of the solvent, a colorless liquid was obtained and dried under vacuum to constant weight (yield, 6.00g, 84%). ^{1}H NMR (300 MHz, $CDCl_3$): δ (ppm) 1.40 (m, 4H, CH_2), 1.51-1.64 (m, 4H, CH_2), 3.24 (t, 2H, CH_2N_3), 3.66 (t, 2H, CH_2O).

4.2.4 Synthesis of 6-Azidohexyl Methacrylate (AHMA)

1-Azido-6-hydroxyhexane (7.34 g, 51 mmol), methacrylic acid (3.87 g, 45 mmol), 4-(dimethylamino)pyridine (DMAP) (1.84 g, 15 mmol) were dissolved in 100 mL methylene chloride and the resulting solution was cooled in an ice bath. A methylene chloride solution (50 mL) of dicyclohexylcarbodiimide (DCC) (10.32 g, 50 mmol) was then added slowly. The resulting solution was then transfered to room temperature and

followed by overnight stirring. After removal of the precipitate and solvent, the crude compound was purified via silica gel column chromatography (hexane : ethyl acetate = 10:1). A colorless liquid was obtained and dried under vacuum to constant weight (yield: 5.91 g, 62.2%). ^{1}H NMR (300 MHz, $CDCl_3$): δ (ppm) 1.40 (m, 4H, CH_2), 1.55-1.70 (m, 4H, CH_2), 1.95 (s, 3H, CH_3C), 3.24 (t, 2H, CH_2N_3), 4.16 (t, 2H, CH_2O), 5.54 (s, 1H, =CH), 6.12 (s, 1H, =CH). ^{13}C NMR (400 MHz, $CDCl_3$): 18.75, 26.04, 26.86, 28.98, 29.28, 51.6, 64.93, 125.78, 136.60, 167.90.

4.2.5 Preparation of Fluorescent Dye and CPDB Coated Silica Nanoparticles

A THF solution of N-[2-{N-(7'-Nitrobenz-2'-oxa-1',3'-diazol-4'-yl)amino} ethyl-carbonyloxy]succinimide (NBD-NHS) (31.6 mg, 90.46 μmol) was added dropwise to amino-functionalized silica nanoparticles (approx. 3 g) dispersed in THF (50 mL). The reaction mixture was stirred at room temperature for 3 h. The solution was precipitated into a large amount of hexane (300 mL), centrifuged at 3000 rpm for 5 minutes, redispersed in dry THF. This procedure was repeated several times until the supernatant solution was colorless after centrifugation. A THF solution (30 mL) of the above fluorescent silica nanoparticles (approx. 3 g) was added dropwise to a THF solution (30 mL) of activated CPDB (0.18 g, 0.468 μmol). After stirring overnight, the solution was precipitated into a large amount of cyclohexane and ethyl ether mixture (500 mL, cyclohexane : ethyl ether = 4 : 1), centrifuged at 3000 rpm for 5 minutes, redispersed in dry THF. This procedure was repeated several times until the supernatant solution was colorless after centrifugation. The final fluorescent dye and CPDB coated silica nanoparticles were dispersed in dry THF for further usage and an aliquot of the

nanoparticles was subjected to UV-vis analysis to determine the graft densities of the coated fluorescent dye and CPDB on the particle surface.

4.2.6 Surface-Initiated RAFT Polymerization of *Tert*-butyl methacrylate from Dye-labeled CPDB Anchored Silica Nanoparticles

Tert-butyl methacrylate (3.85 mL, 2.37×10^{-2} mol), dye-labeled CPDB coated silica nanoparticles (0.54 g, 43.63 μmol/g) and THF (30 mL) were added to a 50 mL Schlenk flask. Anisole (0.50 mL) was added as the standard to monitor the conversion of the polymerization by ^{1}H NMR. After sonication for 1 min, AIBN (237 μL, 0.01 M in THF) was added. The solution was degassed by four freeze-pump-thaw cycles, filled with nitrogen, and then placed in an oil bath of 60 °C for various intervals. The polymerization was stopped by quenching in ice water.

4.2.7 Cleavage of Grafted Poly(*tert*-butyl methacrylate) from Silica Nanoparticles

Generally, 20- 50 mg of poly(*tert*-butyl methacrylate) grafted silica nanoparticles were dissolved in THF (4 mL) in a plastic bottle. HF (1.0 mL, 49% in aq) was added, and the resulting solution was stirred at rt overnight. The solution was poured into a PTFE Petri dish and left in a fume hood overnight to remove the volatiles. The cleaved poly(*tert*-butyl methacrylate) was dissolved in 2 mL THF, and then characterized by GPC.

4.2.8 Ester Cleavage of Poly(*tert*-butyl methacrylate)

Poly(*tert*-butyl methacrylate) grafted silica nanoparticles (100 mg) were dispersed in CH_2Cl_2 (20 mL) and the solution was bubbled with nitrogen for 10 min. Bromotrimethylsilane (3 mL) was added dropwise and the resulting solution was stirred at rt overnight. After removal of the solvent and excess bromotrimethylsilane under reduced pressure, the concentrated solution was precipitated into diethyl ether. After

centrifugation, the polymer was redispersed into ethanol. This procedure was repeated several times until the supernatant was colorless.

4.2.9 Surface-Initiated RAFT Polymerization of Methacrylic acid from Dye-labeled CPDB Anchored Silica Nanoparticles

Methacrylic acid (5.63 mL, 6.64 × 10^{-2} mol), dye-labeled CPDB coated silica nanoparticles (0.80 g, 70.2 μmol/g) and dry DMF (28 mL) were added to a 50 mL Schlenk flask. After sonication for 1 min, AIBN (1.40 mL, 0.005 M in DMF) was added. The solution was degassed by four freeze-pump-thaw cycles, filled with nitrogen, and then placed in an oil bath of 65 °C for various intervals. The polymerization was stopped by quenching in ice water.

4.2.10 Methylation of poly(MAA) Grafted Silica Nanoparticles

Poly(MAA) grafted silica nanoparticles (~ 20 mg) were dissolved in 10 mL DMF. An excess yellow solution of trimethylsilyldiazomethane was added dropwise into the nanoparticle solution at rt. After complete addition, the solution was stirred for 3h at rt. Around 10% by volume of methanol was added to enhance the conversion of the methylation. The excess trimethylsilyldiazomethane was quenched by acetic acid.

4.3 Results and Discussion

4.3.1 Synthesis of dye-labeled poly(carboxylic acid) grafted silica nanoparticles

The first synthetic strategy was based on the “one-pot” click reactions between PAHMA grafted silica nanoparticles and alkyne functionalized molecules (alkyne based coumarin 343 fluorescent dye and 4-pentynoic acid), according to the Scheme 4.1. Thus, fluorescent dye molecules and carboxylic acids were incorporated onto PAHMA grafted nanoparticles sequentially. PAHMA grafted silica nanoparticles were synthesized by

surface-initiated RAFT polymerization of AHMA on CPDB coated silica nanoparticles. The graft density of CPDB coated nanoparticles can be determined by a Uv-vis absorption at 305 nm. A variety of PAHMA grafted silica nanoparticles with different graft densities and chain lengths were prepared, as shown in Table 4.1. The molecular weights of these surface attached PAHMA varied from 12,000 to 28,000 and the PDIs were generally lower than 1.2. The loading of the dye molecules and the amount of carboxylic acids can be controlled by using PAHMA grafted nanoparticles with different graft densities and chain lengths, and the feed ratio between the dyes and 4-pentynoic acid.

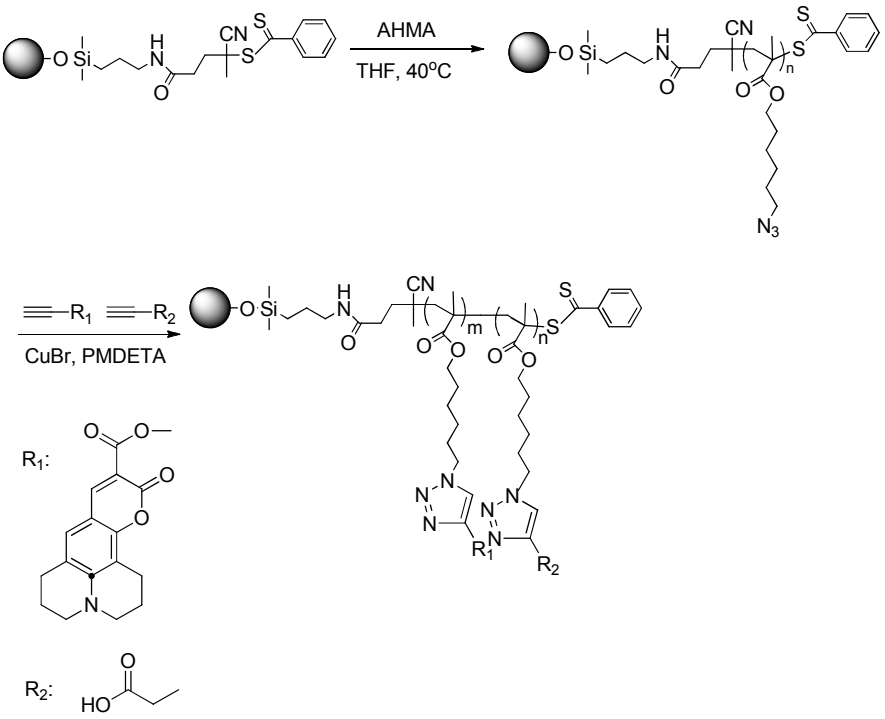

Scheme 4.1. Synthesis of dye-labeled poly(carboxylic acid) grafted silica nanoparticles.

The "click" reaction was conducted between the as-synthesized PAHMA grafted nanoparticles and alkyne functionalized molecules with a ratio of 1: 1.2 between $-N_3$ and the alkyne groups. The amount of alkyne functionalized coumarin 343 accounted for 1

mol % ~ 10 mol % in the alkyne moieties. The CuBr and PMDETA are 0.1 equivalent compared to $-N_3$. After the around 10 h reaction between $-N_3$ and alkyne functionalized coumarin 343, 4-pentynoic acid was added to the reaction solution. IR spectroscopy was used to monitor the progress of the "click" reaction. After 24 - 48 hours, the reaction was completed, which was confirmed by the disappearance of the azide peak around 2100 cm^{-1} according to the Figure 4.1. For "click" reactions involving polymer grafted nanoparticles, the residue copper catalyst was usually removed by passing through an activated alumina column.[20] However, the as-synthesized poly(carboxylic acid) grafted particles were greatly absorbed in the alumina column (as shown in Figure 4.2), resulting a low yield. In addition, it was speculated that those carboxylic acids were able to interact with PMDETA/Cu(I)Br complex, making the copper even harder to be removed. Thus, a new strategy was required to address this challenge.

Table 4.1 Surface-initiated RAFT polymerization of AHMA on silica nanoparticles in THF

Entry	Mn, GPC (g/mol)	PDI	Conversion (%)	Graft Density (chains/nm^2)
1	27282	1.37	-	0.42
2	21309	1.17	-	0.33
3	25246	1.43	-	0.30
4	28051	1.16	-	0.24
5	12355	1.12	11.6	0.23
6	27060	1.10	29.5	0.23

Note: For all the polymerizations, ([AHMA]/[CPDB]/[AIBN] = 500:1:0.1) and the reaction temperature was 40 °C. The conversion of the polymerization was determined by ^{1}H NMR.

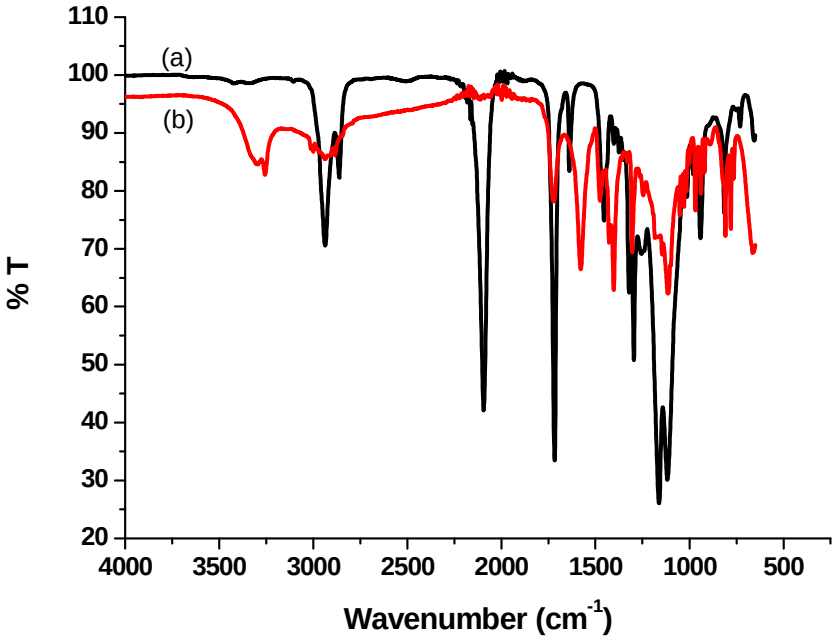

Figure 4.1 IR spectra of PAHMA grafted nanoparticles (a) before and (b) after "click" reaction.

Figure 4.2 Photograph of column purification of polyacid grafted nanoparticles after "click" reaction.

4.3.2 Synthesis of dye-labeled PMAA grafted silica nanoparticles via deprotection of poly(*t*BuMA) grafted nanoparticles

As a new method, the "deprotection" strategy for preparation of dye-labeled PMAA grafted nanoparticles was demonstrated according to Scheme 4.2. The first task was to prepare dye labeled RAFT agent coated silica nanoparticles, and the second task was to synthesize dye labeled poly(*tert*-butylmethacrylate) (P*t*BuMA) grafted nanoparticles which was followed by the last task of deprotection of the *tert*-butyl groups on the nanoparticles.

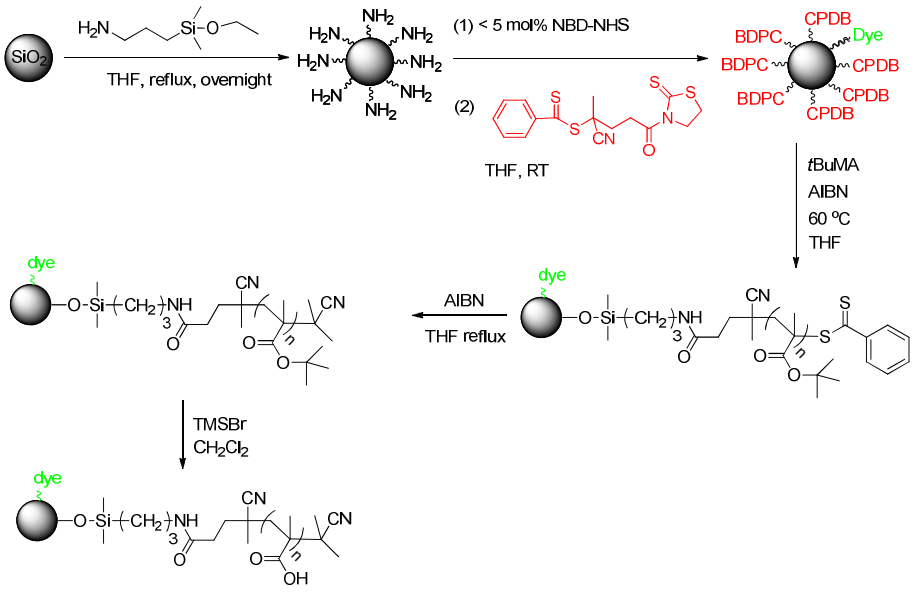

Scheme 4.2 "Deprotection" strategy for preparation of dye-labeled PMAA grafted silica nanoparticles.

Initially, the dye labeled RAFT agent coated silica nanoparticles were synthesized by allowing the amino coated nanoparticles with precisely determined densities to react with a small amount, less than 5 mol % relative to the amines, of activated nitrobenzofurazan derivative followed by an excess of activated CPDB. This method generated a universal platform for surface initiated RAFT polymerization of nanoparticles labeled with

fluorescent dyes for biomedical tracking. The amount of dye covalently bound to the nanoparticle surface (2.33 μmol/g, 0.01 agents/nm^2) was determined quantitatively by comparing the absorbance for the dye modified particles to a standard UV-vis absorption curve prepared from known amounts of free dye (Figure 4.3).

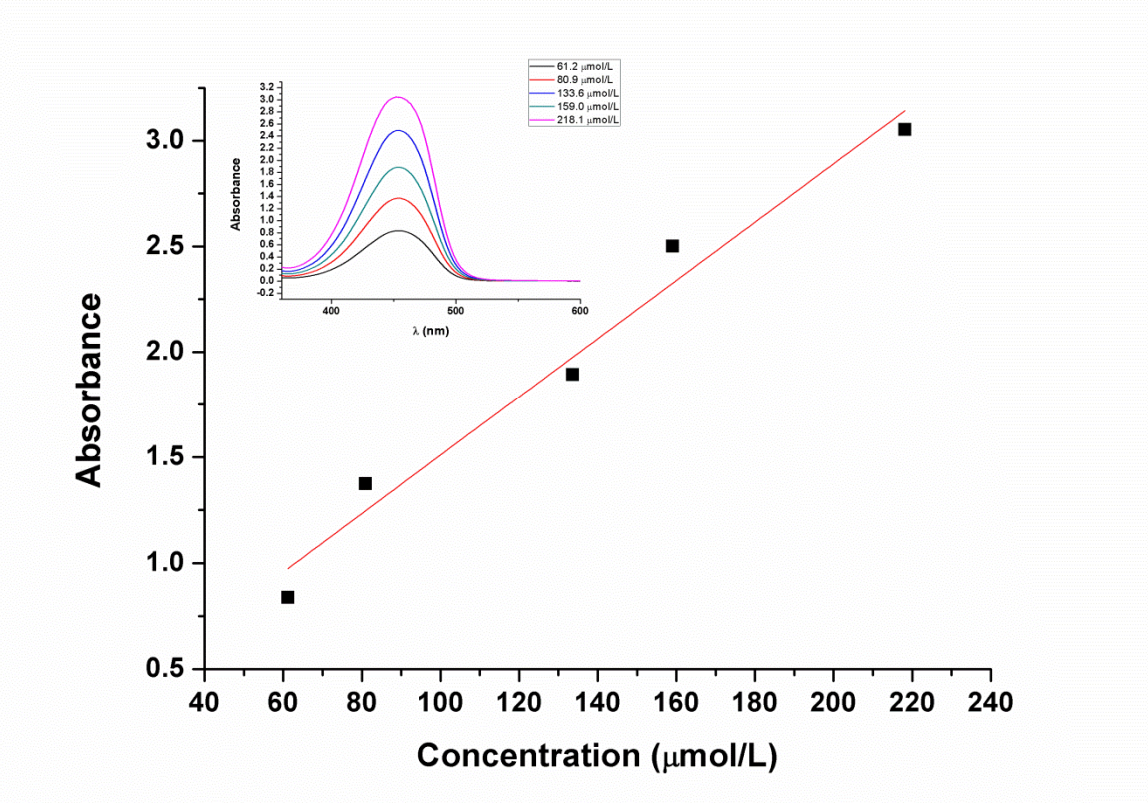

Figure 4.3 UV-vis standard absorption curve of NBD-COOH.

The surface-initiated RAFT polymerization of tBuMA was conducted on dye-labeled CPDB coated silica nanoparticles employing a ratio between species of [*t*BuMA]:[CPDB]:[AIBN] = 1000:1:0.1 at 60 ^{o}C in an appropriate amount of THF. The thermogravimetric analysis (TGA) showed that the grafted poly(*tert*-butylmethacrylate) accounted for 20% by weight (Figure 4.4), which was consistent with the UV analysis. In our previous work,[8] we found that the deprotection of tert-butyl groups in the environment containing thiocarbonylthio moiety with trimethylsilyl iodide (TMSI)

generated ill-defined groups and led to subsequent aggregation. We surmised that the TMSI coordinated to the thiocarbonylthio moiety and caused its decomposition to free thio groups and nanoparticle aggregation by oxidative coupling. Thus, the dye-labeled poly(tert-butylmethacrylate) grafted silica nanoparticles were alternatively treated with excess AIBN to remove the thiocarbonylthio end groups before deprotection of tert-butyl groups.[8] After treatment with excess AIBN, the UV-vis spectrum confirmed that the thiocarbonylthio moiety was removed by the absence of the absorption peak at 300 nm (Figure 4.5).

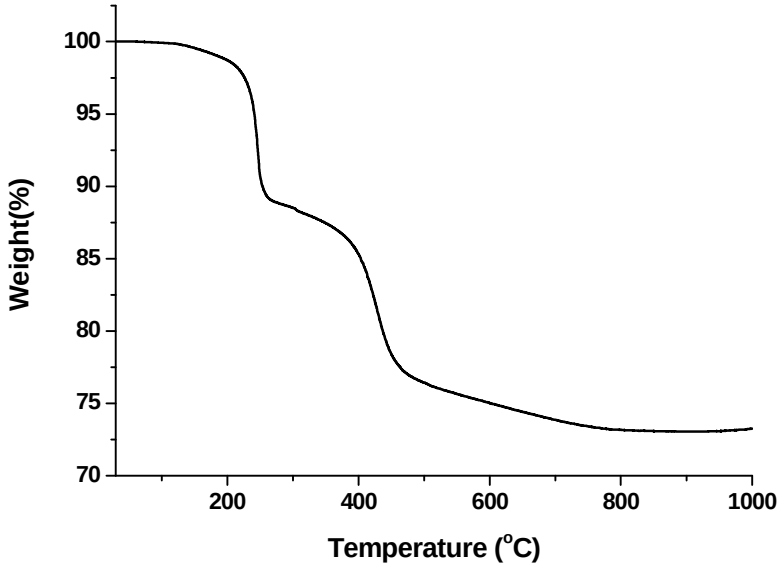

Figure 4.4 TGA of dye-labeled poly(*t*BuMA) grafted silica nanoparticle.

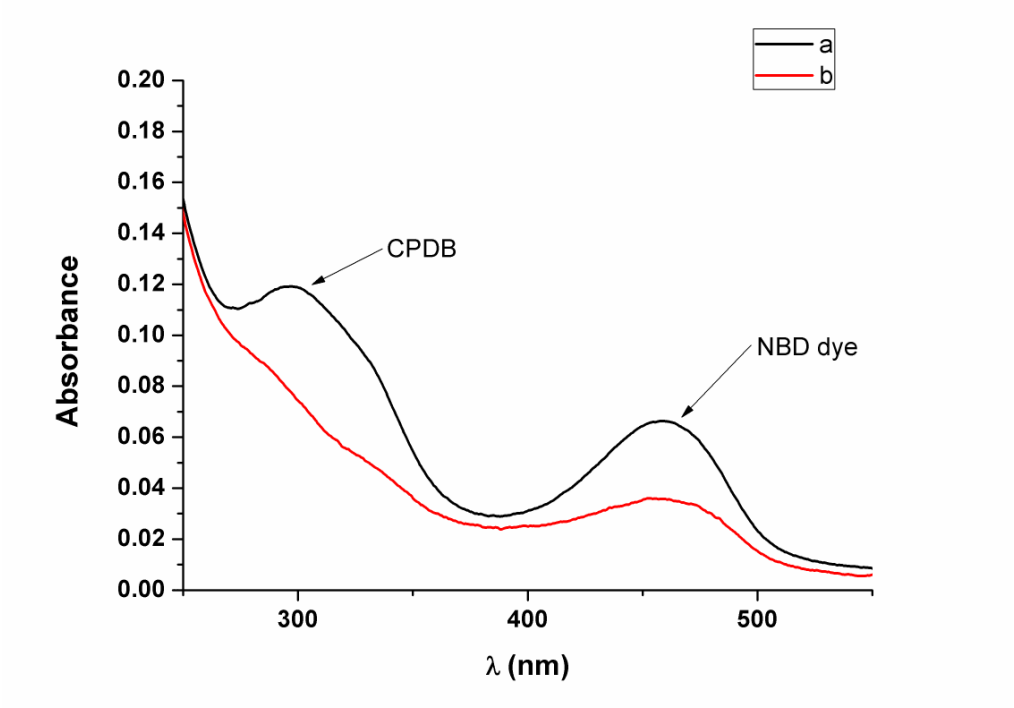

Figure 4.5 UV-vis absorption of (a) dye-labeled CPDB coated silica nanoparticle; (b) dye-labeled CPDB removed silica nanoparticle.

Initially, TMSI was used to deprotect the *tert*-butyl groups. However, the fluorescence of the nanoparticles was destroyed after the treatment with TMSI. It was speculated that the attached dye molecules were decomposed during the process. To exclude the possibility of the unstable NBD dye structure, two other fluorescent dyes, an amino coumarin and fluorescein derivative, with completely different molecular structures (Figure 4.6) were used to investigate the TMSI process in simple solution experiments. Both of them failed to show fluorescence after the treatment. Thus, the reason may be that the side product iodine attacked these fluorescent dyes with highly conjugated structures which resulted in the fluorescence loss. To test this hypothesis, trimethylsilylbromide (TMSBr) was used as alternative under the same conditions. It was found that the fluorescence of the nanoparticles were maintained after the TMSBr

treatment. Thus, TMSBr was used to replace TMSI in the deprotection of the *tert*-butyl groups.

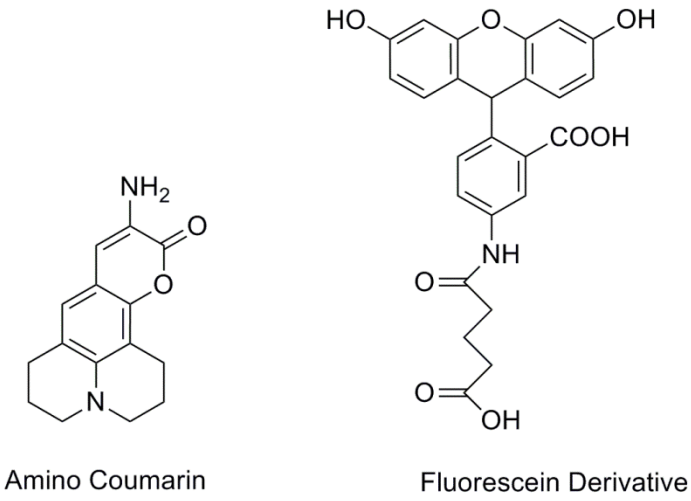

Figure 4.6 The structures of amino coumarin and the fluorescein derivative.

The kinetic study of surface-initiated RAFT polymerization of *t*BuMA on CPDB coated nanoparticles (154.14 μmol/g, 0.65 agents/nm^2) is shown in Figure 4.7. A linear relationship between $\ln(M_0/M_t)$ (where M_0 is the initial monomer concentration and M_t is the monomer concentration at time *t*) and polymerization time was observed, which implies a constant radical concentration. Additionally, the Mn determined by GPC of the polymer chains increased linearly with monomer conversion and agreed closely with the theoretical molecular weight. These features demonstrated the living/controlled nature of the RAFT polymerization of *t*BuMA mediated by CPDB anchored nanoparticles.

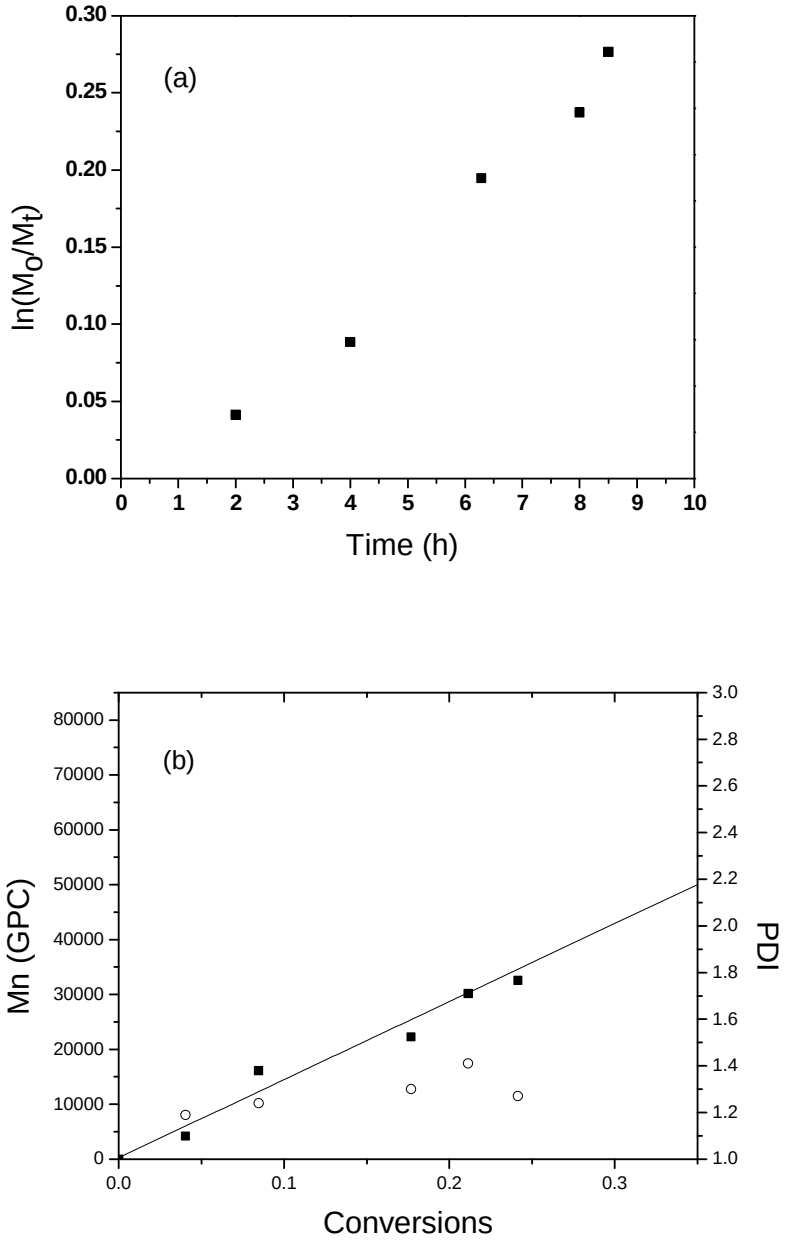

Figure 4.7 (a) Kinetic plots and (b) dependence of the GPC molecular weight (filled squares), theoretical molecular weight (solid line) and polydispersity (unfilled circles) on the conversion for the surface-initiated RAFT polymerization of *tert*-butylmethacrylate ([*t*BuMA]:[CPDB]:[AIBN] = 1000:1:0.1) at 60 ^{o}C.

The FTIR analysis of the nanoparticles (Figure 4.8) confirmed the absence of the strong absorption peak at ~ 2900 cm^{-1}ascribed to the *tert*-butyl moiety after TMSBr treatment. In addition, the presence of a broad peak at ~ 3400 cm^{-1} ascribed to the

hydroxyl group in –COOH and the shift of the carbonyl stretch peak to 1700 cm^{-1} demonstrated the generation of grafted PMAA chains. The ^{1}H NMR (Figure 4.9) reveals the successful formation of the PMAA grafted nanoparticles after the TMSBr treatment. The disappearance of the peak at 1.4 ppm confirmed the complete removal of the *tert*-butyl group. The TGA demonstrated that the grafted PMAA (graft density: 0.23 chains/nm^2) accounted for 79.3% by weight difference measured at 40 ^{o}C and 900 ^{o}C (Figure 4.10), which was consistent with the UV analysis. Figure 4.10 also shows TGA in nitrogen of P*t*BuMA, P*t*BuMA-grafted sNPs. The weight loss for each sample was consistent with the grafting density and chemical modifications across different polymer molecular-weights investigated in this study. The TEM image illustrates the PMAA grafted silica nanoparticles were well dispersed and shows that the diameter of the individual nanoparticles was around 30 nm.

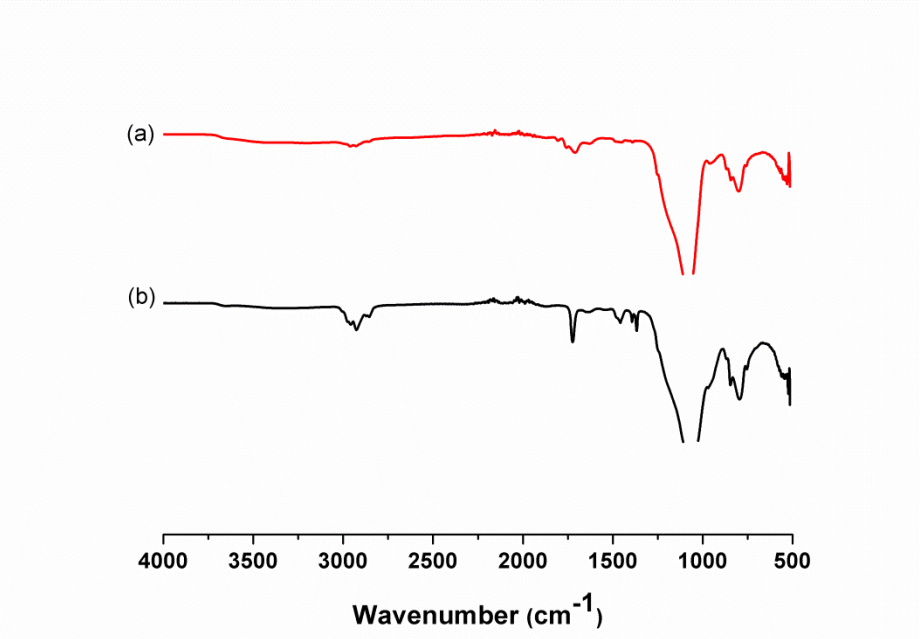

Figure 4.8 IR spectra of SiO_2-g-poly(*t*BuMA) (a) after and (b) before TMSBr treatment.

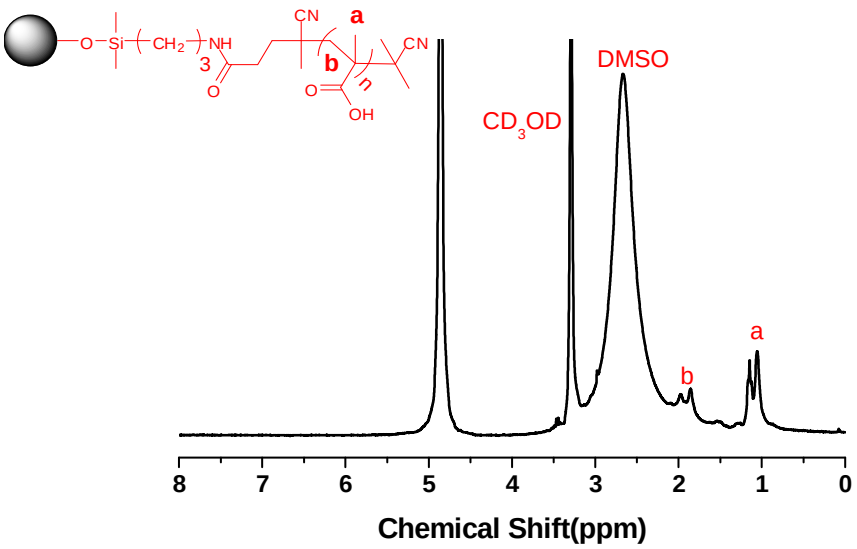

Figure 4.9 ^{1}H NMR spectra of PMAA grafted silica nanoparticles.

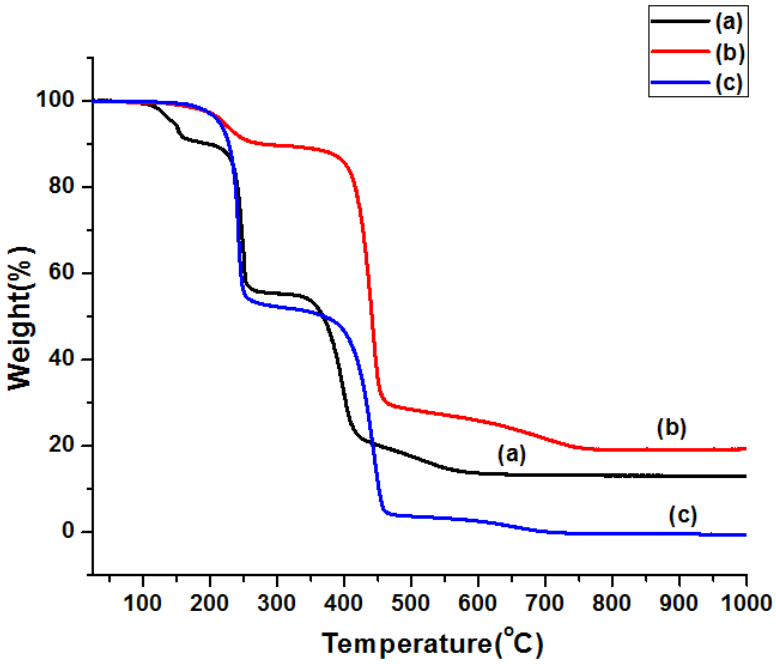

Figure 4.10 TGA in nitrogen: (a) poly(*tert*-butyl methacrylate), Mn=7000 g/mol; (b) poly(*tert*-butyl methacrylate) grafted silica nanoparticles without RAFT group chain end capped); (c) PMAA grafted silica nanoparticles.

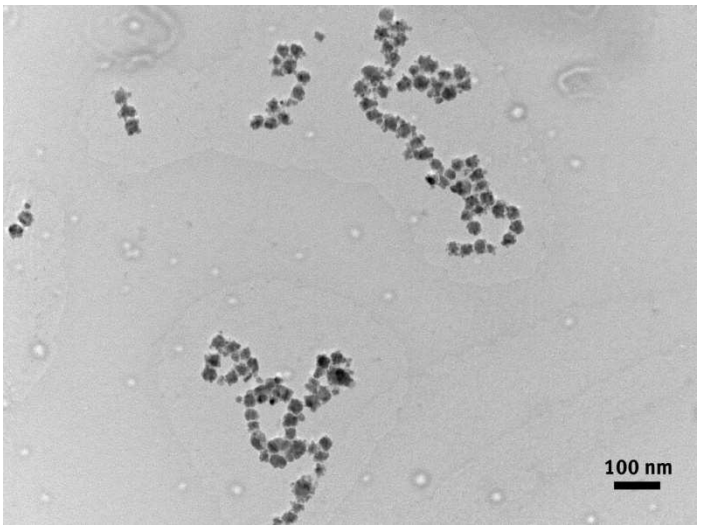

Figure 4.11 TEM image of poly(methacrylic acid) grafted silica nanoparticles.

4.3.4 Synthesis of dye-labeled PMAA grafted silica nanoparticles via direct polymerization of MAA

We found that surface-initiated RAFT polymerization of MAA directly on dye-labeled silica nanoparticles can be well controlled in DMF at 60 ^{o}C with a ratio between species of [MAA]:[CPDB]:[AIBN] = 1000:1:0.1 (Scheme 4.3). A small amount of 1,3,5-trioxane was added to the solution to monitor the monomer conversion by ^{1}H NMR (Figure 4.12). The spectra clearly showed an increase of proton peaks at 1.1 ppm and 1.9 ppm over time assigned to the anchored polymer backbone. The IR analysis of the nanoparticles (Figure 4.13) confirmed the presence of the strong absorption peak at ~ 2900 cm^{-1}ascribed to the methyl moiety after methylation. In addition, the disappearance of a broad peak at 3500 ~ 2500 cm^{-1} ascribed to the hydroxyl group in –COOH and the shift of the carbonyl stretch peak from 1700 cm^{-1} to 1725 cm^{-1} demonstrated the methylation of the anchored PMAA chains. The ^{1}H NMR spectra (Figure 4.14) shows the PMAA grafted silica nanoparticle before and after methylation by trimethylsilyldiazomethane. The appearance of the peak

at ~ 3.6 ppm ascribed to the new methyl group further confirms the successful methylation. The TGA demonstrated that the grafted PMAA accounted for 75% by weight difference measured at 31 ^{o}C and 1000 ^{o}C (Figure 4.15), which was consistent with the UV analysis. The dye-labeled PMAA grafted silica nanoparticle solution was yellow and transparent in dimethylsulfoxide (DMSO) (Figure 4.16). The nanoparticles were dispersed well in water as well (Figure 4.17). Under UV light with 365 nm wavelength, the nanoparticles showed very strong fluorescence. The TEM image (Figure 4.18) illustrates the dye-labeled PMAA grafted silica nanoparticles were well dispersed and shows that the diameter of the individual nanoparticles was around 30 nm.

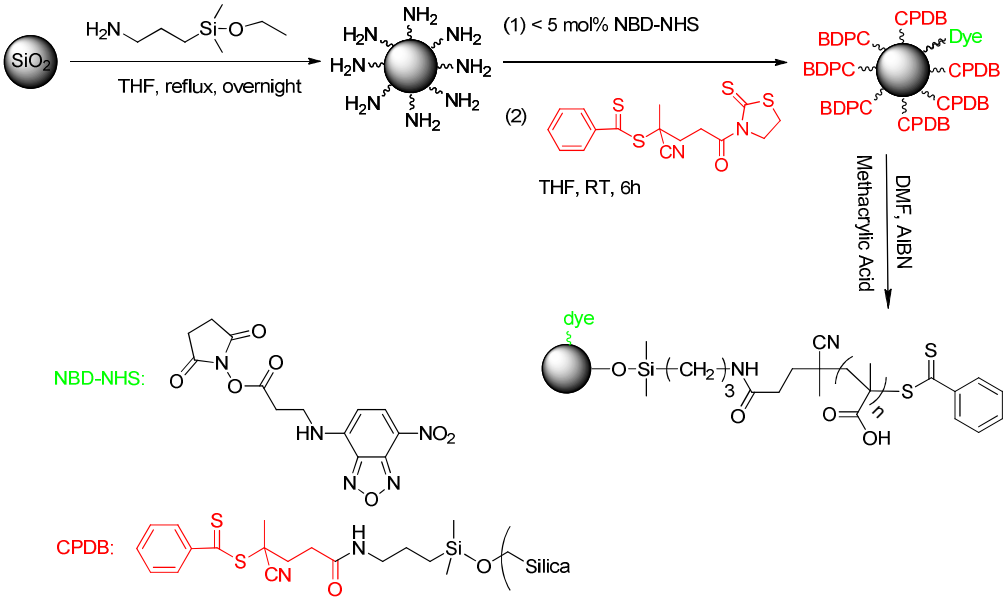

Scheme 4.3 Synthetic scheme for preparation of dye-labeled PMAA grafted silica nanoparticles via direct polymerization of MAA.

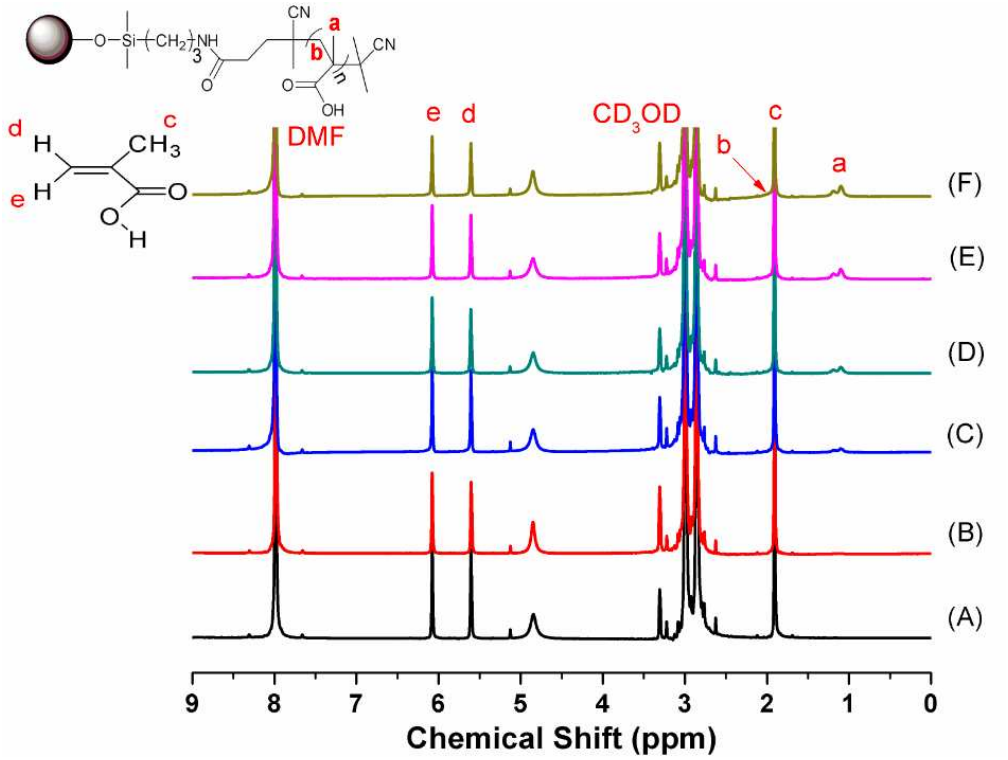

Figure 4.12 ^{1}H NMR spectra of PMAA grafted silica nanoparticles at different time in the kinetic study (for calculation of the conversion at certain time in the polymerization). (A): t=0 h; (B): t=1.58 h; (C): t=4.05 h; (D): t= 6 h; (E): t= 8.7 h; (F): t=10.82 h.

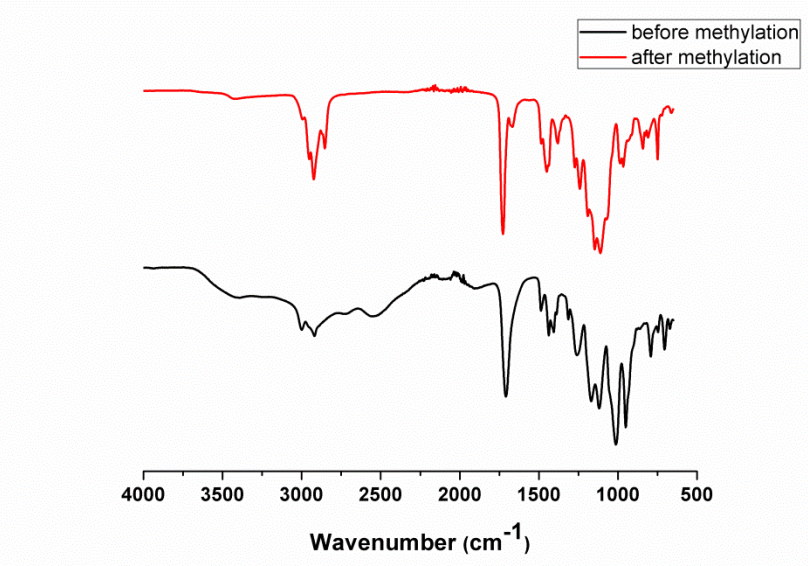

Figure 4.13 IR spectra of PMAA grafted silica nanoparticle before and after methylation by trimethylsilyldiazomethane.

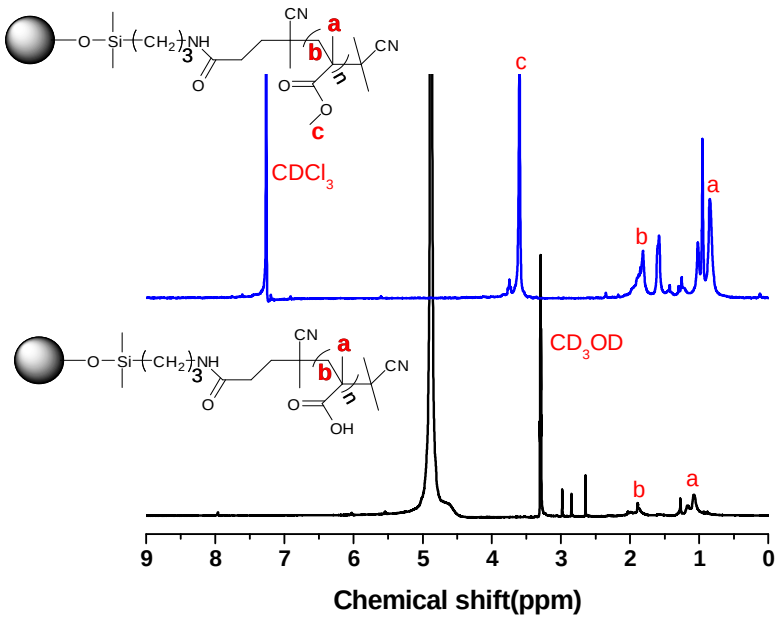

Figure 4.14 ^{1}H NMR of PMAA grafted silica nanoparticle before and after methylation by trimethylsilyldiazomethane.

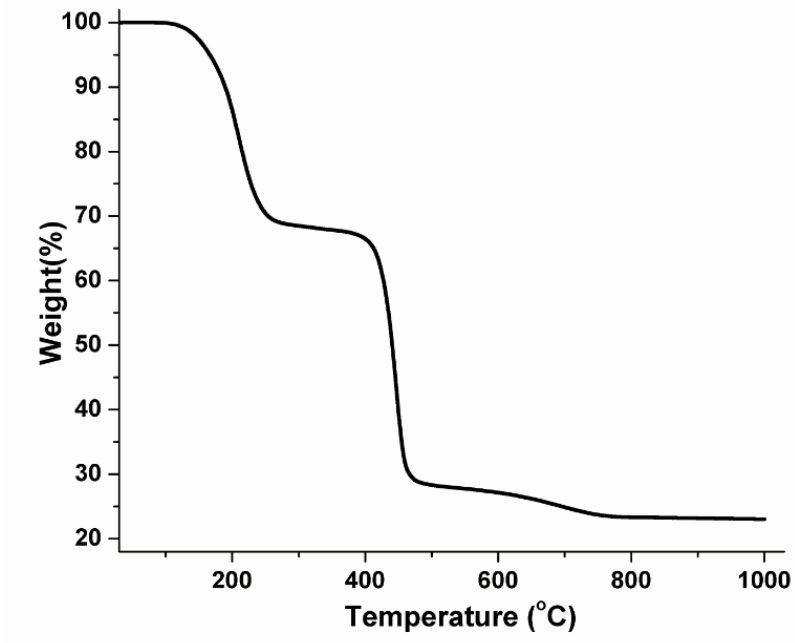

Figure 4.15 TGA of dye-labeled PMAA grafted silica nanoparticle.

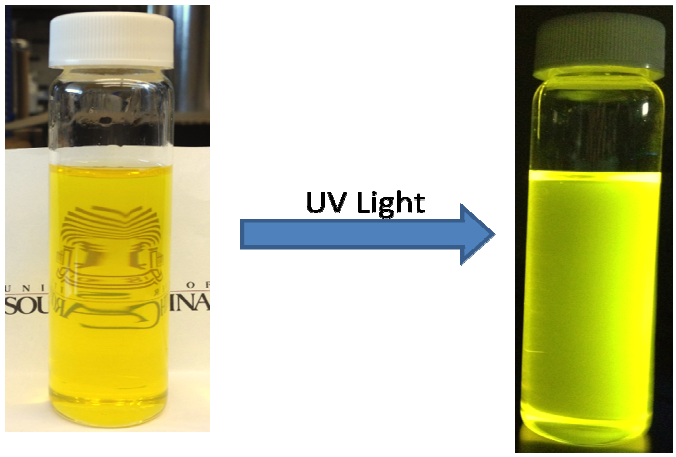

Figure 4.16 Photograph of dye-labeled PMAA grafted silica nanoparticles in DMSO.

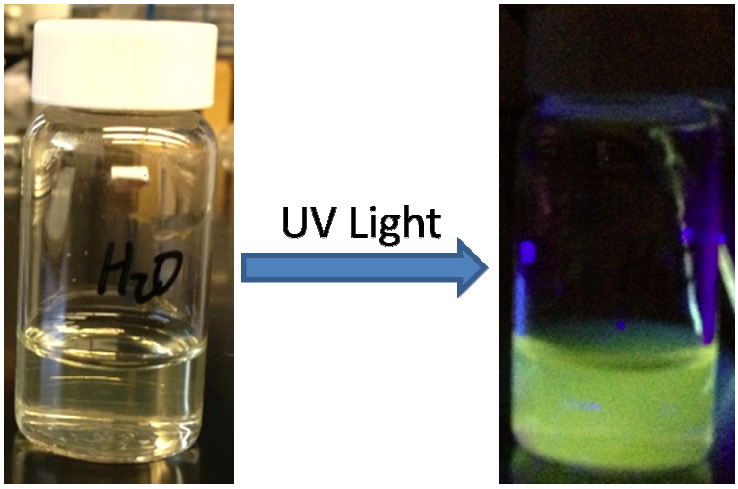

Figure 4.17 Photograph of dye-labeled PMAA grafted silica nanoparticles in water.

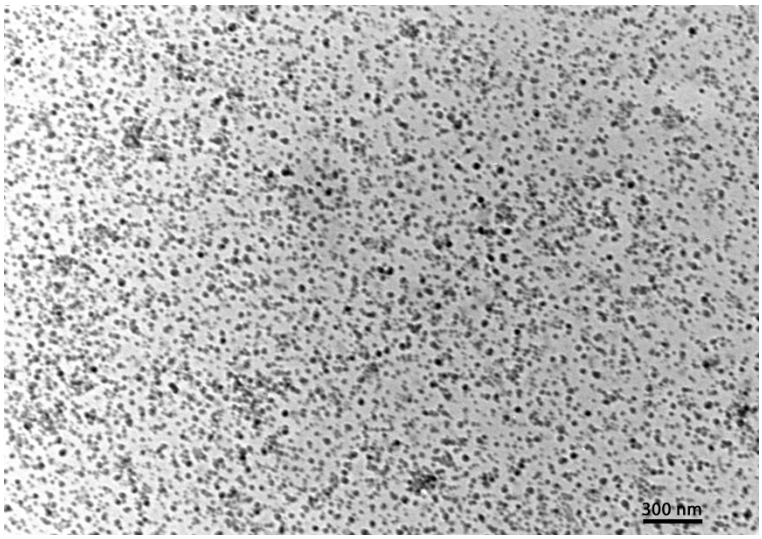

Figure 4.18 TEM of dye-labeled PMAA grafted silica nanoparticles. Size bar = 300 nm.

The kinetic study of surface-initiated RAFT polymerization of MAA on nanoparticles is shown in Figure 4.19. A linear relationship between $\ln(M_0/M_t)$ (where M_0 is the initial monomer concentration and M_t is the monomer concentration at time *t*) and polymerization time was observed, which implies a constant radical concentration. Additionally, the Mn determined by GPC of the methylated PMAA chains (calibrated with PMMA standards) increased linearly with monomer conversion and agreed closely with the theoretical molecular weight. The PDIs were approximately 1.1 during the polymerization. These features demonstrated the living/controlled nature of the RAFT polymerization of MAA mediated by CPDB surface anchored nanoparticles. We have previously demonstrated that we can achieve a variety of surface grafting densities of 0.01 – 0.68 chains/nm^2 using similar surface chemistry to anchor RAFT agents.[21,22] Thus, the surface-initiated RAFT polymerization of MAA was conducted on silica nanoparticles with a high surface density of 0.65 RAFT agents/nm^2, measured by UV-vis spectroscopy.[23] The molecular weight (M_n) of the attached PMAA chains was 41077 g/mol and the PDI was 1.11. Thus, a variety of PMAA brushes with controllable lengths and densities can be synthesized on silica nanoparticles using the direct surface-initiated polymerization approach and with grafting densities as high as 0.65 chains/nm^2.

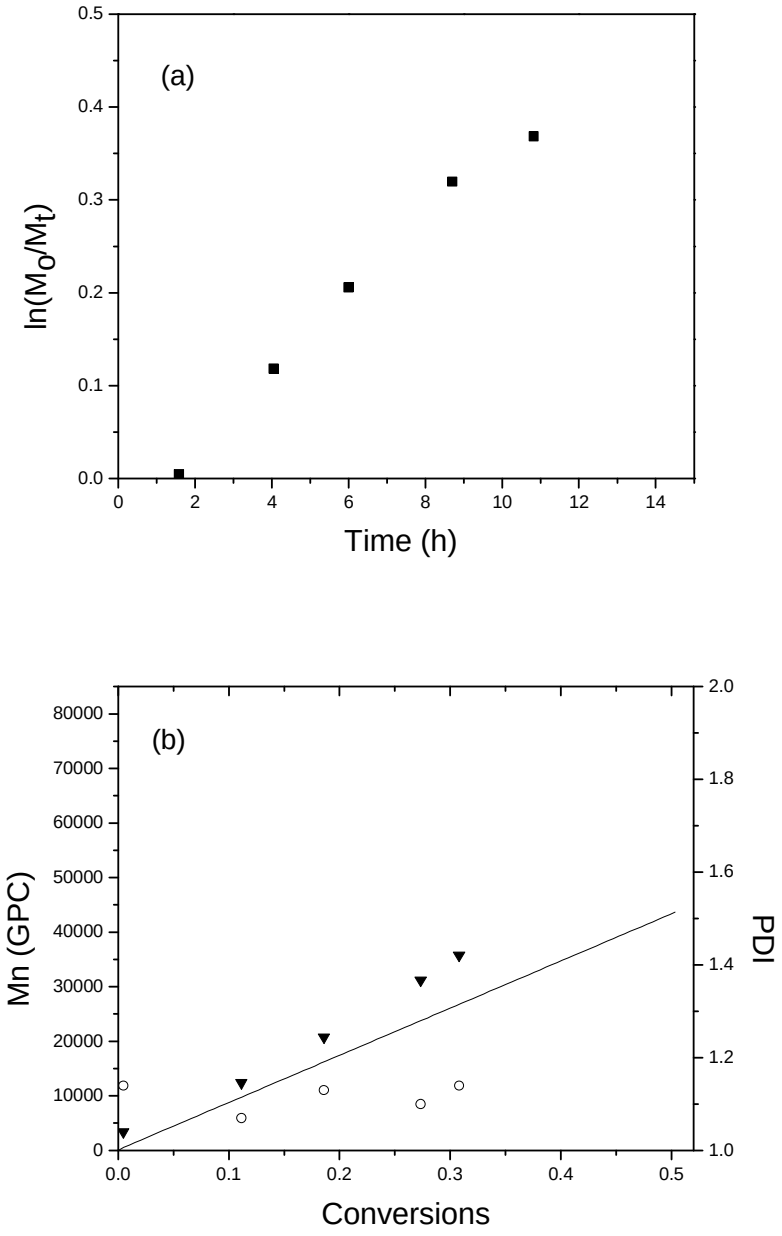

Figure 4.19 (a) Kinetic plot and (b) dependence of the GPC molecular weight (inverted triangle), theoretical molecular weight (solid line) and polydispersity (unfilled circles) on the conversion for the surface-initiated RAFT polymerization of methacrylic acid ([MAA]:[CPDB]:[AIBN] = 1000:1:0.1).

Compared to our initial synthetic strategy, the direct polymerization of MAA on dye-labeled CPDB coated silica nanoparticles is more straightforward. It also prevents the loss of nanoparticles that occurs in the washing processes after each step in the reaction

scheme. These concerns are critical for small diameter nanoparticles which are particularly prone to agglomeration. These challenges are largely addressed by the direct polymerization approach described herein. The kinetic study demonstrated the living/controlled nature of the RAFT polymerization of MAA on small diameter nanoparticle surfaces. The dye-labeled PMAA grafted silica nanoparticles generated in this process dispersed well in DMF and DMSO and were stable in these solvents for more than six months.

4.4 Summary

In conclusion, we demonstrated two methods for the synthesis of dye-labeled PMAA or poly(carboxylic acid) grafted silica nanoparticles. In the first synthetic strategy, "one-pot" click reactions between PAHMA grafted silica nanoparticles and alkyne functionalized molecules (alkyne based coumarin 343 fluorescent dye and 4-pentynoic acid) were conducted to prepare dye-labeled poly(carboxylic acid) grafted silica nanoparticles. In the second strategy, dye-labeled CPDB coated silica nanoparticles were prepared by treating amino functionalized nanoparticles with activated dyes and followed by activated CPDB. Then surface-initiated RAFT polymerization of *t*BuMA was conducted followed by sequential removal of thiocarbonylthio end groups and *tert*-butyl groups to generate dye-labeled PMAA grafted silica nanoparticles. The second method of direct surface-initiated RAFT polymerization of MAA on small size (15 nm) nanoparticles is more straightforward. A variety of PMAA brushes with different lengths and densities were prepared on nanoparticles with excellent control and surface grafting densities as high as 0.65 chains/nm^2. The synthesis of the dye-labeled PMAA grafted silica nanoparticle was confirmed by FTIR, TGA, ^{1}H NMR analysis and TEM. The dye-

labeled PMAA grafted silica nanoparticles provide a platform to bind biologically active molecules and to monitor the presence and movement of the nanoparticles for bioapplications.

4.5 Reference

1. Hollman, A. M.; Scherrer, N. T.; Cammers-Goodwin, A.; Bhattacharyya, D. *J. Membr. Sci.* **2004**, *239*, 65-79.
2. Chen, H.; Hsieh, Y. L. *Biotechnol. Bioeng.* **2005**, *90*, 405-413.
3. Moya, S.; Azzaroni, O.; Farhan, T.; Osborne, V. L.; Huck, W. T. S. *Angew. Chem., Int. Ed.* **2005**, *44*, 4578-4581.
4. Tugulu, S.; Arnold, A.; Sielaff, I.; Johnsson, K.; Klok, H.-A. *Biomacromolecules* **2005**, *6*, 1602-1607.
5. Treat, N. D.; Ayres, N.; Boyes, S. G.; Brittain, W. J. *Macromolecules* **2006**, *39*, 26-29.
6. Wu, T.; Gong, P.; Szleifer, I.; Vlček, P.; Šubr, V.; Genzer, J. *Macromolecules* **2007**, *40*, 8756-8764.
7. Li, D.; Sheng, X.; Zhao, B. *J. Am. Chem. Soc.* **2005**, *127*, 6248-6256.
8. Cash, B.; Wang, L.; Benicewicz, B. *J. Polym. Sci., Part A: Polym. Chem.* **2012**, *50*, 2533-2540.
9. Hojjati, B.; Sui, R.; Charpentier, P. A. *Polymer* **2007**, *48*, 5850-5858.
10. Inoue, M.; Fujii, S.; Nakamura, Y.; Iwasaki, Y.; Yusa, S. *Polym. J.* **2011**, *43*, 778-784.
11. Klevens, R. M.; Edwards, J. R.; Richards, C. L.; Horan, T. C.; Gaynes, R. P.; Pollock, D. A.; Cardo, D. M. *Publ. Hlth. Rep.***2002**, *122*, 160-165.
12. Santra, S.; Xu, J.; Wang, K.; Tan, W. *J. Nanosci. Nanotechnol.* **2004**, *4*, 590-599.
13. Chen, C.; Geng, J.; Pu, F.; Yang, X.; Ren, J.; Qu, X. *Angew. Chem., Int. Ed.* **2011**, *50*, 882-886.
14. De, M.; Ghosh, P.; Rotello, V. *Adv. Mater.* **2008**, *20*, 4225-4241.
15. Yao, G.; Wang, L.; Wu, Y.; Smith, J.; Xu, J.; Zhao, W.; Lee, E.; Tan, W. *Anal. Bioanal. Chem.* **2006**, *385*, 518-524.
16. Wu, T.; Zou, G.; Hu, J.; Liu, S. *Chem. Mater.* **2009**, *21*, 3788-3798.
17. Pothayee, N.; Pothayee, N.; Jain, N.; Hu, N.; Balasubramaniam, S.; Johnson, L.; Davis, R.; Sriranganathan, N.; Riffle, *J. Chem. Mater*. **2012**, *24*, 2056-2063.
18. Li, C.; Benicewicz, B. C. *Macromolecules* **2005**, *38*, 5929-5936.
19. Couvreur, L.; Lefay, C.; Belleney, J.; Charleux, B.; Guerret, O.; Magnet, S. *Macromolecules* **2003**, *36*, 8260-8267.
20. Li, Y.; Benicewicz, B. C. *Macromolecules* **2008**, *41*, 7986-7992.
21. Douglas, D.; Li, Y.; Lewis, S.; Benicewicz, B.; Schadler, L.; Kumar S. K. *Macromolecules* **2010**, *43*, 1564-1570.
22. Akcora, P.; Liu, H.; Kumar, S. K.; Moll, J.; Li, Y.; Benicewicz, B. C.; Schadler, L. S.; Acehan, D.; Panagiotopoulos, A. Z.; Pryamitsyn, V.; Ganesan, V.; Ilavsky, J.; Thiyagarajan, P.; Colby, R. H.; Douglas, J. F. *Nat. Mater.* **2009**, *8*, 354-359.

23. Li, C.; Han, J.; Ryu, C. Y.; Benicewicz, B. C. *Macromolecules* **2006**, *39*, 3175-3183.

CHAPTER 5

PREPARATION AND CHARACTERIZATION OF RECYCLABLE MAGNETIC NANOPARTICLES WITH SURFACE-GRAFTED POLY(METHACRYLIC ACID) VIA RAFT POLYMERIZATION

5.1 Introduction

Magnetic nanoparticles with controlled size and high magnetization are important materials with wide application in magnetic recording, magnetic resonance imaging (MRI), drug delivery and therapeutics.[1,2] However, there are some problems with the application of bare iron oxide nanoparticles in these applications, such as easy aggregation, quick biological-caused decomposition and the environmentally induced loss of the magnetic properties.[3] Silica coated iron oxide magnetic nanoparticles provide a biocompatible silica shell, which can effectively protect the iron oxide in biological systems and preserve the magnetic properties. The silica coating is also a convenient platform for subsequent surface functionalization via a powerful silica surface chemistry toolbox.

Many of the biomedical applications require that the sizes of the magnetic nanoparticles are smaller than 100 nm with a low polydispersity and that the particles are superparamagnetic. Usually, small size magnetic nanoparticles can be completely secreted from the human body through the kidneys. Thus, the synthesis of functionalized

magnetic nanoparticles with a small size and high stability is an ongoing challenge.

There are several traditional methods to prepare iron oxide nanoparticles, namely thermal decomposition of iron (Fe^{3+}) chelates at high temperature in high boiling point organic solvents[2] and coprecipitation of Fe^{2+} and Fe^{3+} salts in basic aqueous solutions.[1] The nanoparticles prepared by the former method possess high saturation magnetization, however the high temperature used in the synthesis (usually above 200 ^{o}C) is an obstacle for scale-up fabrication, especially for industrial applications. The coprecipitation method generally leads to larger size nanoparticles (above 20 nm). In this work, a modified coprecipitation strategy was employed to synthesize Fe_3O_4/ SiO_2 superparamagnetic nanoparticles with a ~10 nm size using mild synthetic conditions while maintaining a high saturation magnetization.

As a significant controlled radical polymerization (CRP) technique, reversible addition-fragmentation chain transfer (RAFT) polymerization has been widely applied to synthesize polymers in a controlled manner (controllable molecular weight and low polydispersities).[4,5] RAFT polymerization has emerged as a powerful tool to modify nanoparticle surfaces to prepare polymer grafted nanoparticles with significant advantages, such as applicability to many radical polymerizable monomers, low metal contamination in the final polymer, and mild polymerization conditions.[6-10] Polymer grafted nanoparticles have important applications in biomedical areas such as drug delivery and tumor therapy.[11]

Poly(methacrylic acid) (PMAA) represents an important class of pH-responsive polymers and has been used in membrane transport,[12] coatings,[13] sensors[14] and biomedical applications.[15] There are a few reports about the surface functionalization of

nanoparticles with PMAA or other multi-acid containing polymers. Some research groups reported the strategy of deprotection of surface attached poly(*tert*-butylacrylate) or poly(*tert*-butylmethacrylate).[16-19] However, the deprotection of *tert*-butyl moiety is tedious and usually uses harsh conditions which may cleave the surface attached polymers. The direct surface-initiated polymerization of acid containing monomers on particles has been reported by very few groups.[20,21] However, these particles are very large (up to 11 μm diameter) and are not appropriate for many biomedical applications. Direct surface-initiated polymerization of acid containing monomers on small size nanoparticles while maintaining good dispersibility is critical and also a challenge for biomedical applications. Surface-initiated RAFT polymerization provides a convenient technique which can be used to precisely control the PMAA chain lengths and densities on surfaces while other CRP techniques (*e.g.* ATRP) cannot be used for this acid containing monomer due to catalyst poison issues.[22,23] In this work, we report the investigation of the direct polymerization of MAA on small size (10 nm) Fe_3O_4/SiO_2 magnetic nanoparticles via surface-initiated RAFT polymerization while maintaining good dispersibility in solutions.

The significantly growing phenomenon of bacterial resistance to antibiotics causes high morbidity and mortality, which is an extremely critical problem in the healthcare area.[24] A variety of antibiotics used over several decades, such as penicillin, become much less active or inactive to bacterial strains. Nanoparticles have been used as drug delivery materials because of their unique properties, such as high specific surface area, nano-size effects and easy surface engineering to introduce new functionalities.[25]

Magnetic nanoparticles have exhibited a variety of advantages in biomedical applications.[1,2] The unique property of stimulus response under magnetic fields can be used to direct the antibiotic attached magnetic nanoparticles to penetrate complicated bacterial environments, such as biofilms, which are much more resistant to antibiotics than individual bacteria. The delivery platform of nanoparticles can be easily recycled via a magnet without leaving residual nanomaterials in the environment which avoids public health concerns. Magnetic particles have been widely used as drug delivery vehicles to eukaryote cells, however there are few reports for applications to bacterial cells. In addition, the recyclability of the delivery vehicles in bacterial system has not yet been reported yet. Thus, in this work, we used PMAA grafted magnetic nanoparticles as a recyclable platform, with high surface area to volume ratio, to deliver large amounts of penicillin-G and examined their effectiveness in killing bacteria. The recyclability of the magnetic particles is also discussed. The small-size water soluble PMAA grafted Fe_3O_4/ SiO_2 magnetic nanoparticles also have great potential in applications such as MRI, multiple drug delivery and therapeutics.

5.2 Experimental

5.2.1 Materials

All chemicals were obtained from Fisher or Acros and used as-received unless otherwise specified. Trimethylsilyldiazomethane (2.0 M in hexanes) was purchased from TCI. 4-Cyanopentanoic acid dithiobenzoate (CPDB) was obtained from Strem Chemical Inc. CPDB immobilized silica nanoparticles were synthesized according to the literature.[26] 3-Aminopropyldimethylethoxysilane was obtained from Gelest and used as

received. Methacrylic acid (99.5%, Acros) was purified by passing through an activated neutral alumina column. AIBN was recrystallized from methanol before use.

5.2.2 Instrumentation

^{1}H NMR (Varian Mercury spectrometer 300/400) was conducted using CD_3OD as the solvent. Molecular weights and PDI were determined using a gel permeation chromatography (GPC) equipped with a 515 HPLC pump, a 2410 refractive index detector, and three Styragel columns. The columns consisted of HR1, HR3 and HR4 in the effective molecular weight ranges of 100-5000, 500-30000, and 5000-500000, respectively. The GPC used THF as eluent at 30 °C and a flow rate of 1.0 mL/min and was calibrated with poly(methyl methacrylate) or polystyrene standards obtained from Polymer Laboratories. The PMAA grafted nanoparticles were methylated by trimethylsilyldiazomethane[27] and then cleaved by HF before GPC analysis. Samples were filtered through microfilters with a pore size of 0.2 μm before injection. Infrared spectra were recorded with a PerkinElmer Spectrum 100 spectrometer. UV-vis spectra were measured with a Perkin-Elmer Lambda 4C UV-vis spectrophotometer. TEM images were examined using a Hitachi 8000 transmission electron microscope with an operating voltage of 200 kV. Carbon-coated copper grids were used to prepare samples by dropping sample solutions on the grids followed by drying in a fume hood before use. XRD characterization was conducted using a Rigaku D/Max 2100 Powder X-ray Diffractometer with Cu Kα radiation. The saturation magnetization of nanoparticles was determined using a Vibrating Sample Magnetometer (VSM). Tapping mode AFM measurements were operated using a Multimode Nanoscope III system (Digital Instruments, Santa Barbara, CA). The characterization was conducted using commercial

Si cantilevers with a spring constant and resonance frequency of 20–80 N m^{-1} and 230–410 kHz respectively. The sample of PMAA grafted nanoparticles was prepared via spin-coating on silicon wafers with a speed of 3000 rpm. TGA measurement was conducted using a TA Instruments Q5000 with a heating rate of 10°C/min form 25°C to 950°C under nitrogen flow.

5.2.3 Synthesis of Fe_3O_4/SiO_2 Magnetic Nanoparticles

Two methods were employed to prepare Fe_3O_4/SiO_2 magnetic nanoparticles. The first method was a microemulsion strategy reported previously.[3] The second method was based on the following procedure: 6.94 g $FeCl_3$ and 6.04 g $FeSO_4 \cdot 7H_2O$ were dissolved in 400 mL N_2 purged DI water. To this solution was added slowly 15 mL 29 wt% NH_4OH at 90 °C under N_2 protection. Then, 9 mL oleic acid was added dropwise 1 hour later and the resulting solution was stirred at 90 °C for 2 hours. The solution was precipitated into a large amount of acetone to remove extra oleic acid. Then, Triton X-100 (2.5 mL) and 42 mL cyclohexane were added to a 250 mL round-bottom flask. After sonication for 1 min, 1 mL above prepared cyclohexane solution of Fe_3O_4 with a concentration of 22.4 mg/mL and 350 µL 29 wt% NH_4OH were added slowly to the stirring solution at room temperature (RT). TEOS was added slowly and the resulting solution was stirred at RT for 18 hours. The final solution was washed with methanol to remove the surfactant by precipitation and centrifugation at 4000 rpm for 5 min, which was repeated 4 times.

5.2.4 Synthesis of Amino-Functionalized Fe_3O_4/SiO_2 Magnetic Nanoparticles

3-Aminopropyldimethylethoxysilane (1.29 g, 8.0 mmol) was added to Fe_3O_4/SiO_2 nanoparticles (approx. 112 mg) dispersed in dry DMF (15 mL). The reaction mixture was stirred at 75 °C overnight under N_2 protection. The solution was precipitated into diethyl ether (200 mL), centrifuged at 3000 rpm for 5 minutes, and redispersed in dry THF. The solution was precipitated again into hexane and redispersed in dry THF for further use.

5.2.5 Synthesis of CPDB-Functionalized Fe_3O_4/SiO_2 Magnetic Nanoparticles

Activated CPDB (202.4 mg, 532 mmol) was dissolved in dry THF (10 mL). The above amino-functionalized nanoparticles (approx. 110 mg, in 20 mL THF) were added slowly and the resulting solution was stirred at RT overnight. After the reaction, the solution was precipitated into cyclohexane and ethyl ether mixture. (200 mL, cyclohexane : ethyl ether = 4 : 1), centrifuged at 3000 rpm for 5 minutes, and redispersed in dry DMF. The solution was precipitated again into ethyl ether and redispersed in dry DMF. This procedure was repeated several times until the supernatant solution was colorless after centrifugation. The final nanoparticles were dispersed in dry DMF for further usage.

5.2.6 Surface-Initiated RAFT Polymerization of Methacrylic Acid from CPDB Anchored Fe_3O_4/SiO_2 Nanoparticles

Methacrylic acid (0.99 mL, 1.17×10^{-2} mol), CPDB coated Fe_3O_4/SiO_2 nanoparticles (17 mg) and dry DMF (2.88 mL) were added to a 20 mL Schlenk tube. After sonication for 1 min, AIBN (233 μL, 5mM in DMF) was added. The solution was degassed by four

freeze-pump-thaw cycles, filled with nitrogen, and then placed in an oil bath of 65 °C for various intervals. The polymerization was stopped by quenching in ice water.

5.2.7 Methylation of PMAA Grafted Fe_3O_4/SiO_2 Nanoparticles

The procedure was similar to the literature.[27]

5.2.8 Cleavage of Grafted PMMA (After Methylation) from Fe_3O_4/SiO_2 Nanoparticles

The procedure was similar to the literature.[23]

5.2.9 Synthesis of PenG-Nanoparticle Complex

33 µl of PMAA grafted nanoparticles (35 mg/ml) was added to 500 µl of Penicillin solution (1 mg/ml), followed by an incubation at 28 ^oC with shaking (186 rpm) for 2 hours. The resulting PenG-nanoparticle complex was collected and washed via Amicon centrifuge tubes.

5.2.10 Bacteria Inhibition Efficiency Determination

10 µl of *E. coli* suspensions were added into 2 mL TSB solutions at 37°C for incubation overnight. Three tubes of the same bacterial culture solutions were prepared. Tube 1 was used as blank group without adding any PenG or nanoparticles. Tube 2 was employed to test the activity of free PenG. 50 µl of PenG-nanoparticle complex was added to Tube 3 before incubation. Bacterial growth was measured at OD_{600}, and was compared to the Tube 1. Thus, the inhibition efficiency was calculated as follows: inhibition efficiency (%) = (Sample OD_{600}/Background OD_{600}) × 100. The Background OD_{600} was determined from Tube 1.

5.3 Results and Discussion

5.3.1 Synthesis and Characterization of Fe_3O_4/SiO_2 Magnetic Nanoparticles

Table 5.1 The Microemulsion Method for Preparation of Fe_3O_4/SiO_2 Magnetic Nanoparticles

Group	Microemulsion	Surfactant (Triton X-100)	Solvent (oil) cyclohexane	Cosurfactant (*n*-hexanol)	Water (µL)	TEOS (µL)	$FeCl_3$ (0.15 M)	$FeSO_4$ (0.1 M)	NH_4OH (29 wt%)
A	ME1	5.3 mL	22.5 mL	5.4 mL	620	10	500 µL	500 µL	
	ME2	5.3 mL	22.5 mL	5.4 mL	810	10			810 µL
B	ME1	5.3 mL	22.5 mL	5.4 mL	620	100	500 µL	500 µL	
	ME2	5.3 mL	22.5 mL	5.4 mL	810	100			810 µL
C	ME1	5.3 mL	22.5 mL	5.4 mL	620	50	500 µL	500 µL	
	ME2	5.3 mL	22.5 mL	5.4 mL	810	50			810 µL
D	ME1	5.3 mL	22.5 mL	5.4 mL	620	10	1000 µL	1000 µL	
	ME2	5.3 mL	22.5 mL	5.4 mL	810	10			810 µL
E	ME1	5.3 mL	22.5 mL	5.4 mL	1240	10	500 µL	500 µL	
	ME2	5.3 mL	22.5 mL	5.4 mL	1620	10			810 µL

The Fe_3O_4/SiO_2 magnetic nanoparticles were synthesized by two methods. The first strategy was a microemulsion method employing the mixing of two separate microemulsions (ME1 and ME2) resulting in the formation of nanoparticles. ME1 had Triton X-100, cyclohexane, *n*-hexanol, water, TEOS, $FeCl_3$ and $FeSO_4$, while ME2 contained Triton X-100, cyclohexane, *n*-hexanol, water, TEOS and the base (NH_4OH). A variety of Fe_3O_4/SiO_2 nanoparticles were prepared according to the first strategy

(microemulsion) using the recipes in the Table 5.1, which were similar to reports in the literature.[3]

In Table 5.1, the group A was chosen as the standard recipe to prepare Fe_3O_4/SiO_2 nanoparticles. The Fe_3O_4/SiO_2 nanoparticle solution using recipe A was light brown and transparent (Figure 5.1). The TEM image (Figure 5.2) illustrates that the Fe_3O_4/SiO_2 nanoparticles were well dispersed and shows that the diameter of the individual nanoparticles was approximately 11 nm. In order to tailor the proportion of iron oxide and silica, the recipes were systematically varied (Group B-D) with different amounts of Fe(III), Fe(II) salts and TEOS, as listed in Table 5.1. The colors of the nanoparticles corresponding to each recipe are shown in Figure 5.3 and varied from dark brown to light yellow. The lighter color of the magnetic nanoparticles was observed in compositions containing higher amounts of TEOS. The nanoparticles with 10X TEOS usage have higher weight loss (18.6%) compared to the particles with 5X TEOS usage (17.3% weight loss) at 940 ^oC in TGA analysis. Increasing the proportion of TEOS would be helpful to enhance the SiO_2 part of the nanoparticles. In this water-in-oil microemulsion strategy, it has been reported that the amount of water is critical in determining the size of water-in-oil microemulsions,[28] which will further affect the size of magnetic nanoparticles. Thus, to investigate the influence of the amount of water on the size of nanoparticles, an altered recipe (Group E in Table 5.1) was employed. The TEM image (Figure 5.4) illustrates the Fe_3O_4/SiO_2 nanoparticles were well dispersed and showed that the diameter of the individual nanoparticles was around 12 nm, which is almost the same as the nanoparticles prepared by the standard recipe (Group A in Table 5.1). Thus, the influence of the amount of water over the nanoparticle size was not observed in the water

range listed in the Table 5.1. Even though well dispersed nanoparticles were obtained using the microemulsion method, the nanoparticles did not have high saturation magnetization (less than 5 emu/g) and strong magnetic responses, similar to other Fe_3O_4/SiO_2 magnetic nanoparticles.[3] Thus, we were motivated to develop a new strategy to prepare Fe_3O_4/SiO_2 magnetic nanoparticles with high magnetization, excellent dispersity, and small size.

Figure 5.1 Photograph of Fe_3O_4/SiO_2 magnetic nanoparticles prepared via the microemulsion method.

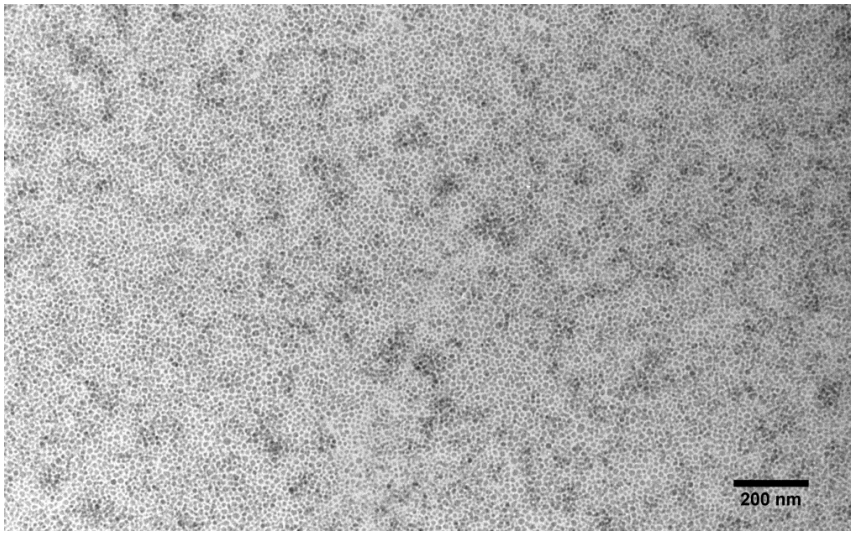

Figure 5.2 TEM of Fe_3O_4/SiO_2 nanoparticles prepared by microemulsion method with the standard recipe (Group A in Table 5.1).

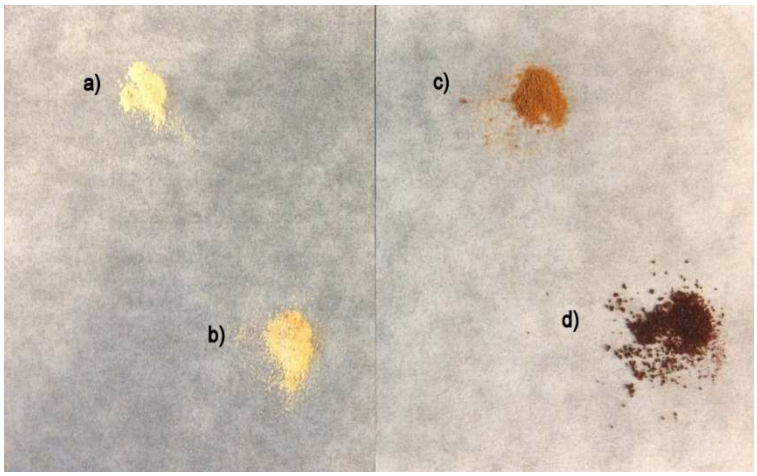

Figure 5.3 Photograph of Fe_3O_4/SiO_2 nanoparticles prepared via microemulsion method: a)10X TEOS of the standard recipe; b) 5X TEOS of the standard recipe; c) Standard Recipe; d) 2X iron of the standard recipe.

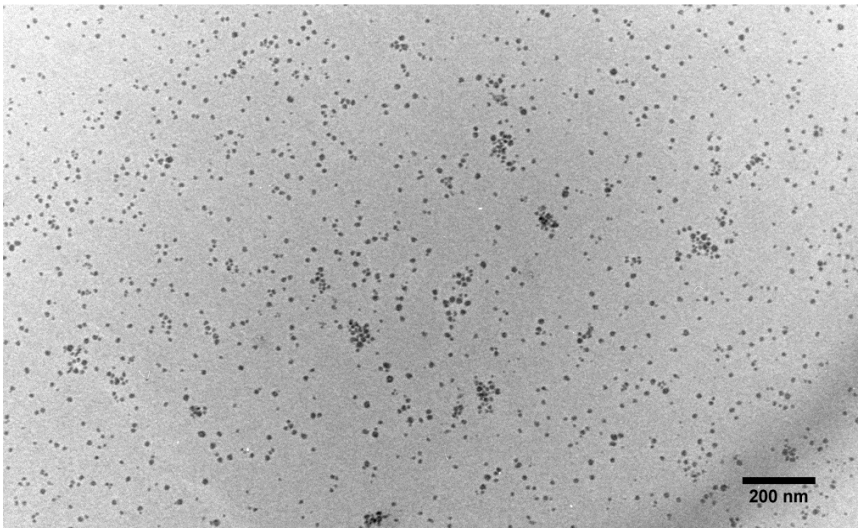

Figure 5.4 TEM of Fe_3O_4/SiO_2 nanoparticles prepared by the recipe with 2X water (Group E in Table 5.1).

The second strategy was based on the coprecipitation of Fe^{2+} and Fe^{3+} salts in basic aqueous solutions at low temperature to form nanoparticles. Fe(III) and Fe(II) salts were coprecipitated with NH_4OH at 90 ^oC to form iron oxide nanoparticles followed by the hydrolysis of TEOS on the Fe_3O_4 nanoparticle surface to form Fe_3O_4/SiO_2 magnetic nanoparticles. The XRD pattern (Figure 5.5) confirmed the non-crystalline SiO_2 shell

ascribed to the broad peak at 10° – 30° and the cubic spinel structure of Fe_3O_4 due to the strong diffraction peaks at 30.1°, 35.6°, 43.2°, 53.9°, 57.2, 62.8°, and 74.2° which were indexed to (220), (311), (400), (422), (511), (440) and (533) planes. The IR analysis of Fe_3O_4 (Figure 5.6) confirmed the absorption peaks at 2924 cm^{-1}, 2854 cm^{-1}, and 1710 cm^{-1} ascribed to the $–CH_2$ and C=O of Fe_3O_4 surface physically absorbed oleic acid respectively. The peak at 1409 cm^{-1}revealed chemically bound oleic acid on Fe_3O_4 ascribed to the stretch of COO^- resulting from the coordination with iron of Fe_3O_4.[29] The IR spectra of Fe_3O_4/SiO_2 demonstrated the existence of SiO_2 after surface hydrolysis of TEOS on Fe_3O_4 nanoparticles based on the appearance of strong absorption peaks at 1135 cm^{-1}, 1056 cm^{-1}, 947 cm^{-1} and 805 cm^{-1}. The magnetic nanoparticle solution was dark brown and the nanoparticle powder (after washing and drying) was capable of lifting a medium size (1.5 cm diameter, 0.9 cm thickness) magnet off the ground, which qualitatively demonstrated the high magnetic moment of the as-synthesized magnetic nanoparticles (Figure 5.7). A vibrating sample magnetometer (VSM) was employed to determine the magnetization strength of the magnetic nanoparticles (Figure 5.8). The VSM measurement demonstrated the superparamagnetivity of both Fe_3O_4 and Fe_3O_4/SiO_2 nanoparticles with a high magnetic moment of 59.5 emu/g and 29.1 emu/g respectively. The silica coated nanoparticles possess a lower magnetic moment than the bare Fe_3O_4, which is consistent with reports from other groups.[3] The TGA showed that the weight loss of Fe_3O_4/SiO_2 nanoparticles (after the addition of SiO_2 on Fe_3O_4) was 35% at 900 ^oC, which is significantly higher than the 24% of bare Fe_3O_4 nanoparticles (Figure 5.9). The TEM image (Figure 5.10) illustrates the Fe_3O_4/SiO_2 nanoparticles were well dispersed. The average diameter of the Fe_3O_4/SiO_2 nanoparticles was around 10 nm. Compared to

the traditional thermal decomposition of Fe(III) chelate in high boiling point solvent (>200 ^{o}C) strategy, [2] this method uses much more mild synthetic conditions and still provides high-magnetization superparamagnetic nanoparticles with a small size.

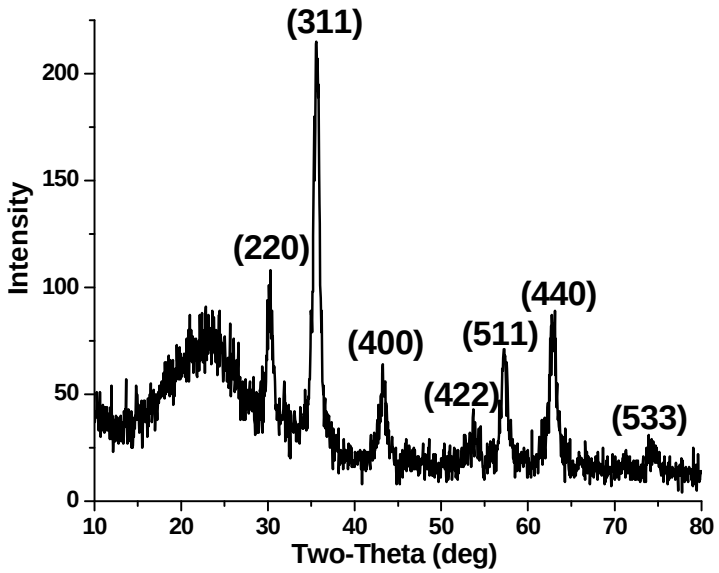

Figure 5.5 XRD of Fe_3O_4/SiO_2 magnetic nanoparticles.

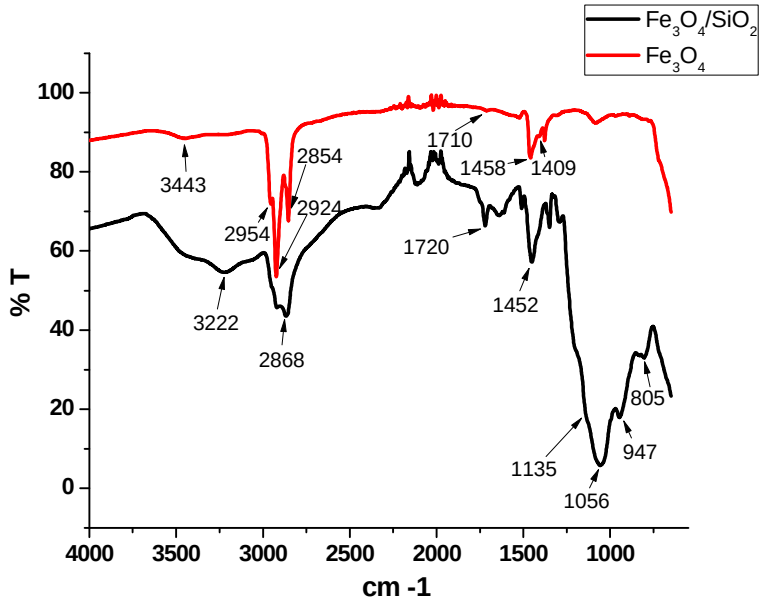

Figure 5.6 IR of Fe_3O_4/SiO_2 and Fe_3O_4 magnetic nanoparticles.

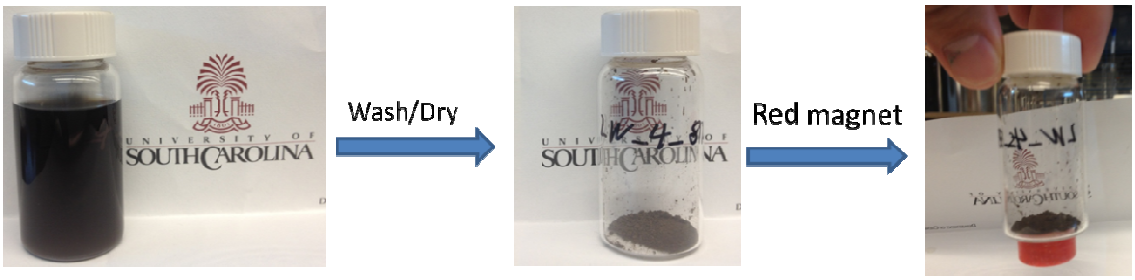

Figure 5.7 General procedure of fabrication of Fe_3O_4/SiO_2 magnetic nanoparticles.

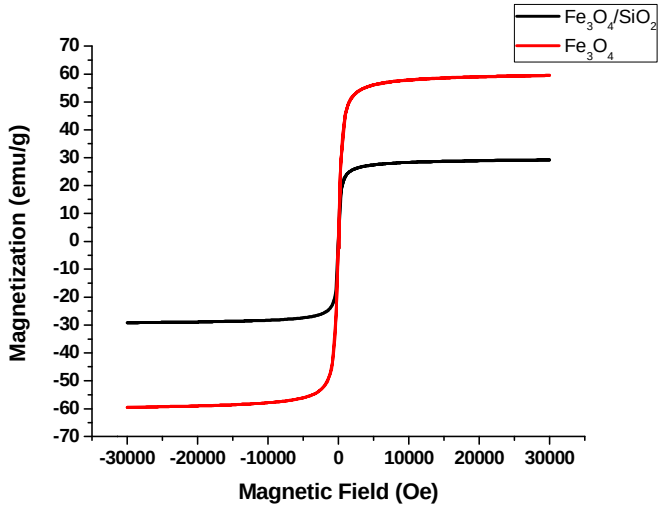

Figure 5.8 VSM of superparamagnetic Fe_3O_4 nanoparticles (59.5 emu/g) and Fe_3O_4/SiO_2 nanoparticles (29.1 emu/g).

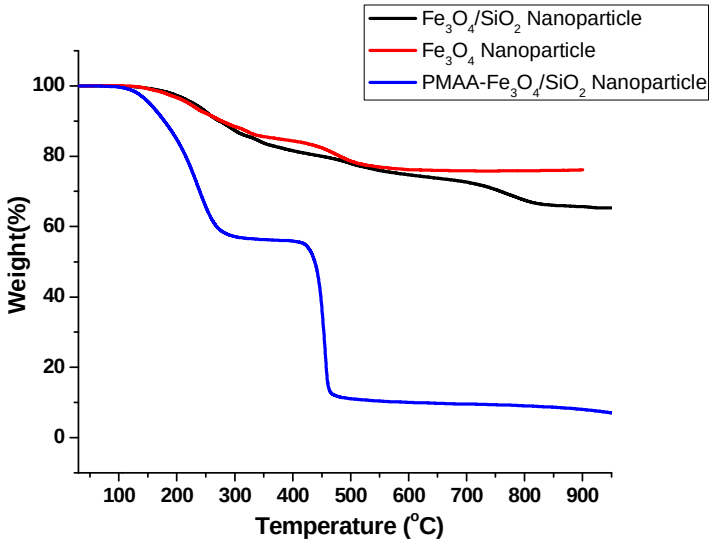

Figure 5.9 TGA of Fe_3O_4, Fe_3O_4/SiO_2, and PMAA grafted Fe_3O_4/SiO_2 magnetic nanoparticles.

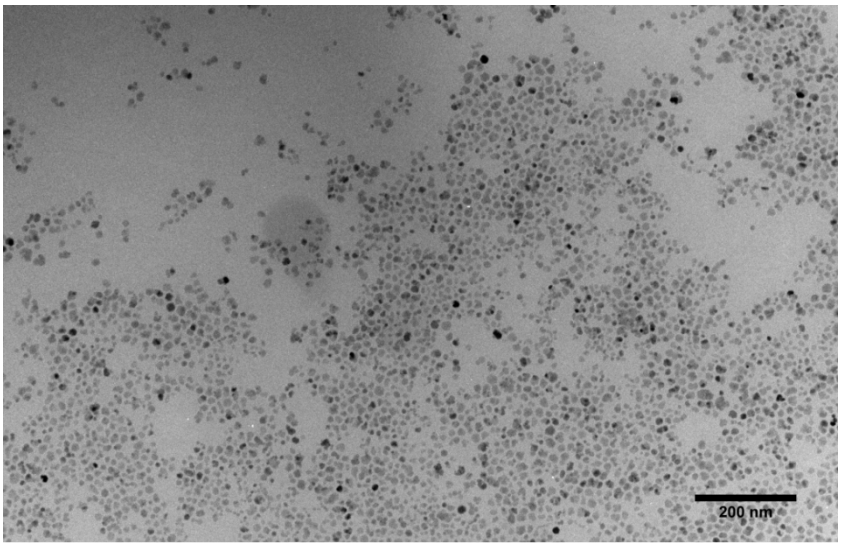

Figure 5.10 TEM of Fe_3O_4/SiO_2 nanoparticles.

5.3.2 Synthesis and Characterization of PMAA Grafted Fe_3O_4/SiO_2 Magnetic Nanoparticles

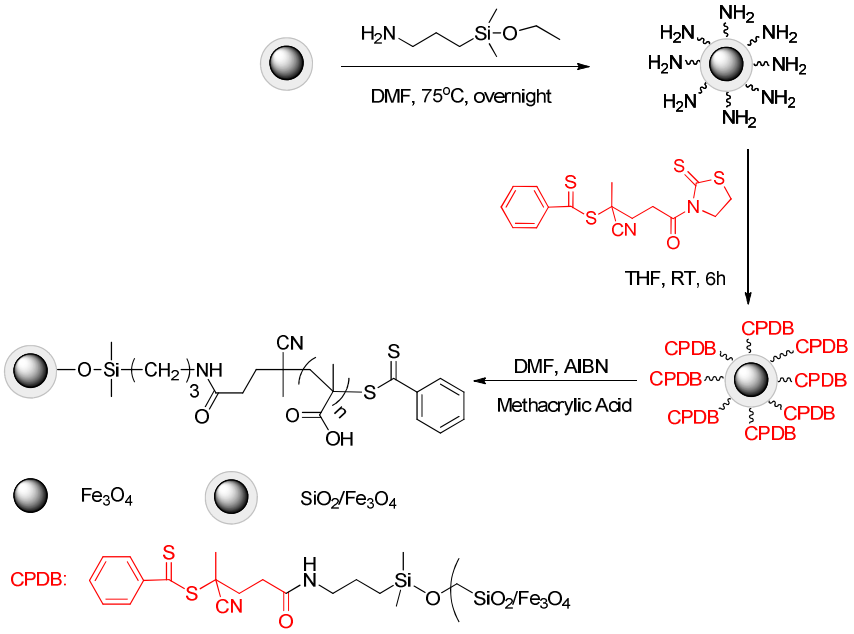

Scheme 5.1 Synthetic scheme for preparation of PMAA grafted Fe_3O_4/SiO_2 nanoparticles via direct polymerization of MAA.

The strategy for preparation of PMAA grafted Fe_3O_4/SiO_2 magnetic nanoparticles is shown in Scheme 5.1. Amino coated Fe_3O_4/SiO_2 nanoparticles were prepared by the

reaction between as-synthesized Fe_3O_4/SiO_2 particles and 3-aminopropyldimethylethoxysilane. The RAFT agent coated Fe_3O_4/SiO_2 nanoparticles were synthesized by allowing the amino coated Fe_3O_4/SiO_2 nanoparticles with accurately determined densities to react with an excess of activated CPDB. This method generated a universal platform for surface initiated RAFT polymerization of nanoparticles with magnetic properties. The CPDB covalently bound to the nanoparticle surface was confirmed via UV-vis absorption at 305 nm (Figure 5.11). Finally, the surface-initiated RAFT polymerization of MAA was conducted in DMF to generate PMAA brushes grafted onto magnetic nanoparticles.

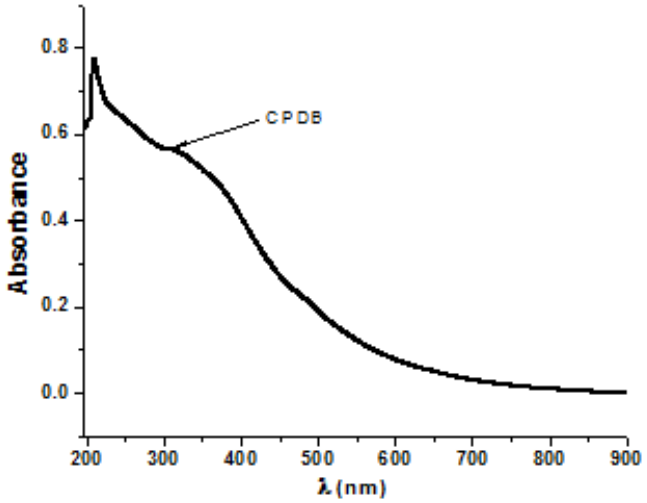

Figure 5.11 CPDB coated Fe_3O_4/SiO_2 nanoparticles.

Surface-initiated RAFT polymerization of MAA directly on Fe_3O_4/SiO_2 nanoparticles was conducted in DMF at 65 ^oC with a ratio between species of [MAA]:[CPDB]:[AIBN] = 1000:1:0.1. The PMAA grafted Fe_3O_4/SiO_2 nanoparticles were methylated by trimethylsilyldiazomethane followed by cleavage of the methylated chains from the nanoparticle surface with hydrofluoric acid solution to conduct accurate measurement of the molecular weights via organic phase (THF) GPC characterization. The FTIR analysis

of the methylated polymer grafted nanoparticles (Figure 5.12) confirmed the appearance of the strong absorption peak at ~ 2951 cm^{-1}due to the generated methyl moiety. Additionally, the absence of a broad peak at 3500 ~ 2500 cm^{-1} due to the hydroxyl group in –COOH and the shift of the carbonyl stretch peak from 1700 cm^{-1} to 1729 cm^{-1} confirmed the successful methylation of the polymer chains. The TGA demonstrated that the surface anchored PMAA accounted for 91% by weight (Figure 5.9). The PMAA grafted Fe_3O_4/SiO_2 nanoparticle solution was brown and transparent in dimethylformamide (DMF) (Figure 5.13). The magnetic nanoparticles had a strong magnetic responsive property and could be easily redispersed in DMF after sonication maintaining the excellent dispersity in solution for at least 2 weeks. The grafted magnetic nanoparticles also readily dispersed in water. The TEM image (Figure 5.14) reveals the PMAA grafted Fe_3O_4/SiO_2 hybrid nanoparticles were well dispersed, and shows that the size of the individual nanoparticles was around 40-50 nm, which is consistent with the AFM image (Figure 5.15).

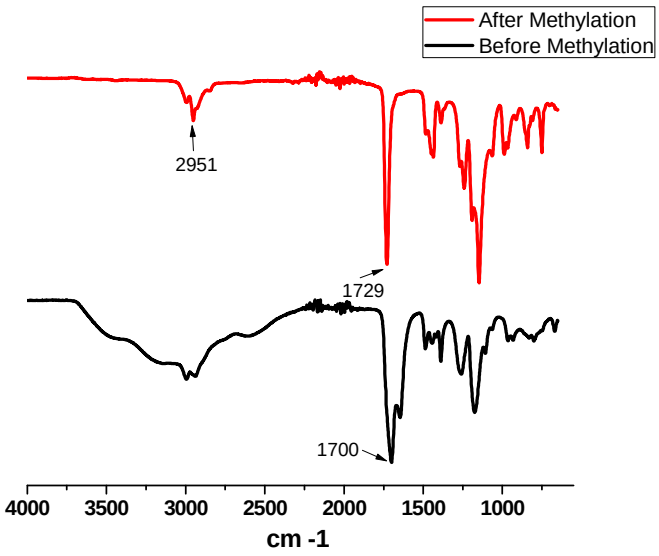

Figure 5.12 IR spectra of PMAA grafted Fe_3O_4/SiO_2 magnetic nanoparticles before and after methylation.

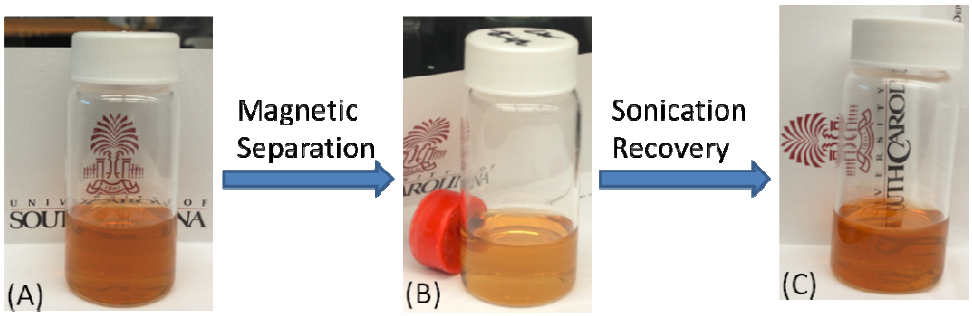

Figure 5.13 PMAA grafted SiO_2/Fe_3O_4 nanoparticles in DMF: (A) Normal state; (B) After magnetic separation; (C) Sonication Recovery and 14 days later.

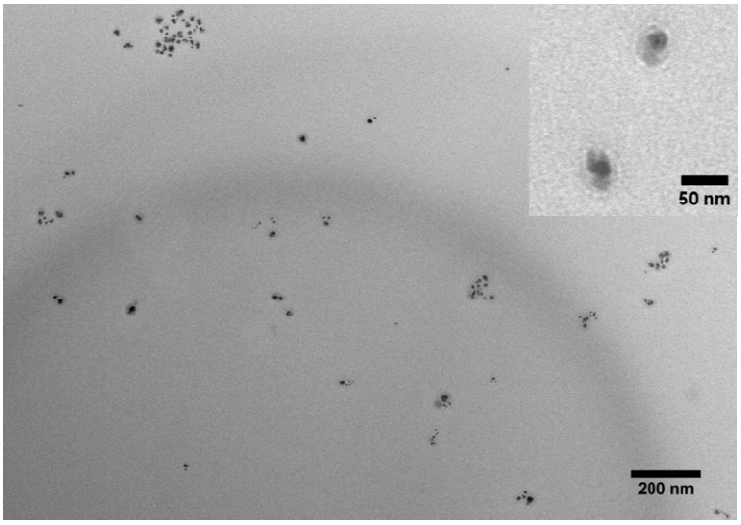

Figure 5.14 TEM of PMAA grafted magnetic nanoparticles.

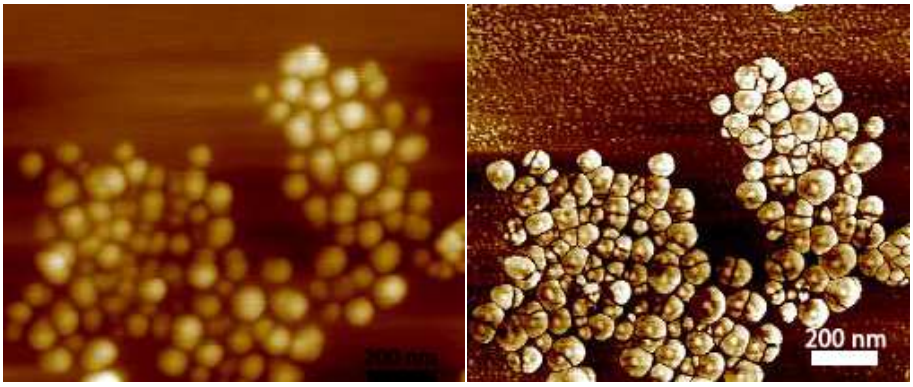

Figure 5.15 AFM of PMAA grafted Fe_3O_4/SiO_2 magnetic nanoparticles. Size bar = 200 nm.

5.3.3 Inhibition Activity and Recyclability of Magnetic PenG-Nanoparticle Complexes

The PMAA grafted magnetic nanoparticles were used to physically bind the beta-lactam antibiotic penicillin-G (PenG) and tested against bacteria. *Escherichia coli* (Gram-negative) and *Staphylococcus aureus* (Gram-positive) were selected as the target pathogens. The culture solution method was used to evaluate the inhibition activity and recyclability of PMAA grafted magnetic particles on antibiotic conjugation for killing bacteria. As a control group, the PMAA grafted nanoparticles exhibited no activity to *E. coli* at the experimental conditions. The PenG-nanoparticle complex was added to the tryptic soy broth based *E. coli* culture solution with shaking at 37 ^{o}C. After treatment overnight, the bacterial growth of the suspension was determined by recording absorbance at OD_{600}, and was compared to the standard bacterial culture solution without PenG and nanoparticles. Another control group of free PenG was tested in the same way.

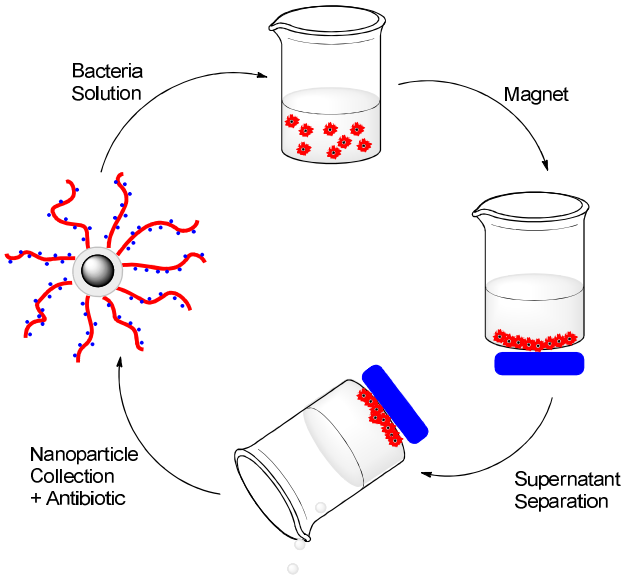

Scheme 5.2 Scheme of recycling magnetic nanoparticles to deliver antibiotics for killing bacteria.

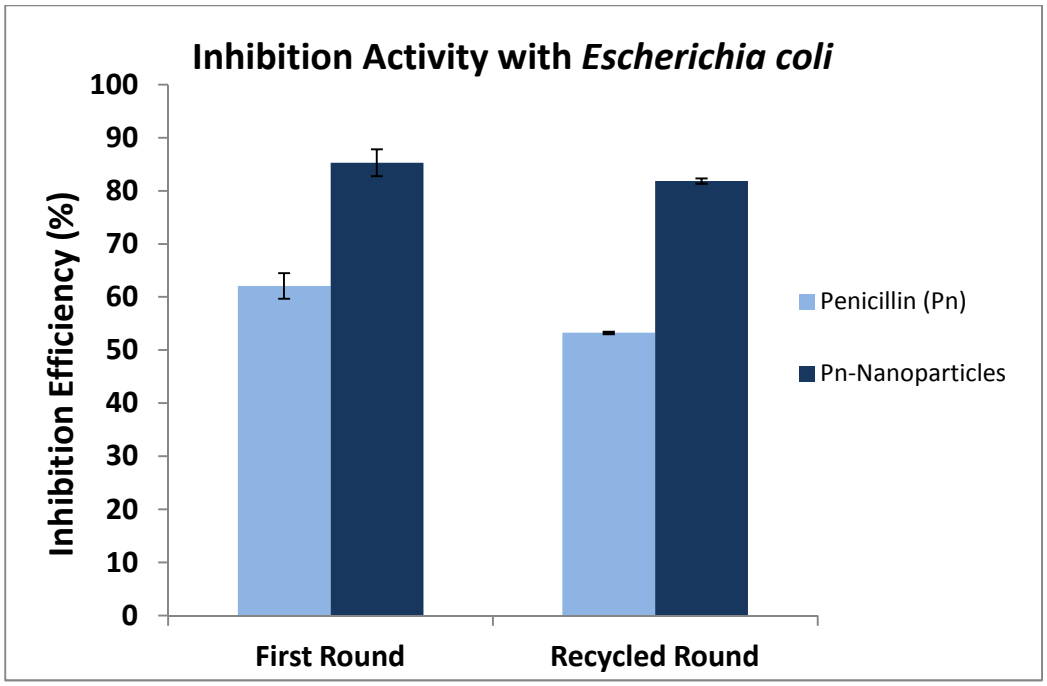

Figure 5.16 Inhibition activities of free-PenG (light blue), and PenG complexed to carboxylated polymers on magnetic nanoparticles (navy) as tested by bacterial culture solution with *E. coli.*

The PMAA grafted magnetic nanoparticles can be readily recycled with a magnet. The nanoparticles were attracted at the bottom of the tube via a magnet and the supernatant was removed. The collected nanoparticles were washed several times and used again to bind PenG and tested again for their ability to kill bacteria employing the above mentioned method (Scheme 5.2). The inhibition efficiency of PenG-nanoparticle complex remained at 82% using the recycled magnetic nanoparticles, which is much higher than the free PenG of around 53% (Figure 5.16).

Thus, PMAA grafted magnetic nanoparticles enhanced the bioactivity of PenG against bacteria when the nanoparticles were physically bound with PenG. We hypothesize that the increased antimicrobial activity is ascribed to locally high concentrations of antibiotics bound to nanoparticles, which overwhelms the resistance of bacterial strains.

The small size PMAA grafted magnetic nanoparticles with precisely controllable surface polymer brush lengths and PDIs provide an important platform to restore the activities of ineffective antibiotics via a new combination of materials to overcome bacterial resistance. The magnetic properties offer a significant stimulus technique to direct the nanoparticles to complicated bacterial environments, such as biofilms, while free antibiotic are not able to access cells in the sticky extracellular polymeric substances (EPS) of biofilms.

5.4 Summary

In conclusion, we demonstrated an effective method for the preparation of Fe_3O_4/SiO_2 superparamagnetic nanoparticles with sizes as low as 10 nm and a high saturation magnetization using very mild synthetic conditions. CPDB coated Fe_3O_4/SiO_2 magnetic nanoparticles were prepared by treating amino functionalized Fe_3O_4/SiO_2 nanoparticles with activated CPDB. The direct surface-initiated RAFT polymerization of MAA was conducted on very small size Fe_3O_4/SiO_2 superparamagnetic nanoparticles while maintaining good dispersibility in solutions. The synthesis of the PMAA grafted Fe_3O_4/SiO_2 superparamagnetic nanoparticle was confirmed by FTIR, TGA, VSM, TEM and AFM. The PMAA grafted Fe_3O_4/SiO_2 magnetic nanoparticles enhanced the bioactivity of PenG over bacteria when physically bound with PenG. The particles were removed from water solutions using a magnet after antimicrobial testing without nano-based pollution of the environment. The recycled PMAA grafted magnetic particles were able to bind PenG and retained high activity over bacteria. The water soluble PMAA grafted Fe_3O_4/ SiO_2 magnetic nanoparticles may also find applications in MRI, multiple drug delivery and therapeutic fields.

5.5 Reference

1. Fried, T.; Shemer, G.; Markovich, G. *Adv. Mater.* **2001**, *13*, 1158-1161.
2. Pothayee, N.; Pothayee, N.; Jain, N.; Hu, N.; Balasubramaniam, S.; Johnson, L.; Davis, R.; Sriranganathan, N.; Riffle, J. *Chem. Mater.* **2012**, *24*, 2056-2063.
3. Santra, S.; Tapec, R.; Theodoropoulou, N.; Dobson, J.; Hebard, A.; Tan, W. *Langmuir* **2001**, *17*, 2900-2906.
4. Chiefari, J.; Chong, Y. K.; Ercole, F.; Krstina, J.; Jeffery, J.; Le, T. P. T.; Mayadunne, R. T. A.; Meijs, G. F.; Moad, C. L.; Moad, G.; Rizzardo, E.; Thang, S. H. *Macromolecules* **1998**, *31*, 5559-5562.
5. Semsarilar M.; Perrier, S. *Nature Chemistry* **2010**, *2*, 811-820.
6. Ohno, K.; Ma, Y.; Huang, Y.; Mori, C.; Yahata, Y.; Tsujii, Y.; Maschmeyer, T.; Moraes, J.; Perrier, S. *Macromolecules* **2011**, *44*, 8944-8953.
7. Moraes, J.; Ohno, K.; Maschmeyer, T.; Perrier, S. *Chem. Commun.*, **2013**, *49*, 9077-9088.
8. Moraes, J.; Ohno, K.; Maschmeyer, T.; Perrier, S., *Chem. Mater.*, **2013**, *25*, 3522-3527.
9. Li, J.; Wang, L.; Benicewicz, B. *Langmuir* **2013**, *29*, 11547-11553.
10. Ranjan, R.; Brittain, W. J. *Macromol. Rapid Commun.* **2007**, *28*, 2084-2089.
11. R. Mout, D. F. Moyano, S. Rana, V. M. Rotello, *Chem. Soc. Rev.* **2012**, *41*, 2539-2544.
12. Hollman, A. M.; Scherrer, N. T.; Cammers-Goodwin, A.; Bhattacharyya, D. *J. Membr. Sci.* **2004**, *239*, 65-79.
13. Moya, S.; Azzaroni, O.; Farhan, T.; Osborne, V. L.; Huck, W. T. S. *Angew. Chem., Int. Ed.* **2005**, *44*, 4578-4581.
14. Tugulu, S.; Arnold, A.; Sielaff, I.; Johnsson, K.; Klok, H.-A. *Biomacromolecules* **2005**, *6*, 1602-1607.
15. Chen, H.; Hsieh, Y. L. *Biotech. Bioeng.* **2005**, *90*, 405-413.
16. Treat, N. D.; Ayres, N.; Boyes, S. G.; Brittain, W. J. *Macromolecules* **2006**, *39*, 26-29.
17. Wu, T.; Gong, P.; Szleifer, I.; Vlček, P.; Šubr, V.; Genzer, J. *Macromolecules* **2007**, *40*, 8756-8764.
18. Li, D.; Sheng, X.; Zhao, B. *J. Am. Chem. Soc.* **2005**, *127*, 6248-6256.
19. Cash, B.; Wang, L.; Benicewicz, B. *J. Polym. Sci. Part A: Polym. Chem.* **2012**, *50*, 2533-2540.
20. Hojjati, B.; Sui, R.; Charpentier, P. A. *Polymer* **2007**, *48*, 5850-5858.
21. Inoue, M.; Fujii, S.; Nakamura, Y.; Iwasaki, Y.; Yusa, S. *Polym. J.* **2011**, *43*, 778-784.
22. Matyjaszewski, K.; Xia, J. *Chem. Rev.* **2001**, *101*, 2921-2990.
23. Wang, L.; Benicewicz, B. *ACS Macro Lett.* **2013**, *2*, 173-176.
24. Evans, H. L.; Lefrak, S. N.; Lyman, J.; Smith, R. L.; Chong, T. W.; McElearney, S. T.; Schumlan, A. R.; Hughes, M. G.; Raymond, D. P.; Pruett, T. L.; Sawyer, R. G. *Crit. Care Med.* **2007**, *35*, 89-95.
25. Mahapatra, I.; Clark, J.; Dobson, P. J.; Owenc, R.; Lead, J. R. *Environ. Sci.: Processes & Impacts.* **2013**, *15*, 123-144.
26. Li, C.; Benicewicz, B. C. *Macromolecules* **2005**, *38*, 5929-5936.

27. Couvreur, L.; Lefay, C.; Belleney, J.; Charleux, B.; Guerret, O.; Magnet, S. *Macromolecules* **2003**, *36*, 8260-8267.
28. Zhang, J; Liu, Z.; Han, B.; Li, Z.; Yang, G.; Li, J.; Chen, J. *J. of Supercritical Fluids* **2006**, *36*, 194-201.
29. Wu, N.; Fu. L.; Su, M.; Aslam, M.; Wong, K. C.; Dravid, V. P. *Nano Letters* **2004**, *4*, 383-386.

CHAPTER 6

SURFACE FUNCTIONALIZATION OF NANOPARTICLES: FROM THE SIMPLE TO THE ADVANCED[4]

[4] Cash, B.; Wang, L.; Benicewicz, B. The Preparation and Characterization of Carboxylic Acid-Coated Silica Nanoparticles. *J. Polym. Sci. Part A: Polym. Chem.* **2012**, *50*, 2533-2540.
Reprinted here with permission of publisher.

6.1 Introduction

The increasing prevalence, perseverance, and adaptability of bacterial resistance to antibiotics is a vexing healthcare problem; one which results in high morbidity/mortality and healthcare costs exceeding $20 billion annually.[1-5] A wide range of infectious strains now exhibit antibiotic resistance. Common examples include MRSA (methicillin-resistant *Staphylococcus aureus*), *Pseudomonas aeruginosa* lung- and wound-infections, VREs (vancomycin-resistant *Enterococci*), bacterial pneumonia strains, and urinary tract-infections (UTIs), as well as a host of infections that occur in association with human conditions such as AIDs, and intestinal/colon breaches.[6-8] The frequency of community-acquired methicillin-resistant *Staphylococcus aureus* (MRSA) increased more than seven-fold from 1999 to 2006.[9] Patients who acquire such infections are at increased risk for death and disease. Such patients can more than double inpatient hospital costs[1] and account for increased outpatient treatment costs[10] and spending on long-term care.

Many widely-used antibiotics *(e.g.*, beta lactam antibiotics) share similarities in molecular structure and modes of action.[11] Since genetic mechanisms underlying antibiotic resistance can be readily exchanged among bacterial cells, a growing number of pathogenic strains now exhibit multiple antibiotic resistance (MAR).[12] Overuse of antibiotics selects for the emergence and later persistence of a resistant infection following antibiotic treatment,[13] a number that has been increasing over the past two decades. Consequently, many previously-used antibiotics (*e.g.* penicillin) have been rendered either less-effective or ineffective because of the preponderance of bacterial strains having genetically-transferable antibiotic resistance.[14] In order to overcome the

growing patterns of resistance, a more effective utilization of antibiotics against infections is required.

Nanoparticles (NP) and other nanotechnology-based approaches are now being investigated as therapeutic delivery-vehicles for antibiotics and other antimicrobial compounds to bacterial cells. While NPs have been used extensively for the delivery of anti-cancer drugs and other types of molecules to eukaryote cells,[15-17] they have not been utilized to a great extent to bacterial cells.[18] However, the size-dependent properties of NPs coupled to their high specific surface area and surface energies, potentially provide NPs with increased delivery capabilities when compared to dissolved molecules.[19] NPs additionally offer new design possibilities because their chemistry can be engineered with high-specificity to possess surfaces having different types and densities of chemical functional groups, charges and other properties.[20-22] This can permit pre-determined quantities of antibiotic molecules to be carried by a single nanoparticle, and subsequently delivered to an infectious bacterial cell. The interiors or surfaces of nanoparticles similarly can be engineered with fluorophores to facilitate quantitative detection. These properties, when used in combination, also offer a unique and improved potential for probing bacterial infections with increasing resolution.

In the present study, we conjugated the antibiotic penicillin-G using specifically-engineered nanoparticles, against bacterial pathogens, some of which were highly-resistant to the antibiotic. The activities of relatively non-effective antibiotics were significantly enhanced by nanoparticle-conjugation and avert certain forms of antibiotic resistance, especially if nanoparticles can specifically target bacteria. The antibiotic was conjugated to engineered silica nanoparticles having their surfaces functionalized with

monolayer carboxylic acids, and poly(methacrylic acid) (PMAA) prepared by the RAFT polymerization technique. Both forms of antibiotic-sNPs complexes demonstrated enhanced inhibition of the bacteria.

Cyclodextrin is an effective molecule to capture the signal molecules acylated homoserine lactones (AHLs), which are released by bacteria in their quorum sensing (QS) process.[23] QS allows bacteria to communicate with each other and thus makes bacteria much more resistant to antibiotics compared to individual bacteria. Thus, we are motivated to prepare cyclodextrin grafted nanoparticles to bind AHLs, lower its concentration to a certain degree and finally shut down the QS. Cyclodextrin grafted nanoparticles could be very important in capturing signal molecules in biofilms, in which bacteria are protected by extracellular polymeric secretions (EPS). Free cyclodextrin will be blocked by the sticky EPS barrier before accessing bacterial cells whereas nanoparticles can penetrate the biofilms EPS.

Bimodal polymer grafted nanoparticles allow polymers to behave synergistically on a nanoparticle. Polyethylene glycol (PEG) is used in the biomedical area as a biocompatible polymer. It also has been reported on preventing protein absorption and minimizes cell attachment.[24] PMAA has been applied to bind functional molecules for various applications. Thus, we are motivated to develop advanced bimodal PMAA and PEG grafted silica nanoparticles.

Polymer grafted nanoparticles are important materials and have found applications in chemosensors, biomedical devices and coatings.[25,26] The preparation of polymer grafted nanoparticles is usually conducted in organic solvents in both “grafting to” and “grafting from” strategies. The organic solvent based surface functionalization limits the

application of such materials, especially in the cosmetics, food and biomedical industries because the residual volatile organic compounds (VOCs) are toxic to human health. Thus, aqueous processes are desirable in the preparation of these materials. We were thus motivated to develop the surface functionalization of particles with polymer in aqueous environments.

6.2 Experimental

6.2.1 Materials

All chemicals were obtained from Fisher or Acros and used as-received unless otherwise specified. Trimethylsilyldiazomethane (2.0 M in hexanes) was purchased from TCI. 4-Cyanopentanoic acid dithiobenzoate (CPDB) was obtained from Strem Chemical Inc. CPDB immobilized silica nanoparticles were synthesized according to the literature.[27] Alkyne-oligoglutamate was obtained from Dr. Richard Gross group at RPI. 3-Aminopropyldimethylethoxysilane was obtained from Gelest and used as-received. NBD based fluorescent dye was prepared according to the literature.[28] Methacrylic acid (99.5%, Acros) was purified by passing through an activated neutral alumina column. AIBN was recrystallized from methanol before use. The beta-lactam antibiotic penicillin-G was obtained from Sigma-Aldrich Inc. and used for all experiments.

6.2.2 Instrumentation

^{1}H NMR (Varian Mercury spectrometer 300/400) was conducted using CD_3OD or $CDCl_3$ as the solvent. Molecular weights and PDI were determined using a gel permeation chromatography (GPC) equipped with a 515 HPLC pump, a 2410 refractive index detector, and three Styragel columns. The columns consisted of HR1, HR3 and

HR4 in the effective molecular weight ranges of 100-5000, 500-30000, and 5000-500000, respectively. The GPC used THF as eluent at 30 °C and a flow rate of 1.0 mL/min and was calibrated with poly(methyl methacrylate) or polystyrene standards obtained from Polymer Laboratories. Samples were filtered through microfilters with a pore size of 0.2 μm before injection. Infrared spectra were recorded with a PerkinElmer Spectrum 100 spectrometer. UV-vis spectra were measured with a Perkin-Elmer Lambda 4C UV-vis spectrophotometer. TEM images were examined using a Hitachi 8000 transmission electron microscope with an operating voltage of 200 kV. Carbon-coated copper grids were used to prepare samples by dropping sample solutions on the grids followed by drying in a fume hood before use. Tapping mode AFM measurements were operated using a Multimode Nanoscope III system (Digital Instruments, Santa Barbara, CA). The characterization was conducted using commercial Si cantilevers with a spring constant and resonance frequency of 20–80 N m^{-1} and 230–410 kHz respectively. The sample of PMAA grafted nanoparticles was prepared via spin-coating on silicon wafers with a speed of 3000 rpm. TGA measurement was conducted using a TA Instruments Q5000 with a heating rate of 10°C/min form 25°C to 950°C under nitrogen flow.

6.2.3 Bacterial Strains

List of organisms used: *Staphylococcus aureus* ATCC 25423; *Bacillus cereus* ATCC 11778; *Escherichia coli* ATCC 25922; *Pseudomonas aeruginosa* ATCC 27853; *Proteus vulgaris* ATCC 29905; *Salmonella typhimurium* ATCC 133111; *Enterobacter aerogenes* ATCC 13048; *Alcaligenes faecalis* ATCC 8750; *Staphylococcus aureus* ATCC 29213 (community acquired-MRSA); *Staphylococcus aureus* ATCC BAA 1717 (hospital associated-MRSA); *Klebsiella pneumoniae* ATCC 27736. The Gram-negative bacterium

strain *Escherichia coli* M8820 was obtained from the American Type Culture Collection (ATCC #25922). The *E. coli* were grown in tryptic soy broth (TSB, 30 mg/L) at 37°C with vigorous agitation. Growth of the cultures was assayed by measuring the optical density (600 nm) using absorbance spectrophotometry (Shimadzu, Inc). Several strains of the Gram-positive bacterium *Staphylococcus aureus*, were used for experiments. These included strains that are either sensitive or resistant to the antibiotic Penicillin-G: *S. aureus* (subsp. *aureus*; ATCC No. BAA-1717)[10] and *S. aureus* ATCC 25423. All Gram-positive strains were grown at 37^{o}C in tryptic soy broth. The bioactivity tests against these bacteria were conducted by Dr. Yung Pin Chen and Kristin Miller in Prof. Alan W. Decho lab at the University of South Carolina.

6.2.4 Synthesis of Silica Nanoparticles

200 mL ethanol, 5 mL ammonium hydroxide (29 wt%) and 2.5 mL deionized water were added into a round-bottom flask and the mixture was stirred for 15 min. Tetraethyl orthosilicate (TEOS) (5 mL) was then added quickly and the resulting solution was stirred at rt with a speed of 125 rpm overnight. $MgSO_4$ was added to the reaction solution to absorb the water. After filtration of $MgSO_4$, the filtrate was concentrated and precipitated into ethyl ether. The nanoparticles were recovered by centrifuge at 3000 rpm for 5 min and redispersed in THF. The process was repeated two more times and the silica nanoparticles were finally dispersed in THF for further use.

6.2.5 Method for Preparation of Lanthanide (Europium III) Doped Silica Nanoparticles

200 mL ethanol, 5 mL ammonium hydroxide (29 wt%) and 2.5 mL deionized water were added into a round-bottom flask and the mixture was stirred for 15 min. Tris

(2,2,6,6-tetramethyl-3,5-heptanedionato) europium (III) [$Eu(TMHD)_3$] (51.72 mg, 7.37×10^{-5} mol) was added and the resulting solution was stirred for another 15 min. Then the tetraethyl orthosilicate (TEOS) (5 mL) was added rapidly and the resulting solution was stirred smoothly (125 rpm) at room temperature overnight. $MgSO_4$ was added to the reaction solution to absorb the water. After filtration of $MgSO_4$, the filtrate was concentrated and precipitated into ethyl ether. The nanoparticles were recovered by centrifuge at 3000 rpm for 5 min and redispersed in THF. The process was repeated two more times and the europium (III) doped nanoparticles were finally dispersed in THF for further use.

6.2.6 Ruthenium (II) Doped Silica Nanoparticles

The synthesis of ruthenium (II) doped silica nanoparticles is similar to europium (III) doped silica nanoparticles. 55.17 mg ruthenium complex of tris(2,2'-bipyridine)ruthenium(II) dichloride hexahydrate, 200 mL ethanol, 5 mL ammonium hydroxide (29 wt%), 2.5 mL deionized water and 5 mL TEOS were used in the nanoparticle synthesis.

6.2.7 Preparation of Dye and Carboxylic Acid Functionalized Silica Nanoparticles

NBD-NHS (2.72 mg, 7.786 μmol), as a solution in THF (344 μL), was added dropwise to amino-functionalized silica nanoparticles (2.6 g, 56.9 μmol/g) dispersed in THF (30 mL). The reaction was stirred at rt. After 3 h, succinic anhydride (7.0 mg, 0.7 mmol) was added as a 1 mM solution in DMF and the mixture was stirred overnight. The reaction solution was then poured into 200 mL ethyl ether. The particles were recovered by centrifugation at 3000 rpm for 5 min. The particles were then redispersed in 30 mL of ethanol and re-precipitated in ethyl ether (200 mL). This procedure was repeated three

more times until the supernatant remained colorless. The NBD-NHS and carboxylic acid anchored silica nanoparticles were finally dissolved in ethanol (44.8 g/L). The NBD-NHS accounted for 4.8% in the total functionalized surface groups.

6.2.8 Acidification of Penicillin G Potassium Salt

8 g Penicillin G potassium salt was dissolved in 400 mL DI water followed by cooling to 0 °C. The pH was adjusted to 2 with 1 M H_2SO_4 and a large amount of white precipitates were generated. The precipitates were extracted using ethyl ether and further washed three times using saturated sodium chloride solution. After drying with sodium sulfate, the concentrate was poured into a mixture (~250 mL) of isopropylamine and acetone (1:1) followed by filtration and drying (yield: 2.88 g, 36%).

6.2.9 Synthesis of Penicillin G Physically Attached Nanoparticles

To complex PenG to nanoparticles, 0.5 ml of dye-labeled monolayer carboxylic acid coated nanoparticles (12.8 mg/ml) and 1.5 mL DI water were mixed. Then, 5 mg Penicillin was added and incubated at 28 ^{o}C with shaking (200 rpm/min) for 6 hours. The nanoparticle-penicillin complex sample was collected by Amicon centrifuge tubes. For Dye-labeled poly(methacrylic acid) grafted nanoparticles (22 mg/ml), the same procedure was performed.

6.2.10 Synthesis of Glutamate Grafted Silica Nanoparticles

A THF solution of PAHMA grafted silica nanoparticles (554.2 mg, 4.078×10^{-4} mol N_3 group) and alkyne-oligoglutamate (0.5 g, 4.078×10^{-4} mol) was treated with nitrogen purging for 30 min. Then CuBr (5.85 mg, 4.078×10^{-5} mol) and PMDETA (7.067 mg, 4.078×10^{-5} mol) were added and the resulting solution was stirred under nitrogen

protection at rt for more than 48 hours. The mixture was concentrated and dialyzed in water to remove the copper catalyst. The glutamate grafted silica nanoparticles were collected, dried and dispersed in DMSO for further use.

6.2.11 Preparation of Monolayer Dye-labeled β-CD Functionalized Silica Nanoparticles

A DMF solution of β-CD (70.56 mg, 62.16 μmol), N,N'-dicyclohexylcarbodiimide (DCC, 10.3 mg, 49.73 μmol) and 4-dimethylaminopyridine (DMAP, 0.5063 mg, 4.144 μmol) were added to a 15 mL DMF solution of dye-labeled carboxylic acid-functionalized silica nanoparticles (graft density: 0.24 groups/nm^2, 0.7281g). The reaction was stirred at room temperature overnight. Then the reaction solution was then poured into 200 mL ethyl ether followed by centrifugation at 3000 rpm for 5 min. The recovered particles were then redispersed in ethanol and subjected to dialysis process to further remove impurities. The isolated dye-labeled β-CD coated silica nanoparticles were finally dissolved in ethanol/water mixture solvents for further use.

6.2.12 Preparation of Dye-labeled Poly(β-CD) Grafted Silica Nanoparticles

A DMF solution of β-CD (3.711 g, 3.27 mmol), N,N'-dicyclohexylcarbodiimide (DCC, 0.54 g, 2.616 mmol) and 4-dimethylaminopyridine (DMAP, 26.6 mg, 0.218 mmol) were added to a 10 mL dry DMF solution of dye-labeled poly(methacrylic acid) grafted silica nanoparticles (graft density: 0.30 chains/nm^2, 252 mg). The reaction was stirred at room temperature overnight. Then the reaction solution was then poured into 200 mL ethyl ether followed by centrifugation at 3000 rpm for 5 min. The recovered particles were then redispersed in 20 mL of ethanol and subjected to dialysis process to

further remove impurities. The isolated dye-labeled poly(β-CD) grafted silica nanoparticles were finally dissolved in water for further use.

6.3 Results and Discussion

6.3.1 Preparation of Doped Silica Nanoparticles

Silica nanoparticles were synthesized via the Stober method which is based on the hydrolysis of TEOS under basic conditions.[29] A variety of silica nanoparticles with different sizes were prepared by using various amounts of TEOS, NH_4OH and water. Figure 6.1 shows the TEM images of 20 nm and 90-100 nm (diameter) silica nanoparticles and indicates that the nanoparticles were mono-distributed and dispersed well in solution. NaOH (around same pH value to NH_4OH solution) was also used to hydrolyze TEOS in the system and the resulting nanoparticles dispersed well in solution.

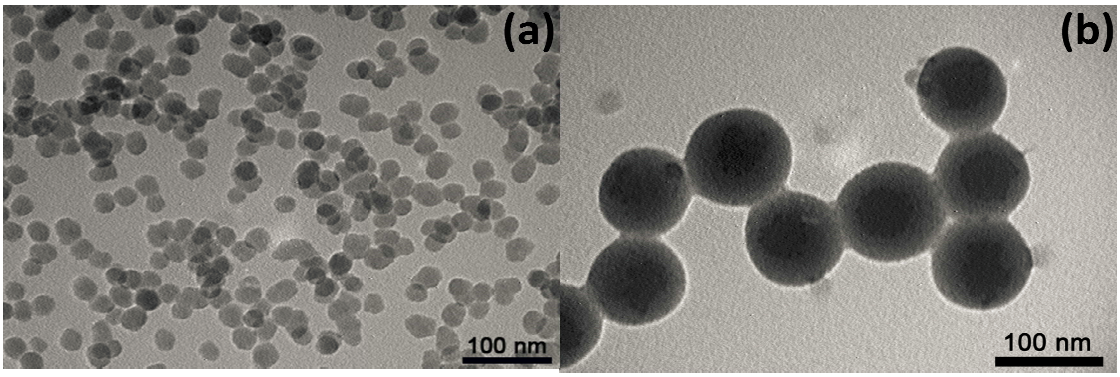

Figure 6.1 TEM image of silica nanoparticles prepared by Stober method with different sizes (a) 20 nm; (b) 90-100 nm.

Lanthanide probes, such as europium (III) enhance the ability to quantify and detect nanoparticles. Lanthanide metals exhibit time-resolved luminescence with emissions specific to the molecular environment.[30] The nanoparticles were synthesized with europium (III) in order to directly incorporate the europium (III) into the silica matrix.

When excited at 365 nm, the emission of the modified silica nanoparticles could be measured at 538 nm (Figure 6.2). Despite the ultra-small size of the nanoparticles, their luminescence was detectable using confocal scanning laser microscopy (CSLM; Figure 6.3). The Eu (III)-doped silica nanoparticles were synthesized in a range of sizes (Table 6.1**)**, with diameters between 25 nm to 170 nm. The diameters of the Eu (III)-doped silica nanoparticles varied depending on the europium ligands and molar ratios of Eu and Si. Figure 6.4 shows the TEM images of Eu (III)-doped silica nanoparticles and indicates that the nanoparticles were mono-distributed and dispersed well in tetrahydrofuran (THF). The relative transparency of solutions containing Eu (III)-doped silica nanoparticles changed depending on the size of the nanoparticles, and larger diameter nanoparticles resulted in more "milky" solutions (Figure 6.5)**.** The photoluminescent nanoparticles were allowed to react with 3-aminopropyldimethylethoxysilane to obtain amino group functionalized Eu (III)-doped silica nanoparticles, followed by the reaction with succinic anhydride to prepare carboxylic acid coated Eu (III)-doped silica nanoparticles.

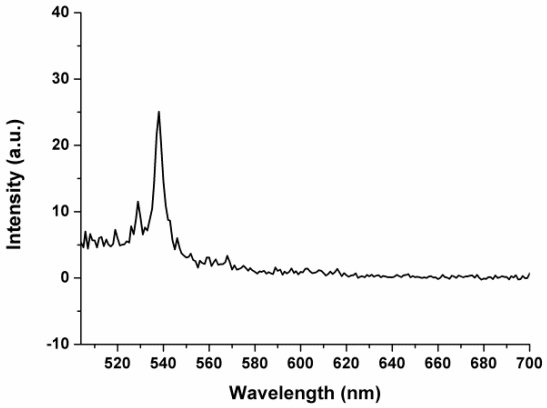

Figure 6.2 Photoluminescence spectrum of Eu (III)-doped silica nanoparticles. Using the excitation wavelength of 365 nm, the maximum emission was 538 nm.

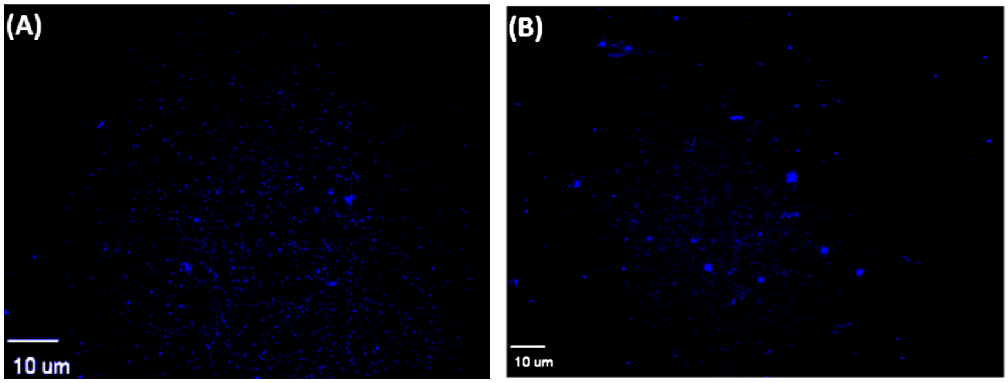

Figure 6.3 Confocal scanning laser micrographs showing time-resolved fluorescence of Eu (III)-doped silica nanoparticles: (A) 25-30 nm size; (B) 95-100 nm size. Note: the sizes of light spots are larger than the actual particle size due to inherent resolution limitations of light microscopy and partial agglomeration of particles prepared on glass slides.

Table 6.1 Europium (III)-doped silica nanoparticles size distribution

Entry	Eu (III) ligand	Molar Ratio Eu:Si (mol%)	Nanoparticle diameter (nm)
1	Tris(2,2,6,6-tetramethyl-3,5-heptanedionato) europium	0.33	25-30
2	Europium chloride hexahydrate	0.68	40-50
3	Europium chloride hexahydrate	1.34	150-170
4	Europium acetate hydrate	0.5	95-100

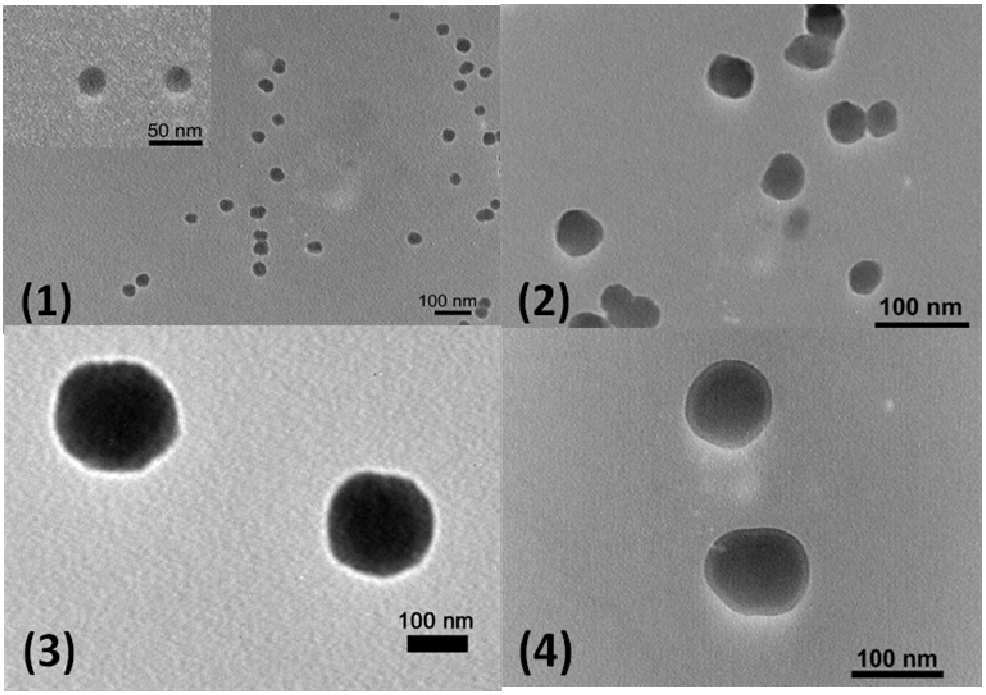

Figure 6.4 Transmission electron microscopy (TEM) micrographs of Eu (III)-doped silica nanoparticles with a variety of ligands: (1) Tris(2,2,6,6-tetramethyl-3,5-heptanedionato) Europium (Eu : Si = 0.33 mol%), 25-30 nm; (2) Europium chloride hexahydrate (Eu : Si = 0.68 mol%), 40-50 nm; (3) Europium chloride hexahydrate (Eu : Si = 1.34 mol%),150-170 nm; (4) Europium acetate hydrate (Eu : Si = 0.5 mol%), 95-100 nm.

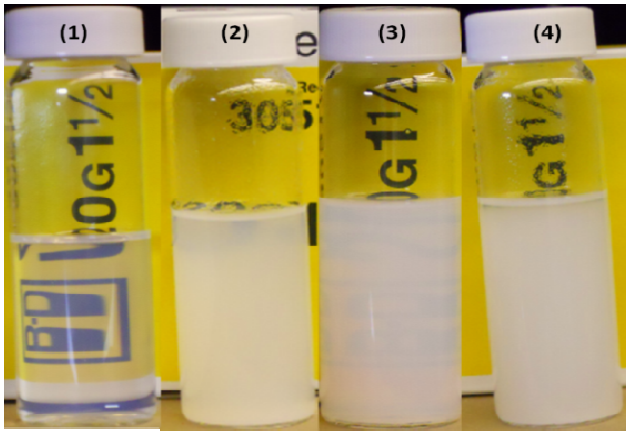

Figure 6.5 Eu (III)-doped silica nanoparticles with a variety of ligands: (1) Tris(2,2,6,6-tetramethyl-3,5-heptanedionato) Europium (Eu : Si = 0.33 mol%), 25-30 nm; (2) Europium chloride hexahydrate (Eu : Si = 0.68 mol%), 40-50 nm; (3) Europium acetate hydrate (Eu : Si = 0.5 mol%), 95-100 nm; (4) Europium chloride hexahydrate (Eu : Si = 1.34 mol%), 150-170 nm.

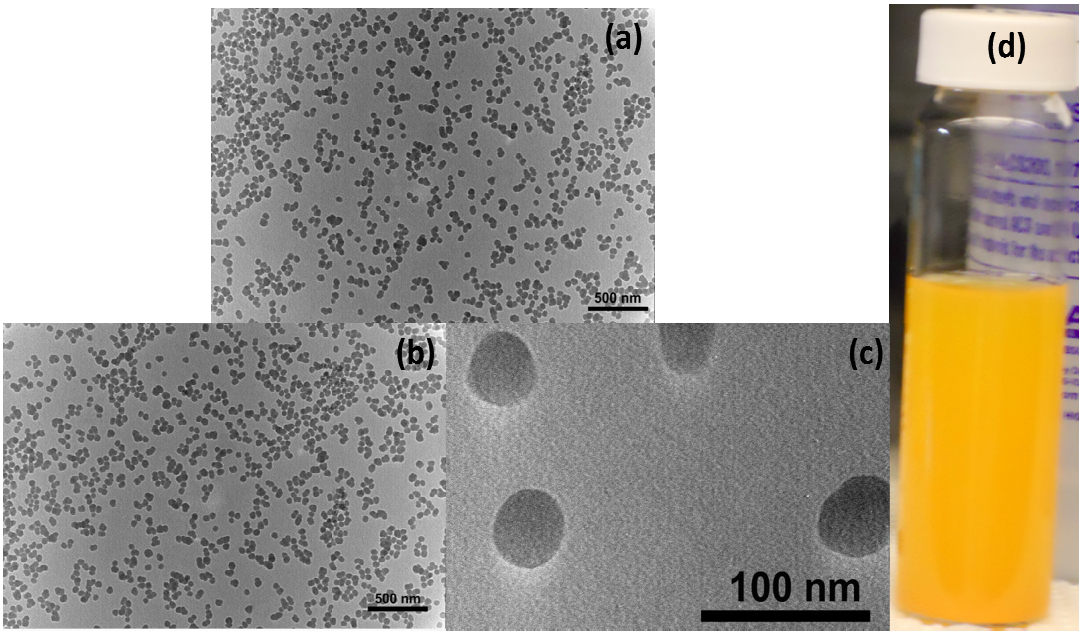

Figure 6.6 (a), (b), (c): TEM micrographs of Ru(II)-doped silica nanoparticles, 40-50 nm; (d): photograph of ruthenium(II) doped silica nanoparticles.

Tris(2,2'-bipyridine)ruthenium(II) $[Ru(bpy)_3]2^+$] were incorporated into the silica nanoparticles during the formation of particles. $[Ru(bpy)_3]Cl_2$ is red while the ruthenium(II) doped silica nanoparticles are orange, as shown in Figure 6.6 (d). Figure 6.6 shows the TEM images of Ru (II)-doped silica nanoparticles and indicates that the nanoparticles were mono-distributed and dispersed well in ethanol. The feed ratio between ruthenium(II) complex and TEOS is Ru : Si = 0.33 mol% and the diameter of the generated spherical nanoparticles is 40-50 nm**.**

6.3.2 Synthesis of Dye-Labeled Monolayer Carboxylic Acid Coated Silica Nanoparticles (sNPs)

The carboxylic acid engineered sNPs were labeled with fluorescent dyes for monitoring the presence and movement of the sNPs using UV-vis and confocal scanning laser microscope (CSLM). A carboxylic acid monolayer was coated on sNPs with fluorescent tags in two steps (Scheme 6.1). First, amino-coated nanoparticles (with a

predetermined amount of amino groups) were allowed to react with a small amount (< 5 mol % relative to the amines) of 7-nitrobenzofurazan-(NBD)-based dye molecules. Secondly, an excess of succinic anhydride was added to the reaction solution to generate fluorescent dye-labeled carboxylic acid-coated nanoparticles. The amount of dye molecules attached to the nanoparticle surface was determined by absorbance of functionalized nanoparticles (326 nm) and compared to a standard UV-vis absorption curve of free NBD-COOH (Figure 6.7). The dye-labeled silica nanoparticles with surface functionalized carboxylic acids were yellow and the ethanol solution was transparent (Figure 6.8).

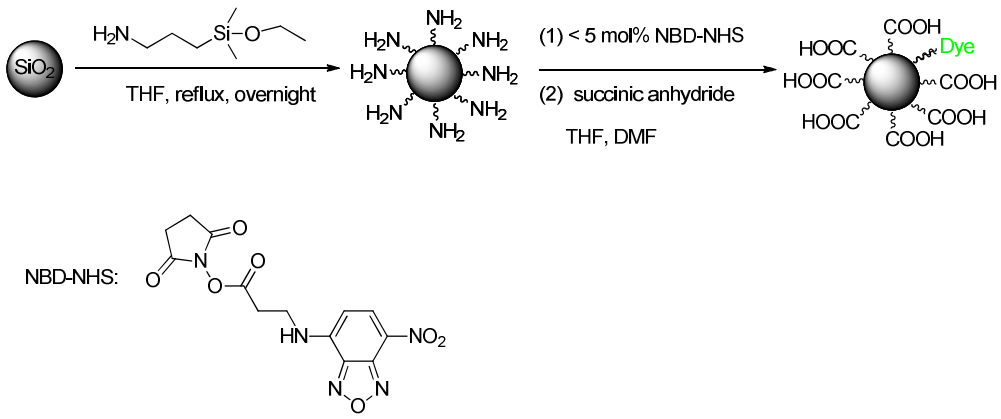

Scheme 6.1 Synthesis of dye and carboxylic acid functionalized nanoparticles.

A series of dye- and carboxylic acid-functionalized sNPs at low-, medium-, and high-density were prepared, as shown in Table 6.2. Samples labeled ‘Entry 1’ and ‘Entry 5’were used as control groups to test the toxicity of functionalized sNPs to bacteria. Bare sNP (Entry 1, Table 6.2) and 100% fluorescent dye-surface functionalized sNP (Entry 5, Table 6.2) demonstrated no detectable toxicity to either *E. coli* or *S. typhimurium*. Dynamic-light-scattering (DLS) indicated the mean diameter of bare nanoparticles was 18.9 ±0.4 nm. The mean diameter of carboxylic acid coated-nanoparticles was 22.7 nm, with an increase of 3.8 nm after surface modification.

Table 6.2 Dye-labeled monolayer carboxylic acid coated nanoparticles

Entry	Total surface density (groups/nm^2)	Total surface density-equivalent (μmol/g)	Dye in the surface groups (mol%)	Carboxylic Groups/Nanoparticle
1	0	0	0	0
2	0.24	56.91	4.80	287
3	0.40	93.53	3.05	487
4	0.65	154.14	3.40	788
5	0.24	56.91	100	0

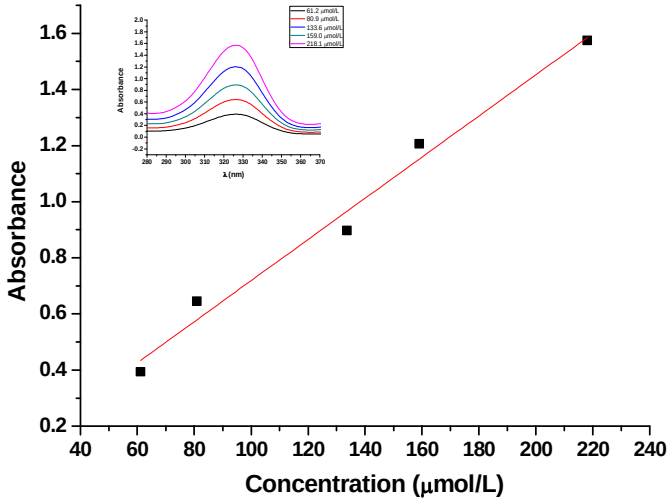

Figure 6.7 UV-vis standard absorption curve of NBD-COOH at 326 nm.

Figure 6.8 Photograph of dye-labeled carboxylic acid coated nanoparticles in ethanol after several washes.

6.3.3 Synthesis and Characterization of Poly(methacrylic acid) Grafted Silica Nanoparticles

Poly(methacrylic acid) grafted sNPs were synthesized by preparation of poly(*tert*-butylmethacrylate) (P*t*BuMA) grafted nanoparticles followed by the deprotection of the *tert*-butyl groups on the surface-attached polymers. Poly(*tert*-butyl methacrylate) grafted sNPs were prepared by RAFT polymerization of *tert*-butyl methacrylate mediated by 4-cyanopentanoic acid dithiobenzoate (CPDB) coated sNPs in THF employing azobisisobutyronitrile (AIBN) as the initiator at 60 °C. In addition, an extra step of treatment with excess AIBN is required to remove the thiocarbonylthio moiety before the deprotection process because the deprotection agent trimethylsilyl iodide (TMSI) would coordinate to the thiocarbonylthio group, generate free thio groups and lead to nanoparticle aggregation by oxidative coupling. The extremely large abundance of carboxylic acid on the poly(methacrylic acid) extending from the nanoparticles provides

the capability for complexation of enormous numbers of antibiotic molecules to a single nanoparticle.

Figure 6.9 shows TEM images of poly(tert-butyl methacrylate) and poly(methacrylic acid) grafted sNPs, and reveals an excellent dispersion of nanoparticles after each step of chemical modifications. The diameter of individual poly(methacrylic acid)-coated sNPs was approx. 30 nm, and consistent with AFM-based measurements (Figure 6.9, d).

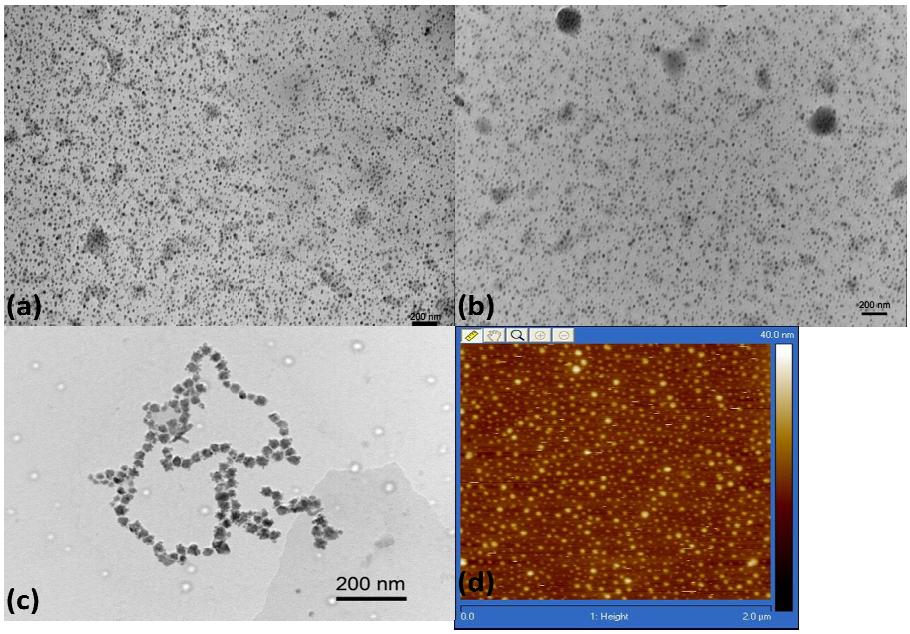

Figure 6.9 TEM and AFM image of polymer grafted sNPs: (a) poly(tert-butyl methacrylate) grafted sNPs with RAFT group chain end capped; (b) poly(tert-butyl methacrylate) grafted sNPs without RAFT group chain end capping; (c) poly(methacrylic acid) grafted sNPs. Scale bar for all the TEM images: 200 nm. (d) AFM image of poly(methacrylic acid) grafted sNPs.

6.3.4 Preparation of Antibiotic-Nanoparticle Complexes

Penicillin G (PenG) is a bactericidal antibiotic, which kills cells through the inhibition of cell wall synthesis.[11] PenG was non-selectively conjugated to monolayer carboxylic acid or PMAA grafted sNPs via physical interactions. Basically, PenG was added to the water solution of monolayer carboxylic acid or PMAA grafted nanoparticles for

incubation at 28 ^{o}C with shaking for 3 hours. The PenG/nanoparticle complex was collected and separated from unbound PenG using Amicon Ultra Centrifuge Filters.

PenG was also covalently attached onto silica nanoparticles to investigate the antimicrobial activity of the complex (Scheme 6.2). In the covalently anchoring process, the acidification step of PenG potassium salt is critical because there is no other functional group in the structure which is suitable for further chemical modification. The process was conducted using 1M H_2SO_4 to adjust the pH to 2. The treatment should be conducted very carefully to avoid potential hydrolysis of the β-lactam structure. The covalently attachment of PenG acid was achieved via the coupling reaction with amino-functionalized silica nanoparticles. In the process, choosing the right reaction solvent is critical. Typically, dichloromethane (DCM) is a good solvent for the coupling reaction between organic molecules. However, amino-anchored particles did not dissolve in DCM. After a series of tests, a mixture solvent of DCM and DMF (DCM/DMF=2:1) was selected. As another strategy, PenG acid was activated with N-hydroxysuccinimide (NHS) to obtain PenG-NHS. This can then be used to react with amino-functionalized particles, which is a highly efficient reaction. The as-synthesized nanoparticles were washed several times to remove the small molecules and then dispersed in ethanol or DMSO.

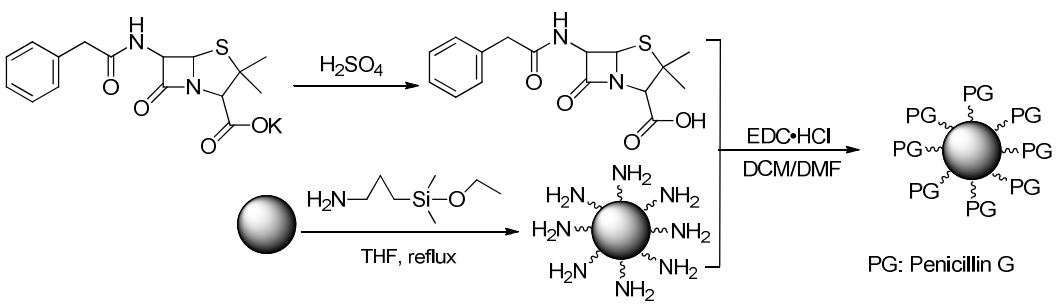

Scheme 6.2 Synthesis of Penicillin G covalently attached nanoparticles.

6.3.5 The Antimicrobial Activity of Antibiotic-Nanoparticle Complexes

Standardized agar disk-diffusion assays and broth dilution approach were used to measure the antimicrobial activities of PenG and sNP-PenG complexes. Our investigation studied ten bacterial pathogens (six Gram-negative and four Gram-positive bacteria), including methicillin-resistant *Staphylococcus aureus* (MRSA) strains. In disk-diffusion assays, treatment disks containing the nanoparticle complexes were tested on the same agar plates as the control (soluble PenG) disks to ensure that the dosage and growth stage of the bacterial lawn was comparable. The inhibition activity of nanoparticle-complexed antibiotic was verified by its presence in the inhibition zones of agar plates (Figure 6.10). Bare sNPs did not result in observable zones of inhibition. Free penicillin at a low dose (2.5 µg) had an activity of 0 in both assays, while the nano-complexed form of penicillin with the same dose of PenG enhanced activity significantly (Figure 6.11).

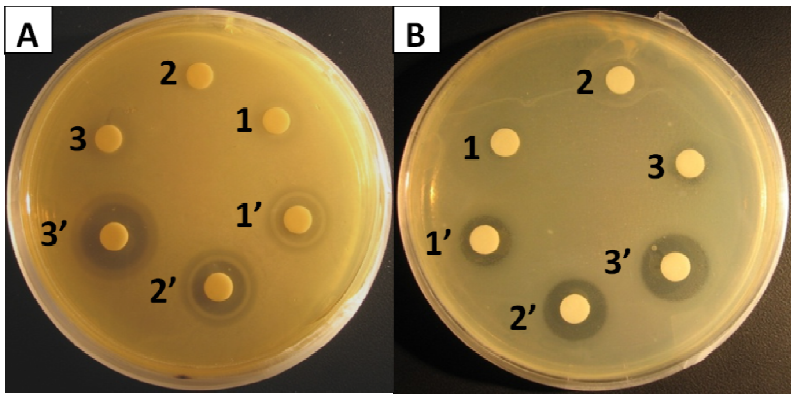

Figure 6.10 Results of disk-diffusion assays using (A) S. typhimurium and (B) E. coli. Disks 1, 2, and 3 represent 2.5, 5.0, and 7.5 µg of PenG added in soluble form, respectively. Disks 1', 2', and 3' have 2.5, 5.0, and 7.5 µg of PenG complexed to 'monomeric' surface-carboxylated silica nanoparticles (sNPs), respectively.

The results (Figure 6.11) showed that in disk-diffusion assays using Gram-negative bacteria (B, D and I), both PenG-conjugated to monolayer carboxylic acid and to PMAA grafted nanoparticles, exhibited much greater inhibition zones (> 7 mm in B; > 7.5 mm in D; > 8 mm in I) while inhibition zones of free-PenG were effectively 0 mm when the PenG doses were low. Differences in observed inhibition zones between nanoparticle-complexed PenG and free-PenG decreased when PenG doses were increased. The same trends were also observed in tests using Gram-positive bacteria and MRSA. The ability of PenG, when conjugated to either monolayer carboxylic acid- or PMAA-nanoparticles, to inhibit MRSA strains (Figure 6.11 F, G) illustrates the increased effectiveness of nanoparticle-conjugated antibiotics.

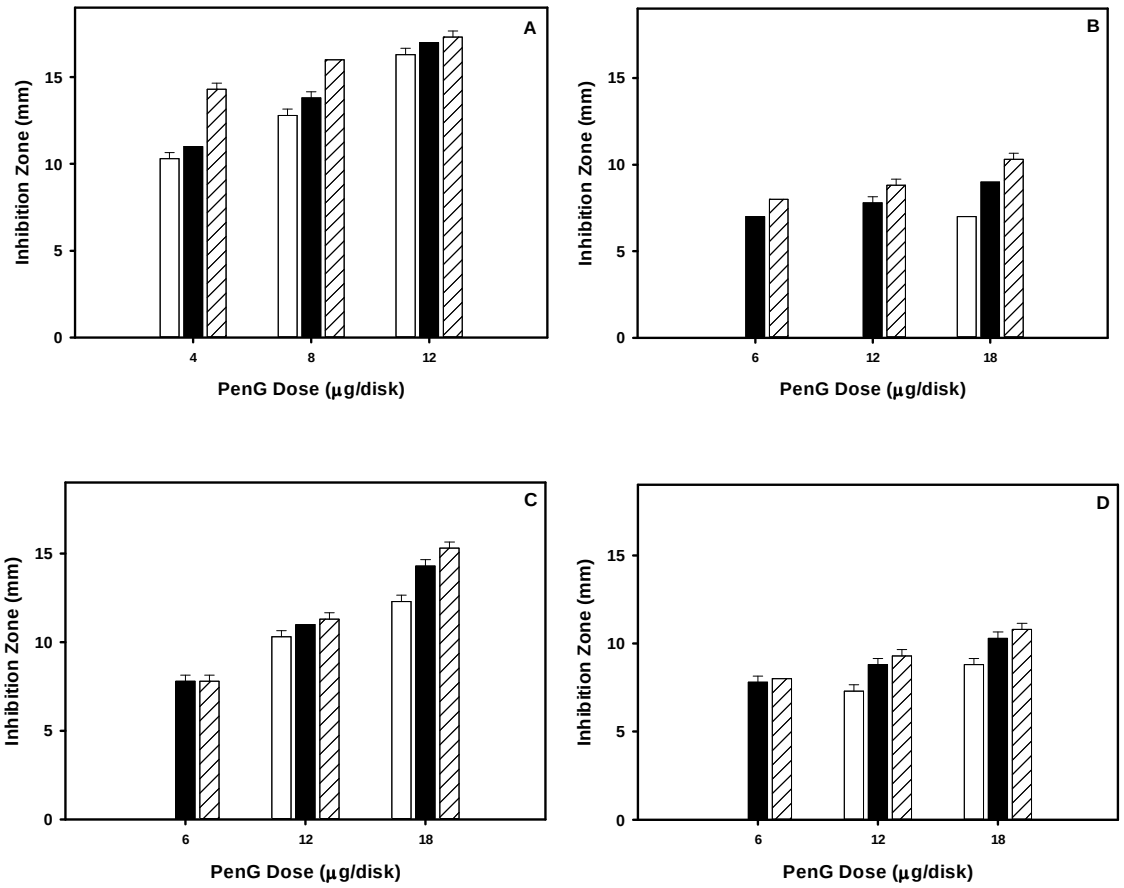

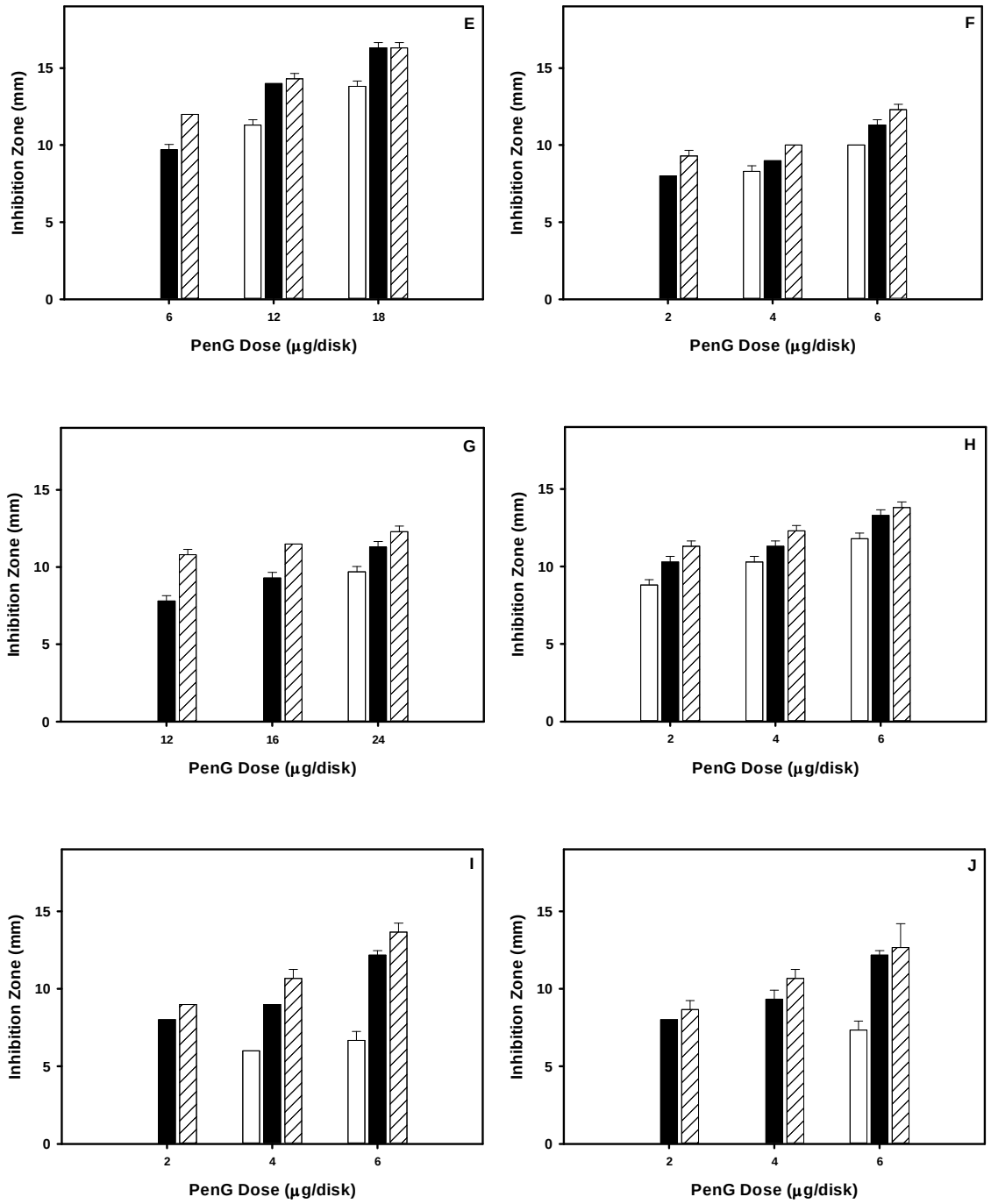

Figure 6.11 Inhibition activity of free-PenG (white), PenG-complexed to the surface monolayer on sNPs (black), and PenG-complexed to carboxylated polymers on sNPs (hatched), as tested by disk-diffusion assays using B. cereus (A), P. aeruginosa (B), K. pneumoniae (C), P. vulgaris (D), E. aerogenes (E), S. typhimurium (F), CA-MRSA (G), HA-MRSA (H), E. coli (I), and S. aureus (J).

The disk-diffusion assays illustrate the high antimicrobial activity of the nanocomplexed antibiotics against both Gram-negative and Gram-positive bacteria, especially antibiotic-resistant MRSA. These results were surprising because PenG is not typically effective against MRSA. The question emerges from our results: Why do nanoparticle-conjugated antibiotics have increased antibacterial activity? In order to answer this question, control groups of dye-labeled monolayer carboxylic acid and PMAA grafted sNPs were used to conduct the same experiment as the sNP-PenG complex. It was found that these particles did not show any activities to the Gram-negative and Gram-positive bacteria, including MRSA. Thus, the real moiety which demonstrated the antimicrobial activity in the complex is the conjugated PenG.

Beta-lactam antibiotics, such as PenG, work by interfering with the cross-linkage of peptidoglycan, a major component of the bacterial cell wall.[24] Resistant bacterial strains often possess beta-lactamases, enzymes that specifically degrade the lactam structure and render the antibiotic ineffective. In order to verify the resistance mechanism, we tested the effects of nanoparticle-PenG complex on beta-lactamases by incubation of free PenG or nanoparticle-conjugated PenG (both on monolayer carboxylic acids and PMAA coated sNPs) and *E. coli* (ATCC 25922) followed by the nitrocefin disk assays. Nitrocefin, containing a beta-lactam ring, is a chromogenic cephalosporin and usually used to rapidly detect beta-lactamase.[31] Usually, nitrocefin solution is yellow with a UV-vis absorption peak around 380 nm. Beta-lactamase is able to hydrolyze the beta-lactam ring of nitrocefin, resulting in a color change from yellow (negative) to red (positive), with a corresponding UV-vis absorption peak around 480 nm. The incubation with monolayer carboxylic acid coated sNPs remained a yellow color, which indicated no- or little

hydrolysis; while the incubation with PMAA resulted in a very light red color which reveals more hydrolysis. However, compared to the control group of free PenG on nitrocefin disk (no sNPs) that resulted in a dark red color, incubations with the PenG-nanoparticle complexes generated much less beta-lactamases. This low concentration of beta-lactamase leads us to hypothesize that the binding of PenG on nanoparticle surfaces resulted in less recognization by the cell and a lower generation of beta-lactamases.

We hypothesize that another reason for the high antimicrobial activities is the locally high concentrations of surface-attached antibiotic molecules on a nanoparticle. This may overwhelm a targeted bacterial cell's ability to degrade the antibiotics using enzymes (i.e. beta-lactamases). In contrast, a typical antibiotic once solubilized will typically diffuse to form a rather homogeneous dispersion of molecules spread over bacterial cells, but results in a relatively low concentration of antibiotic molecules reaching a single bacterium. Our studies suggest that when antibiotics are concentrated on a nanoparticle surface, they can supply a more locally-concentrated dose. The ability of PenG to prevent bacteria from building a peptidoglycan layer weakens the cell wall of the bacterium, which ultimately results in cell lysis.

6.3.6 β-Cyclodextrin Grafted Silica Nanoparticles

Fluorescent and multifunctional silica nanoparticles were synthesized via a coupling reaction between the hydroxyl groups on β-CD and dye-labeled, carboxylic acid coated silica nanoparticles using DCC. The carboxylic acid coated nanoparticles were prepared based on a ring opening reaction between succinic anhydride and amino-functionalized silica nanoparticles with a variety of surface graft densities ranging 0.24-0.65 groups/nm^2. Thus, the graft density of β-CD functionalized nanoparticles can be tailored by varying

the feed ratio between bare silica nanoparticles and amino-silane compound. The as-synthesized β-CD functionalized nanoparticles were purified via dialysis to completely remove un-reacted free β-CD molecules. The ^{1}H NMR spectra confirmed the removal of free β-CD from the β-CD coated nanoparticles after dialysis (Figure 6.12). The TGA data showed an increase in weight from the attached monolayer β-CD which accounted for 2.78% by weight (Figure 6.13).

2-Hydroxypropyl-β-CD was used to replace β-CD to investigate the effects of trapping signal molecules secreted by bacterial cells. Employing the same surface attachment chemistry, 2-hydroxypropyl-β-CD was attached on silica nanoparticles.

Polymer grafted silica nanoparticles containing β-CD side groups were prepared via the condensation reaction between the grafted poly(methacrylic acid) and the hydroxyl groups on β-CD. The dye-labeled poly(methacrylic acid) grafted silica nanoparticles were prepared by direct surface-initiated RAFT polymerization of methacrylic acid on dye-labeled silica nanoparticles. Thus, the carboxylic acid loading can be controlled by tailoring the surface grafted poly(methacrylic acid) brushes length as well as the graft densities. The TGA data showed that the surface polymer supported chains with multiple β-CD is accounted for 61.7% by weight for particles have a PMAA brush density of 0.18 chains/nm^2 and molecular weight of 54,900 mol/g (Figure 6.14). The β-CD side chain based polymer grafted nanoparticles showed strong fluorescence under UV light even after multiple-step surface chemical modifications (Figure 6.15).

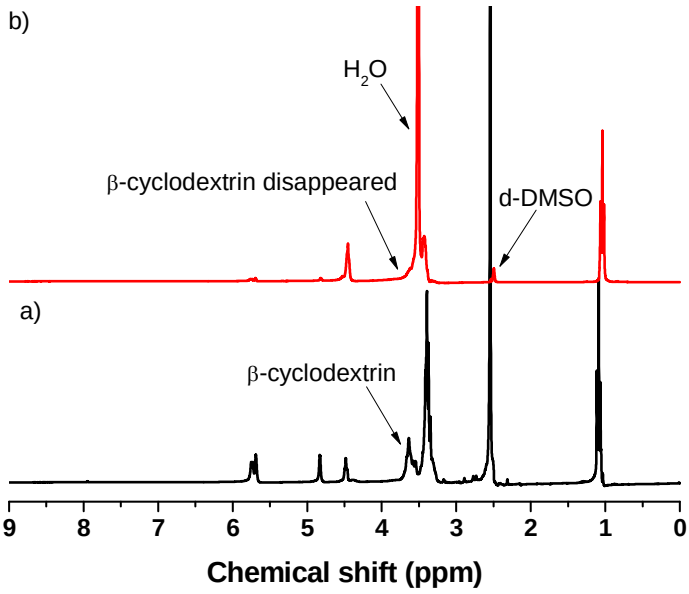

Figure 6.12 ^{1}H NMR spectra of the as-synthesized β-CD coated silica nanoparticles. a) before dialysis; b) after dialysis.

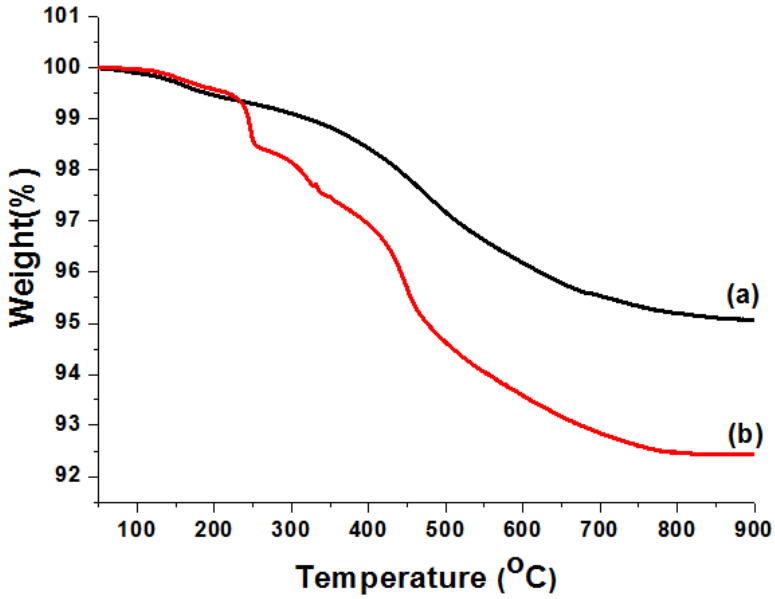

Figure 6.13 TGA of (a) dye-labeled monolayer carboxylic acid coated silica nanoparticles; (b) dye-labeled monolayer β-CD coated silica nanoparticles.

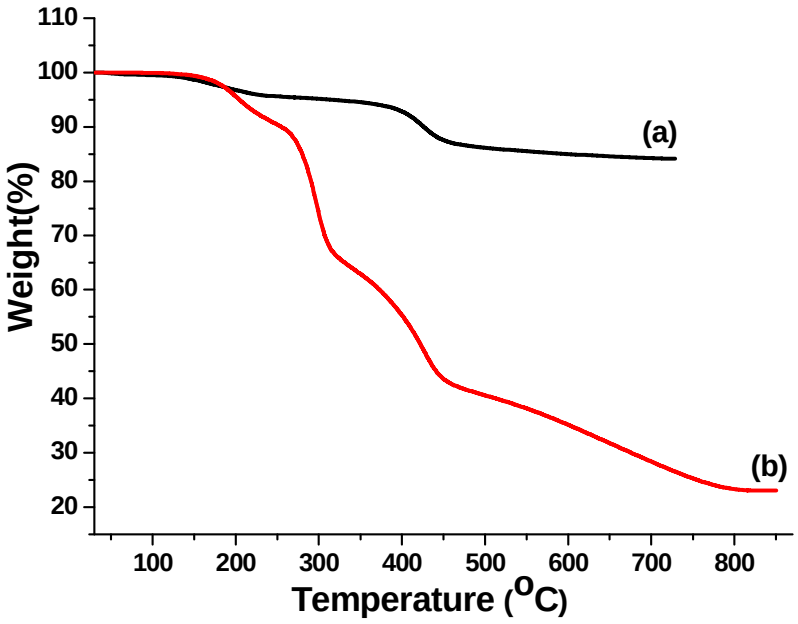

Figure 6.14 TGA of (a) dye-labeled poly(methacrylic acid) grafted silica nanoparticles (graft density: 0.18 groups/nm^2); (b) dye-labeled poly(β-CD) grafted silica nanoparticles.

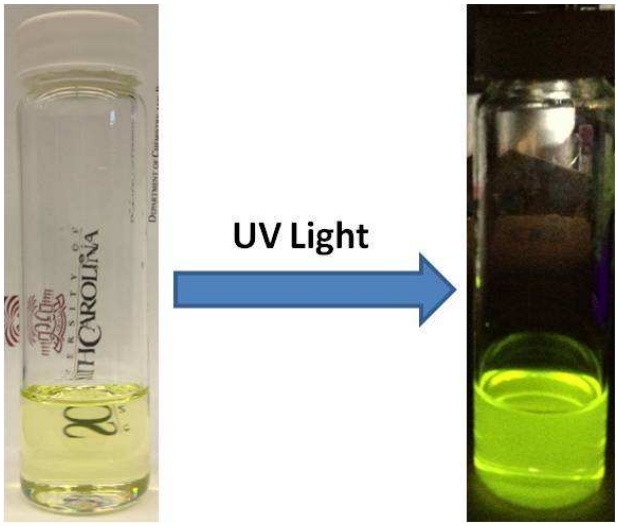

Figure 6.15 Photograph of dye-labeled poly(β-CD) grafted silica nanoparticles in DMSO.

6.3.4 Glutamate Grafted Silica Nanoparticles

The synthesis of glutamate grafted silica nanoparticles was demonstrated according to Scheme 6.3. The alkyne functionalized oligo(γ-ethyl-L-glutamate) has an average DP of

7 and the molecular weight is 1,226 g/mol. Considering the potential steric hindrance received from the surface attached PAHMA chains for the oligomers, a relatively low graft density (0.09 chains/nm^2) of PAHMA grafted silica nanoparticles with a polymer molecular weight of 8,400 g/mol and PDI of 1.27 was used for the click reaction. Thus, the oligomers can more easily diffuse into the inner area of the polymer grafted particles. The PAHMA grafted nanoparticles were prepared by surface-initiated RAFT polymerization of AHMA on CPDB coated nanoparticles, which were synthesized by the reaction between activated CPDB and amino-functionalized silica nanoparticles. IR spectroscopy was used to monitor the progress of the click reaction. The IR spectra (Figure 6.16) showed that the reaction was not completed due to appearance of the azide peak around 2100 cm^{-1} after 24 hours. The azide peak was still observed after 48 hours even though it was very weak. The increase in the N-H peak (3285 cm^{-1}) and the C=O peak (1625 cm^{-1}) were also noted, showing the attachment of oligoglutamate on the nanoparticles. This phenomena is ascribed to the steric effect for the diffusion of the oligomer to the inner area of surface attached polymers, which has also been reported in the literature.[32] The TGA (Figure 6.17) showed that the surface attached glutamate accounted for around 33.8% based on the theoretical calculation on the weight percentage of PAHMA in PAHMA grafted silica particles. The as-synthesized glutamate attached nanoparticles are being tested for antimicrobial activity.

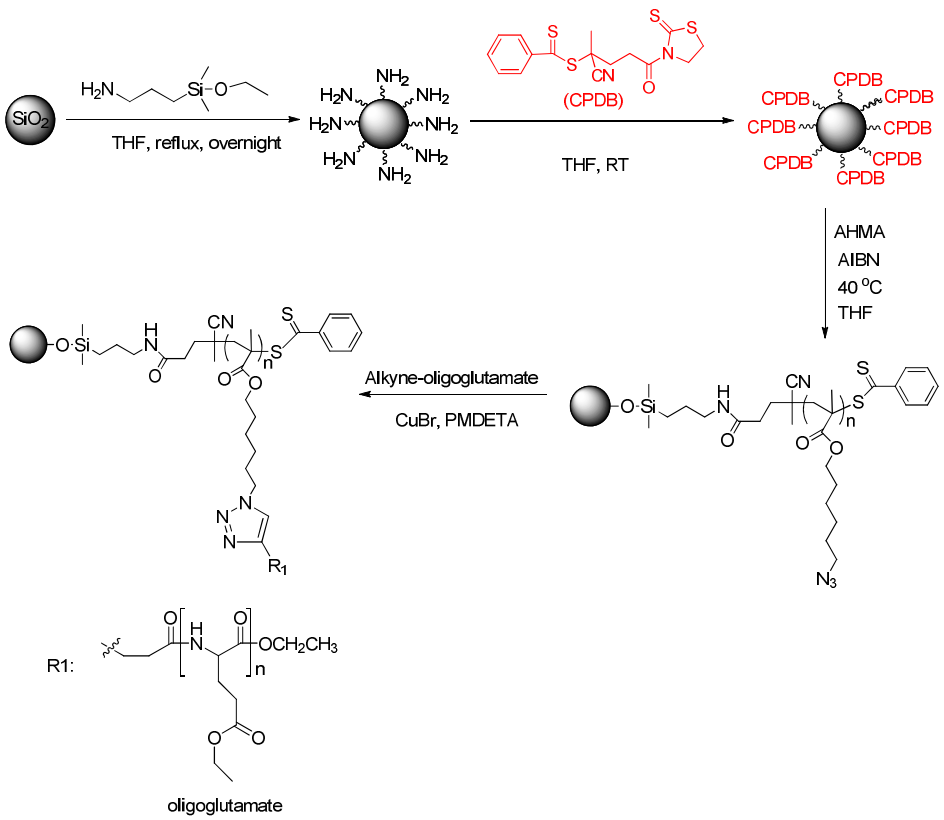

Scheme 6.3 Synthetic method for preparation of glutamate attached nanoparticles.

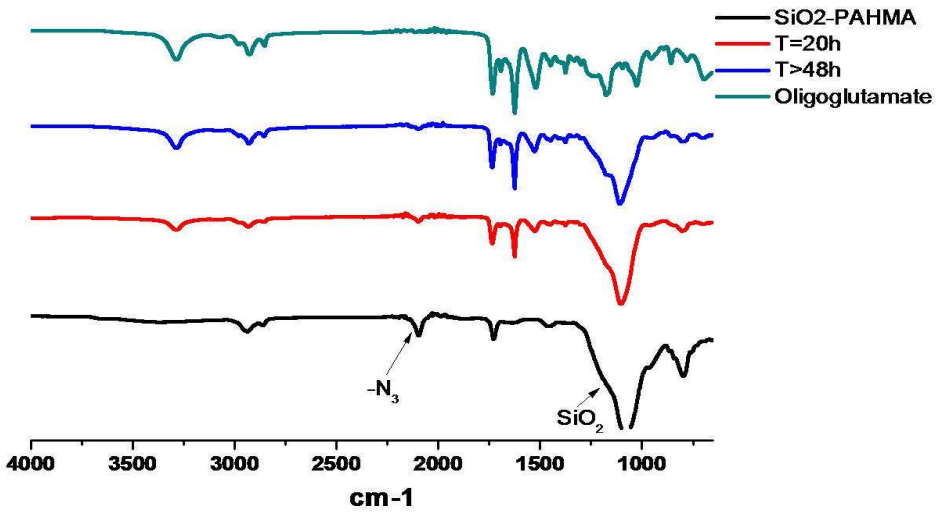

Figure 6.16 IR spectra of the click reaction progress between alkyne-oligoglutamate and PAHMA grafted silica nanoparticles.

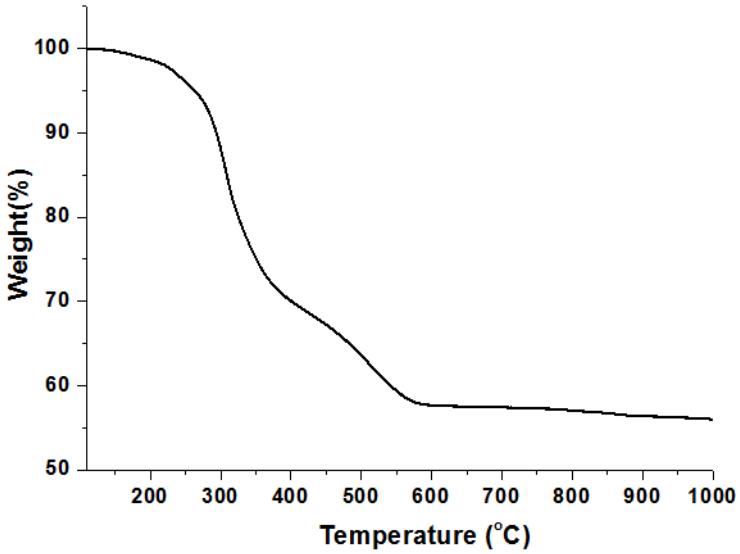

Figure 6.17 TGA of glutamate attached nanoparticles.

6.3.5 Advanced Bimodal Polymer Grafted Silica Nanoparticles

The synthesis of bimodal PMAA and PEG grafted nanoparticles was conducted according to Scheme 6.4. The first step is to make nanoparticles water soluble. Thus, the click reaction (azide-alkyne Huisgen cycloaddition) was used to attach azide-PEG onto alkyne partially functionalized silica nanoparticles, which were synthesized by the reaction between 1-(2-thioxothiazolidin-3-yl)pent-4-yn-1-one and amino-functionalized nanoparticles with a suitable ratio. An excess of 1-(2-thioxothiazolidin-3-yl)pent-4-yn-1-one will consume all the amino groups without leaving free amino groups for subsequent CPDB attachment. If the amount of 1-(2-thioxothiazolidin-3-yl)pent-4-yn-1-one is too low, the resulting PEG grafted particles would not be water soluble for the limited PEG chains. 1-(2-thioxothiazolidin-3-yl)pent-4-yn-1-one was synthesized by activation of 4-pentynoic acid using DCC/DMAP coupling reaction. The ^{1}H NMR spectra confirmed the successful formation of 1-(2-thioxothiazolidin-3-yl)pent-4-yn-1-one (Figure 6.18).

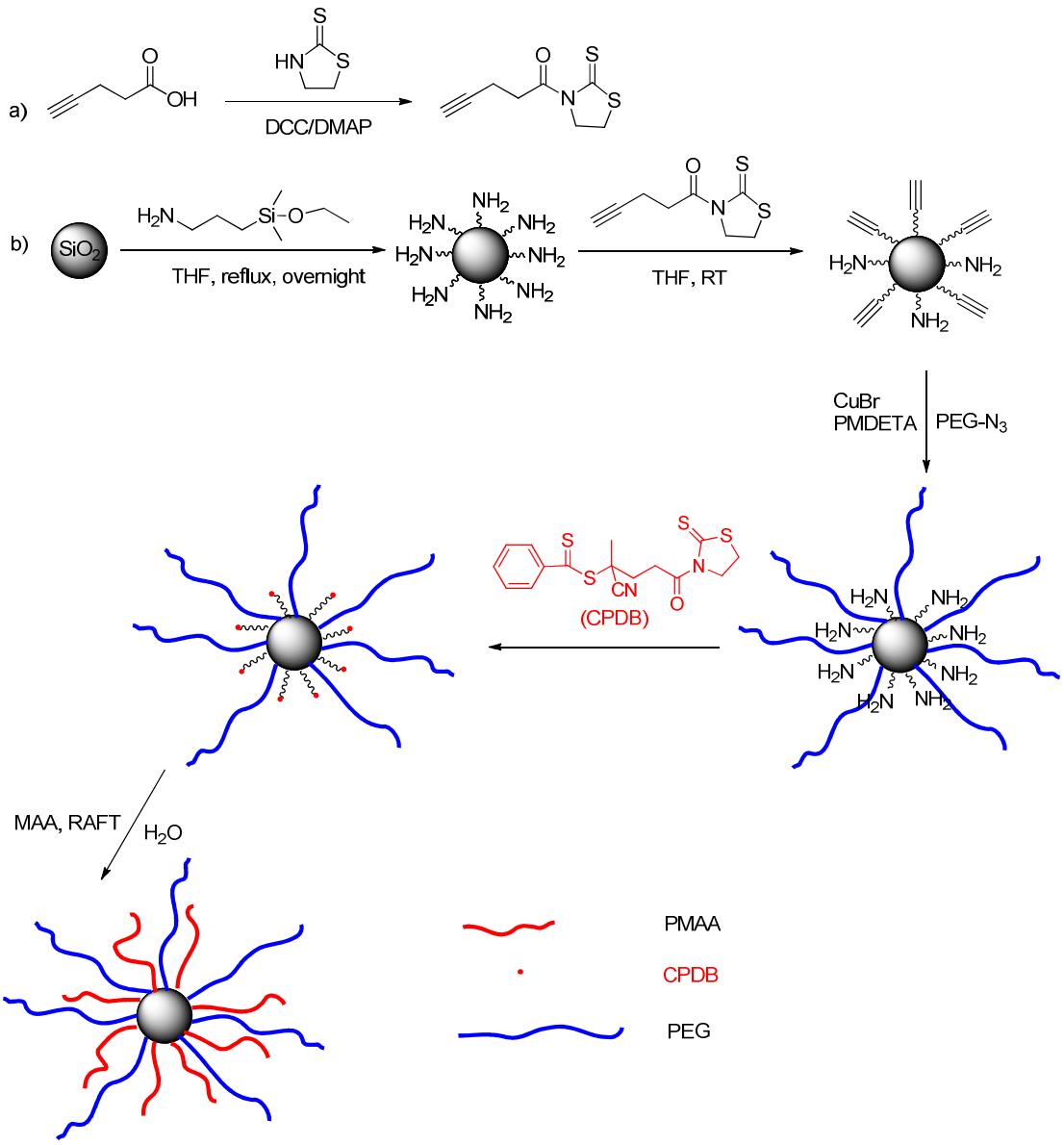

Scheme 6.4 Synthetic method for bimodal PMAA and PEG grafted silica nanoparticles via RAFT polymerization in water.

Non-functionalized silica nanoparticles were not soluble in water (Figure 6.19, A), while PEG grafted nanoparticles with two different molecular weights (550 g/mol and 5,000 g/mol) were soluble in water (Figure 6.19 B and C). The TGA data showed that the graft density of short chain PEG (Mn=550 g/mol) grafted particles was around 0.32 chains/nm^2 while the grafted density of long chain PEG (Mn=5,000 g/mol) grafted

particles was around 0.18 chains/nm^2 (Figure 6.20). Usually, in the "grafting to" strategy, the longer the polymer chains, the lower the graft density because there is much stronger steric hindrance between longer chains. Thus, the graft densities of the two groups were consistent with their polymer chain lengths.

Azide functionalized PEG (Mn=5,000 g/mol) was used to attach on particles via the click reaction and the resulting water soluble particles were used to anchor RAFT agent CPDB followed by surface-initiated RAFT polymerization of MAA in water. The TGA data showed that the surface-attached PEG accounted for around 14.7% in the PEG grafted particles (Figure 6.21). The CPDB graft density was 16 µmol/g in the CPDB coated PEG grafted nanoparticles. The TGA confirmed that new polymer was attached on particles and the bimodal polymer (PEG and PMAA) totally accounted for around 27.9% in the materials (Figure 6.21).

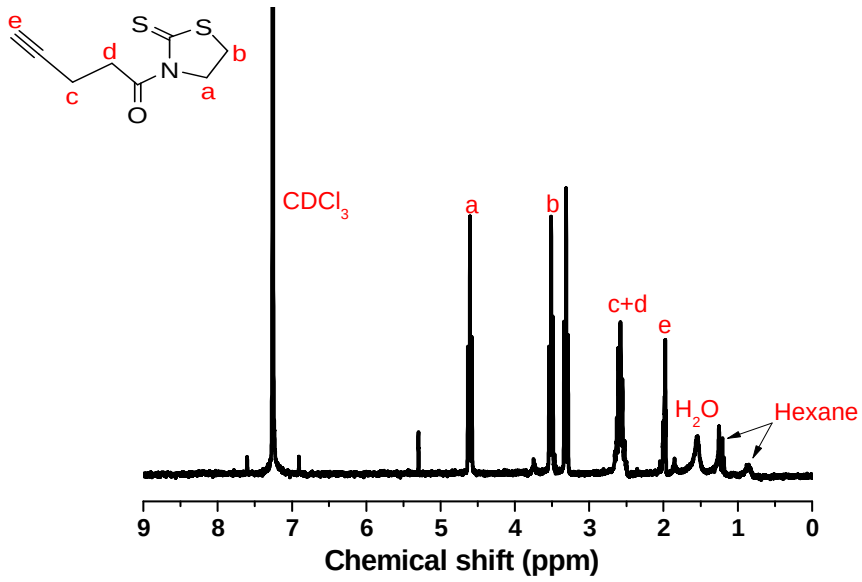

Figure 6.18 ^{1}H NMR of 1-(2-thioxothiazolidin-3-yl)pent-4-yn-1-one.

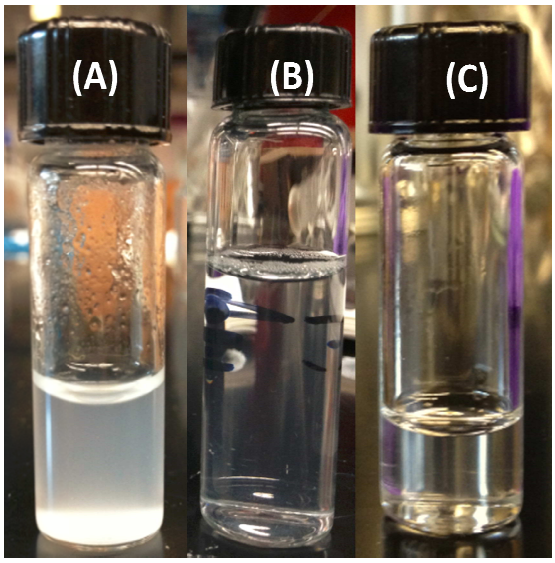

Figure 6.19 Photograph of nanoparticles in water (a) SiO_2; (b) PEG (Mn=550 g/mol) functionalized SiO_2; (c) PEG (Mn=5000 g/mol) functionalized SiO_2.

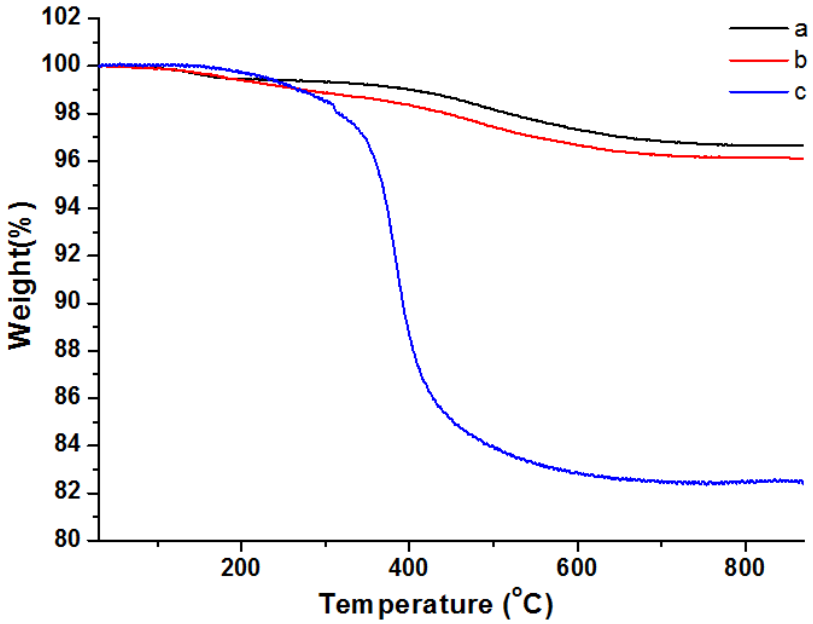

Figure 6.20 TGA of (a) SiO_2-COOH; (b) PEG (Mn=550 g/mol) functionalized SiO_2; (c) PEG (Mn=5000 g/mol) functionalized SiO_2.

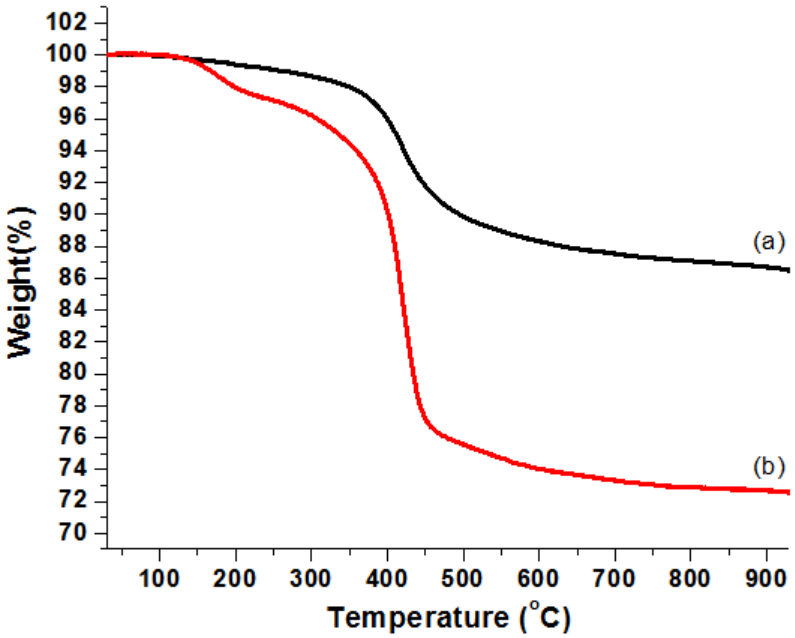

Figure 6.21 TGA of (a) PEG (Mn=5000 g/mol) grafted SiO_2 nanoparticles; (b) Bimodal PEG and PMAA grafted SiO_2 nanoparticles.

6.3.6 Poly(MAA-*b*-NIPAM) Grafted Silica Nanoparticles

There are many concerns of antibiotic leakage before arriving at the desired site during drug delivery. In order to avoid this problem, an advanced platform of poly(MAA-*b*-NIPAM) grafted silica nanoparticles was designed and synthesized, which is shown in Scheme 6.5. In this system, the inner block of PMAA is used to physically bind with antibiotics, and the outer block of PNIPAM is used to cover the inner layer using temperature control because PNIPAM is a thermal stimulus polymer. When the temperature is higher than the lower critical solution temperature (LCST), the PNIPAM transits from a swollen hydrated phase to a shrunken dehydrated phase. When the temperature is lower than the LCST, the reverse phase transition occurs. Thus, the inner layer containing conjugated antibiotics are in a constrained environment when the outer layer of PNIPAM is in a shrunken dehydrated state and the antibiotics can be stimulated

to release by adjusting the pH value when the PNIPAM layer is in a swollen hydrated state. The poly(MAA-*b*-NIPAM) grafted nanoparticles were synthesized by sequential RAFT polymerization of MAA and NIPAM in DMF on CPDB coated silica nanoparticles.

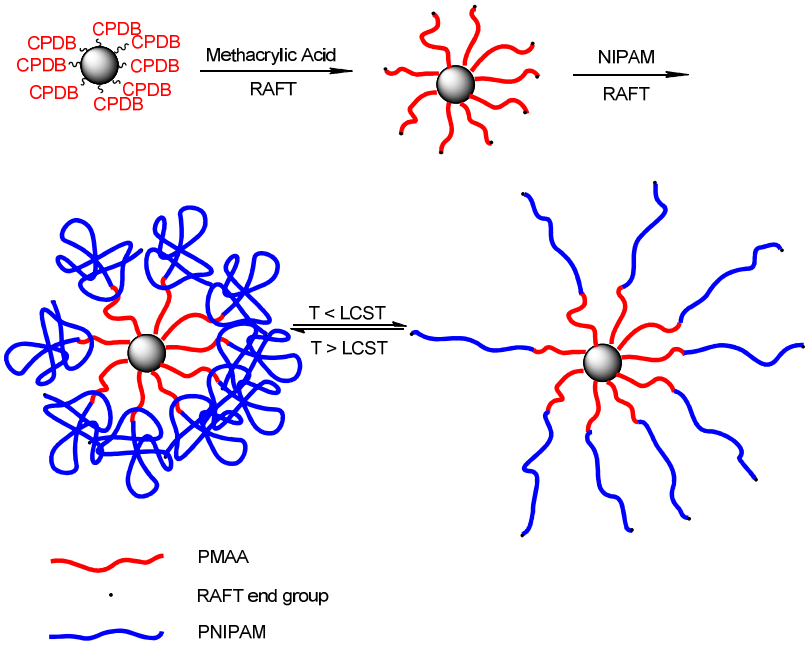

Scheme 6.5 Synthetic method for poly(MAA-*b*-NIPAM) grafted silica nanoparticles.

RAFT polymerization of NIPAM in free solution or on CPDB coated silica nanoparticles was conducted before building the second block on PMAA grafted particles. As shown in Table 6.3, the free solution RAFT polymerization generated PNIPAM with low PDI. A considerable long polymer brush was obtained after 15 h reaction. CPDB mediated nanoparticles were also able to mediate the RAFT polymerization of NIPAM.

Table 6.3 RAFT Polymerization of NIPAM

Entry	Time (h)	Mn (g/mol)	PDI	DMF (Volume, mL)
1[a]	21.5	32,368	1.04	2.5
2[a]	15.67	20,037	1.05	2
3[b]	16	13,519[c]	-	4

Note: The reaction temperature was 65 °C. (a): Polymerization in free solution ([NIPAM]/[CPDB]/[AIBN] = 500:1:0.1; CPDB: 0.018 mmol); (b): Polymerization on CPDB coated nanoparticles ([NIPAM]/[CPDB]/[AIBN] = 1000:1:0.1; CPDB-SiO_2: 135 mg, 0.4 chains/nm^2); (c) Theoretical Mn based on the conversion determined by ^{1}H NMR.

A variety of PMAA grafted particles were synthesized with different chain lengths. A sample with attached polymer molecular weight of 35,798 g/mol and PDI of 1.14 was used to conduct the second round of RAFT polymerization of NIPAM. 1,3,5-Trioxane was used as the standard to monitor the conversion of NIPAM by ^{1}H NMR (Figure 6.22).After 10 h, the conversion of NIPAM was 16.1 %. The TGA (Figure 6.23) showed that the surface attached poly(MAA-b-NIPAM) accounted for 86.7 % in the nanocomposite while the precursor PMAA accounted for 83% in the nanocomposite, which exactly matches with the theoretical calculation of ^{1}H NMR. In order to completely fulfil the idea, a design of short chain of PMAA and long chain of PNIPAM was used. The ideal ratio between the chain length of PMAA and PNIPAM is expected to be lower than 1:2 (DP_{PMAA} : DP_{PNIPAM} < 1:2), thus PNIPAM is long enough to cover the surface of the particles. Therefore, PMAA grafted particles with lower polymer molecular weight of 13,633 g/mol were prepared and could be used in further experiments.

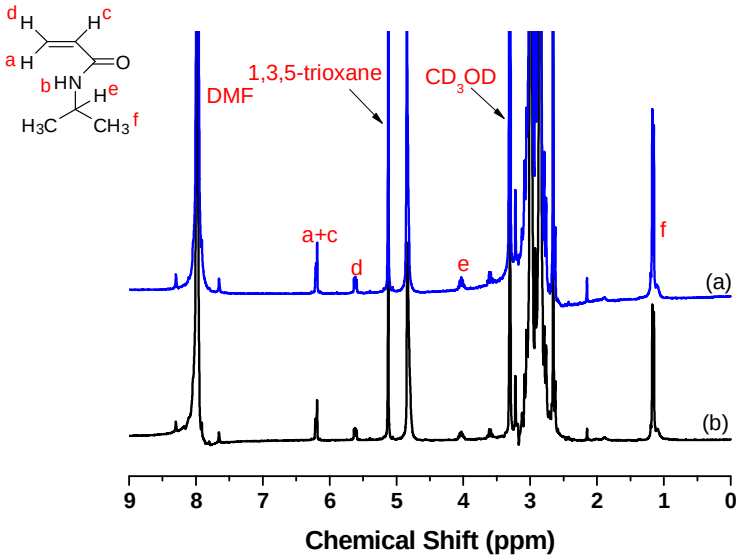

Figure 6.22 ^{1}H NMR of (a) PMAA grafted silica nanoparticles; (b) poly(MAA-*b*-NIPAM) grafted nanoparticles.

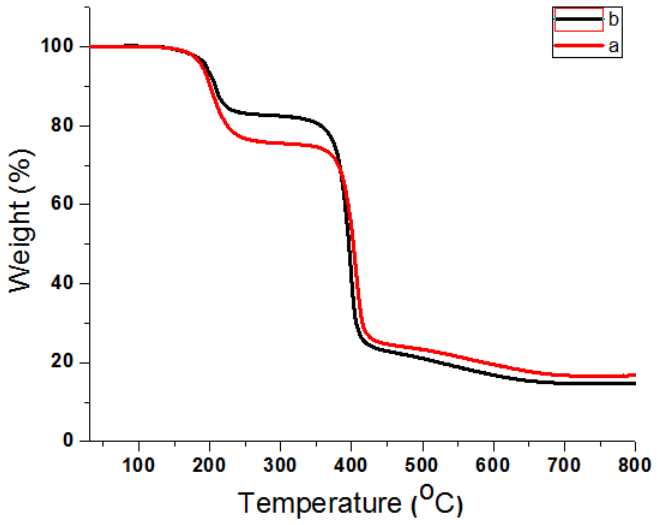

Figure 6.23 ^{1}H NMR of (a) PMAA grafted silica nanoparticles; (b) poly(MAA-*b*-NIPAM) grafted nanoparticles.

6.4 Summary

In conclusion, the surface of silica nanoparticles was modified with a variety of functionalities, from the simple to the advanced. A series of Europium (III) and

Ruthenium (II) doped silica nanoparticles with different sizes were prepared. Dye-labeled monolayer carboxylic acid coated silica nanoparticles with a range of graft densities were synthesized and the particles possessed strong fluorescence. Antibiotic penicillin-G was conjugated on nanoparticles physically and covalently with low to high amounts of loading. Carboxylic acid grafted sNPs were engineered and examined to bind antibiotics and to further kill bacterial cells. It was shown that when the commonly-used antibiotics, such as penicillin-G, were linked to nanoparticles, their bacteriocidal efficiencies were increased significantly, even to antibiotic-resistant MRSA. Therefore, much lower concentrations of the antibiotic were needed to kill these bacteria under laboratory conditions. In addition, penicillin-G conjugated to PMAA grafted nanoparticles demonstrated higher antimicrobial activity compared to penicillin-G conjugated to monolayer carboxylic acid coated particles. We hypothesize that the increased antimicrobial activity is affected by the locally high concentrations of antibiotics bound to nanoparticles, which overwhelms the resistance of bacterial strains. β-Cyclodextrin grafted nanoparticles have been prepared to capture acyl-homoserine lactone molecules in the bacterial quorum sensing (QS) process. Glutamate coated nanoparticles were prepared by the click reaction on PAHMA grafted particles for antimicrobial applications. Lastly, bimodal PEG and PMAA grafted nanoparticles, and poly(MAA-*b*-NIPAM) grafted particles were designed and prepared via the “grafting to” and “grafting from” techniques.

6.5 Reference

1. Evans, H. L.; Lefrak, S. N.; Lyman, J.; Smith, R. L.; Chong, T. W.; McElearney, S. T.; Schumlan, A. R.; Hughes, M. G.; Raymond, D. P.; Pruett, T. L.; Sawyer, R. G. *Crit. Care Med.* **2007**, *35*, 89-95.

2. Klevens, R. M.; Edwards, J. R.; Richards, C. L. Jr.; Horan, T. C.; Gaynes, R. P.; Pollock, D. A.; Cardo, D. M. *Publ. Hlth. Rep.* **2002**, *122*, 160-165.
3. Klevens, R. M.; Morrison, M. A.; Nadle, J.; Petit, S.; Gershman, K.; Ray, S.; Harrison, L. H.; Lynfield, R.; Dumyati, G.; Townes, J. M.; Craig, A. S.; Zell, E. R.; Fosheim, G. E.; McDougal, L. K.; Carey, R. B.; Fridkin, S. K. *JAMA*. **2007**, *15*, 1763-1771.
4. Fischbach, M. A.; Walsh, C. T. *Science* **2009**, *325*, 1089-1093.
5. Greene, S. E.; Reid, A. Report from the American Academy of Microbiology; 1752 N Street, NW, Washington, DC 20036/academy.asm.org. **2012**, pp 44-44.
6. Percival, S. L.; Bowler, P. G.; Russell, D. *J. Hosp. Infect.* **2005**, *60*, 1-7.
7. Kim, C. K.; Ghosh, P.; Pagliuca, C.; Zhu, Z-J.; Menichetti, S.; Rotella, V. M. *J. Am. Chem. Soc.* **2008**, *191*, 1960-1961.
8. Kallen, A. J.; Mu, Y.; Bulens, S.; Reingold, A.; Petit, S.; Gershman, K.; Ray, S. M.; Harrison, L. H.; Lynfield, R.; Dumyati, G.; Townes, J. M.; Schaffner, W.; Patel, P. R.; Fridkin, S. K. *JAMA.* **2010**, *6*, 641-647.
9. Klein, E.; Smith, D. L.; Laxminarayan, R. *Emerg. Infect. Dis.* **2007**, *13*, 1840–1846.
10. Asche, C.; McAdam-Marx, C.; Seal, B.; Crookston, B.; Mullins, C. D. *J Antimicrob Chemother*. **2008**, *61*, 1162–1168.
11. Wright, G. D. *Nat. Rev. Microbiol.* **2007**, *5*, 175-186.
12. Levy, S. B.; Marshall, B. *Nat. Med. Publ. Hlth.* **2004**, *10*, S122–S129.
13. Hannan, S.; Ready, D.; Jasni, A. S.; Rogers, M.; Pratten, J.; Roberts, A. P. *Med. Microbiol.* **2010**, *59*, 345-349.
14. Nikaido, H.; Pages, J-M. *FEMS Microbiol. Rev.* **2011**, *36*, 340-363.
15. Harris, J. M.; Chess, R. B. *Nat. Rev. Drug Discov.* **2003**, *2*, 214-221.
16. Steiniger, S. C. J.; Kreuter, J.; Khalansky, A. S.; Skidan, I. N.; Bobruskin, A. I.; Smirnova, Z. S.; Severin, S. E.; Uhl, R.; Kock, M.; Geiger, K. D.; Gelperina, S. E. *Int. J. Cancer* **2004**, *109*, 759-767.
17. Liong, M.; Lu, J.; Kovochich, M.; Xia, T.; Ruehm, S. G.; Nel, A. E.; Tamanoi, F.; Zink, J. I. *ACS Nano* **2008**, *2*, 889-896.
18. Kell, A. J.; Stewart, G.; Ryan, S.; Peytavi, R.; Boissinot, M.; Huletsky, A; Bergeron, M. G; Simard, B. *ACS Nano* **2008**. *2*, 1777–1788.
19. Mahapatra, I.; Clark, J.; Dobson, P. J.; Owenc, R.; Lead, J. R. *Environ. Sci.: Processes & Impacts.* **2013**, *15*, 123-144.
20. Akcora, P.; Liu, H.; Kumar, S. K.; Moll, J.; Li, Y.; Benicewicz, B. C.; Schadler, L. S.; Acehan, D.; Panagiotopoulos, A. Z.; Pryamitsyn, V.; Ganesan, V.; Ilavsky, J.; Thiyagarajan, P.; Colby, R. H.; Douglas, J. F. *Nat. Mater.* **2009**, *8*, 354-359.
21. Cash, B. M.; Wang, L.; Benicewicz, B. C. *J. Polym. Sci. Part A: Polym. Chem.* **2012**, *50*, 2533-2540.
22. Wang, L.; Benicewicz, B. C. *ACS Macro Lett.* **2013**, *2*, 173-176.
23. Fuqua C.; Parsek M. R.; Greenberg, E. P. *Annu Rev Genet* **2003**, *35*, 439-468.
24. Lan, S.; Veiseh, M.; Zhang, M. *Biosens. Bioelectron.* **2005**, *20*, 1697-1708.
25. Zou, H.; Wu, S.; Shen, J. *Chem. Rev*. **2008**, *108*, 3893-3957.
26. Pothayee, N.; Pothayee, N.; Jain, N.; Hu, N.; Balasubramaniam, S.; Johnson, L.; Davis, R.; Sriranganathan, N.; Riffle, J. *Chem. Mater.* **2012**, *24*, 2056-2063.
27. Li, C.; Benicewicz, B. C. *Macromolecules* **2005**, *38*, 5929-5936.

28. Mayer, T. G.;Weingart, R.;Münstermann, F.;Kawada, T.;Kurzchalia, T.;Schmidt R. R. *Eur. J. Org. Chem.* **1999**, 2563-2571.
29. Stöber, W.; Fink, A.; Bohn, E. *J. Colloid Interface Sci.* **1968**, *26*, 62-69.
30. M. Tagaya, T. Ikoma, T. Yoshioka, S. Motozuka, F. Minami, J. Tanaka. *Materials Letters* **2011**, *65*, 2287–2290.
31. Ocallagh, C.; Shingler, A. H.; Kirby, S. M.; Morris, A. *Antimicrob. Agents Chemother*. **1972**, *1*, 283−288.
32. Li, Y.; Benicewicz, B. C. *Macromolecules* **2008**, *41*, 7986-7992.

CHAPTER 7

CONCLUSIONS AND FUTURE WORK

Conclusions

A series of RAFT agents were synthesized to mediate the polymerization of styrene, MA, MMA, VAc and isoprene. The polymerizations of styrene, methyl acrylate, vinyl acetate mediated by O-ethyl based MADIX agents with primary R groups: O-ethyl S-prop-2-yn-1-yl carbonodithioate and tertiary R groups: 6-azidohexyl 2-((ethoxycarbonothioyl)thio)-2-methylpropanoate were not well-controlled which probably was due to the low chain transfer constants of these MADIX agents. Both RAFT agents containing the tertiary and α-EWG R groups: S-(2-cyanopropan-2-yl) O-ethyl carbonodithioate and the trithiocarbonate: 4-cyano-4-(dodecylsulfanylthiocarbonyl)sulfanylpentanoic (CDSS) demonstrated excellent control over the polymerization of styrene. The former generated polystyrene has a high PDI (~ 2.0) while the later generated polymer has a low PDI (~ 1.1). These differences can result in either sharp or fuzzy interfaces on nanoparticles with similar chain lengths and chain densities. The fuzzy interface could be helpful to improve the dispersion of these nanoparticles in polymer matrices by overcoming the loss of interface entropy. (4-Cyano-4-diethyldithiocarbamyl) pentanoic acid exhibited excellent control over the polymerization of vinyl acetate. Polyisoprene grafted silica particles were prepared via surface-initiated RAFT polymerization of isoprene mediated by CDSS coated

nanoparticles. They are expected to improve the dispersion of particles in rubber matrices, which is critical for mechanical reinforcement.

Two classes of water soluble polymers, namely poly(vinylpyrrolidone) (PVP) and poly(methacrylic acid) (PMAA), were grafted on nanoparticles via "grafting from" strategies. A new dithiocarbamate, 4-cyanopentanoic acid N-pyrroledithiocarboxylate (CPDC) was invented for mediating the RAFT polymerization of N-vinylpyrrolidone. CPDC can also mediate the polymerization of styrene and methyl acrylate in a controlled manner. CPDC was coated on silica nanoparticles (sNPs) via surface silane coupling chemistry. The surface-initiated RAFT polymerization of NVP was conducted on 15 nm (diameter) silica nanoparticles resulting in well-dispersed particles. PVP grafted silica nanoparticles appear to be a new vehicle to efficiently restore antibiotic activity. Dye-labeled poly(methacrylic acid) (PMAA) grafted silica nanoparticles was prepared by two methods. In the first method, "one-pot" click reactions between poly(azidohexylmethacrylate) grafted silica nanoparticles and alkyne functionalized molecules (alkyne based coumarin 343 fluorescent dye and 4-pentynoic acid) were conducted to prepare dye-labeled poly(carboxylic acid) grafted particles. In the second method, dye-labeled CPDB coated silica nanoparticles were prepared by treating amino functionalized nanoparticles with activated dyes, followed by activated CPDB. Then surface-initiated RAFT polymerization of *t*BuMA was conducted followed by sequential removal of thiocarbonylthio end groups and *tert*-butyl groups. Another strategy of direct surface-initiated RAFT polymerization of MAA on small size (15 nm) nanoparticles is more straightforward. The synthesis of the dye-labeled PMAA grafted silica nanoparticle was confirmed by FTIR, TGA, ^{1}H NMR analysis and TEM. The dye-labeled PMAA

grafted silica nanoparticles provide a platform to bind bio-molecules and to monitor the presence and movement of the nanoparticles for bioapplications.

We demonstrated an effective method for the preparation of Fe_3O_4/SiO_2 superparamagnetic nanoparticles with sizes as low as 10 nm and a high saturation magnetization using very mild synthetic conditions. CPDB coated Fe_3O_4/SiO_2 magnetic nanoparticles were prepared by treating amino functionalized Fe_3O_4/SiO_2 nanoparticles with activated CPDB. The direct surface-initiated RAFT polymerization of MAA was conducted on very small size Fe_3O_4/SiO_2 superparamagnetic nanoparticles while maintaining good dispersibility in solutions. The PMAA grafted Fe_3O_4/SiO_2 magnetic nanoparticles enhanced the bioactivity of PenG over bacteria when physically bound with PenG. The particles were removed from water solutions using a magnet after antimicrobial testing without nano-based pollution of the environment. The recycled PMAA grafted magnetic particles were able to bind PenG and retained high activity over bacteria. The water soluble PMAA grafted Fe_3O_4/ SiO_2 magnetic nanoparticles may also find applications in magnetic resonance imaging (MRI), multiple drug delivery and therapeutic fields.

We developed a toolbox of surface functionalization methods: from the simple to the advanced. These enabling techniques were used to build a variety of architectures on particles to tailor the properties for various applications. A series of luminescent particles, namely europium (III) and ruthenium (II) doped silica nanoparticles with different sizes were prepared based on the Stober method. Dye-labeled monolayer carboxylic acid coated silica nanoparticles were prepared with strong fluorescence and low-to-high graft densities. Carboxylic acid grafted sNPs were engineered and examined to bind antibiotics

and to further kill bacterial cells. It was shown that when the commonly-used antibiotics, such as penicillin-G, were linked to nanoparticles, their bacteriocidal efficiencies are increased significantly, even to antibiotic-resistant MRSA. Therefore, much lower concentrations of the antibiotic were needed to kill these bacteria under laboratory conditions. We hypothesize that the increased antimicrobial activity is ascribed to locally high concentrations of antibiotics bound to nanoparticles, which overwhelms the resistance of bacterial strains. β-Cyclodextrin grafted nanoparticles were prepared to capture acyl-homoserine lactone molecules in the bacterial quorum sensing (QS) process. Advanced bimodal PEG and PMAA grafted nanoparticles, and poly(MAA-*b*-NIPAM) grafted particles were designed and prepared via the "grafting to" and "grafting from" techniques.

Future Work

Following the design and synthesis of RAFT agents for mediating the polymerizations of styrene, methyl acrylate, methyl methacrylate, vinyl acetate and isoprene in solutions, these polymer grafted particles should be thoroughly prepared and tested for improvements of dispersion in polymer matrices, which is very important for applications in optoelectronics and mechanical reinforcement. Based on the current work, polystyrene can be prepared on nanoparticles with controllable molecular weights but with a high PDI of ~2.0, which is helpful to form fuzzy interfaces on nanoparticles. The fuzzy interfaces can overcome the loss of interface entropy, which is helpful to improve the dispersion of nanoparticles. Poly(methyl acrylate) and poly(methyl methacrylate) based nanocomposites with high PDIs can also be prepared like polystyrene. Thus, it is now

possible to prepare polymer grafted nanoparticles with identical grafte densities, polymer type, and polymer molecular weight, but differency only on the “sharpness” of the interface. Polyisoprene grafted nanoparticles could also be tested for their dispersion in rubber matrices and compared to non-functionalized silica. The surface attached polyisoprene layer is expected to improve the dispersion of particles via the interaction with the matrices. The resulting rubber composites with well-dispersed silica are expected to enhance the modulus and tensile strength of the materials.

We also propose a method to prepare block copolymer grafted nanoparticles with very different monomer activities. This is very difficult to achieve by traditional sequential RAFT polymerization using the same RAFT agent because it is hard to subsequently mediate the polymerization of a monomer with totally different activity. This problem can be addressed by using universal or switchable RAFT agents (usually dithiocarbamates) which can be easily protonated by Lewis acids to be able to mediate the polymerizations of “more activated” monomers, such as styrene and acrylates. Thus, a variety of surface grafted block copolymer with greatly different monomer activities can be prepared using switchable RAFT agent coated nanoparticles.

In addition to the current work of grafting water soluble polymers on nanoparticles, more simple and environmentally friendly processes could be explored. For example, some work in this thesis explored grafting of polymers on particles for solubility in water. The surface-initiated polymerization in water can avoid the toxicity issue of residual volatile organic compounds (VOCs), especially for applications in the cosmetics, food and biomedical industries. However, a remaining challenge in this water-based polymer grafting technique is how to ensure that the inorganic nanoparticles are initially well-

dispersed in water for subsequent processing. The typical method is coating multiple hydrophilic groups on the surfaces. Different size particles require different amounts of hydrophilic units to achieve an aqueous well-dispersed state, thus a balance between the graft density and the repeating units of these hydrophilic groups should be considered to avoid over coverage of these groups resulting in a lack of space for aqueous polymer grafting. We propose a more effective method which is introducing charged moieties as the hydrophilic groups. Usually, lower quantities of charged species are required to make particles water soluble compared to hydroxyl, oxyl alkyl, or ester groups.

More protocols could be designed and prepared for advanced surface functionalization to obtain bimodal polymer or block copolymer grafted nanoparticles. For example, targeting or recognition ligands can be anchored on the terminal sites of the surface attached polymers, which is helpful to interact with cells or proteins for biomedical applications. Multimodal functionalization is also required to incorporate three (or more) blocks or populations of polymers on a single nanoparticle to further enhance the dispersion in polymer matrices and bring new functionalities to the composite materials while maintaining the necessary mechanical properties.

APPENDIX A

PERMISSION TO REPRINT

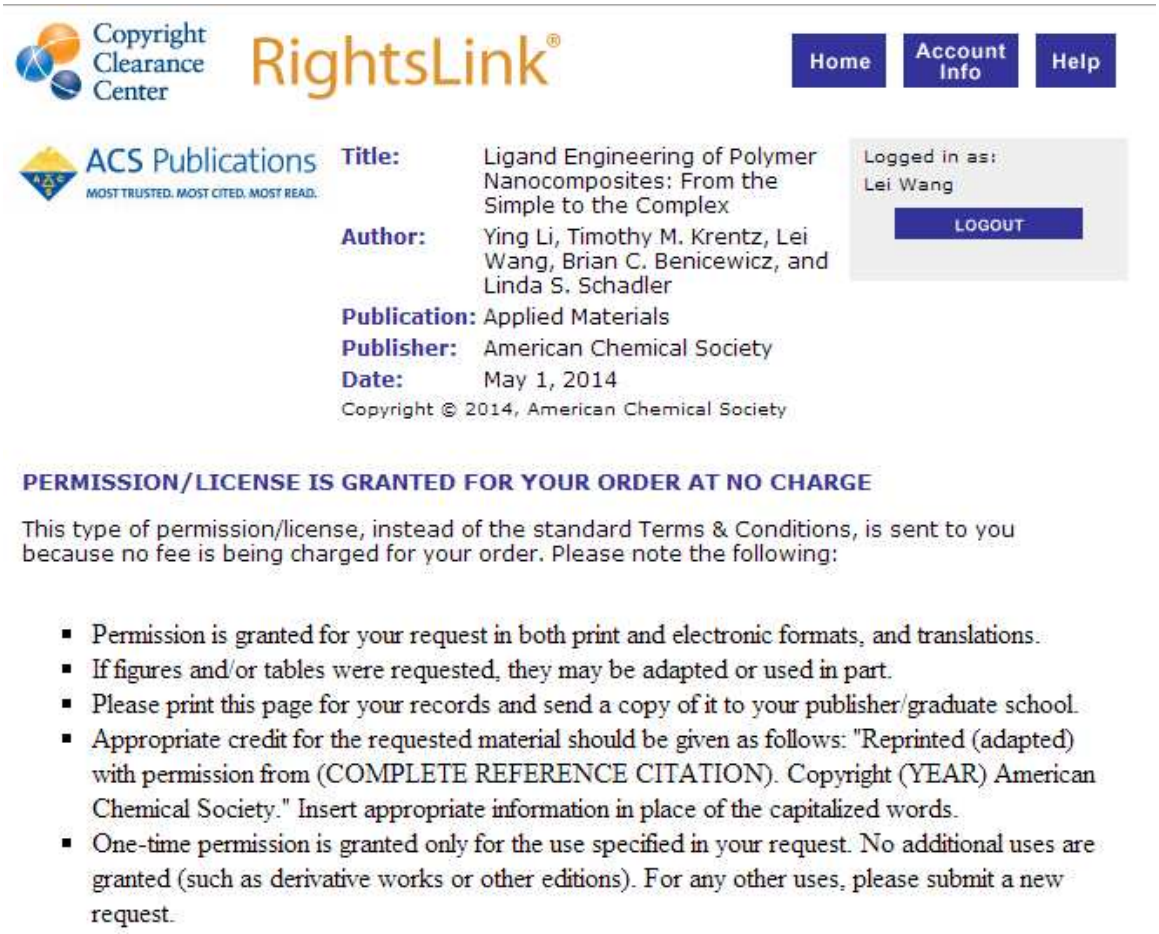

Copyright Clearance Center RightsLink®

Home | Account Info | Help

ACS Publications
MOST TRUSTED. MOST CITED. MOST READ.

Title: Ligand Engineering of Polymer Nanocomposites: From the Simple to the Complex

Author: Ying Li, Timothy M. Krentz, Lei Wang, Brian C. Benicewicz, and Linda S. Schadler

Publication: Applied Materials

Publisher: American Chemical Society

Date: May 1, 2014

Copyright © 2014, American Chemical Society

Logged in as: Lei Wang

LOGOUT

PERMISSION/LICENSE IS GRANTED FOR YOUR ORDER AT NO CHARGE

This type of permission/license, instead of the standard Terms & Conditions, is sent to you because no fee is being charged for your order. Please note the following:

- Permission is granted for your request in both print and electronic formats, and translations.
- If figures and/or tables were requested, they may be adapted or used in part.
- Please print this page for your records and send a copy of it to your publisher/graduate school.
- Appropriate credit for the requested material should be given as follows: "Reprinted (adapted) with permission from (COMPLETE REFERENCE CITATION). Copyright (YEAR) American Chemical Society." Insert appropriate information in place of the capitalized words.
- One-time permission is granted only for the use specified in your request. No additional uses are granted (such as derivative works or other editions). For any other uses, please submit a new request.

Figure A.1 Permission to reprint for Chapter 1.

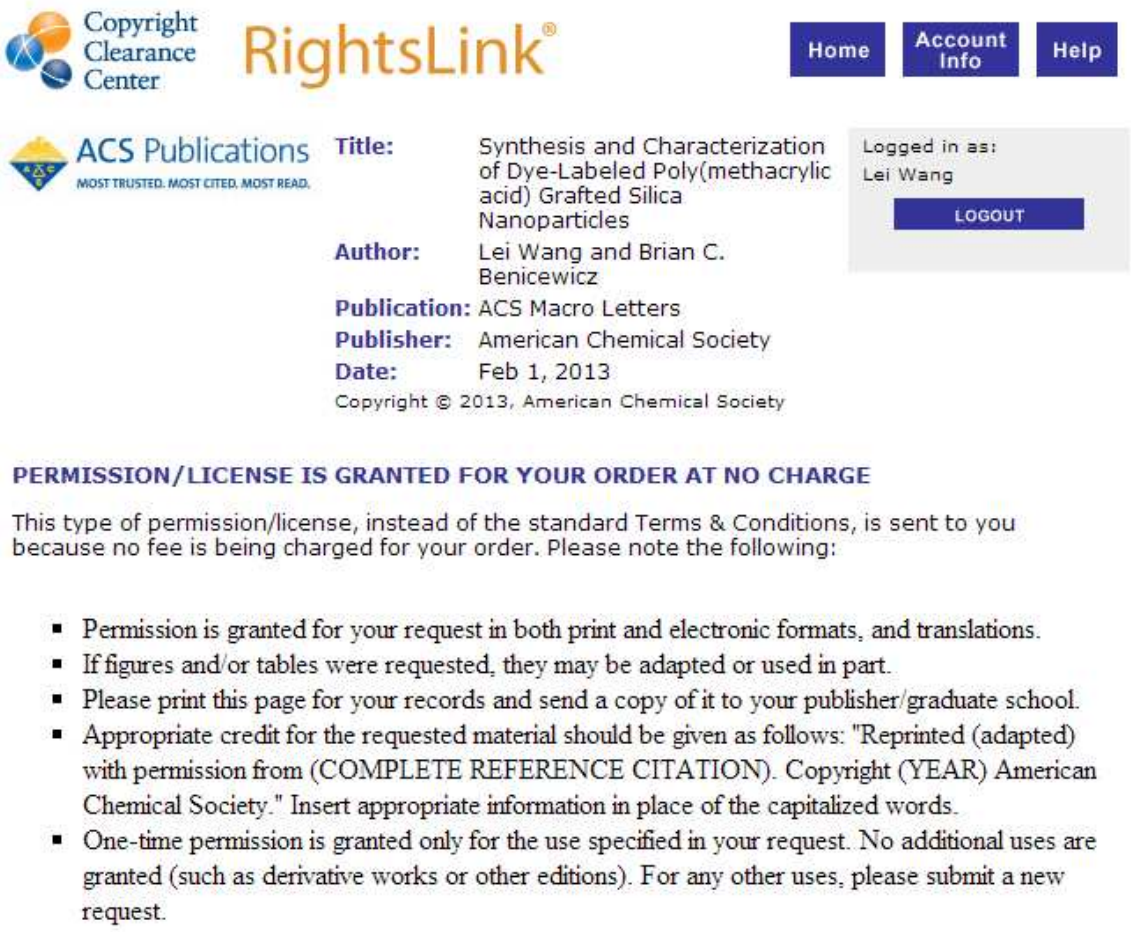

Figure A.2 Permission to reprint for Chapter 4.

Copyright Clearance Center RightsLink®

Home | Account Info | Help

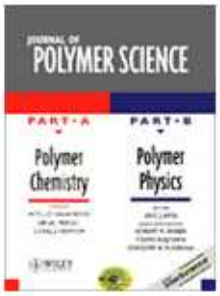

Title: The preparation and characterization of carboxylic acid-coated silica nanoparticles
Author: Brandon M. Cash,Lei Wang,Brian C. Benicewicz
Publication: Journal of Polymer Science Part A: Polymer Chemistry
Publisher: John Wiley and Sons
Date: Mar 27, 2012

Logged in as:
Lei Wang
LOGOUT

Order Completed

Thank you very much for your order.

This is a License Agreement between Lei Wang ("You") and John Wiley and Sons ("John Wiley and Sons"). The license consists of your order details, the terms and conditions provided by John Wiley and Sons, and the payment terms and conditions.

Get the printable license.

License Number	3405101291739
License date	Jun 09, 2014
Licensed content publisher	John Wiley and Sons
Licensed content publication	Journal of Polymer Science Part A: Polymer Chemistry
Licensed content title	The preparation and characterization of carboxylic acid-coated silica nanoparticles
Licensed copyright line	Copyright © 2012 Wiley Periodicals, Inc.
Licensed content author	Brandon M. Cash,Lei Wang,Brian C. Benicewicz
Licensed content date	Mar 27, 2012
Start page	2533
End page	2540
Type of use	Dissertation/Thesis
Requestor type	Author of this Wiley article
Format	Print and electronic
Portion	Text extract
Number of Pages	1
Will you be translating?	No
Title of your thesis / dissertation	Synthesis and Characterization of Polymer Nanomaterials Using Controlled Radical Polymerization
Expected completion date	Jun 2014
Expected size (number of pages)	209
Total	0.00 USD

ORDER MORE... CLOSE WINDOW

Figure A.3 Permission to reprint for Chapter 6.

Copyright Clearance Center RightsLink®

Home | Account Info | Help

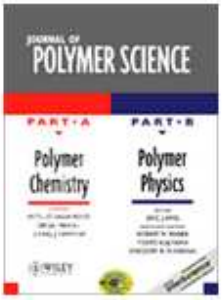

Title: The preparation and characterization of carboxylic acid-coated silica nanoparticles
Author: Brandon M. Cash,Lei Wang,Brian C. Benicewicz
Publication: Journal of Polymer Science Part A: Polymer Chemistry
Publisher: John Wiley and Sons
Date: Mar 27, 2012

Logged in as:
Lei Wang
LOGOUT

Order Completed

Thank you very much for your order.

This is a License Agreement between Lei Wang ("You") and John Wiley and Sons ("John Wiley and Sons"). The license consists of your order details, the terms and conditions provided by John Wiley and Sons, and the payment terms and conditions.

Get the printable license.

License Number	3405110160908
License date	Jun 09, 2014
Licensed content publisher	John Wiley and Sons
Licensed content publication	Journal of Polymer Science Part A: Polymer Chemistry
Licensed content title	The preparation and characterization of carboxylic acid-coated silica nanoparticles
Licensed copyright line	Copyright © 2012 Wiley Periodicals, Inc.
Licensed content author	Brandon M. Cash,Lei Wang,Brian C. Benicewicz
Licensed content date	Mar 27, 2012
Start page	2533
End page	2540
Type of use	Dissertation/Thesis
Requestor type	Author of this Wiley article
Format	Print and electronic
Portion	Figure/table
Number of figures/tables	4
Original Wiley figure/table number(s)	Figure 2, Figure 4, Figure 9 and Figure 10
Will you be translating?	No
Title of your thesis / dissertation	Synthesis and Characterization of Polymer Nanomaterials Using Controlled Radical Polymerization
Expected completion date	Jun 2014
Expected size (number of pages)	209
Total	0.00 USD

Figure A.4 Permission to reprint for Chapter 4 and Chapter 6.